A geochemical traverse across the North Chilean Andes

Thesis

A GEOCHEMICAL TRAVERSE ACROSS THE NORTH CHILEAN ANDES

A thesis presented for the degree of

Doctor of Philosophy

Graeme Rogers

(B.A. Oxon.)

Department of Earth Sciences

The Open University

Milton Keynes

July 1985

Date of submission : July 1985

Date of award : 28 November 1985

Abstract

A transect across the Andean cordillera at latitude 22°S in Chile is investigated using geochemical and geochronological techniques.

The oldest rocks in the region are the Limon Verde schists, which yield a Rb-Sr whole rock age of 251±50 Ma. This is considered to reflect resetting by the intrusion of the adjacent Limon Verde pluton. T^{Nd}_{DM} ages range from 913 - 1308 Ma indicating the presence of old lithosphere on the western flanks of the Andes. The Limon Verde pluton gives a whole rock Rb-Sr age of 266±42 Ma (ε^{i}_{Sr} = 26.5). Its Sr and Nd isotopes are slightly enriched relative to 'bulk Earth' and derivation from isotopically enriched mantle or equilibration of the whole, more depleted magma with a crustal melt prior to high level fractionation is favoured. Rhyolitic lavas of the Cerro Crespo Formation yield a whole rock Rb-Sr age of 233±36 Ma (ε^{i}_{Sr} = 40.2). Their petrogenesis is considered to be similar to that of the Limon Verde pluton.

The La Negra Formation outcrops in the Cordillera de la Costa, and marks the start of the 'Andean Orogeny' in this transect. The lavas yield a whole rock Rb-Sr age of 186±14 Ma (ε^{i}_{Sr} = -18.8). They are mainly plagioclase phyric, high K basaltic andesites exhibiting tholeiitic fractionation trends. Sr and Nd isotope systematics indicate derivation from a depleted mantle source. More than 80% of Sr, K, Rb, Ba and Th, and less than 60% Ce, Nd, P and Sm are introduced as the subduction zone component. Plots of Hf/LILE and Hf/HFSE against these proportions yield information regarding the elemental concentrations in the mantle prior to the addition of the subduction zone component. This mantle had $\varepsilon^{i}_{Nd} \sim +10$, and the subduction zone component had

$\varepsilon^{i}_{Nd} \sim -2$. To satisfy trace element criteria, the addition of the subduction zone component must have been a multistage process. The La Negra Formation is considered to have been erupted through fissures in an ensialic back arc basin.

Jurassic plutons in the Cordillera de la Costa yield ages between 158 - 154 Ma. Parts of the Tocopilla pluton experienced late-stage alkali metasomatism resulting in the formation of "monzonites". Trace element and isotopic differences between the plutons are due to derivation from a heterogeneous, isotopically depleted mantle source.

Jurassic marine and lower Cretaceous continental sedimentation around Cerritos Bayos was succeeded by the lavas of the Indio Muerto Formation. Immobile inter HFSE ratios suggest derivation from a variety of mantle sources: Nd isotope data imply that significant crustal contamination may have occurred. The Augusta Victoria Formation gives an age of 105±19 Ma ($\varepsilon^{i}_{Sr} = -4.3$). Two magma types are present, the high K group being derived from a more trace element enriched source than the low K group. The Cerro Negro Formation, which is composed mainly of tuffs with isolated lavas, was derived from an isotopically depleted source within the garnet stability field.

Emplacement of plutons during the Cretaceous occurred at 100 Ma in the Cerros de Montecristo and at Cerritos Bayos, at 79 Ma in the Pampa Negra and at 66 Ma at Cerro Colorado. Whilst Cerro Colorado is highly potassic, the other plutons follow calcalkaline trends. The Cerritos Bayos pluton has been affected by late-stage alkali metasomatism and post consolidation silicification which has disturbed much of its geochemistry. Isotope systematics suggest that the Cerros de Montecristo, Cerritos Bayos

and Cerro Colorado plutons have tapped isotopically distinct sources, whereas the Pampa Negra pluton may have experienced complex crustal interaction.

The El Abra pluton yields an age of 39±2 Ma (ε^{i}_{Sr} = -2). There is no evidence to indicate that it has suffered significant crustal contamination. Tertiary volcanics between 15.2 and 2.5 Ma all have slightly enriched isotopic characteristics. Their T^{Nd}_{DM} ages range from 798 - 1151 Ma, again implying that the Western Cordillera is underlain by old lithosphere. Recent basic monogenetic centres also have enriched isotopic characteristics and subduction-related trace element geochemistry. An alkali basalt from Bolivia, however, is unrelated to subduction and has more depleted isotope systematics; its source is probably below the continental lithosphere. Revised and additional Sr and Nd isotope data for San Pedro and Ecuador are presented.

There has been a general eastwards migration in the locus of magmatism since the Jurassic. Isotope data show that younger, more easterly units tap progressively less depleted sources, and that to the east of the Rio Loa these are enriched relative to 'bulk Earth'. Trace element data indicate that the proportion of the subduction zone component in volcanic rocks decreases from the Jurassic - Recent. Variations in the subduction zone component and progressively increasing degrees of crustal contamination of depleted mantle derived magmas are not thought to be responsible for the observed isotopic and trace element variations. Instead, as the locus of magmatism has migrated eastwards it has tapped more trace element and isotopically enriched, and probably older mantle source regions.

The increase in crustal thickness since the Miocene may be attributable to tectonic underthrusting of the continental margin. The thickening crust promotes the likelihood of crustal anatexis and contamination. This contamination, however, operates on magmas derived from old, enriched mantle sources.

CONTENTS

List of Figures

List of Tables

List of Plates

Acknowledgements

I would like to express my thanks to the following people:

1. Chris Hawkesworth - for supervision and guidance throughout the project.

2. Everyone in the isotope lab., especially Andy Gledhill and Peter van Calsteren for ensuring the smooth running of the chemical separation facilities and the mass spectrometer.

3. Lindsey O'Callaghan - for field assistance in Chile and Peru.

4. Peter Francis - for getting us thrown into jail in Peru.

5. Senor Carlos Ricketts (Honorary British Consul, Arequipa) - for getting us out of jail.

6. Senora Doris MacFarlane - for logistical help in Antofagasta.

7. Lindsey O'Callaghan - for providing powders from Cerro Colorado and San Pedro, and rocks from several other localities.

8. John Watson and Peter Webb (XRF, Open University); P.K. Harvey and B.P. Atkin (XRF, Nottingham University); Phil Potts, Olwen Williams Thorpe and Nick Rogers (INAA); Ian Chaplin et al. (thin sections).

9. John Taylor, Helen Boxall and Sue Button for cartographic advice.

10. Arthur Baldwin, Peter van Calsteren, Peter Francis, Martin Menzies, Lindsey O'Callaghan, Julian Pearce, Nick Rogers, Andy Saunders, Richard Thorpe, and Andy Tindle - for discussions and criticisms.

11. Andy Saunders - for patience. "There's still a small problema..."

12. Janet Dryden and Carol Whale - for typing this thesis.

13. My parents - for continual encouragement and support.

14. Liz - without whom this thesis would have been finished ages ago.

CHAPTER 1

INTRODUCTION

1.1 Location and physiography of the field area

The location of the study area is a narrow transect across northern Chile at approximately latitude 22°S between the port of Tocopilla in the west and the San Pedro volcano near the Chile-Bolivia frontier (Figures 1.1 and 1.2). The area is part of the Atacama Desert, and is completely arid; the nitrate mine at Maria Elena is the driest place on Earth, no rain having fallen for at least 400 years (Guinness Book of Records, 1983). Below 3000 m altitude there is no vegetation whatsoever, except briefly after rare rainstorms when there is an explosion of tiny flowers in certain places; above this level sparse cacti, tough grasses and yareta survive on the scant seasonal precipitation. The region is cut by one river, the Rio Loa which has small tributaries in the Western Cordillera. Water from these streams is extracted to supply the towns of Calama, Chuquicamata, Maria Elena, Pedro de Valdivia and Tocopilla. Lower down the Rio Loa is probably fed by underground springs, but its meagre waters are always brackish and its channel very narrow. This arid climate is thought to have persisted since at least the Oligocene (Galli-Olivier, 1967). A consequence of these conditions is that exposure is 100% in the sense that there is no vegetation cover, but because of solar heat exfoliation and, above 3000 m, freeze-thaw action much of the desert surface is simply composed of boulders, forming *in situ* scree. This frequently obscures geological contact relationships. The best exposure is that of the La Negra Formation forming the coastal escarpment.

Access to the area is limited. Roads connect the main towns, and these provide a framework from which to enter the more remote areas.

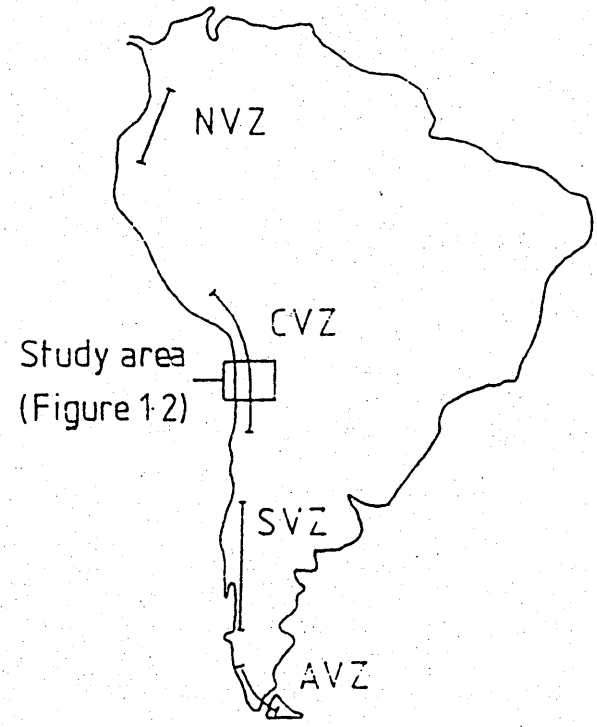

Figure 1.1

Map of South America showing location of study area and the active volcanic zones in the Andes. NVZ = Northern Volcanic Zone; CVZ = Central Volcanic Zone; SVZ = Southern Volcanic Zone; AVZ = Austral Volcanic Zone

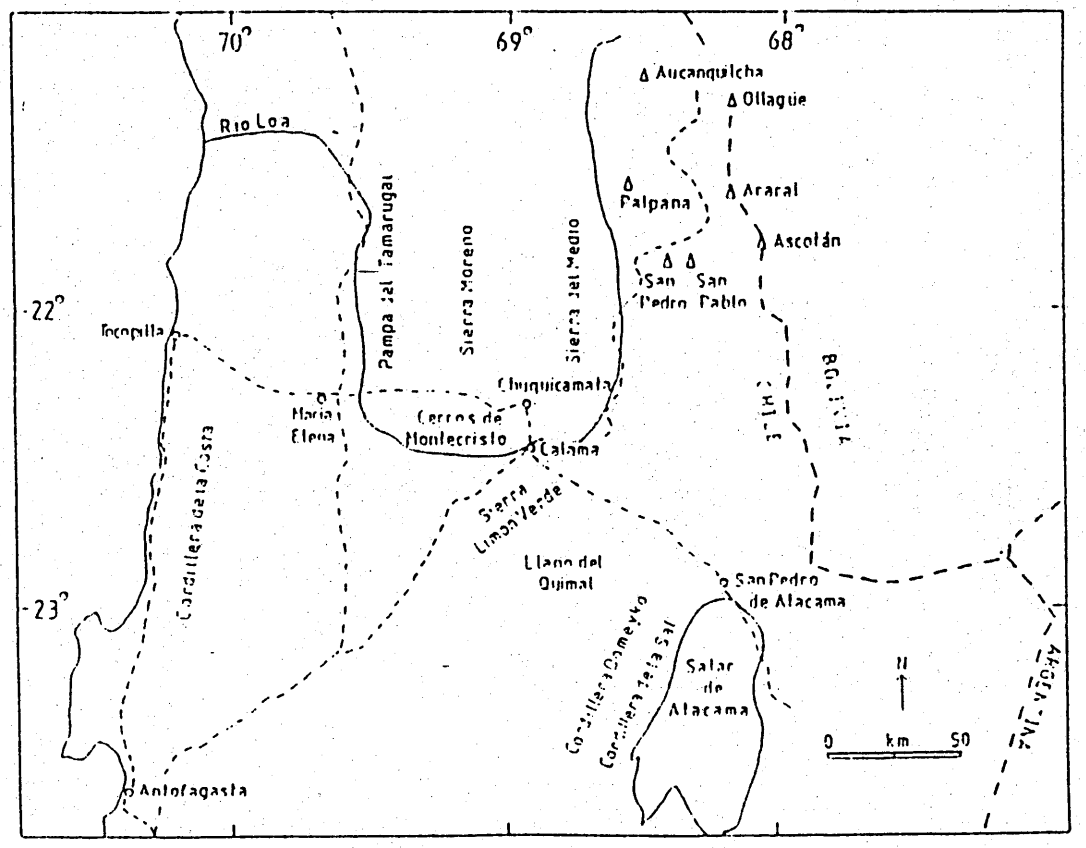

Figure 1.2

Map of the study area at ∿ 22°S showing major towns, roads and topographic features.

Mineral exploration over the years has created rough tracks across much of the desert, but these are often washed out by any rainstorms.

The Andean margin can be divided into a number of physiographic provinces (Figure 1.3): many terms exist in the literature to cover the same areas and diverse authors may use the same term for different provinces. The nomenclature for gross provinces presented below will be adhered to in this thesis.

i) Cordillera de la Costa

This forms a narrow (50-60 km) horst structure parallel to the coast. It is bounded to the west by a steep fault escarpment which locally attains a height of 1700 m; the highest summits of this range in the study area reach 2000 m. To the east the mountains descend gradually by small faults into the Pampa del Tamarugal: these faults are part of the extensive Atacama Fault System.

ii) Longitudinal Valley (Pampa del Tamarugal)

The longitudinal (or Central) Valley forms a prominent but intermittent feature along much of northern and central Chile. In the study area and further north it is named the Pampa del Tamarugal. Its elevation rises gently from about 1100-1200 m in the west to about 1700 m in the east where it is fault-bounded against the Sierra Moreno and Cerros de Montecristo (Figure 1.2). Much of this fault is obscured by Quaternary and older gravels.

iii) Precordillera

The region between the Pampa del Tamarugal and the Western Cordillera is composed of a series of horsts and grabens oriented roughly

north-south (Figure 1.2). The westernmost of these is the block which includes the Sierra Moreno and the Cerros de Montecristo. The former rises to about 3700 m whereas the highest point in the Cerros de Montecristo is 2920 m. To the east of these mountains is a narrow tilted pampa followed by a range termed the Sierra del Medio which contains peaks up to 4500 m high. This is separated from the Western Cordillera by the north-south faulted depression of the Rio Loa. South-west of Calama the extension of the Sierra Moreno block is poorly defined, the Cerros de Guacate near Cerritos Bayos being the southerly equivalent. Here the Pampa del Tamarugal extends further east into the Pampa Limon Verde which rises to 2700 m. This is fault-bounded to the east against the Sierra Limon Verde which reaches 3620 m. The Sierra Limon Verde, like the Cordillera de la Costa drops gently to the east into the Llano del Quimal before rising to the northernmost bastions of the important Cordillera Domeyko, the Cerros de Purilactis. These attain a height of 3600 m, some 600 m above the level of the aforementioned plain. The internal drainage basin of the Salar de Atacama is separated from the Cerros de Purilactis by the narrow Llano de Paciencia and the spectacular Cordillera de la Sal.

iv) Western Cordillera

The Western Cordillera is here defined as the region immediately to the east of the Rio Loa and Salar de Atacama. At 22°S it is separated from the Precordillera by the valley of the Rio Loa. Although faults just to the east of the valley downthrow to the east, the topography rises gently from this valley, the slope formed by tilted upper Tertiary ignimbrites now covered by Quaternary deposits. Surmounting this slope (Puna slope) at 22°S are two north-south lines of stratovolcanoes separated by a chain of salars. The western line of cones includes San Pedro (6141 m), San Pablo (6022 m), Palpana (6023 m) and

Aucanquilcha (6176 m), while the eastern one includes Ascotan (5478 m), Araral (5688 m) and Ollague (5863 m). San Pedro, Aucanquilcha and Ollague have fumerolic activity (Casertano, 1963; Roobol et al., 1976). The chain of salars - Ollague, Carcote (San Martin) and Ascotan - is at a height of about 3700 m.

v) Altiplano

Between the Western Cordillera and the Eastern Cordillera in Bolivia is a large plateau with some internal drainage extending northwards into southern Peru: this is termed the Altiplano. It has an average elevation of about 3800 m and contains several extensive lakes and salt flats (e.g. Salar de Uyuni, Lake Poopo, Lake Titicaca).

1.2 Economic geology

The major mining activity in the area is centred on the huge porphyry copper deposit at Chuquicamata. Other porphyry copper deposits include El Abra and Quebrada Blanca, both related to the same fault system as Chuquicamata. These mines have also been used to obtain molybdenum. Copper, too, is mined from small workings in the La Negra Formation (Chapter 3) and granitic plutons of the Cordillera de la Costa, from around Cerritos Bayos, and from the plutons near Sierra Gorda. This latter locality has also been worked for gold, lead and zinc. Silver has been recovered from Jurassic marine sediments near Caracoles.

The most important non-metallic deposits are the nitrate fields at Maria Elena and Pedro de Valdivia. In the 19th and early 20th centuries these oficinas were numerous, but, with the advent of chemical synthesis of nitrate the industry entered rapid decline. Details of the methods currently employed at the oficinas are given in Crozier (1981). Sulphur

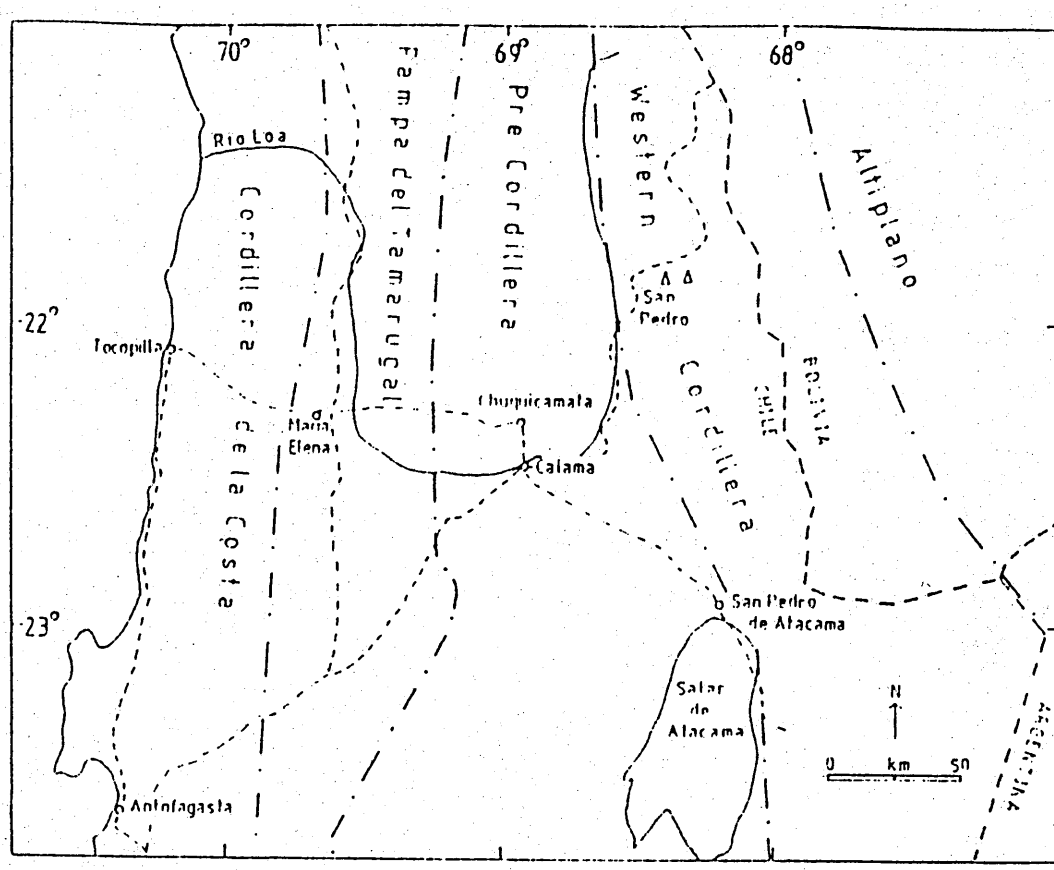

Figure 1.3

Map of the study area showing the division of the Andes into physiographic provinces. Towns and roads are marked for comparison with Figure 1.2.

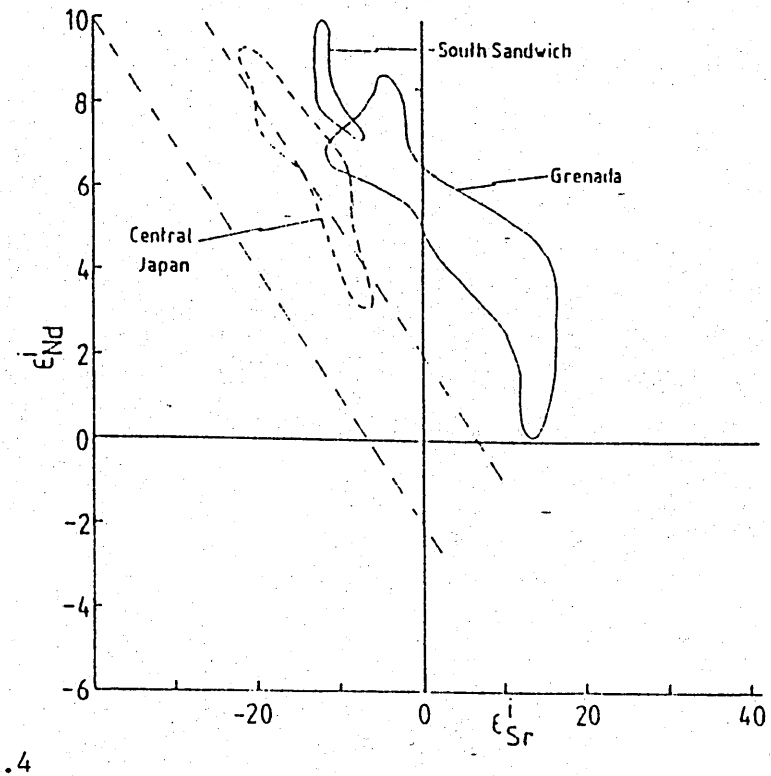

Figure 1.4

ε_{Sr}-ε_{Nd} diagram illustrating the displacement of certain island arcs to the high ε_{Sr} side of the mantle array. Data sources: South Sandwich Islands: Hawkesworth et al. (1977); Cohen and O'Nions (1982): Grenada; Hawkesworth et al. (1979); White and Patchett (1984): Central Japan; Nohda and Wasserburg (1981); White and Patchett (1984).

is mined from high on the volcanoes of Ollague and Aucanquilcha. Gypsum has been exploited from several localities. The Salar de Ascotan contains appreciable quantities of borax. In the past guano was an important product from the coastal region. The strangest deposit, however, is the alteration associated with Alcaparrosa near Cerritos Bayos. Here, because of the extreme aridity unique minerals, mostly anhydrous iron sulphates, may be found. An extensive review of the economic deposits is given in Ruiz et al. (1965).

1.3 Magmagenesis at destructive plate margins

The generation of magma at destructive plate margins is a complex process. Several putative sources which may contribute towards the final magma include:

(i) the subducted oceanic lithosphere in either amphibolite or eclogite facies (Green and Ringwood, 1968; Ringwood, 1974) by melting or by dehydration reactions. This lithosphere may be fresh or altered by hydrothermal or halmyrolitic processes (Hart et al., 1974).

(ii) pelagic sediments deposited on the oceanic lithosphere which include calcareous oozes, ferruginous clays and volcanic ash (Hole et al., 1984).

(iii) detrital sediments eroded from the arc and/or from an approaching landmass into the trench. This may be particularly important in continental arcs where the provenance of the sediments could be from ancient rocks.

(iv) the overriding mantle wedge.

(v) the continental crust through which magmas in continental arcs rise. This may partially melt and contaminate the ascending liquid, or given appropriate geothermal gradients may melt more extensively to yield acid

magmas (Hawkesworth et al., 1982).

Coupled with these potential sources, processes of partial melting, low and high pressure fractional crystallization and magma mixing fundamentally affect the nature and composition of magmatic products. The participation or otherwise of the differing sources, and the degree of involvement of the various processes has been assessed in several arcs using trace element and isotope geochemistry. Gill (1981) and Thorpe (1982) have extensively reviewed the geochemical characteristics of arc magmatism to which the reader is referred for detailed discussions. Briefly, magmas erupted in island arc environments are enriched in large ion lithophile elements (LILE) relative to high field strength elements (HFSE), thus producing higher ratios of, for instance, Ba/Zr, Ce/Ta and Th/Ta compared to those found in mid ocean ridge basalts (MORB) (Pearce, 1982, 1983; Saunders et al., 1980; Hole et al., 1984). In continental arcs there is also a decrease in Zr/Nb ratios reflecting an intra-plate component (Pearce, 1983). These variations are often best displayed on a MORB normalised diagram (Pearce, 1982, 1983). Isotopically, on a diagram of $^{143}Nd/^{144}Nd$ against $^{87}Sr/^{86}Sr$, some destructive plate margin lavas are displaced to the right (high $^{87}Sr/^{86}Sr$) of the mantle array (e.g. Hawkesworth et al., 1977, 1979a, b; Hawkesworth and Powell, 1980; DePaolo and Wasserburg, 1977; Figure 1.4). The trace element and isotopic signature of subduction-related magmatism is considered to be due to dehydration of the subducting oceanic lithosphere enriching the overlying mantle wedge in LILE (but not HFSE) which subsequently melts to produce arc magmas. The lower light rare earth element (LREE) and P_2O_5 content of island arc tholeiites compared to island arc calcalkaline basalts may be due to melting of sediments producing the

latter (Hawkesworth and Powell, 1980), though it is interesting to note that HFSE are not enriched suggesting that dehydration processes are still the dominant mechanism. The depletion of HFSE relative to LILE has also been attributed to stabilisation of minor phases (e.g. zircon, sphene, ilmenite and rutile) in the overriding mantle wedge under conditions of high P_{H_2O} (Saunders et al., 1980).

Of particular value in eliminating the effects of fractional crystallization and partial melting is the use of elements which are highly incompatible in the relevant phase assemblages as their interelement ratios are unaltered by these processes (e.g. Wood et al., 1979). Radiogenic isotope studies are important for similar reasons, but additionally they can yield information pertaining to the timing of the events which fractionate parent-daughter elemental ratios (e.g. Rb/Sr, Sm/Nd, U/Pb, Lu/Hf; Hawkesworth and van Calsteren, 1983). Thus, if the isotopic and incompatible trace element characteristics of the various sources are known it may be possible to assess whether one particular domain has been involved in magmagenesis and to constrain the degree of participation. As mentioned earlier, in continental arcs there is the possibility that ascending magmas may be contaminated by the continental crust: it is thus necessary to determine the geochemical and isotopic characteristics of potential local contaminants in order to confirm or otherwise their suitability. The realisation of contamination trends is most successfully performed using combinations of radiogenic and stable isotopes, and fractionation indices (e.g. Taylor, 1980; DePaolo, 1981; Hawkesworth, 1982; Thirlwall and Jones, 1983), and, as emphasised by Hawkesworth et al. (1983), the need is for integrated isotope, major and trace element studies to constrain, as far as possible, conflicting hypotheses.

1.4 The Andes - Previous work

The Andean mountain chain is the type example of subduction of oceanic lithosphere beneath a continental margin with the descent of the oceanic Nazca Plate beneath the western margin of the continental South American Plate. The geology of the Andes has been reviewed by Zeil (1964, 1979), and more specifically the geochemistry by various authors in Harmon and Barreiro (1984) and in Bell (1984). There has been an extensive survey of the coastal batholith and its cover rocks in Peru by Livrpool University (e.g. Cobbing and Pitcher, 1972a, b; Pitcher, 1978; Atherton et al., 1979, 1983; Atherton, 1981; McCourt, 1981): workers at the Carnegie Institute of Washington have studied the geochemistry of Jurassic - Recent lavas in southern Peru (e.g. James et al. 1974, 1975, 1976; Margaritz et al., 1978; James, 1978, 1981a, b, 1982) and the geophysics of the plate interaction (e.g. James 1971a, b; Sacks and Okada, 1974; Sacks et al., 1976). Various aspects of the geology and geophysics of the Nazca Plate are discussed in Kulm et al. (1981).

In northern Chile major geological reviews have been presented by Brueggen (1950), Ruiz et al. (1965) and Garcia (1967). During the 1960's a group from London University studied the Upper Tertiary evolution around San Pedro de Atacama (23°S) paying particular attention to the ignimbrite formations and their ages (e.g. Hollingworth, 1964; Rutland et al., 1965; Hollingworth and Rutland, 1968; Guest, 1969). German workers provided numerous geochemical analyses from northern Chile; they considered that the Recent andesitic stratovolcanoes post-dated the voluminous ignimbrite sheets, and that both were the products of intracrustal melting (e.g. El Hinnawi et al., 1969; Siegers et al., 1969: Pichler and Zeil, 1969, 1972; Zeil and Pichler, 1967).

More recently their investigations have concentrated on the rocks of the Cordillera de la Costa between 26^{o}-27^{o}S. (Zeil et al., 1980; Damm et al., 1981; Berg and Breitkreuz, 1983; Berg et al., 1983). Studies at the Open University over the last decade have primarily concentrated on the Upper Tertiary-Recent volcanic succession (e.g. Francis et al., 1974, 1977, 1978, 1984; Roobol et al., 1976; Thorpe, et al., 1976; Baker, 1977a, b; Baker and Francis, 1978; Hawkesworth et al., 1979a, 1982; O'Callaghan, in prep.), but mineralization has also been studied in Tertiary rocks around the El Salvador porphyry copper deposit (Baldwin and Pearce, 1982). These studies have attempted to elucidate the petrogenesis and geochronology of the ignimbrites and lavas by detailed geochemistry and K-Ar dating: the temporal overlap between the ignimbrites and lavas has also been demonstrated. Further south in Chile, between 26^{o}-27^{o}S, Canadian workers have investigated the evolution of the cordillera using K-Ar geochronology, major and trace element geochemistry, and Sr, Pb and O isotope systematics (Farrar et al., 1970; Quirt, 1972; Clark et al., 1967, 1973, 1976; Zentilli, 1974; McNutt et al., 1975, 1979; Haynes, 1975; McBride et al., 1976; Dostal et al., 1977; Longstaffe et al., 1982). The Chilean Geological Survey - the Servicio Nacional de Geologia y Mineria (formerly the Instituto de Investigaciones Geologicas (I.I.G.)) - has an active program of mapping in the region and several sheets have been produced (Ferraris, 1978; Ferraris and Di Biase, 1978; Maksaev, 1978; Ramirez and Huete, 1981).

1.5 Regional variations in the Andes

The interaction between the South America and Nazca Plates has been investigated seismically by Barazangi and Isacks (1976) and Jordan et

al. (1983) who identified regional segmentation in the dip of the Benioff zone: between latitudes $5^{o}N$-$2^{o}S$ (south Colombia - north Ecuador), 16^{o}-$28^{o}S$ (south Peru - north Chile) and 33^{o}-$46^{o}S$ (south Chile) the Benioff zone dips at about 30^{o} whereas between $2^{o}S$-$15^{o}S$ and 27^{o}-$33^{o}S$ the dip is much shallower ($\sim 10^{o}$). These authors noted that there is a close correspondence between those segments with steeply dipping Benioff zones and regions of Quaternary volcanism, and argued that the presence of a wedge of asthenospheric mantle between the subducting oceanic lithosphere and the continental crust was a prerequisite for volcanic activity (see also Thorpe et al., 1981). Comparative reviews of the geochemistry of these three regions - the northern volcanic zone (NVZ), central volcanic zone (CVZ) and southern volcanic zone (SVZ) - have been given by Thorpe and Francis (1979a, b), Thorpe et al. (1981, 1982), Harmon et al. (1981, 1984) and Thorpe (1984). Additionally Stern et al., (1984) have classified the volcanic centres between 49^{o}-$55^{o}S$ as the Austral volcanic zone (AVZ) (figure 1.1); these are mainly related to a small convergence rate between the Antarctic and South America plates, though the southernmost edifice, Isla Cook, may be related to transcurent tectonics and ridge subduction (Stern et al., 1984; Puig et al., 1984; Rogers et al., in press). The salient points to emerge by comparing the NVZ, CVZ and SVZ are as follows:-

i) The crustal thickness beneath the NVZ is 40 - 50 km (Messiner et al., 1972; Case et al., 1973) and is Palaeozoic - Mesozoic in age (Thorpe et al., 1981; Thorpe, 1984). Beneath the CVZ the crust attains a thickness of 70 km (Draguicevic, 1962; James, 1971a, b) parts of which are Precambrian (Lehmann, 1978; Shackleton et al., 1979; Pacci et al., 1980); the extent of this basement beneath the active cordillera is a matter of conjecture. The SVZ is built upon Palaeozoic -

Mesozoic basement (Hickey et al., 1984) which is 30 - 45 km thick (Lomnitz, 1962; Cummings and Schiller, 1971)

(ii) The lavas from the NVZ are mainly basaltic andesites and andesites (Pichler et al., 1976; Thorpe et al., 1981), whereas those from the SVZ are predominantly basalts and basaltic andesites with minor andesites, dacites and rhyolites (Lopez-Escobar et al., 1977; Hickey et al., 1984). In contrast basic rocks are rare in the CVZ and andesites and dacites dominate (Francis et al., 1974; Roobol et al., 1976; Dostal et al., 1977). Additionally there are voluminous dacitic - rhyolitic ignimbrite sheets.

(iii) Radiogenic and stable isotope characteristics vary between the three zones as summarised in Table 1.1 and Figure 1.5 and reviewed in detail by Harmon et al. (1984). The CVZ is distinguished by having higher $^{87}Sr/^{86}Sr$, lower $^{143}Nd/^{144}Nd$ and higher $\delta^{18}O$. $^{207}Pb/^{204}Pb$ and $^{208}Pb/^{204}Pb$ from the SVZ are slightly lower than the NVZ and CVZ: $^{206}Pb/^{204}Pb$ ratios from northern Chile and NVZ are higher than from the SVZ whereas $^{206}Pb/^{204}Pb$ ratios from southern Peru are very unradiogenic. These very low $^{206}Pb/^{204}Pb$ values are interpreted as being due to contamination by old granulite basement gneisses during magma ascent (Tilton and Barreiro, 1980; James, 1982; Barreiro, 1984; Barreiro and Clark, 1984).

The contrasting $^{87}Sr/^{86}Sr$ ratios between Ecuador and north Chile, and the gross correlation between these and crustal thickness (Figure 1.5) led Francis et al. (1977) to conclude that the higher ratios in Chile were due to crustal contamination of basic magmas with an isotopic signature similar to Ecuador by slow uprise through the thick crust. This view has been repeatedly stressed by Thorpe and Francis (1979a, b); Francis et al. (1980); Harmon et al. (1981, 1984);

Table 1.1 Isotopic characteristics of the NVZ, CVZ and SVZ of the Andes

	NVZ		CVZ		SVZ	
	Colombia	Ecuador	S. Peru	N. Chile, Bolivia, NW Argentina	S. Chile	Refs.
$^{87}Sr/^{86}Sr$	0.7040-0.7048	0.7036-0.7044	0.7054-0.7092	0.7050-0.7149	0.7037-0.7046	1-11
$^{143}Nd/^{144}Nd$	0.51273-0.51285	0.51285-0.51300	0.51199-0.51247	0.51224-0.51257	0.51269-0.51291	4,6,7,10-12
$^{206}Pb/^{204}Pb$	18.95-20.00	18.72-18.99	17.38-18.29	18.63-19.01	18.48-18.59	9,11,13,14
$^{207}Pb/^{204}Pb$	15.55-15.72	15.59-15.68	15.53-15.63	15.61-15.69	15.58-15.62	9,11,13,14
$^{208}Pb/^{204}Pb$	38.55-38.82	38.46-38.91	38.47-38.78	38.52-39.14	38.32-38.51	9,11,13,14
$\delta^{18}O$	6.5-7.8	6.3-7.7	6.8-8.6	7.3-14.0	5.2-6.8	6,8,9,11,15-17

References: (1) James et al. (1976); (2) Francis et al. (1977); (3) Klerk et al. (1977); (4) DePaolo and Wasserburg (1977); (5) Francis et al. (1980); (6) James (1982); (7) Hawkesworth et al. (1982); (8) Deruelle et al. (1983); (9) Harmon et al. (1984); (10) Hickey et al. (1984); (11) James and Murcia (1984); (12) Hawkesworth et al. (1979a); (13) Tilton and Barreiro (1980); (14) Barreiro (1982a); (15) Margaritz et al. (1978); (16) Harmon et al. (1981); (17) Gerlach et al. (1983).

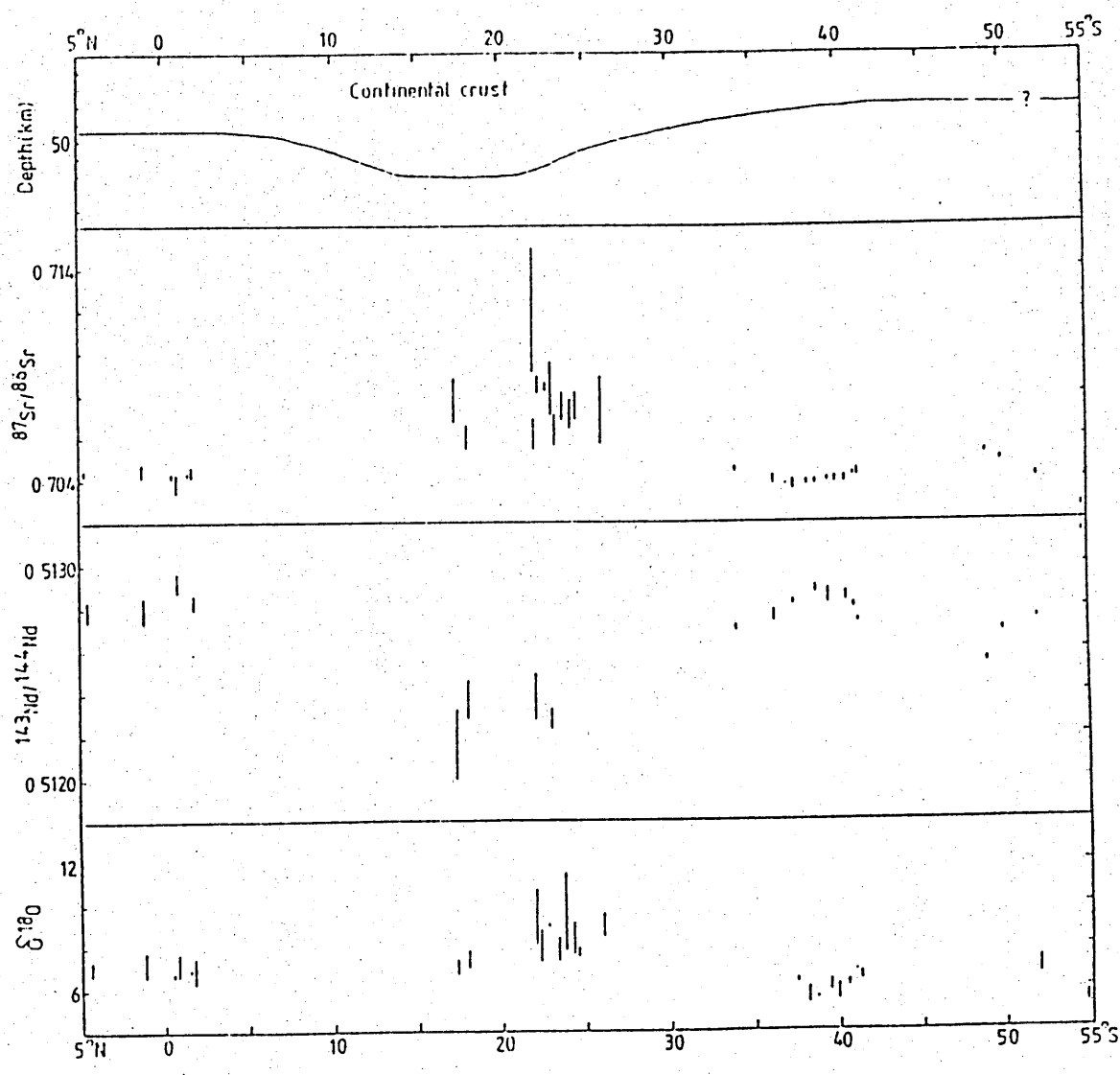

Figure 1.5

Latitudinal variation along the Andes in crustal thickness and the $^{87}Sr/^{86}Sr$, $^{143}Nd/^{144}Nd$ and $\delta^{18}O$ ratios of Recent Volcanics. Data sources as in Table 1.1 except for south of latitude 49°S which are from Stern and Futa (1982) and Stern et al. (1984)

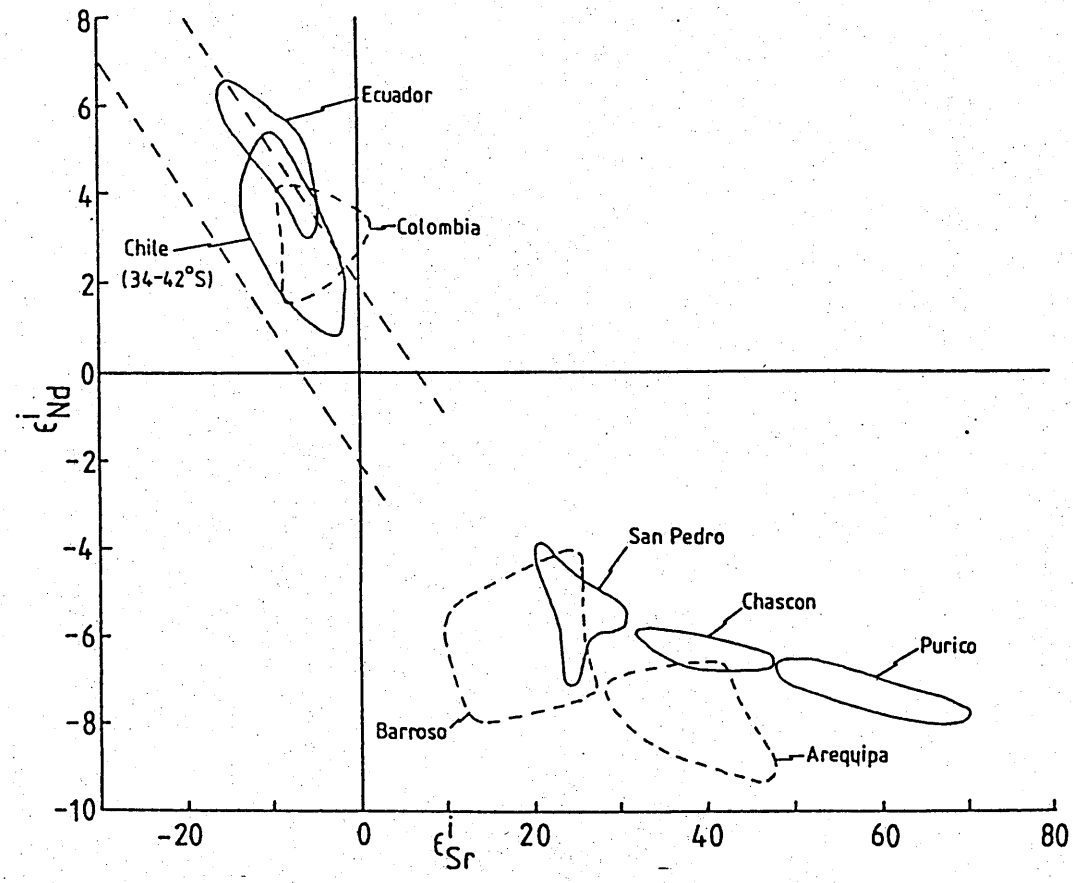

Figure 1.6

ε_{Sr}-ε_{Nd} diagram for Recent Andean rocks from the NVZ (Colombia and Ecuador), CVZ (Arequipa, Barroso, San Pedro, Chascon and Purico) and SVZ (Chile, 34°-42°S). The rocks of the CVZ have much more enriched isotopic signatures than those from the NVZ and SVZ. Data sources; Colombia; James and Murcia (1984): Ecuador; this work: Arequipa and Barroso; James (1982): San Pedro; this work: Purico and Chascon; Hawkesworth et al. (1982): Chile (34°-42°S); Hickey et al. (1984).

Thorpe et al. (1981, 1982, 1984) and Deruelle et al. (1983) who consider that any $^{87}Sr/^{86}Sr$ ratios and $\delta^{18}O$ values above the "normal" mantle values of 0.7040 ± 0.0005 and 6.0 ± 0.5‰ respectively must be contaminated by continental crust en route to the surface. The lower $^{143}Nd/^{144}Nd$ ratios of north Chile compared to Ecuador reported by Hawkesworth et al. (1979a) have also been taken as support for the above opinion (Figure 1.6). Thorpe and Francis (1979b) suggested that the former represent 20% crustal contamination of a mantle-derived melt with an isotopic signature the same as Ecuador. Hawkesworth et al. (1979a), however, argued that these more enriched isotopic characteristics could also be generated from a mantle which had had a time-integrated Rb/Sr and Nd/Sm enrichment relative to "bulk earth". Hawkesworth (1979, 1982) later pointed out that if the rocks were contaminated then the contaminant must be old to explain the low $^{143}Nd/^{144}Nd$ ratios. In southern Peru James (1982) proposed that the parental magmas for the Arequipa and Barroso volcanics had enriched isotopic characteristics but was reluctant to invoke that this was due to the nature of the sub-Andean mantle: instead he favoured lower crustal contamination of a mantle-derived magma (presumably analogous to Ecuador) in the absence of plagioclase to produce this signature. This view, with a notable emphasis on the lower crustal role has been reiterated by James (1984).

Hawkesworth et al. (1982) reported trace element and Sr and Nd isotope data for the Cerro Purico ignimbrite shield volcano in north Chile. They concluded that for evolved centres such as this a petrogenesis involving intracrustal melting was consistent with the data, although some of the observed trends could also have been generated by mixing between crustal and mantle melts.

1.6 Aims of this thesis

In view of the spectacular geochemical and physiographical differences noted above between the CVZ and the other active volcanic zones it was important to study the Mesozoic - Recent rocks of a specific transect across the central Andes to assess how the source regions for magmas have changed with time. In particular the geochemistry of magmatic products of differing ages was investigated in terms of contributions from the continental crust, subcontinental mantle and the subduction zone, which in turn enabled the effects of temporal versus spatial control on the geochemistry to be determined. Geochronological data in the literature for northern Chile are sparse, and so each unit investigated was subjected to a whole-rock Rb-Sr study. Although crustal contamination mechanisms had been proposed for the petrogenesis of San Pedro (Francis et al., 1977) the composition and age of the basement in northern Chile was unknown. Consequently basement rocks were characterised geochemically to place some constraints on models. The transect chosen was at 22°S from Tocopilla on the coast through to Volcan San Pedro in the Western Cordillera (Figures 1.2 and 1.3), as this volcano had been studied by the Open University and vehicular access was possible further west.

The units studied are considered in subsequent chapters in geochronological order, and described in terms of their field relations, petrography, geochronology, geochemistry and petrogenesis. Chapter 8 amalgamates this data and assesses the processes responsible for the spatial and temporal variations across the transect of the cordillera as a whole.

1.7 Methodology

1.7.1 Isotope systematics

It is not the purpose of this study to explain the principles of Sm-Nd isotope systematics; the reader is referred to the papers and reviews by DePaolo and Wasserburg (1976a, b), O'Nions et al. (1979) and Hawkesworth and van Calsteren (1983). A number of the isotopic concepts used herein, however, require quantification as different authors use various values in their calculations. All the data presented and quoted in this study have been normalised to, and calculated using the values in Appendix F.

1.7.2 MORB normalised diagrams

The geochemistry of many rocks analysed in this thesis may be portrayed on a diagram normalised to the mid ocean ridge basalt (MORB) values of Pearce (1982). These diagrams have been used to identify the broad tectonic setting of rocks of unknown affinity by comparing them with samples from known tectonic scenarios. During fractional crystallization the shapes of the patterns for incompatible elements do not change provided that minor phases are not precipitating. Obvious exceptions are Sr and Ti which may not be incompatible and whose values will decrease with increasing fractionation of plagioclase and titanomagnetite respectively. When considering more evolved rocks any fractionation of minor phases can be detected by negative anomalies in the pattern (e.g. a P anomaly in response to apatite fractionation).

Pearce, moreover, has divided those diagrams pertaining to subduction-related rocks into segments which represent the contribution from the subduction zone and from the overriding mantle wedge (Figure 1.7). Using this division he calculated by simple mass balance the

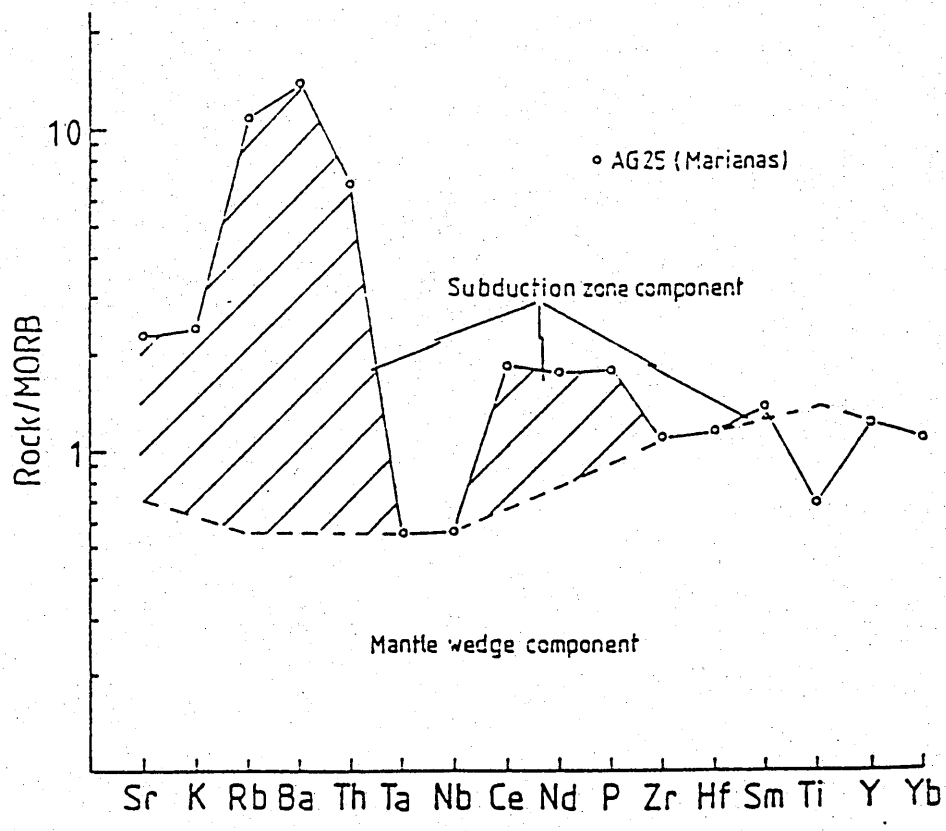

Figure 1.7

MORB normalised diagram (Pearce, 1982) for basaltic andesite, AG25, from the Marianas (Hole et al., 1984) to illustrate the division into the subduction zone components and mantle wedge components.

proportion of any element found in a rock derived from each of the components. When quantifying proportions of the subduction zone component in this study only elements and/or trace element ratios which are little affected by fractional crystallization of likely phases are considered. This in turn precludes Sr as it is often difficult to assess the amount of plagioclase fractionation. The diagrams are also not applicable to rocks which have demonstrably undergone crustal contamination or which have experienced post-consolidation alteration.

1.7.3 Definition of the 'Andean Orogeny'

The Phanerozoic geological history of the central Andes has been traditionally divided into two main orogenic episodes: firstly, up to the end of the Palaeozoic and including the early Triassic; secondly from the late Triassic - Recent. This latter episode has generally been termed the Andean Orogeny (Rutland, 1971; McNutt *et al.*, 1975; Coira *et al.*, 1982) though late Triassic rocks are not present throughout the region. The lower Jurassic marks the widespread initiation of volcanism and plutonism in the present coastal regions of north Chile, the locus of which has subsequently migrated eastwards (Farrar *et al.*, 1970; McNutt *et al.*, 1975) in contrast to the Palaeozoic trend of westwards magmatic migration (McNutt *et al.*, 1975; McBride *et al.*, 1976). Whereas the Andean Orogeny is broadly described in terms of the subduction of oceanic lithosphere beneath the western margin of South America, the tectonic setting of the Palaeozoic is obscure, and may either represent the evolution of an ensialic basin underlain by thinned continental crust (Dalmayrac *et al.*, 1980), or an earlier period of subduction (Coira *et al.*, 1982).

CHAPTER 2

PALAEOZOIC EVOLUTION

2.1 Introduction

Whilst most of the published research in northern Chile has concentrated on the Tertiary and Recent volcanism (e.g. Baker, 1977b; Thorpe et al., 1976; Deruelle, 1982; Hawkesworth et al., 1982), and more sparsely on the Mesozoic evolution (Farrar et al., 1970; McNutt et al., 1975) there has been negligible work on the Palaeozoic basement. McBride et al. (1976) reviewed K-Ar ages between 225 and 450 Ma from western Argentina and Garcia (1967) gave some Pb/α ages (233 - 292 Ma) for the Palaeozoic batholith near Calama. More recently Berg et al. (1983) reported a number of Rb-Sr biotite ages between 199 and 285 Ma for plutons in the Cordillera de la Costa between $25^{o}30'$ and $26^{o}35'$S. Detailed geochemical analyses are absent. Nonetheless it is important to study these older rocks, in order to attempt to characterise potential crustal contaminants which certain authors (e.g. Francis et al., 1977; Harmon et al ., 1984) deem necessary in the Recent volcanics. The rock units are considered in geochronological order commencing with the Limon Verde metamorphics.

2.2 Limon Verde Metamorphics

2.2.1 Field relations and Petrography

On the western margins of the Sierra Limon Verde there is a thin strip of schists about 12 km long and 2 km wide (Harrington, 1961; Baeza, 1976; Figures 2.1, 2.2). To the east they have a faulted contact with the Limon Verde pluton (Section 2.4) although smaller outcrops of the latter to the west of the fault zone do have intrusive relations with the schists. In the west they are unconformably overlain by the Upper Palaeozoic Cerro Crespo Formation, Jurassic marine sediments and the

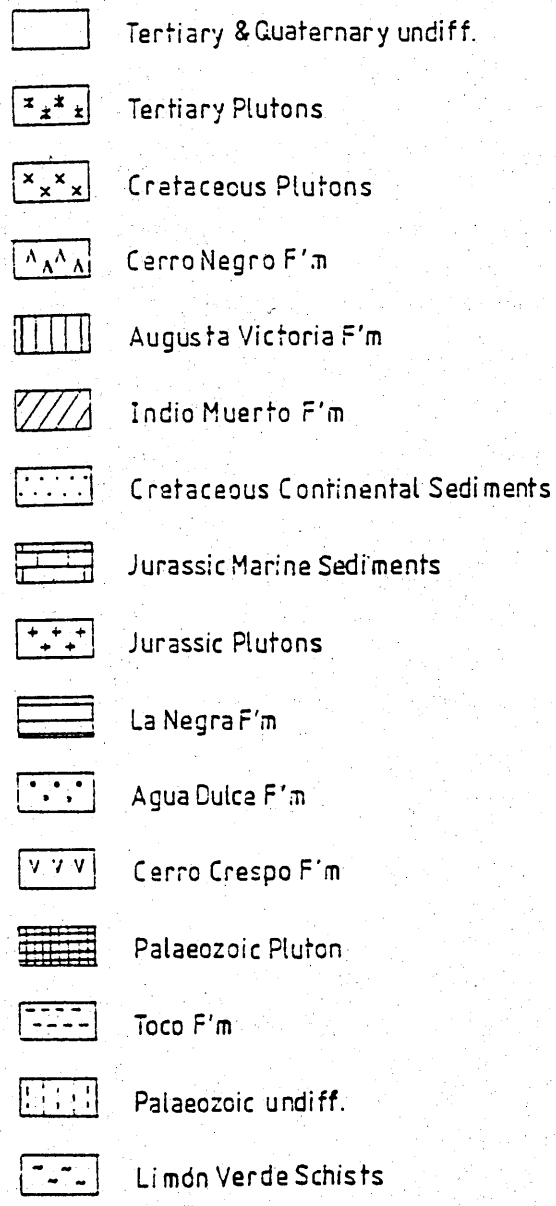
Tertiary & Quaternary undiff.
Tertiary Plutons
Cretaceous Plutons
Cerro Negro F'm
Augusta Victoria F'm
Indio Muerto F'm
Cretaceous Continental Sediments
Jurassic Marine Sediments
Jurassic Plutons
La Negra F'm
Agua Dulce F'm
Cerro Crespo F'm
Palaeozoic Pluton
Toco F'm
Palaeozoic undiff.
Limón Verde Schists

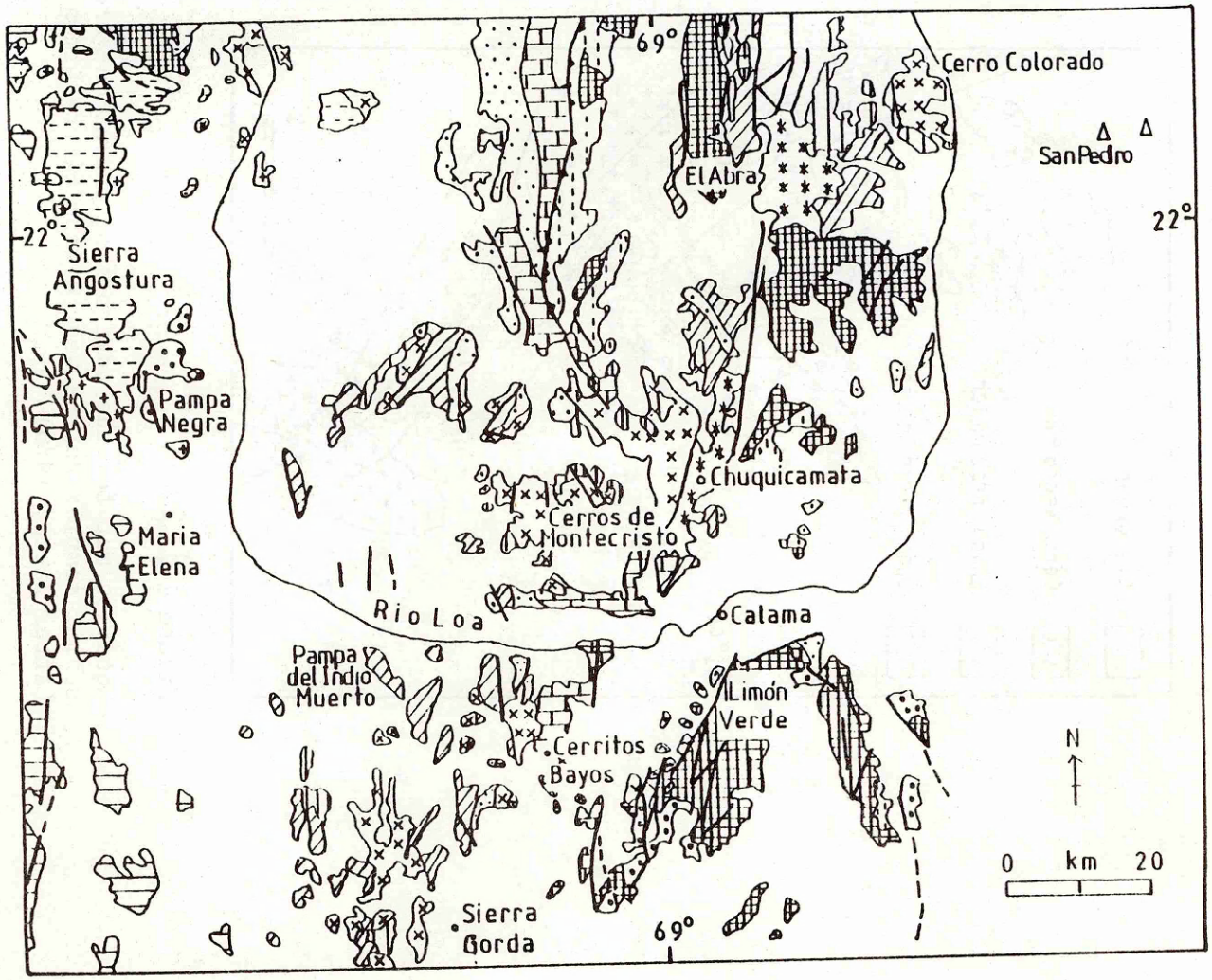

Figure 2.1

Generalised geological map showing the locations of Palaeozoic rocks studied in this work (after Servicio Nacional de Geologia y Mineria, 1980). Key on facing page.

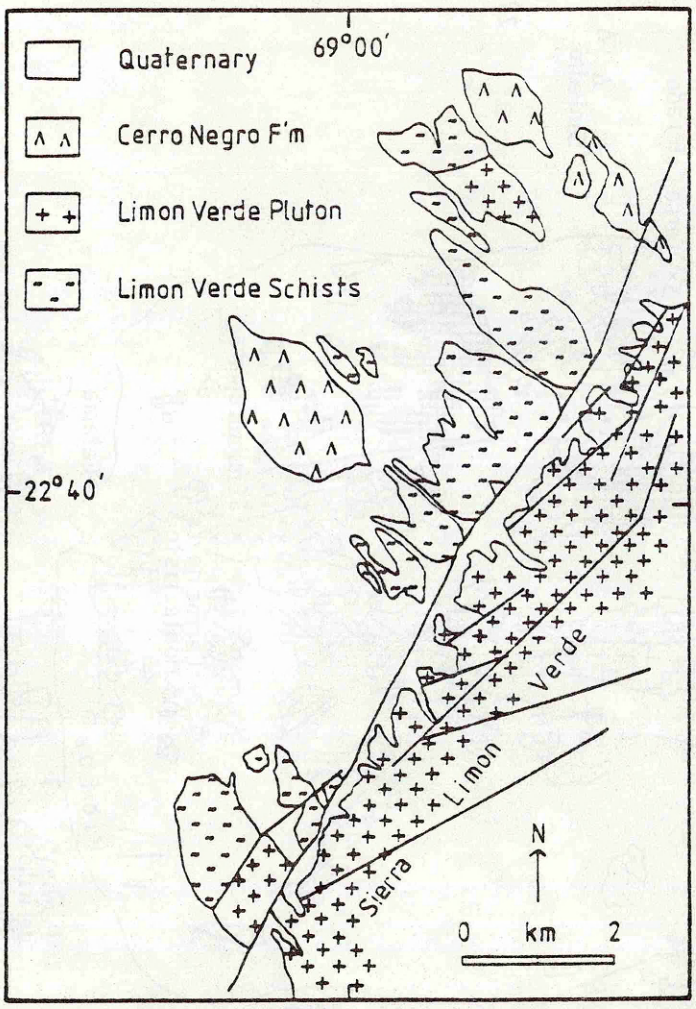

Figure 2.2

Location map for the outcrops of the Limon Verde schist complex to the west of the Sierra Limon Verde. (After Baeza, 1976)

Cretaceous Cerro Negro Formation (Sections 2.5, 5.2 and 5.6). All outcrops are highly weathered with more massive exposures being at a premium. Several interbedded facies are found.

i) Garnet amphibolites consisting of an assemblage of almandine-rich garnet, hornblende, quartz, albite, sphene, apatite, rutile, Fe-Ti oxides and zircon. The garnets form large poikiloblasts with inclusions of apatite, albite, quartz and sphene. Generally, the fabric defined by the long axes of the sphene rhombs cuts across the garnets imparting a helicitic texture and suggesting that the poikiloblasts were syn-tectonic (Plate 2.2a). This is supported by sparse evidence of garnet rotation. However, occasionally sphene wraps around garnet implying that the latter is pre-tectonic in some instances. Some of the garnets have been partially retrogressed to chlorite. Sphene is usually an abundant phase in these rocks portraying its characteristic rhomboid habit; it is sometimes poikiloblastic with inclusions of rutile and apatite. Hornblende has a decussate texture, its growth after garnet being evidenced by its more intense green colour at the contact of the two minerals. The long axes of these prismatic crystals are coincident with those of sphene. Apatite occurs as xenoblasts which occasionally form chains parallel to the rock lineation. Quartz and albite are scarce and have an intergranular habit (Plate 2.1a, b).

ii) Garnet-biotite amphibolites with an assemblage of garnet, biotite, actinolite, quartz, chlorite and minor albite, apatite, muscovite and rutile. The garnets are porphyroblasts and are frequently completely retrogressed to a colourless, low birefringent chlorite. Actinolite has a granoblastic texture with the long axes of prismatic crystals defining a weak lineation. Biotite flakes impart a foliation to

a.

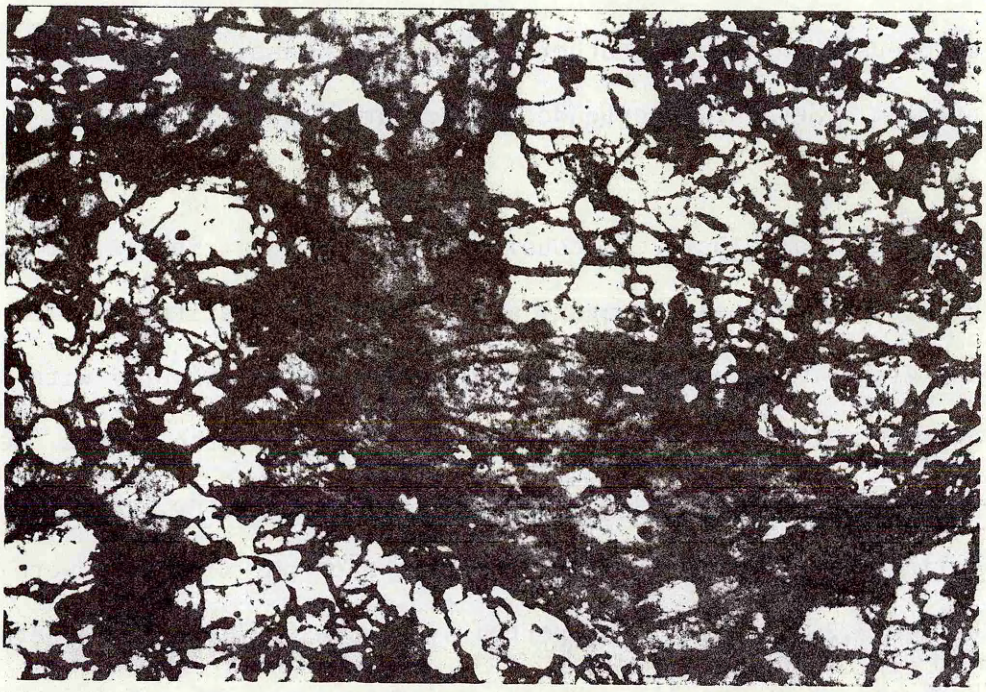

b.

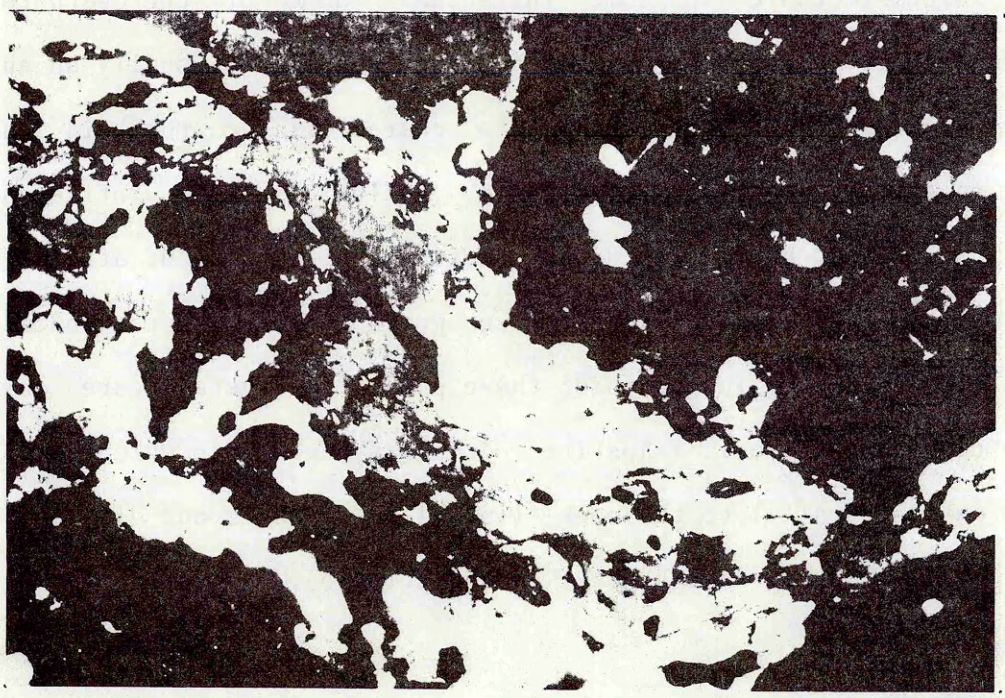

Plate 2.1a. Garnet amphibolite (81010) containing garnet poikiloblasts (pale brown), hornblende (green/brown), rutile (dark brown), quartz (colourless), apatite (colourless - top right) and zircon (brown - included into hornblende). PPL. Field of view = 5.3 mm.

Plate 2.1b. Garnet amphibolite (81010). As above but with XP. Field of view: 5.3 mm.

a.

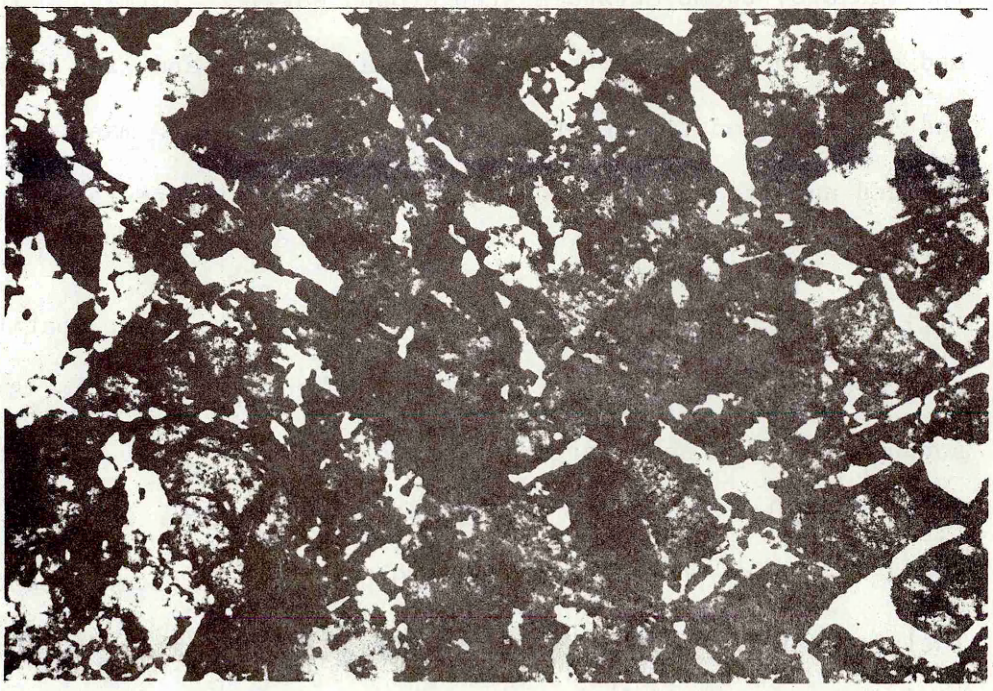

b.

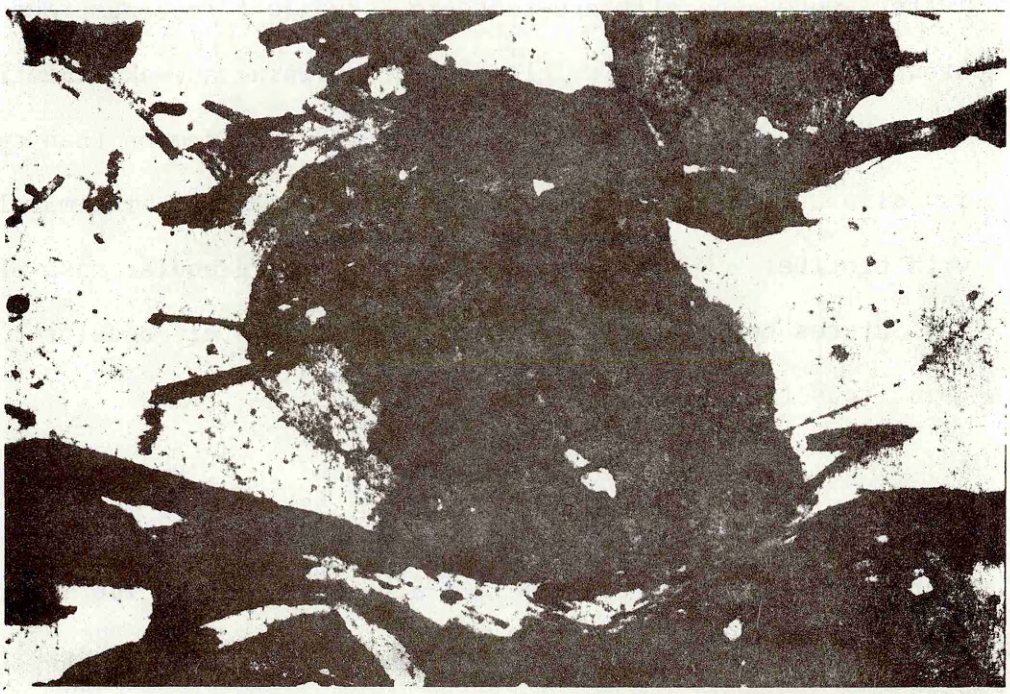

Plate 2.2a. Garnet amphibolite (81150). Rhombs of sphene (dark brown) in fragmented garnet (pale brown). Some of the garnet has been retrogressed to chlorite (pale green).
PPL. Field of view = 3.47 mm.

Plate 2.2b. Snowball garnet (grey) in garnet-quartz-biotite-rutile schist (81151). Sigmoidal trails within the garnet are delineated by whisps of oxide and quartz (colourless). Biotite (orange) contains inclusions of rutile (very dark brown) and zircon (dark brown).
PPL. Field of view = 5.3 mm.

the schists; these crystals wrap around earlier formed actinolite, albite and quartz pods. Apatite and rutile are small and xenoblastic. Quartz and albite constitute the small intergranular mass, the former fine grained and occasionally aggregating into erosion resistant pods.

iii) Garnet-quartz-biotite-rutile schists with minor apatite and zircon, and rare muscovite and Fe-Ti oxides. The garnet forms small, grey porphyroblasts, and larger poikiloblasts. A snowball texture may be present with sigmoidal trails delineated by quartz crystals and fine whisps of oxide (Plate 2.2.b). Other poikilitically enclosed phases include apatite, biotite and rutile. The foliation of these schists is defined by biotite flakes which wrap around the garnets implying that the latter were generally pre-tectonic. Rutile forms numerous small, dark brown xenoblasts, their elongation defining a weak lineation direction. Apatite, too, is xenoblastic, though is less common than rutile. Zircon is also a relatively abundant phase, often being intimately associated with biotite. Quartz forms the main intergranular mass of these rocks, the sutures between grains being highly lobate; undulose extinction is ubiquitous (Plate 2.3).

iv) Amphibolites These are almost monomineralic rocks composed of granoblastic actinolite sometimes altered to talc. The accompanying phase assemblages, however, vary slightly. In some rocks clinozoisite occurs as prismatic crystals, and occasionally segregates into distinct layers less than 0.5 mm thick. Rare accessory phases are quartz and sphene or rutile.

v) Garnet-quartz-muscovite schists with minor apatite and rutile. The garnet of these schists has two habits. The first forms large poikiloblasts, frequently fragmented, with inclusions of

a.

b.

Plate 2.3a. Garnet-quartz-biotite-rutile schist (81011) containing garnet porphyroblasts (pale brown), biotite (orange), rutile (very dark brown) and apatite (light grey) set in a quartz groundmass (colourless).
PPL. Field of view 3.47 mm.

Plate 2.3b. As above, but note the lobate sutures between quartz grains.
XP. Field of view = 3.47 mm.

a.

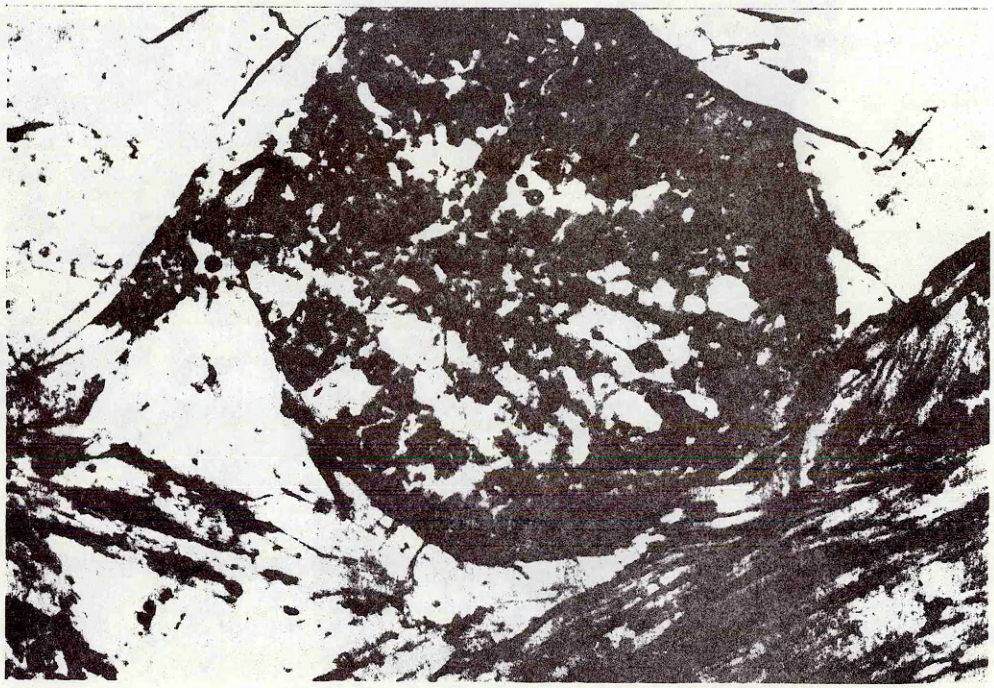

b.

Plate 2.4a. Syntectonic rotated garnet poikiloblast (pale brown) in garnet-quartz-muscovite schist (80214). PPL. Field of view = 5.3 mm.

Plate 2.4b. Pretectonic garnet in 80214 enshrounded by muscovite and set in a groundmass of quartz (white-grey). XP. Field of view = 3.47 mm.

quartz and apatite. Syn-tectonic rotation is exhibited by some (Plate 2.4a) whereas others are enshrouded by muscovite, characteristic of a pre-tectonic origin (Plate 2.4b). The second habit is as small porphyroblasts set within the quartz groundmass, devoid of inclusions and not fragmented; these are later than the poikiloblasts, but still syn-tectonic. Muscovite occurs as large flakes, imparting a strong foliation. This foliation has acted as the plane for migration of iron-rich fluids which have deposited haematite within cracks in the larger garnet and around the mica crystals. Fine - coarse grained quartz with undulose extinction constitutes the groundmass of these schists. It also forms resilient rods around which the micas are bent, implying an early tectonic growth. Rutile and apatite are both xenoblastic, but rare.

The original stratigraphy was of intercalated basic titaniferous volcanics and quartz rich sediments; the relatively high rutile content of the metasediments suggests they may have been in part derived from the associated basalts. The observed assemblages indicate the moderate pressures and temperatures of lower-middle amphibolite grades of metamorphism: there is no evidence of their ever having been in either eclogite or granulite facies. Baeza (1976), however, has described glaucophane schists from this area, though none was found in the present study.

Glaucophane and lawsonite schists occur further south in Chile. At Aguade de la Perdiz ($23^{o}30'S$, $67^{o}30'W$) Garcia *et al.* (1962) described a thick sequence of fossiliferous Ordovician quartzites in which Baeza and Palacios (1977) later claimed to have found blueschists. The latter authors also found similar metamorphic assemblages at $24^{o}37'S$, $68^{o}38'W$ in a sequence of marine

Ordovician quartzites and quartzo-feldspathic arenites described by Cecioni and Frutos (1973). There are metamorphic rocks south of 29°S in the Cordillera de la Costa. Between 32°-36°S they have been divided into two series, the Western and Eastern, by Aguirre et al. (1972). The Western Series contains mica schists, blueschists, greenschists and some serpentinized ultramafics; they have been interpreted as being the product of moderately high P/T conditions of metamorphism. The greenschists and amphibolites of the Eastern Series represent lower P/T gradients, and constitute meta shales and greywackes with occasional calc-silicates. Between Arauco and Valdivia (37°-40°S) Frutos and Tobar (1973) reported Ordovician - Devonian blueschists and serpentinites - a continuation of the Western Series. Amphibolite schists are also found to the south of Antofagasta; these have been equated with the Eastern Series. In the Sierra del Medio micaceous schists, gneisses, and quartzites have been described by Vergara (1978) (Choja Formation), and Maksaev (1978) (Challo Formation) which exhibit metamorphic grades of greenschist and amphibolite facies. These rocks form a thin zone striking roughly north-south, and it seems likely that they are a continuation of the Limon Verde schists. In the Puna of northwest Argentina there are also slates and schists of greenschist-amphibolite facies (Coira et al., 1982); it is uncertain whether these are contiguous with the similar rocks found in Chile.

2.2.2 Geochronology and isotope geochemistry

Four schists from the Limon Verde metamorphic complex (two metavolcanic and two metasedimentary) define a Rb-Sr errochron of 251±50 Ma with an initial $^{87}Sr/^{86}Sr$ ratio of 0.707±4 (ε^{i}_{Sr} = +30.2, Figure 2.3). This date agrees closely with the Rb-Sr age of 266±42 Ma for the Limon Verde pluton which intrudes the

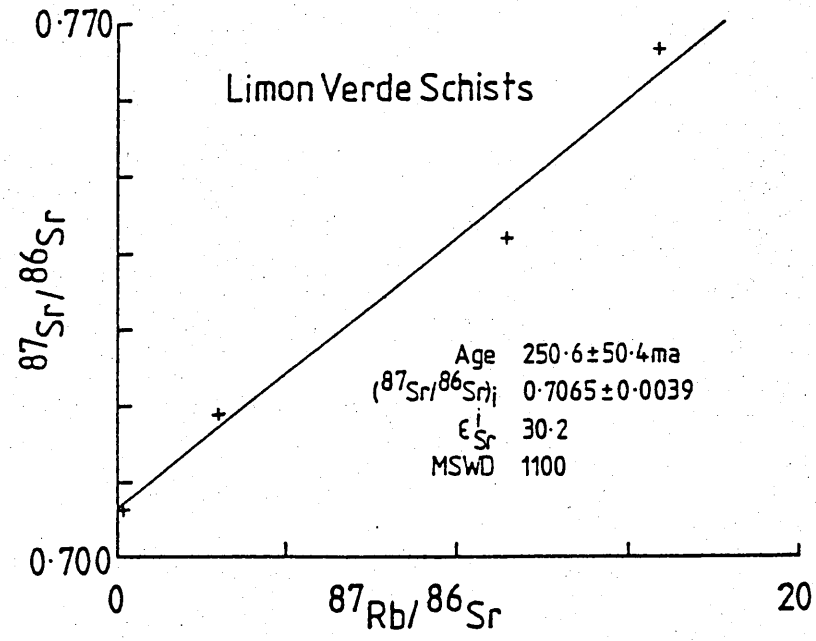

Figure 2.3

Rb-Sr whole rock isochron diagram for the Limon Verde schists.

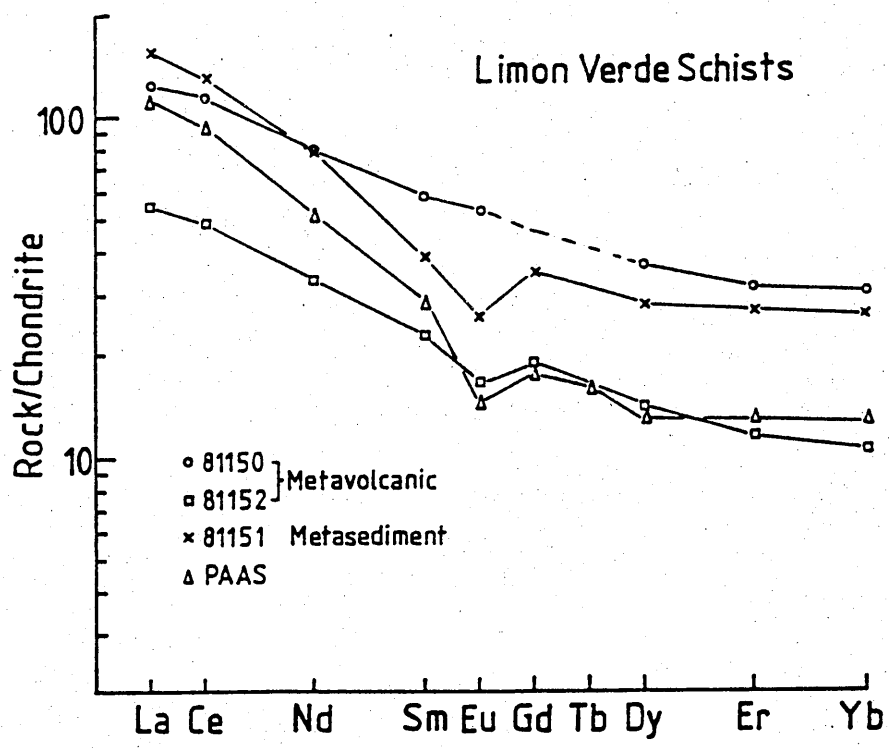

Figure 2.4

Chondrite normalised REE plot for the Limon Verde schists. The Post Archaean Australian Shale (PAAS) of McLennan and Taylor (1981) is shown for comparison.

schists (Section 2.4). It is therefore suggested that the Rb-Sr systematics of the schists were reset during this Permian intrusive episode though complete isotopic homogenization was not achieved, as shown by the considerable scatter of the data (ε^{i}_{Sr} = -45 to +82). A schist from the nearby Sierra del Medio has given a K-Ar age of 292±17 Ma (Huete et al., 1977), but this is interpreted as having been reset by the intrusion of plutons between 318 - 287 Ma.

ε_{Nd} at 251 Ma range from +1.67 to -6.63, with the metavolcanic samples having higher values (ε^{251}_{Nd} +1.67 and -1.01) than the metasedimentary rocks (ε^{251}_{Nd} = -4.38 and -6.63). T^{Nd}_{DM} ages for the former are 913 and 1073 Ma while for the latter they are 1212 and 1308 Ma, thus indicating the presence of Precambrian basement on the western flanks of the Andes in northern Chile.

2.2.3 Geochemistry

Major and trace elements analyses for the schists are presented in Appendix D. REE plots are shown in Figure 2.4. The two metavolcanics (81150 and 81152) have LREE enriched profiles with $(Ce/Yb)_N$ = 3.8 - 4.6; 81152 has a negative Eu anomaly - Eu/Eu* = 0.79. Sample 81151 - a metasediment - has a similar profile to the lavas with LREE enrichment ($(Ce/Yb)_N$ = 5.0) and flattish HREE, but it has more fractionated LREE with $(Ce/Sm)_N$ = 3.4 compared to 2.0 - 2.1 for the lavas. It has a similar overall shape to the Post Archaean Australian Shale (PAAS) of McLennan and Taylor (1981).

Whilst the geochemistry of the alkalis may have been modified by the intrusion of the Limon Verde pluton, the HFSE should be unaffected. It is interesting to note, therefore, the extremely high Nb concentration

of 81150 (266 ppm) which is borne out petrographically by the abundance of sphene. (This sample was analysed at both Nottingham and the Open University, giving similar results from both laboratories). The origin of the Nb spike is unknown. Nonetheless even in 81152 the Zr/Nb and Ce/Nb ratios are low (7.0 and 2.0) and are comparable to those of intraplate alkali basalts (Clague and Frey, 1982). The original tectonic setting of these lavas however remains obscure.

2.3 Toco Formation

In the area immediately to the west of the Pan American highway and north of the Tocopilla-Chuquicamata road a series of hills rise out of the Pampa Negra, the western margin of the Pampa del Tamarugal; these are the Sierra de la Cruz and the Sierra Angostura (Figure 2.1). The latter is composed entirely of clastic sediments, whereas the former has a rim of similar sediments but a core of Mesozoic granitoid. The sediments were originally described by Wetzel (1927), and later by Hoffstetter et al. (1957) who proposed the name "Palaeozoico de El Toco": Harrington (1961) modified this by using the name "Toco Formation". The formation is probably about 1000 m thick and consists of grey-green, massive, fine-grained, quartzose sandstones intercalated with fissile shales and coarser micaceous sandstones. Occasional conglomeratic lenses may be found. In the Sierra de la Cruz where the sediments have been later intruded, hornfelsing has occurred. The formation has been strongly folded with fold axes running approximately ESE, and is cut by dykes trending NNW (Harrington, 1961). (These same dykes also cut the later intrusión in the Sierra de la Cruz (Section 4.2.4)).

The age of these rocks is problematical as they are unfossiliferous. Wetzel, however, discovered several fragments of

silicified wood which were identified as Dadoxylon sp., indicative of the Upper Palaeozoic. This general age is supported on several grounds. Firstly, the folding directions are very much at variance with those of the Mesozoic and Cenozoic evolution of northern Chile which are essentially north-south: the degree of deformation is also much stronger than in any later units. Secondly, the intrusion in the Sierra de la Cruz has been dated as middle Jurassic (Section 4.3), thus giving a minimum age for the sediments. Thirdly, Frutos (1976) indicates that the unit is overlain disconformably by the Triassic Agua Dulce Formation. Thus the Toco Formation belongs to the pre-Andean evolution of western South America and is probably of Upper Palaeozoic age.

2.4 Limon Verde Pluton

2.4.1 Field relations and petrography

The Sierra Limon Verde forms an elongate range of hills running NNE-SSW between Calama and Sierra Gorda. They form the southward continuation of the Sierra del Medio, the intervening area having been breached by the Rio Loa (Figure 2.1). On its western flanks the range is steeply dissected by quebradas which pass out into the braided stream deposits and fanglomerates of the gently tilted Pampa Limon Verde, after crossing the major north-south fault zone which forms the western margin of these hills. The eastern flanks are much gentler and fall into pampa which lead to the northern limits of Cordillera Domeyko 45 km to the east.

The main mass of the Sierra Limon Verde is a Palaeozoic pluton composed of granodiorites and granites (Figure 2.5). In the west it intrudes the metamorphic complex though most of the contact is faulted: the Cerro Crespo Formation (Section 2.5) and the Jurassic marine strata (Section 5.2) overlie the pluton. In the east heat from the intrusion has

hornfelsed a sequence of arenites of presumed lower Palaeozoic age. (These rocks may be of the same age as the Toco Formation (Section 2.3)). Overlying the pluton on this flank are Triassic lavas and tuffs and the Jurassic Moctezuma and Limon Verde Formations (Harrington, 1961) consisting of some 400 m of marine limestones of Liassic-Bajocian age.

The intrusion has been briefly described by Baeza (1976). It is generally equigranular and medium-coarse grained. On the faulted western margins a local foliation defined by felsic and mafic segregations is developed in response to shearing during intrusion. Mineralogically it is more evolved than any of the later plutons of the Andean orogen at this latitude. Plagioclase of oligoclase composition is a ubiquitous early crystallizing phase. The crystals, which are generally fresh, rarely exhibit zoning. Orthoclase, initially interstitial, has a more euhedral habit in the evolved granodiorites and granites. Perthitic textures and interstitial microcline are increasingly developed as fractionation proceeds (Plates 2.5a, b). Quartz, too, is early crystallizing in the majority of these rocks forming large crystals. In the acidic members it becomes the most voluminous phase, and rare granophyric and myrmekitic textures are produced. The mafic content of the pluton varies considerably with values of M' (Strekheisen, 1976) ranging from 43.9 in the most basic to 3.9 in the most acidic. Hornblende, occasionally exhibiting a bluish hue, is euhedral-subhedral almost throughout, being interstitial in the most basic and acidic members. A little marginal alteration to epidote is apparent in a few samples. Biotite, too, is interstitial at first, but soon attains a platey more euhedral habit. It is inclined to form clots which sometimes alter at the margins to chlorite. Sphene is also present in small quantities as euhedral rhombs. The modal proportions of all these mafic minerals tend to decrease with

a.

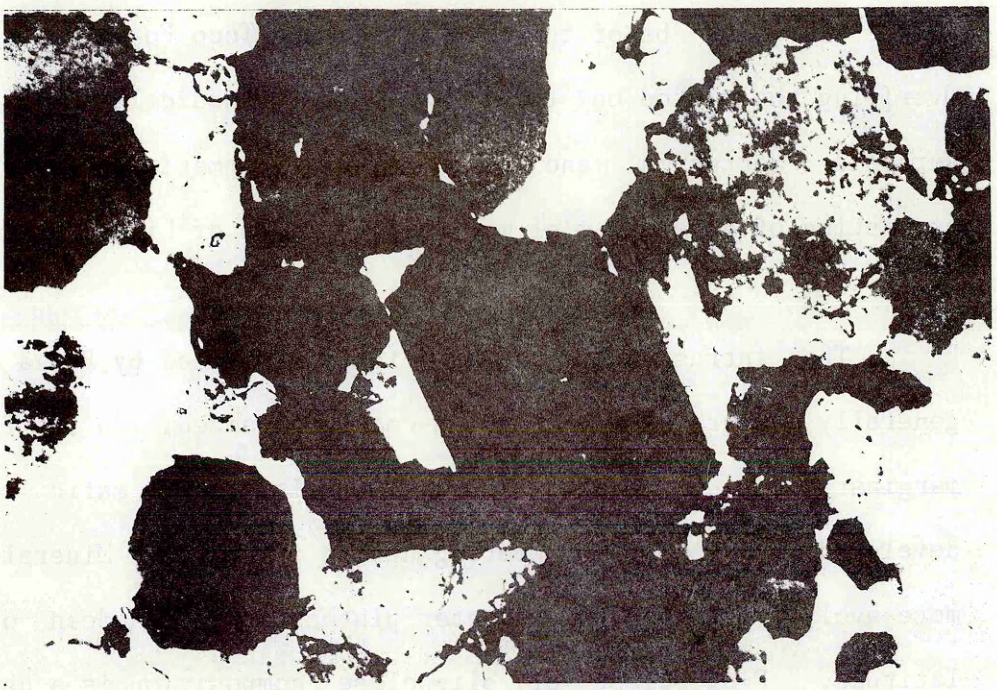

b.

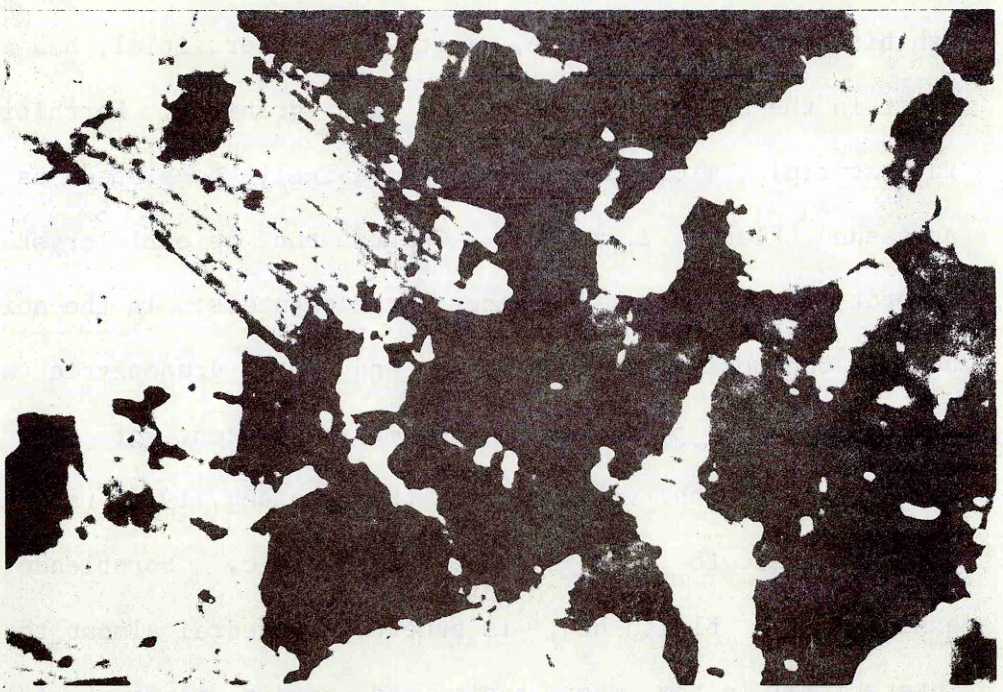

Plate 2.5a. Euhedral perthite (centre) in granite (81119). Other euhedral crystals are mainly potassium feldspar with interstitial quartz and microcline.
XP. Field of view = 3.47 mm.

Plate 2.5b. Interstitial microcline in granite (81119).
XP. Field of view = 3.47 mm.

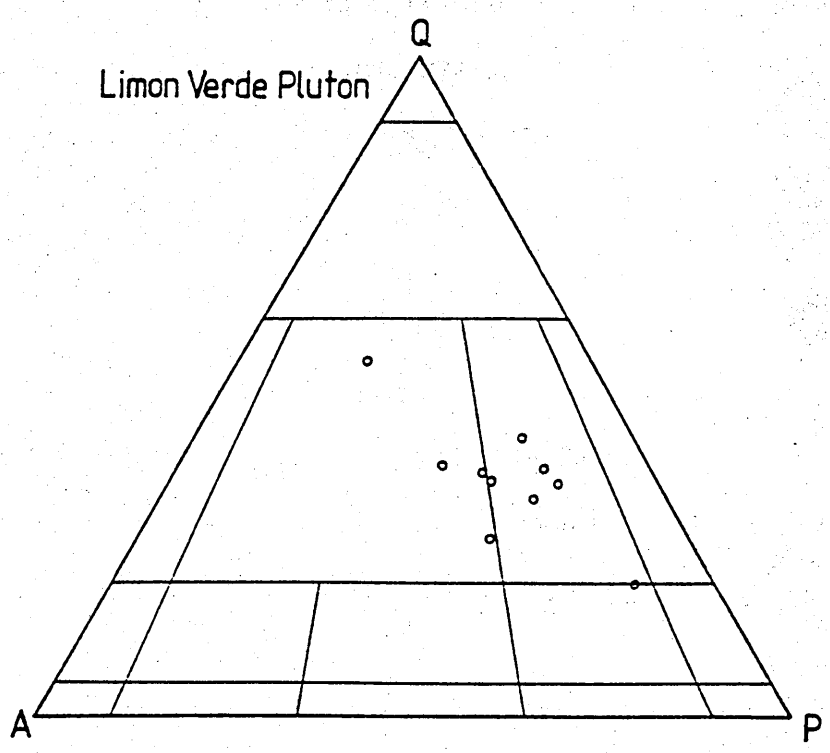

Figure 2.5

Modal QAP diagram for the Limon Verde pluton.

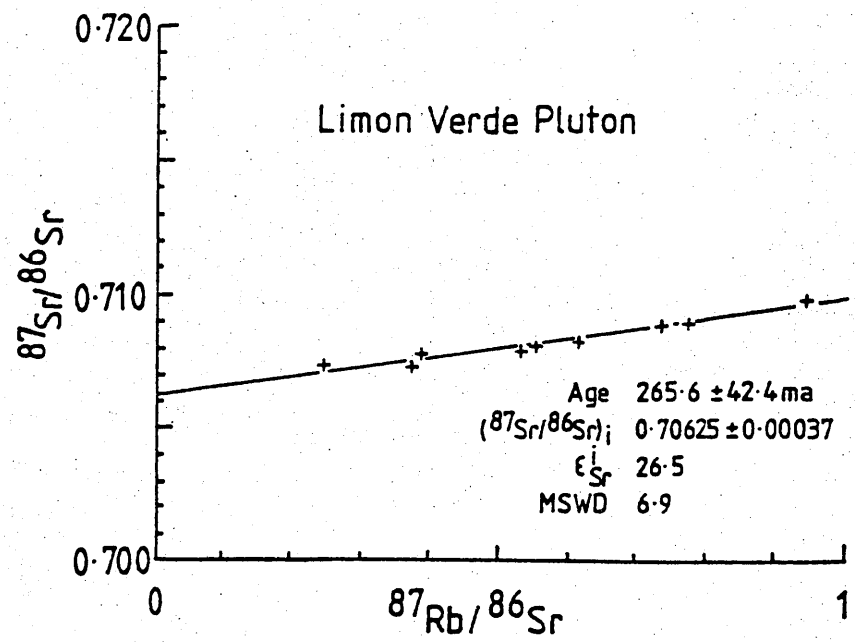

Figure 2.6

Rb-Sr whole rock isochron diagram for the Limon Verde pluton.

fractionation, that of hornblende dramatically. Fe-Ti oxides are usually small and early crystallizing. Minor phases include ubiquitous apatite (often found as euhedral inclusions in sphene, biotite and hornblende), sporadic zircon, and rare allanite.

2.4.2 Geochronology

Nine samples from the Limon Verde pluton yield a Rb-Sr whole rock errorchron of 266±42 Ma with an initial $^{87}Sr/^{86}Sr$ of 0.7062 ± 4 (ε^{i}_{Sr} = +26.5) (Figure 2.6). This is consistent with the Pb/α date of 260 ± 30 Ma reported by Garcia (1967) for the same pluton, and with K-Ar ages of 260 - 272 Ma from the Sierra Moreno (Huete et al., 1977). Further south similar ages have been reported by Farrar et al. (1970), Quirt (1972), Zentilli (1974) and Sepulveda and Naranjo (1982) in Chile, and by Caminos et al. (1982) and McBride et al. (1976) from Argentina. The plethora of coincident ages over such wide areas attests to the regional importance of this intrusive event.

2.4.3 Geochemistry

Harker variation diagrams for the Limon Verde pluton are given in Figure 2.7, and reinforce the petrographic evidence for fractionation governed by plagioclase + hornblende + apatite + Fe-Ti oxides ± orthoclase ± biotite. On an AFM diagram (Figure 2.8) the pluton displays a calcalkaline trend. Of most importance is the behaviour of Y which decreases continuously with fractionation suggestive of hornblende control (Frey et al., 1978a), whereas in the Mesozoic plutons contrary trends are displayed (Figure 2.9) as clinopyroxene is the dominant mafic phase (Chapters 4 and 6). This in turn implies that the parental magma of the Limon Verde pluton was wetter than those of the later intrusions. The scatter in the data for Hf and Zr, and for Ta probably reflects varying

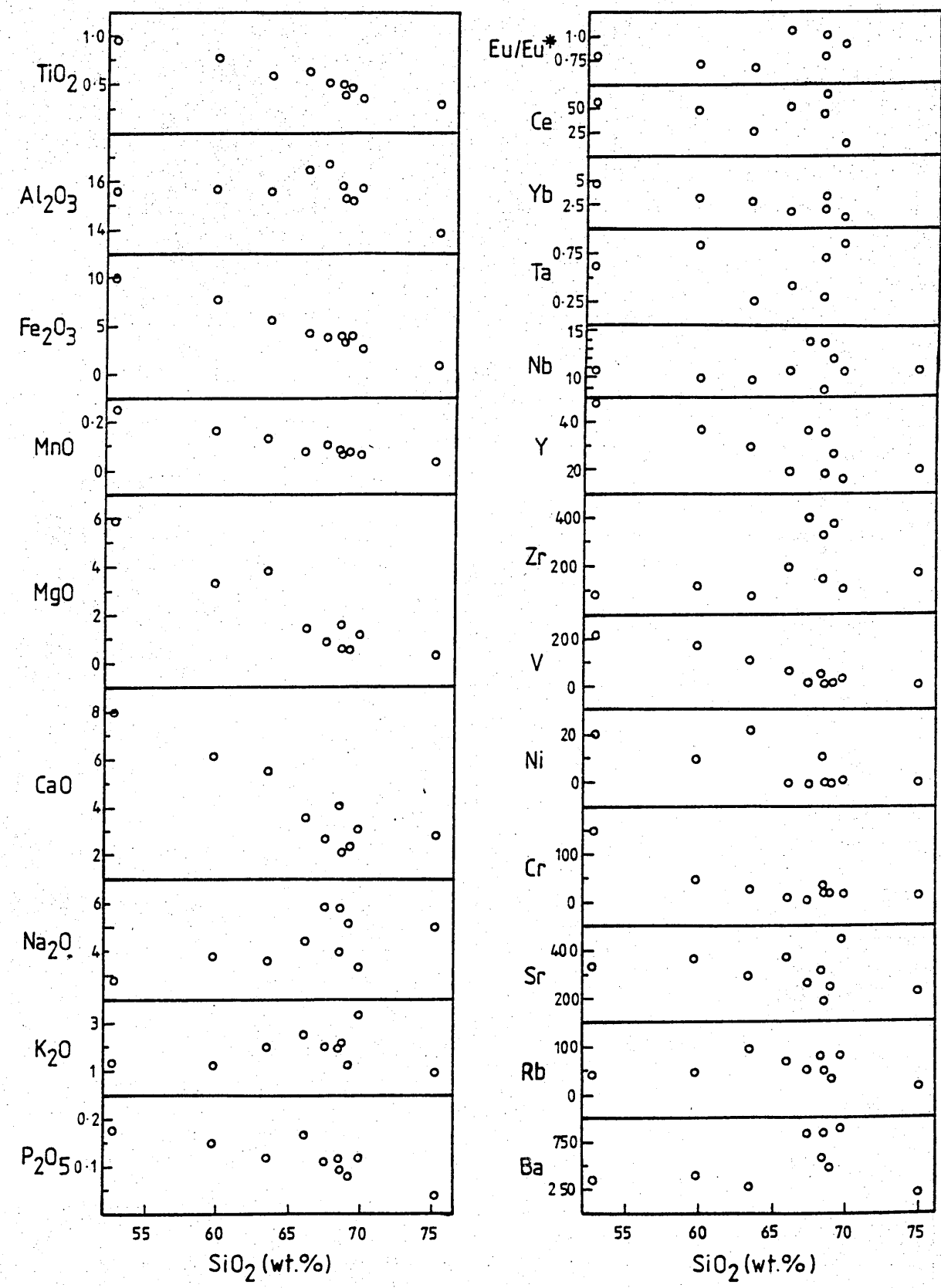

Figure 2.7

Harker variation diagram for the Limon Verde pluton.

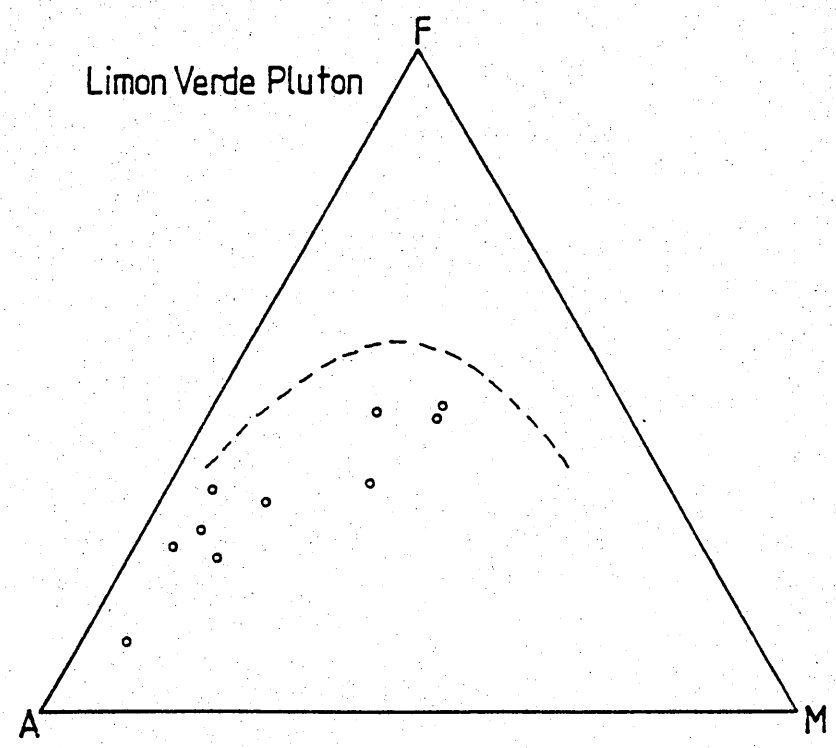

Figure 2.8

AFM diagram for the Limon Verde pluton

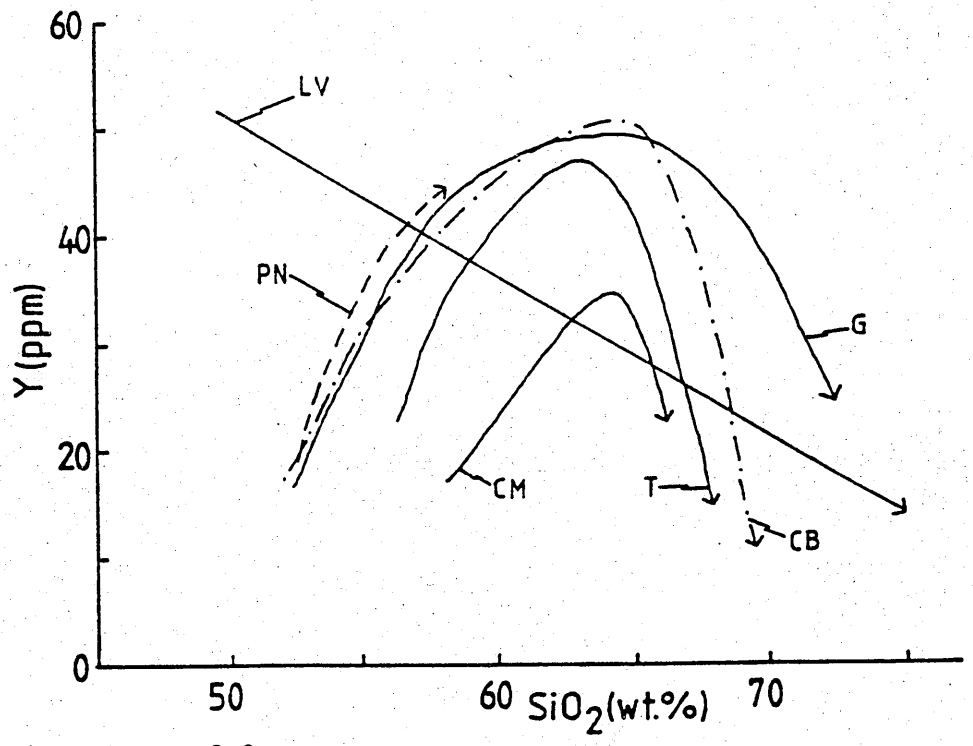

Figure 2.9

Y-SiO_2 plot for plutonic rocks investigated in this study. Note the differing behaviour of the Limon Verde pluton compared to that of the other intrusions. Key to intrusions: LV = Limon Verde: G = Gatico (Jurassic): T = Tocopilla (Jurassic): CM = Cerros de Montecristo (Cretaceous): CB = Cerritos Bayos (Cretaceous): PN = Pampa Negra (Cretaceous).

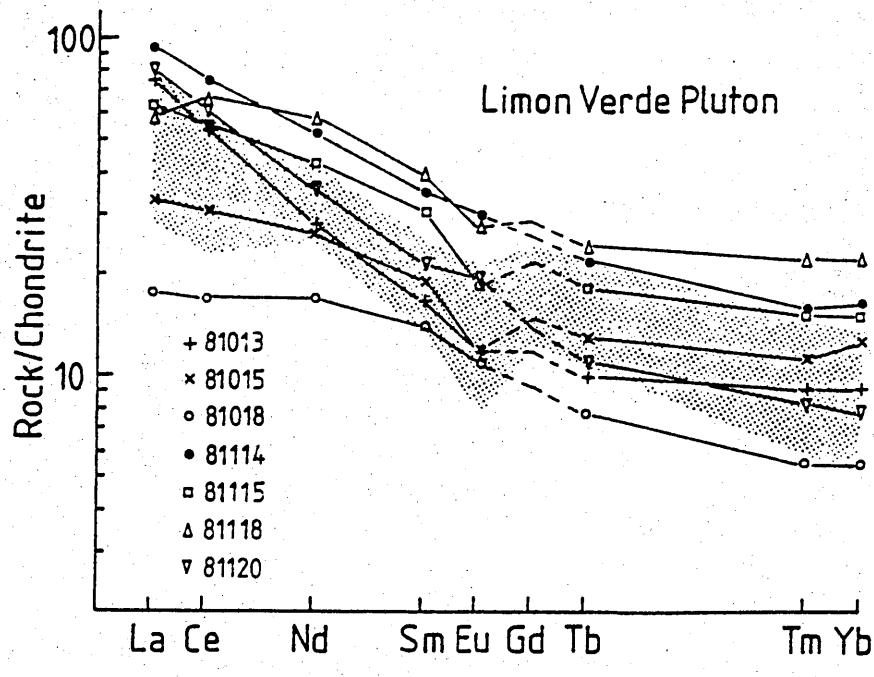

Figure 2.10

Chondrite normalised REE plot for the Limon Verde pluton. The shaded area represents the range for Chilean Palaeozoic granitoids studied by Lopez-Escobar et al. (1979).

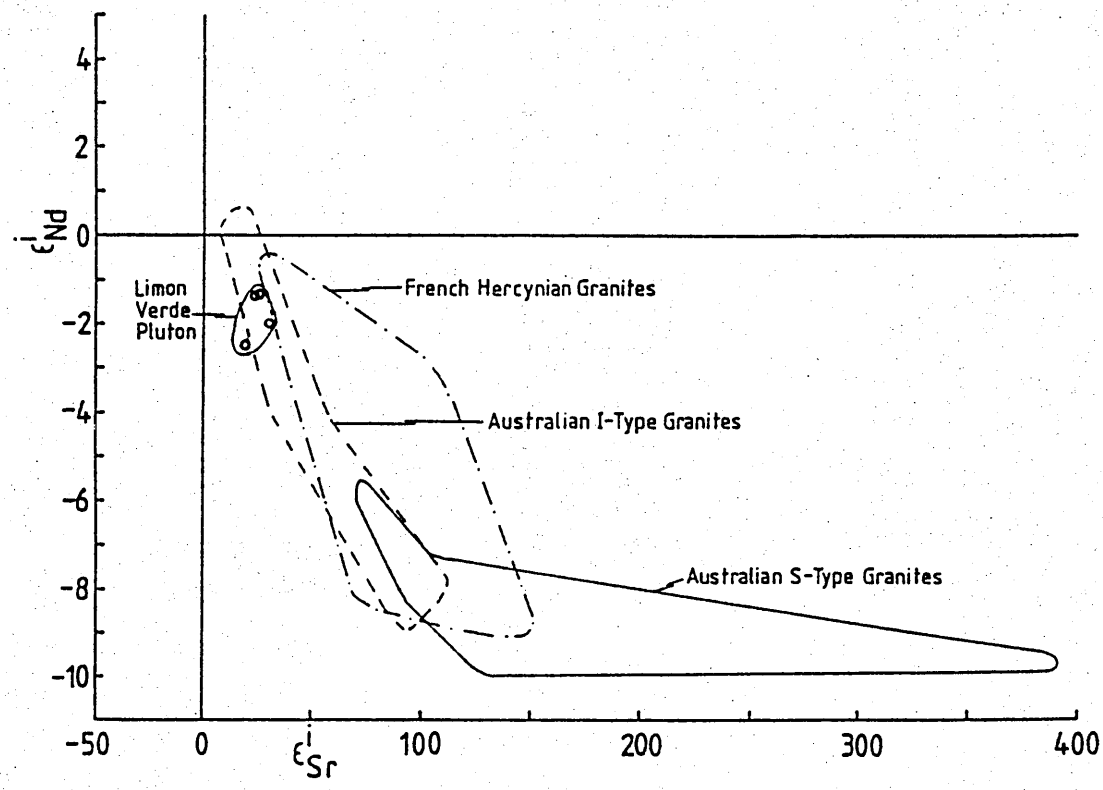

Figure 2.11

ε^i_{Sr} - ε^i_{Nd} diagram for the Limon Verde pluton in comparison to other Phanerozoic granitoids. Data sources: Australia; (McCulloch and Chappell, 1982): French Hercynian granites; (Allegre and Ben Othman, 1980).

degrees of accumulation of zircon and sphene. Ce also has a negative correlation with SiO_2 which is likely to be the result of sphene ± allanite fractionation; sphene is present in all facies of the pluton and allanite was observed in 81117. Moreover, Tindle (1982) has shown that the influence of only trace amounts of these minerals can account for substantial variations in REE contents, and thus they may not necessarily be present in any one thin section.

Chondrite normalised REE plots are presented in Figure 2.10. The rocks are all LREE enriched with $(Ce/Yb)_N$ = 2.4 - 7.7; Ce_N varies from 16.8 - 74.7 and Yb_N from 5.7 - 22.1. Eu/Eu* ranges from 0.68 - 1.07, though as shown in Figure 2.7 this is not related to fractionation in a simple manner; it appears that the Eu anomaly becomes less negative as the rocks evolve which may be due to accumulation of plagioclase and alkali feldspar or increasing fo_2 in the melt. The range of REE concentrations expands that obtained by Lopez-Escobar et al. (1979) for Palaeozoic granitoids from central Chile (33^o-34^oS) (Figure 2.10).

2.4.4 Isotope geochemistry

Initial $^{87}Sr/^{86}Sr$ ratios have a narrow range from 0.70600 - 0.70649 (ε^i_{Sr} = +23.4 to +30.0) : initial $^{143}Nd/^{144}Nd$ varies from 0.512195 - 0.512229 (ε^i_{Nd} = -2.0 to -1.3). If sample 81121 from the southern end of the Sierra Limon Verde is included and assumed to be the same age then the variation is extended to ε^i_{Sr} = +19.0 and ε^i_{Nd} = -2.48. The data plot in the bottom right hand quadrant of an ε^i_{Sr} - ε^i_{Nd} diagram (Figure 2.11) similar to many granitoids studied by Allegre and Ben Othman (1980), Caledonian granites

in Scotland (Hamilton et al., 1980) and Australian granites (McCulloch and Chappell, 1982), but in marked contrast to the Mesozoic-Tertiary intrusions of this part of the Central Andes (Chapters 4, 6 and 7).

2.4.5 Petrogenesis

The petrogenesis of the Palaeozoic batholith in northern Chile presents a number of problems in that on a regional scale the mineralogy and Sr isotope geochemistry vary considerably. Zeil et al. (1980) and Berg et al. (1983) report two mica granitoids around Chanaral varying from 285 - 238 Ma in age which have variable, but usually high, initial $^{87}Sr/^{86}Sr$ ratios of 0.7054 - 0.7141, suggesting an origin in which crustal anatexis has played an important role. Naranjo (pers. comm., 1984) has identified both biotite and two mica plutons, although no geochemical analyses are available on these rocks.

The combined Sr and Nd isotope geochemistry of the Limon Verde pluton is consistent with an origin by crustal anatexis. If this intracrustal melting did not fractionate the Sm/Nd ratio between source and melt then the T^{Nd}_{DM} ages of the rocks place constraints on the maximum age of the crust being melted; these model ages vary from 862 - 1187 Ma, thus militating against Archaean and early Proterozoic crustal precursors. The dates are, however, similar to the T^{Nd}_{DM} ages of the Limon Verde schists (913 - 1308 Ma) suggesting that the same old component may be present in both units. There are, however, an number of arguments against crustal anatexis. Firstly, the broad spectrum in SiO_2 content (52.6-75.1%) is difficult to generate by melting at or near the granite minimum. Secondly, Cornish granites (Alderton et al., 1980) other collision granites (Harris et al., in press), and Bolivian rhyodacites and acidic ignimbrites (Kussmaul et al., 1977)

which are considered to be crustal melts (or to contain a large crustal component) have high Rb/Zr ratios (> 1) reflecting the importance of K feldspar, amphibole and biotite breakdown and the residual nature of zircon during melting in the granite system. The Limon Verde pluton conversely has low Rb/Zr ratios (< 0.8; Figure 2.12) with high Zr concentrations (up to 412 ppm). It is thought, therefore, that intracrustal melting has not been the main mechanism in the petrogenesis of this pluton, though it may have been the case in the generation of other parts of the Palaeozoic batholith elsewhere in Chile.

The uniformity of both initial Sr and Nd isotope ratios over a wide range of compositions argues against the hypothesis of progressive crustal contamination during fractionation (AFC; DePaolo, 1981), and indicates that the source of the Limon Verde pluton had $\varepsilon^{266}_{Sr} \sim +25$ and $\varepsilon^{266}_{Nd} \sim -1.5$. In keeping with this mildly enriched signature the Hf/Ta ratios of the most basic parts of the pluton (4.4 - 5.1) are also more enriched than N-type MORB (13; Pearce, 1982), or chondrites (8.6, Wood et al., 1979), and closely resemble those of the later (Cretaceous) magmatism in the nearby Cerros de Montecristo (Section 5.5). The isotopic characteristics of this mantle, however, present a problem regarding the Cretaceous activity. These later lavas have depleted isotope characteristics with ε^{i}_{Nd} = +3.6 to +5.2 ($(^{143}Nd/^{144}Nd)_i$ = 0.5126870 - 0.512774) and ε^{i}_{Sr} = -7.0 to +0.10 ($(^{87}Sr/^{86}Sr)_i$ = 0.70408 - 0.70458). Thus whilst it is possible to go from a Limon Verde $^{143}Nd/^{144}Nd$ ratio of 0.51223 at 266 Ma to 0.51270 at 105 Ma by radioactive decay, the time integrated Sm/Nd ratio of the source of 0.74 is considered far too high considering depleted MORB sources have Sm/Nd ratios ~0.41. Furthermore the $^{87}Sr/^{86}Sr$ of the Limon Verde

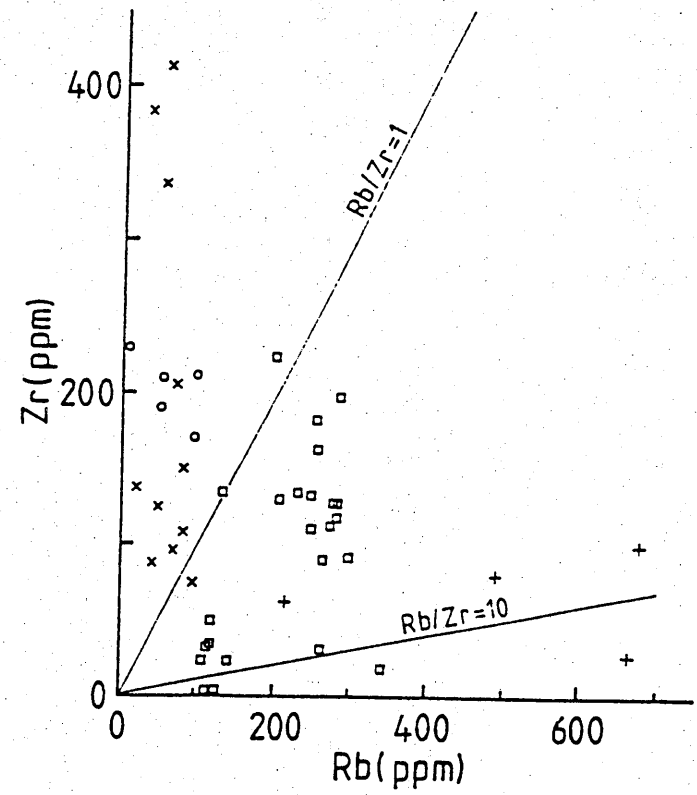

Figure 2.12

Rb - Zr plot for the Limon Verde pluton (✕) and the rhyolites of the Cerro Crespo Formation (○). Supposed crustal melts from Cornwall (+) (Alderton et al., 1980) and S.W. Bolivia (□) (Fernandez et al., 1973; Kussmaul et al., 1977) are also depicted.

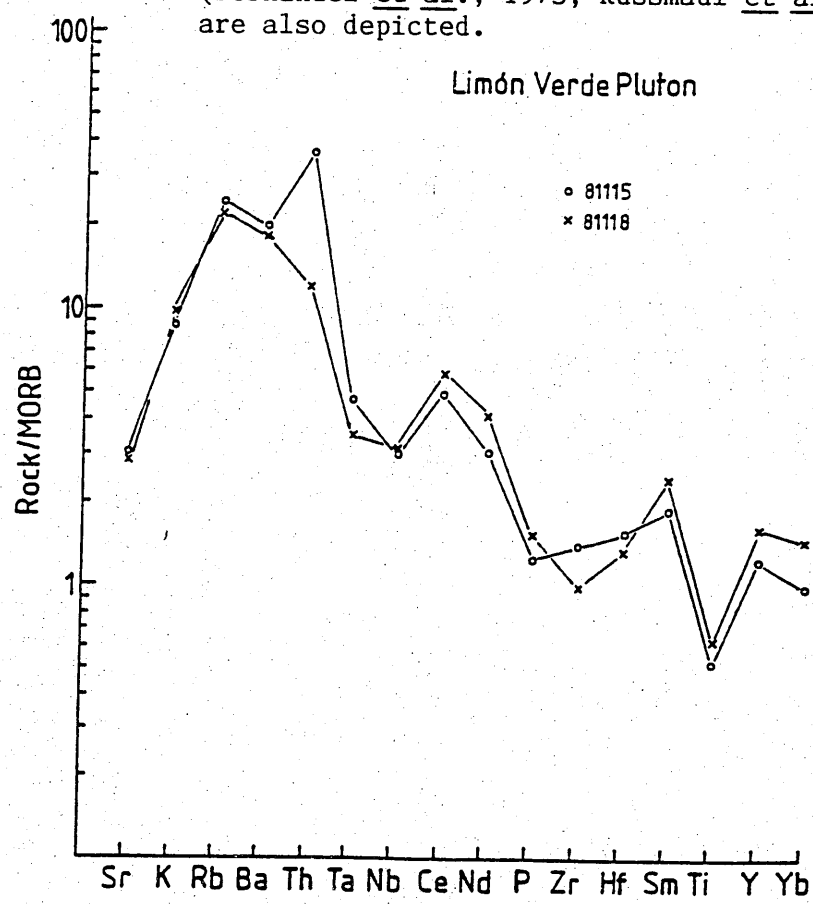

Figure 2.13

MORB normalised plot of basic facies in the Limon Verde pluton.

source (0.7063) is more radiogenic than that of the Cretaceous lavas, and so it is impossible to progress from one to the other by closed system radioactive decay. The input of slab-derived material would also be expected to increase the $^{87}Sr/^{86}Sr$ rather than to decrease it. Consequently, unless one postulates highly distinctive, long lived, isotopic domains in adjacent sectors of the mantle it would appear inevitable to advocate that the Limon Verde pluton was derived from the depleted mantle precursor to the Cretaceous volcanism, and that the magma was contaminated after leaving the mantle source, but prior to high level fractionation. Assuming that the Sm/Nd ratio and ε^{100}_{Nd} of the mantle derived endmember of the Cretaceous magmatism were 0.33 and +4.0 respectively, then, assuming they had previously been closed systems, at the time of intrusion of the Limon Verde pluton (266 Ma) the Nd isotopic composition would have been $\varepsilon^{266}_{Nd} = +3.95$. Additionally the Sr isotope systematics would be constrained to be on the mantle array (i.e. $\varepsilon^{266}_{Sr} = -12$: $(^{87}Sr/^{86}Sr)_{266} = 0.70353$). By consideration of the Sr and Nd contents of the Cretaceous succession values of 600 - 700 ppm and 20 ppm respectively are thought to be reasonable estimates for their concentration in the mantle-derived magma. Apportioning values to the crustal contaminant are even more ad hoc. Possible observed contaminants include the basement schists or the rocks of the Toco Formation which may originally have formed as an accretionary prism. Unfortunately there are no geochemical data for the Toco Formation and so its effects during assimilation are unknown. However, it may have been sufficiently hydrous to increase the P_{H_2O} in the ascending magma and hence bring amphibole onto the liquidus instead of pyroxene. These problems notwithstanding, if the crustal melt is assumed to have a SiO_2 content of 70% (Hawkesworth et al., 1982; Tindle, 1982) then

the basic nature of parts of the pluton constrain the amount of contaminant permitted to enter the melt to 13% (given that the mantle derived melt had SiO_2 = 50%). Furthermore, because of the low Sr content of the likely crustal melt (100 ppm), to increase the $^{87}Sr/^{86}Sr$ ratio from 0.7035 to 0.7063 requires a crustal contaminant with $^{87}Sr/^{86}Sr$ = 0.8175. Accepting Tindle's (1982) value of 40 ppm for the Nd concentration of a greywacke the $^{143}Nd/^{144}Nd$ ratio of the contaminant is 0.51133 ($\varepsilon^{266}Nd$ = -18.9). Interestingly this gives a T^{Nd}_{DM} age of 2732 Ma (if it has an average crustal Sm/Nd ratio of 0.19) lending further support for the presence of ancient crust in the region.

A MORB normalised plot (Pearce, 1982) of the more basic rocks (Figure 2.13) indicates that the pluton has a subduction-related signature with high ratios of LILE/HFSE. Low Hf/Ta ratios in such rocks are considered by Pearce (1983) to represent a continental margin signature rather than that of an oceanic island arc. This is in accord with the palaeogeographic model of Coira et al. (1982) of a subduction zone dipping eastwards beneath the Palaeozoic South American continent. The HREE concentrations of the most basic facies of the pluton preclude a petrogenesis involving garnet as a residual phase during partial melting, and thus indicate that the crust hereabouts was less than 60-70 km thick. The present crustal thickness beneath the Limon Verde is about 60 km (James, 1971a), therefore implying that there has been crustal thickening beneath this area subsequent to the Upper Palaeozoic.

2.5 CERRO CRESPO FORMATION

2.5.1 Field relations and petrography

Overlying the southern reaches of the Sierra Limon Verde on its western margins is a sequence of intercalated rhyolites, rhyolitic tuffs and volcaniclastics generally dipping north-west. Individual lavas and tuffs attain a maximum thickness of 20m whilst the volcaniclastics are generally thinner. All the lavas are sparsely porphyritic, the phenocryst content usually less than 5%. Quartz, plagioclase and magnetite are ubiquitous phenocryst phases, although orthoclase is also often present; rarely sanidine may occur in place of orthoclase. Quartz forms clear rounded crystals with pronounced cuspate embayments up to 1mm across; occasionally it exhibits a glomeroporphyritic texture. Plagioclase, the most common phenocryst phase is always albitized, with relict lamellar twinning still discernible. Idiomorphic laths up to 2mm long are often present, though resorption may produce rounded, allotriomorphic crystals. Orthoclase, while being present in many flows is generally only found in small quantities; it exhibits a similar habit to that of plagioclase. Sanidine occurs as clear idiomorphic crystals. Magnetite, too, is a minor phenocryst phase, displaying very small idiomorphic and hypidiomorphic crystals, and larger allotriomorphic clots. Groundmasses consist predominantly of fine grained quartz, a little potassium feldspar, sparse finely divided opaque oxides and infrequently some very fine plagioclase microlites. Some of the lavas contain small xenoliths of other rhyolites, presumably erupted earlier in the sequence: the contacts between xenolith and host are fairly sharp. No blocks of the underlying pluton or metamorphic belt were found. The tuffs and volcanclastics are often reddened due to staining with haematite; originally the more porous nature of these units compared to the lavas allowed easier fluid circulation.

Baeza (1976) has described this unit as being a porphyritic granite of Tertiary age. However, the petrography and stratigraphic sequences observed indicate an eruptive and sedimentary rather than an intrusive mode of origin for this pile. These rocks were seen overlying the pluton of the Limon Verde, but not to overlie the lavas of Upper Cretaceous age as reported by Baeza (op. cit.). Thus, while not eliminating a Tertiary age for the suite, an older date of formation is still possible. The geochronology is discussed further below.

2.5.2 Geochronology

Five rhyolites from the Cerro Crespo Formation yield a whole rock Rb-Sr errochron of 233 ± 36 Ma with an initial $^{87}Sr/^{86}Sr$ ratio of 0.7073 ± 14 (ε^{i}_{Sr} = +40.2) (Figure 2.14). This date supports the stratigraphic view that the formation is older than the Tertiary age alleged by Baeza (1976). The Choyoi Group of the Cordillera Frontal and the Precordillera in Argentina has yielded similar K-Ar ages as reported in Caminos *et al.* (1982), and analogous rocks in central Chile are associated with sediments of Permian age (Naranjo, pers. comm., 1984).

2.5.3 Geochemistry

The lavas of the Cerro Crespo Formation are all very silicic (70.8 - 80.0% SiO_2) and are classed as rhyolites according to Peccerillo and Taylor (1976). Low concentrations of TiO_2 (<0.50%), V (<24 ppm) and P_2O_5 (< 0.10%) indicate considerable fractionation of titanomagnetite and apatite, and in one sample (81043) depletion of K_2O and Rb suggests significant removal of alkali feldspar. REE patterns (Figure 2.15) show marked negative Eu anomalies (Eu/Eu* = 0.52)

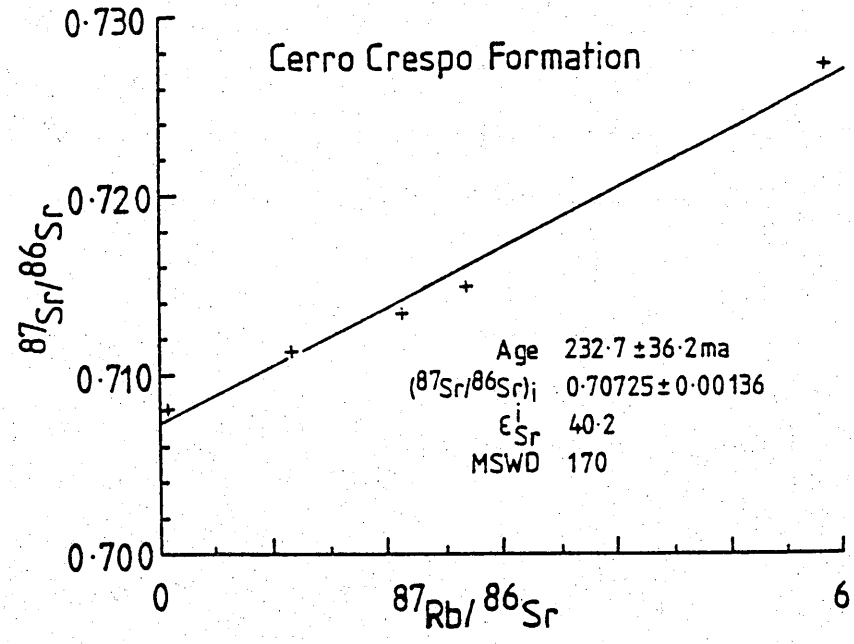

Figure 2.14

Rb - Sr whole rock isochron diagram for the Cerro Crespo Formation.

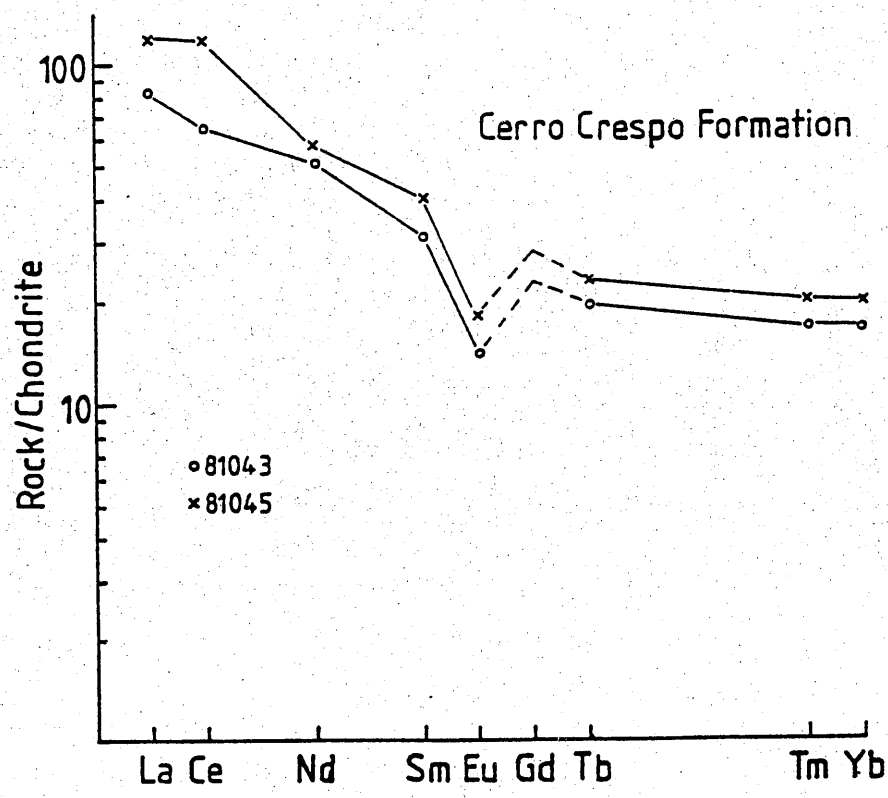

Figure 2.15

Chondrite normalised REE plot for the Cerro Crespo Formation.

attesting to feldspar fractionation. The rhyolites are LREE enriched with $(Ce/Yb)_N$ = 3.9 - 5.8, though the HREE are almost flat ($(Tb/Yb)_N$ = 1.14 - 1.19) : Ce_N varies from 65 - 117 and Yb_N from 16.7 - 20.3.

Sr isotopes were measured on five samples and initial $^{87}Sr/^{86}Sr$ ratios (i.e. at 233 Ma) vary from 0.70618 - 0.70831 (ε^i_{Sr} = +24.9 to +55.2): initial $^{143}Nd/^{144}Nd$ ratios are tightly constrained between 0.512212 - 0.512295 (ε^i_{Nd} = -0.9 to -2.5). All the analyses lie in "enriched" quadrant of an ε_{Sr} - ε_{Nd} diagram and overlap with the isotopic composition of the Limon Verde pluton at that time (ε^{233}_{Sr} = +21.9 to +34.9; ε^{233}_{Nd} = -1.6 to -2.7), though overall the latter has slightly less radiogenic Sr (Figure 2.16).

2.5.4 Petrogenesis

The main problem when considering the petrogenesis of rhyolites is determining whether they have been generated by intracrustal melting (e.g. Siegers et al., 1969; Pichler and Zeil, 1972: Kussmaul et al., 1977), by advanced degrees of fractional crystallization of a basaltic melt (Lanphere et al., 1980; Cameron et al., 1980), or by contamination of a fractionating basaltic melt with crustal material (DePaolo, 1981). In some cases the geochemical evidence is ambiguous, and more than one solution is possible (Hawkesworth et al., 1982).

The position of the Cerro Crespo Formation rhyolites in the bottom right-hand quadrant of the ε_{Sr}- ε_{Nd} diagram (Figure 2.16) creates few constraints on their petrogenesis, and any of the mechanisms outlined above are applicable. Considering firstly the possibility that the

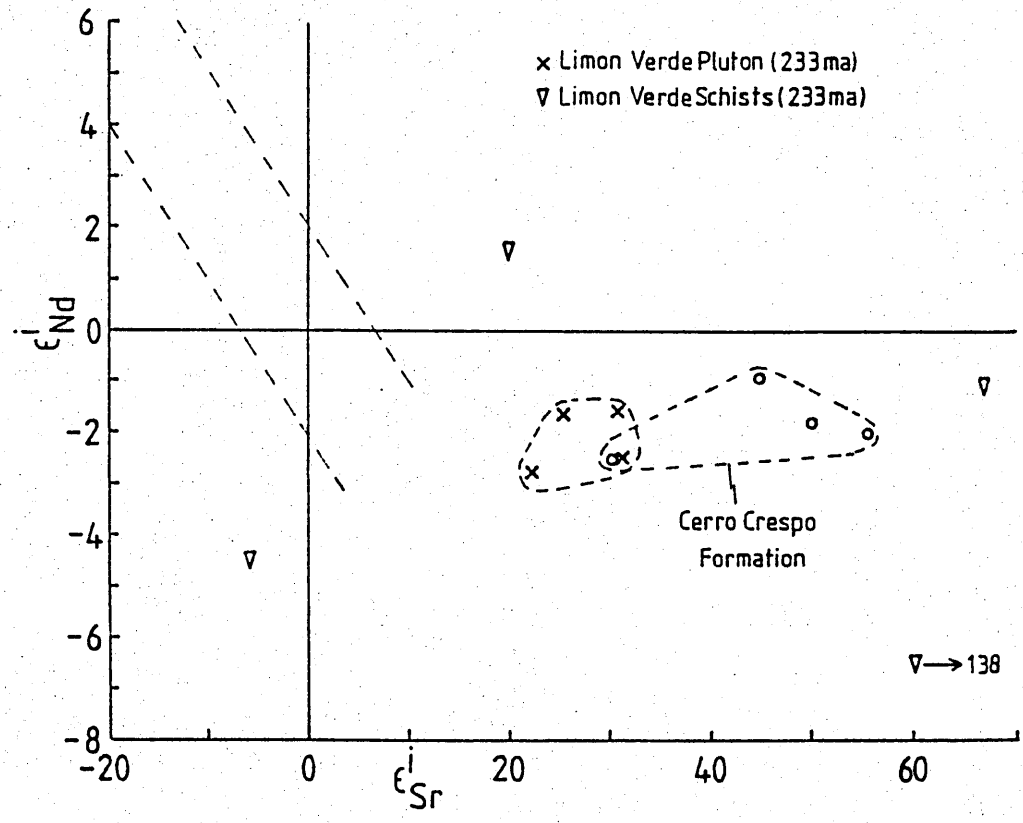

Figure 2.16

ε_{Sr} - ε_{Nd} diagram for the Cerro Crespo Formation, showing also the positions of the Limon Verde pluton and the basement schists at 233 Ma.

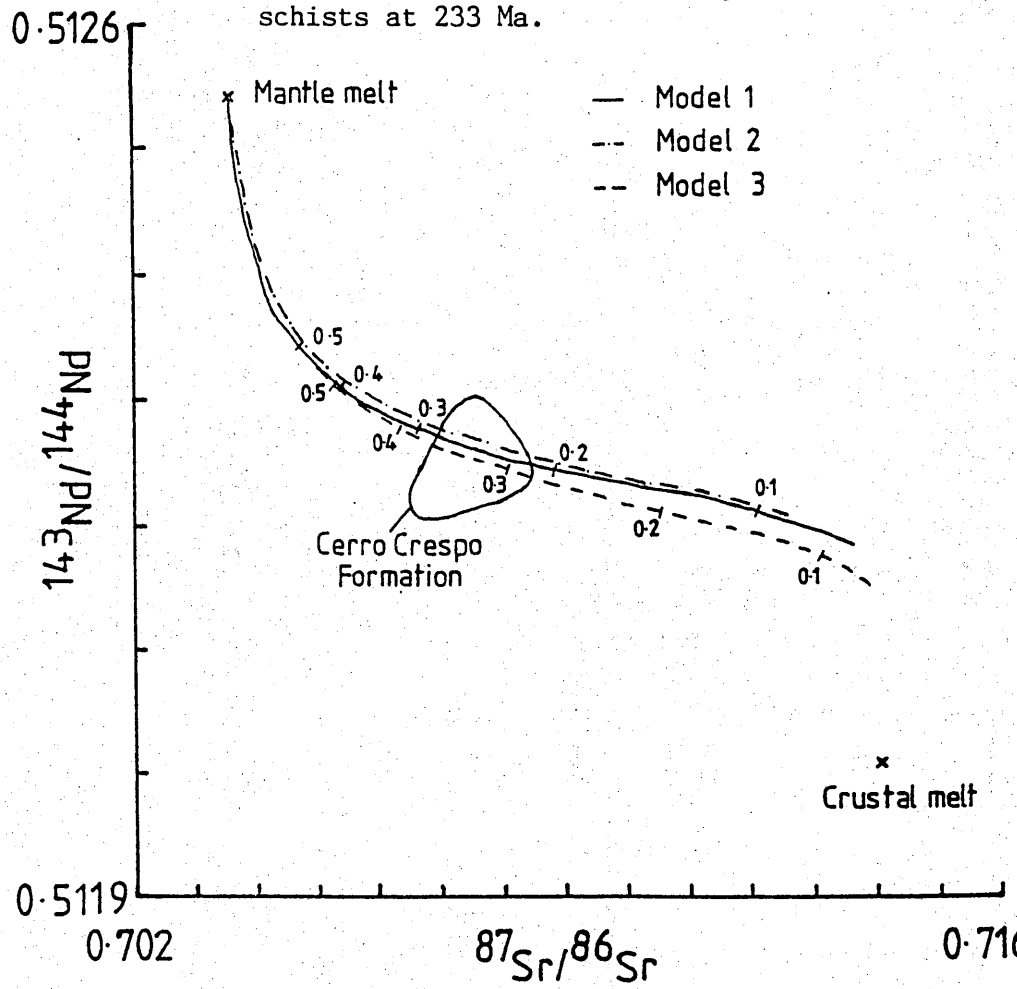

Figure 2.17 AFC curves produced during modelling of the Cerro Crespo Formation. Modelling parameters are given in Table 2.1. Values along curves for models 1 and 3 indicate the mass of magma remaining as a fraction of the mass of the initial magma.

Table 2.1 Parameters used in AFC modelling of the Cerro Crespo Formation

	Model 1		Model 2		Model 3	
	Mantle melt	Crustal melt	Mantle melt	Crustal melt	Mantle melt	Crustal melt
$^{87}Sr/^{86}Sr$	0.70357	0.71411	0.70357	0.71411	0.70357	0.71411
$^{143}Nd/^{144}Nd$	0.51254	0.51201	0.51254	0.51201	0.51254	0.51201
Sr	700	100	600	35	600	35
Nd	20	35	20	35	20	35
K_D^{Sr}	2		2		2	
K_D^{Nd}	0.5		0.5		0.5	
r	0.35		0.35		0.4	

rhyolites were formed by intracrustal melting, their T^{Nd}_{DM} ages of 887 - 996 Ma constrain the maximum age of that crust. If the crustal precursors had been derived from a chondritic mantle then their age could be no greater than 471 Ma. As mentioned in the previous section the isotope data for the underlying Limon Verde pluton at 233 Ma coincide with those of the Cerro Crespo Formation; furthermore their T^{Nd}_{CHUR} ages are also in close agreement (318-471 Ma for the rhyolites and 319-570 Ma for the pluton). Consequently the derivation of the lavas by remelting of the pluton is a distinct possibility. The trace element geochemistry of the rhyolites, however argues against this as their Rb/Zr are very low (<0.6) compared to other crustal melts (e.g. Harris et al., in press; Figure 2.12).

The possibility that the rhyolites are the products of an AFC style of crustal contamination of a basaltic melt, is difficult to assess quantitatively as there is no systematic trace element variation with the degree of fractionation, and one has little control on the composition of either end member. It is always possible to draw mixing lines between hypothetical melts and contaminants to pass through a given set of data points. Nonetheless, the most plausible mantle-derived magma would have the same isotopic composition and Sr and Nd concentrations as that conjectured for the Limon Verde pluton (i.e. ε_{Nd} = +3.95, ε_{Sr} = -12, Nd = 20 ppm, Sr = 600-700 ppm). Data for the metamorphic complex yield a wide range in isotopic composition at 233 Ma with ε^{233}_{Sr} = -6 to +138 and ε^{233}_{Nd} = +1.57 to -6.50 (Figure 2.16); clearly some of these are potential contaminants and sample 81151 with ε^{233}_{Nd} = -6.5 and ε^{233}_{Sr} = +138 was used in the modelling. Concentrations of Sr and Nd in the crustal melt were taken to be 100 ppm and 35 ppm respectively (Hawkesworth et al.,

1982). Three curves were found to pass through the data field (Figure 2.17) although none gives a perfect fit: the parameters used in the models are given in Table 2.1. It can be seen that increasing the Sr content of the mantle-derived magma has roughly the same effect on the shape of the curve as slightly increasing the ratio of mass assimilated/mass crystallized (r). The curves indicate that 70-80% fractional crystallization is required by model 1 whereas model 3 necessitates 60-70%. Either way the amount of fractionation is large. These calculations are not unique solutions to the problem, but merely illustrate that locally available materials coupled with reasonable estimates for K_Ds can approximate to the isotopic data.

If the rhyolites are the product of fractional crystallization of a basaltic magma without any crustal influence then their isotopic characteristics indicate that the original magma must have been derived from an isotopically enriched source. Compared to the lavas of the Jurassic La Negra Formation (Chapter 3) which form part of the Cordillera de la Costa and have a depleted isotopic signature, the Hf/Ta ratio of the Cerro Crespo Formation is considerably lower (6 compared to 14-19) in keeping with the enrichment of the isotopes, and is close to that of the parental magma of the Limon Verde pluton (4.4 - 5.1). However, it has been argued earlier (Section 2.4.5) that the parental magma for this pluton was derived from an isotopically depleted mantle, similar to that which produced the later Cretaceous magmas, and that this equilibrated with a crustal melt before undergoing fractionation. Thus, in view of the geographical and temporal proximity of the Cerro Crespo Formation to the pluton it seems reasonable to assume that the petrogenesis of both was also similar.

2.6 Agua Dulce Formation

This formation was named by Garcia (1967) after a section to the east of Caracoles (just to the south of the present transect) composed of over 1000 m of conglomerates and lavas, unconformably overlain by Jurassic marine sediments. Similar successions were previously recorded from the Limon Verde area by Wetzel (1927), Hausen (1937), Biese (1961), Harrington (1961) and Perez and Levi (1961), though the latter two references indicated a comformable relationship between the continental volcano-sedimentary series and the marine Jurassic around Moctezuma on the north-east flanks of the Sierra Limon Verde. In the present area of study Baeza (1976) has described several sections in the region between Cerritos Bayos and Calama, such as the north-westerly dipping succession at Colina Roja just to the west of the Sierra Limon Verde (Figure 2.1).

The basal part of the section at Colina Roja consists of some 300 m of poorly sorted, immature sandstones, siltstones and conglomerates. The latter contain up to 95% angular - sub-rounded clasts, ranging in size up to 5 cm, and comprising fragments of fine-grained quartzite, granite, several varieties of intermediate and acid lavas, vesiculated pumice, ignimbrite, arenites, quartz rich conglomerates and breccias, as well as crystals of opaque oxides, plagioclase, potassium feldspar and quartz. The matrices of most of these sediments are quartz rich and have been stained with haematite, though some calcite cementation also occurs. These clastics were probably derived from the adjacent Limon Verde during periods of rapid erosion and burial as indicated by their immaturity and clast composition. Overlying these sediments is about 130 m of reddened intermediate lavas, and rhyolitic tuffs and ignimbrites. The ignimbrites display an eutaxitic texture with crystals of plagioclase, quartz, with a

little opaque oxides and occasionally angular lithic fragments. This sequence, too, has suffered extensive alteration by iron-rich fluids. The volcanics are succeeded by 65 m of more fine-grained arenites followed by 3 m of sub-angular and sub-rounded conglomerates containing predominantly andesite clasts. Disconformably overlying these are glauconitic sands, arenites and silicified calcilutites, the latter forming cherts in places. Lower Liassic fossils have been found in these upper beds by Baeza (1976), and consequently the section is interpreted as one of a Jurassic marine transgression over a Triassic continental landmass. Other isolated outcrops on the Pampa Limon Verde yield similar stratigraphic successions, with the Triassic-Jurassic unconformity being more pronounced at some localities, though always of shallow angle.

Further outcrops of the Agua Dulce Formation occur in the west of the area, in the Pampa Negra (Figure 2.1). Here Frutos (1976) described a series of rhyolites and quartz rich continental sediments which overlie the Toco Formation. These rocks form the roof of a small stock of Cretaceous age (Chapter 6) and are extensively hornfelsed. Other regions of Triassic volcanic rocks are found in northern Chile notably in the Cordillera Domeyko where there are interbedded continental sediments and volcanics (Chong, 1977).

The altered nature of the Agua Dulce Formation in the study area precludes meaningful geochemical interpretation. The presence of rhyolitic ignimbrites may attest to processes involving crustal anatexis or crustal contamination of basic magmas, but this is not a certainity (e.g. Cameron et al., 1980). However, this style and composition of volcanism contrasts markedly with the Lower Jurassic eruptions of the La Negra Formation in the Cordillera de la Costa (Chapter 3), and represents

the last phase of igneous activity at this latitude before the switch of locus of eruption to the west.

CHAPTER 3

LA NEGRA FORMATION

3.1 Introduction

The coastal escarpment of northern Chile between 22° - 23° forms an impressive feature, in places rising to 1700 m in less than 8 km horizontal distance, Much of this scarp is composed of lava flows and sedimentary intercalations of the La Negra Formation (Figure 3.1). These flows were first noted by Darwin (e.g. 1876) who called them the "Porphyritic" Formation. The term "La Negra" was introduced by Garcia (1967) after the type section in the Quebrada La Negra to the south of Antofagasta where the sequence has an estimated thickness of 10,000 m. The rocks have been studied by Palacios (1978) who, on chemical evidence, interpreted them as representing a Jurassic arc. The base of the formation is not seen in the study area, but further south fossiliferous marine Liassic sediments are interspersed between flows (Ferraris, 1978): in the Chañaral area (26°20'S) Triassic plutons are cut by basic dykes which are thought to represent the feeder system of the La Negra pile (Damm and Pichowiak, 1981). These observations place a lower limit on the age of the La Negra, and are in accord with the geochronological data presented in Section 3.3. Moreover, the volcanics are intruded by granitic plutons along much of this part of the Cordillera de la Costa, and their age places an upper limit of middle Jurassic on the age of the lavas (Section 4.3).

3.2 Field relations and petrography

To the south of Tocopilla the lavas form very thin basaltic andesite flows dipping uniformly eastwards at about 30° (Plate 3.1). Over a 600 m section at Punta Ampa flow thicknesses vary between 1 - 8 m;

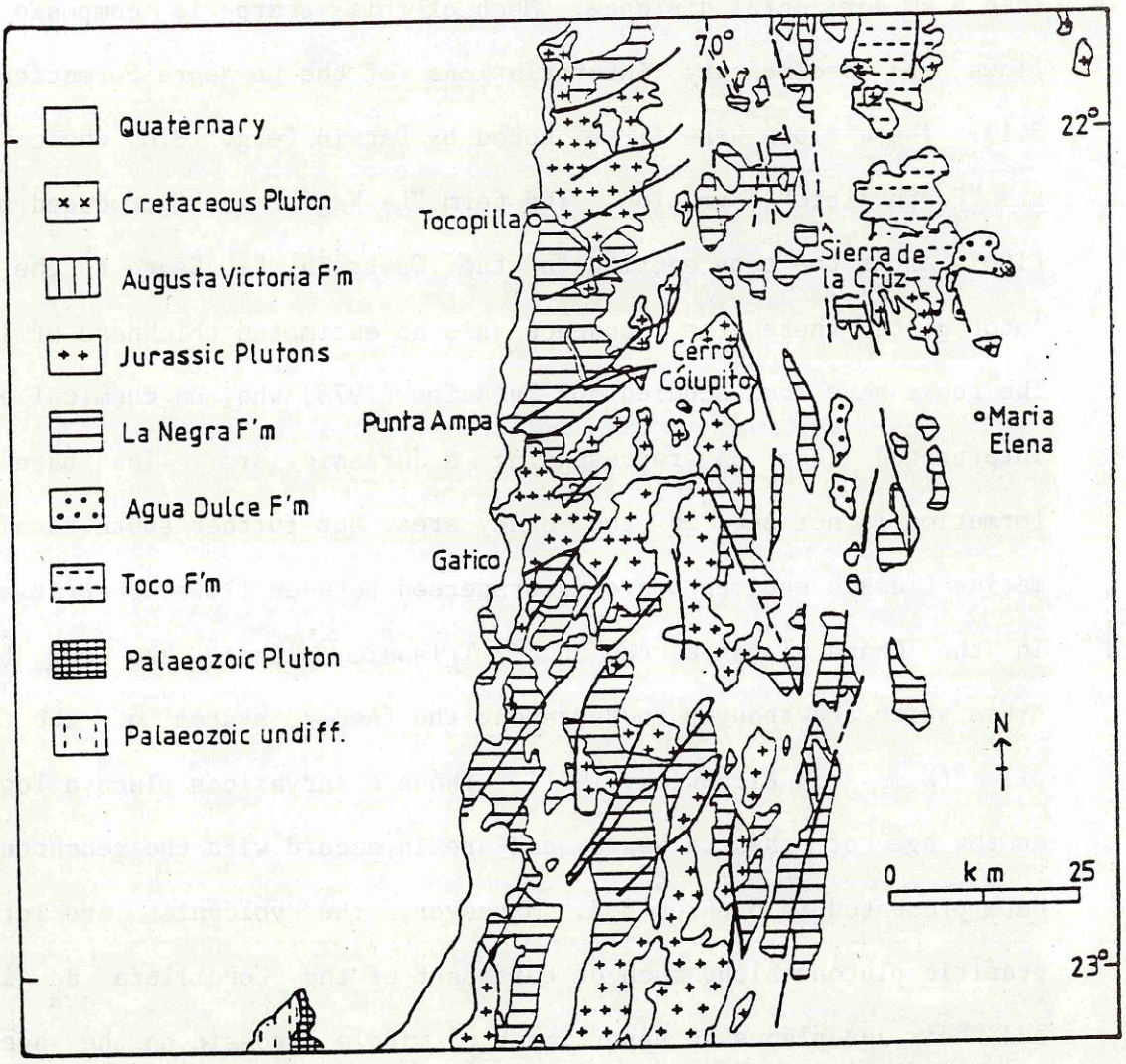

Figure 3.1

Generalised geological map showing the location of the La Negra Formation in the study area (after Servicio Nacional de Geologia y Mineria, 1980).

the section, however, can be divided into three main groups: a lower group composed of thin (1 - 2.5 m) flows, a middle group of thicker (4 - 8 m) flows, and an upper group of thin ($\sim$ 2 m) flows. Many flows have a chilled base (3 - 6 cm), which sometimes contain flattened amygdales, and a brecciated top; the flow surfaces may also be highly oxidised with rounder amygdales. Sporadically intercalated with the flows are reworked sandy tuffs and intraformational volcaniclastics, some of which contain blocks up to 1 m across. The sands sometimes fill in hollows of the underlying flow and thus appear lensoid. The sediments and the brecciated lava tops, being more porous than the lavas, have acted as conduits for the passage of post-consolidation fluids during burial metamorphism. This has led to the development of calcite, epidote, quartz, chlorite, and, more rarely, prehnite and pumpellyite fillings in vesicles, and to the alteration of the matrices of the sediments which in extreme cases have been converted to green epidote sands. During sampling care was taken to select lavas from the massive centres of flows where the abundance of amygdales, and the effects of fluid circulation were minimal. Pillow structures indicative of subaqueous eruptions were observed in isolated flows, particularly near Antofagasta, and in the supposed Jurassic lavas forming the "Morro" at Arica in northernmost Chile. A section at the top of the cliffs at the Buena Esperanza copper mine yielded similar lithologies, but the degree of alteration was much greater. Further inland (i.e. higher stratigraphically) the degree of alteration decreases along with the quality of exposure.

Most of the lavas are strongly prophyritic, though there are sequences of flows where phenocrysts are rare. The dominant phase is plagioclase, never less than 75% of the total phenocryst content. All flows show sericitization of the plagioclase to certain degrees around the

a.

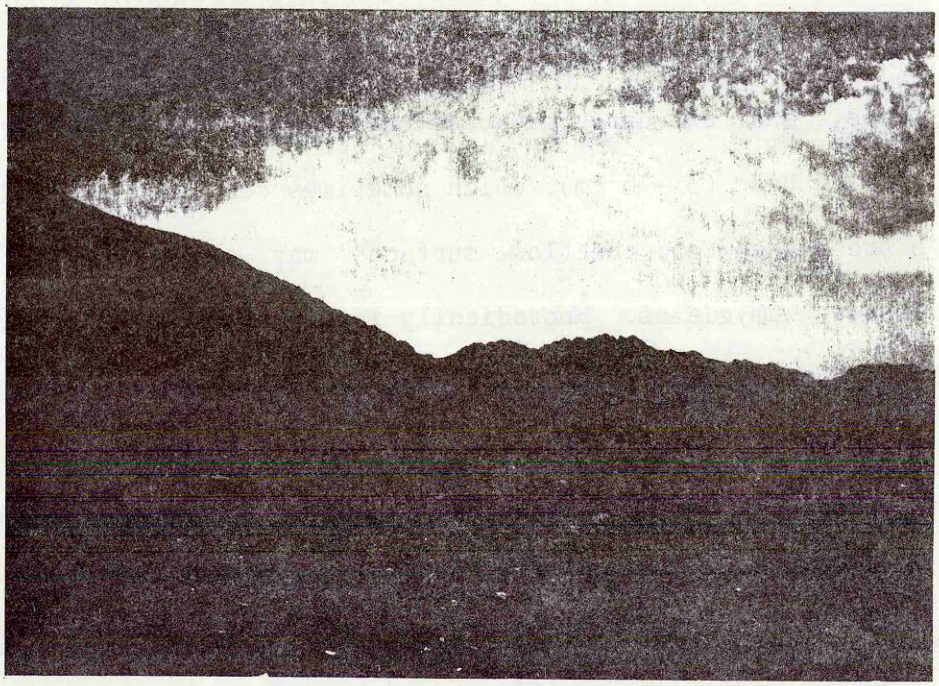

b.

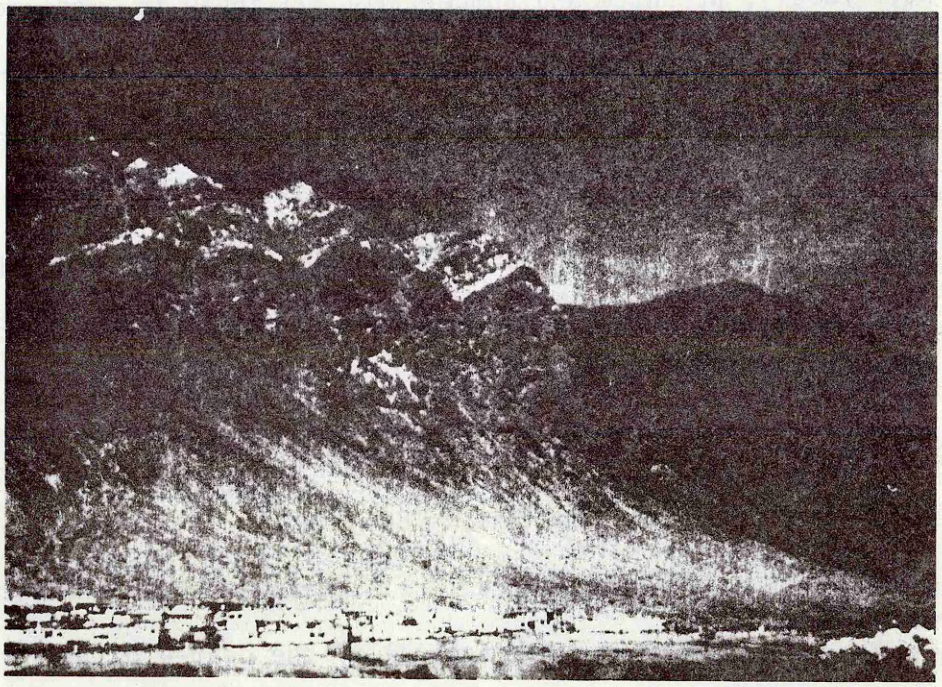

Plate 3.1a. Easterly dipping lavas of the La Negra Formation at Punta Ampa.

Plate 3.1b. Hyaloclastite (white) in the La Negra Formation at Tocopilla. This cannot be traced across the fault which cuts the escarpment between the foreground and background cliffs.

margins and along cracks. Normal zoning is apparent in the fresh crystals ranging from about An_{63} in the cores to An_{30} at the margins. Disequilibrium between phenocryst and liquid is sometimes apparent: phenocrysts may contain glassy inclusions defining an original crystal outline, and which have undergone later growth. This melting may be due to either the crystal moving into a higher temperature magma, or to the influx of a hotter liquid into the magma chamber; during subsequent cooling further crystal growth has occurred. Other evidence for thermal/compositional disequilibrium is the presence of resorbed crystal margins.

Ferromagnesian minerals are rare in these lavas. The most common is augite which in places shows simultaneous crystallization with plagioclase. Orthopyroxene is universally altered to serpentine and specular oxide: it generally appears to have crystallized prior to clinopyroxene. Olivine, too, is highly altered being pseudomorphed either by serpentine or iddingsite. The highly rounded nature of the phenocrysts suggests thermal/compositional disequilibrium. Magnetite is a trace phenocryst in many flows, often included into plagioclase crystals. Groundmasses have an intersertal texture and consist mainly of plagioclase microlites, finely divided oxides, altered ferromagnesians and devitrified glass.

Further inland, towards the Sierra de la Cruz, the lavas are a little more evolved, though plagioclase is still predominant. Hornblende is sometimes present, occasionally cored by clinopyroxene: pyroxenes are frequently converted to serpentine or haematite rich products. Groundmasses are coarser than at Tocopilla, and a little quartz may be present; ferromagnesian components are usually altered.

The thickness of the lava pile is undetermined. North-east striking faults are exploited by quebradas, and have acted as conduits for the circulation of mineralizing fluids. Correlation of flows or sediments across these faults is not possible; for example a prominent hyaloclastite near Tocopilla is faulted out completely in one of the quebradas (Plate 3.2). Other conspicuous faults are aligned north-south, and form part of the major Atacama Fault system; this lineament downthrows to the east into the graben structure of the Pampa del Tamarugal. Thus, if it is assumed that the lava pile has a uniform easterly dip of 30° (reasonable as the La Negra to the west of the Sierra de la Cruz also has this dip), as far east as Maria Elena (60 km from the coast), and that it was deposited horizontally with all the tilting being post-depositional, then the pile would be 30 km thick. Allowing for some downfaulting on the eastern margins further increases this value. As the rocks on the coast south of Tocopilla are above the base of the formation the total thickness is even greater. Therefore, given that the section at Punta Ampa is buried to at least a depth of 30 km, and assuming reasonable geothermal gradients, the rocks would be expected to be in the granulite facies, which is clearly not the case. Levi (1970) has described similar rocks of Cretaceous age from central Chile and their associated burial metamorphism and Aguirre et al. (1978) and Offler et al. (1980) have reported analogous studies in the Casma and Calipuy volcanics in Peru. In these sequences it was noted that "cycles" of burial metamorphic assemblages could be identified, with a high grade facies (greenschist) at the base of one cycle overlying a low grade facies (zeolite) at the top of the previous cycle. Levi (1970) interpreted this as being due to a "sealing" process whereby the growth of early formed assemblages reduced the permeability of the rock, and hence later fluids were unable to

penetrate the strata. Offler et al. (1980), however, questioned this hypothesis, but could come to no rigorous conclusions. No distinct "cycles" of burial metamorphism were observed within the La Negra pile.

Rather than postulate an original pile of horizontal flows with its associated thickness problems, it is envisaged that the lavas formed as imbricate sheets, dipping gently to the east with the locus of eruption migrating eastwards slightly with time. The morphology of the flows suggests that eruptions were in an extensional environment from fissures. One major problem regarding the source of the lavas is the complete absence of dykes cross cutting the pile, especially on the coast where exposure is excellent. Inland, potential dyke systems may be obscured by the thick cover of Quaternary gravels. Contact relations and flow features within the formation preclude thickening by sill intrusion. The logical source, therefore, given an original easterly dip is to the west. Tenure of this hypothesis necessitates the post Liassic removal of some of the continental margin, as the present day Peru-Chile trench is only a few kilometres to the west. Further evidence for the existence of a more extensive continental margin is provided in the Cretaceous Coloso Formation of continental sediments on the coast near Antofagasta where Turner et al. (1984) have determined a provenance from the west. A fuller discussion of this problem is rendered in Chapter 8.

3.3 Geochronology

An eighteen point isochron for the La Negra Formation yielded an age of 186 $\pm$ 14 Ma with an initial $^{87}Sr/^{86}Sr$ of 0.7032 $\pm$ 2 (ε^{i}_{Sr} = -18.8) (Figure 3.2). A similar Rb-Sr age has been reported for the Chocolate Volcanics of southern Peru (James et al., 1975). Farrar et al. (1970), McNutt et al. (1975), and

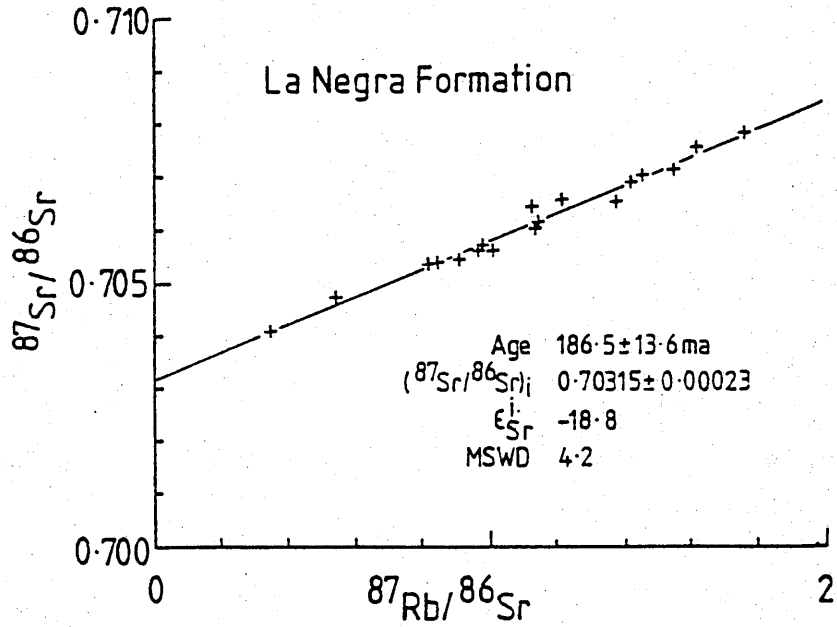

Figure 3.2

Rb - Sr whole rock isochron diagram for the La Negra Formation

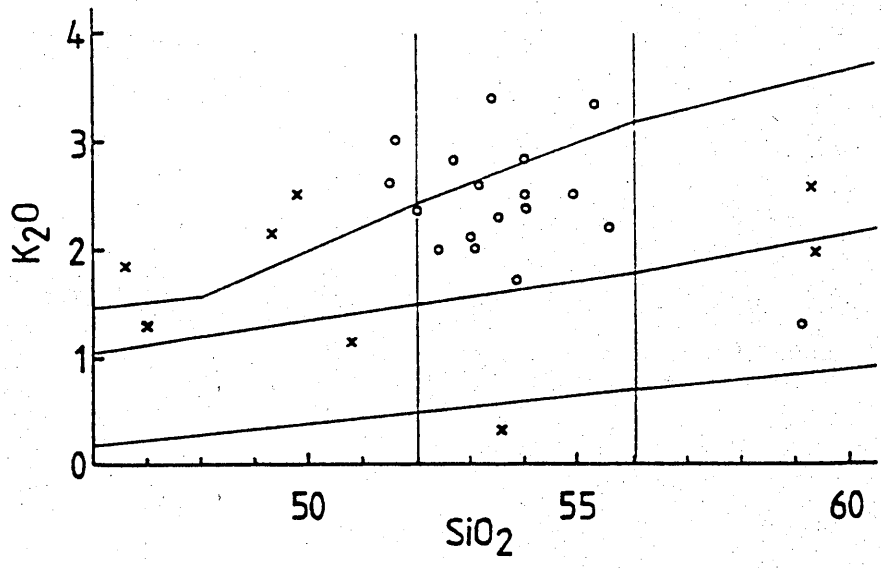

Figure 3.3

K_2O - SiO_2 diagram for the La Negra Formation (O) illustrating its high K nature. Lavas from the Puente Piedra Formation, Peru (Atherton et al., 1983) are shown for comparison (×). Field boundaries are from Peccerillo and Taylor (1976).

Berg et al. (1983) also found intrusive rocks spanning 177 - 191 Ma at about 27°S between Chañaral and Caldera using both K-Ar and Rb-Sr techniques.

The correlation of the La Negra Formation with the post Kimmeridgian lavas of Cerritos Bayos (the Indio Muerto Formation of this study; Section 5.4) given by Baeza (1976) and Palacios (1978) appears incorrect. The Indio Muerto Formation is of Tithonian-Neocomian age, and while the La Negra Formation may be diachronous over the study area, the aforementioned relationship with the middle Jurassic plutons probably as far east as the Sierra de la Cruz (although here the intrusive contact was not seen) implies that it is generally pre-middle Jurassic in age. Thus the La Negra, although a thick pile, was probably erupted over a short period of time during the Liassic. This is not unusual - most of the Deccan traps were erupted over a few million years at the beginning of the Tertiary (Kaneoka, 1980). The petrography of the Indio Muerto Formation is also different from that of the La Negra; in the former olivine is more common in the basaltic andesites, and there is a higher proportion of dacites.

3.4 Major and trace element characteristics

The lavas of the La Negra Formation exhibit little variation in SiO_2 content, with the majority between 51 - 56%; only one analysed sample lies outside this range at 59%. Within the main SiO_2 grouping K_2O varies from 1.73 - 3.93%, the lavas falling in the high-K basaltic andesite, shoshonite and absarkoite fields of the classification of Peccerillo and Taylor (1976) (Figure 3.3); these rocks are hereafter referred to as the basaltic andesites. The higher SiO_2 sample is defined as a calc-alkaline andesite. All the lavas have low

concentrations of MgO (2.98 - 4.62%), Ni (7 - 30 ppm) and Cr (26 - 97 ppm). Coupled with the high K_2O contents the basaltic andesites also have enhanced concentrations of LILE (except Sr) relative to HFSE (Figure 3.4). All the lavas are moderately LREE enriched (Figure 3.5) with $(Ce/Yb)_N$ defining a narrow range between 2.97 - 3.56: Ce_N varies from 46.2 - 71.9 and Yb_N from 13.0 - 21.2 (These ranges are extended to 75.7 and 22.4 if andesite 8098 is included). Ubiquitous negative Eu anomalies vary from Eu/Eu* = 0.84 - 0.65 and are roughly anticorrelated with Ce content. Compared to basaltic andesites from southern Chile (Lopez-Escobar et al., 1977) these lavas have lower concentrations of Al_2O_3, CaO, Sr, Cr and Ni and higher of TiO_2, K_2O, P_2O_5, FeO* (total iron as FeO), Rb, Ba, Th, Hf and REE. They are, however, more comparable with the average composition of unaltered basalt from the Lower Cretaceous Bustamante Hill area in Central Chile near Santiago (Levi et al., 1982), and to the Puente Piedra volcanics of Cretaceous age in Peru (Atherton et al., 1983) (Table 3.1; Figure 3.3).

Due to the restricted range in SiO_2 most Harker variation diagrams simply produce a cloud of data points; consequently Zr (165 - 318 ppm) is used as the differentiation index on account of its apparent incompatibility during the fractional crystallization of these lavas (Figure 3.6). Within the basaltic andesites with increasing Zr (increasing degree of fractionation) there are sympathetic variations in TiO_2, MnO, K_2O, P_2O_5, Ba, Rb, Th, Y, Ta, Nb and REE: Fe_2O_3 forms a scatter, though a poor positive correlation may exist: Na_2O remains essentially constant: Al_2O_3, CaO, Sr, $(Ce/Yb)_N$ and Eu/Eu* show pronounced anticorrelations: MgO, Cr, Ni and Y exhibit clouds with no defined trends. These variations support the

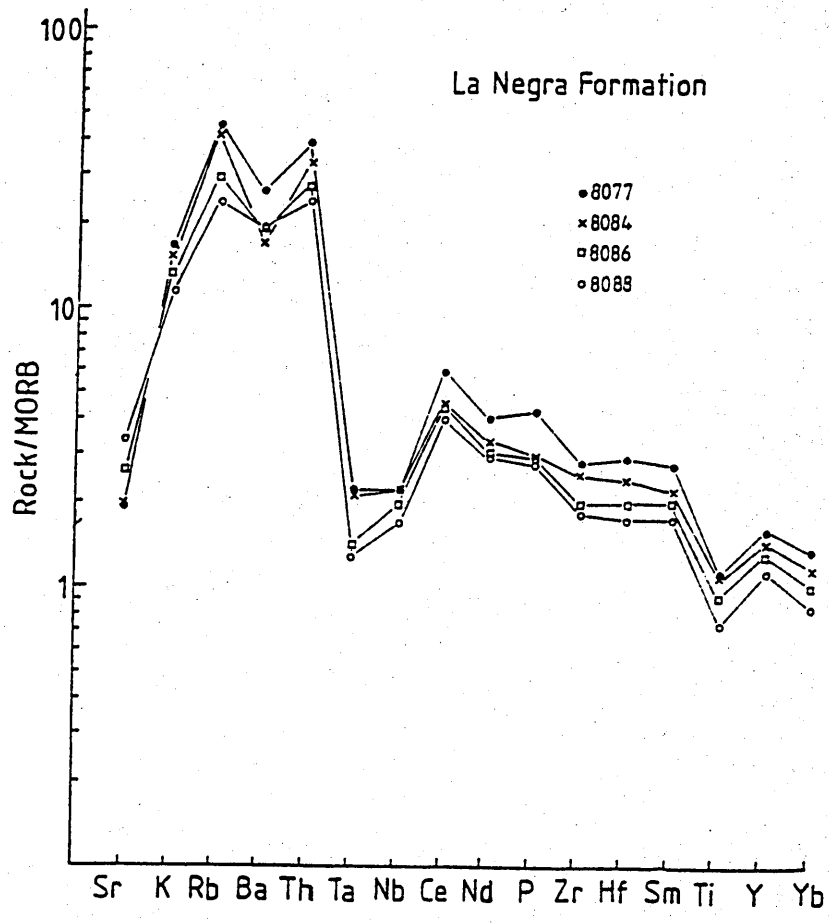

Figure 3.4

MORB normalised plot of the La Negra Formation

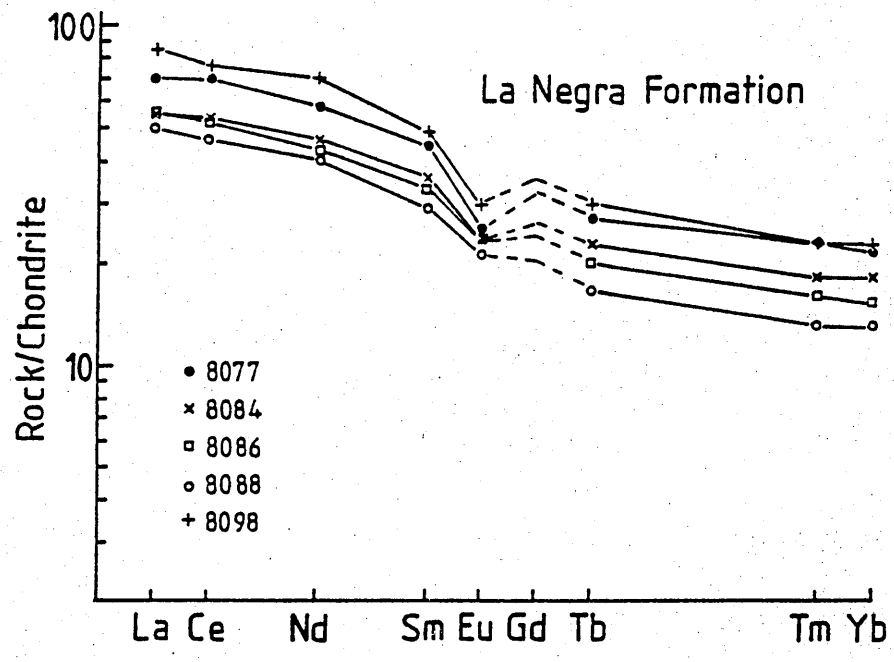

Figure 3.5

Chondrite normalised REE plot for selected lavas of the La Negra Formation.

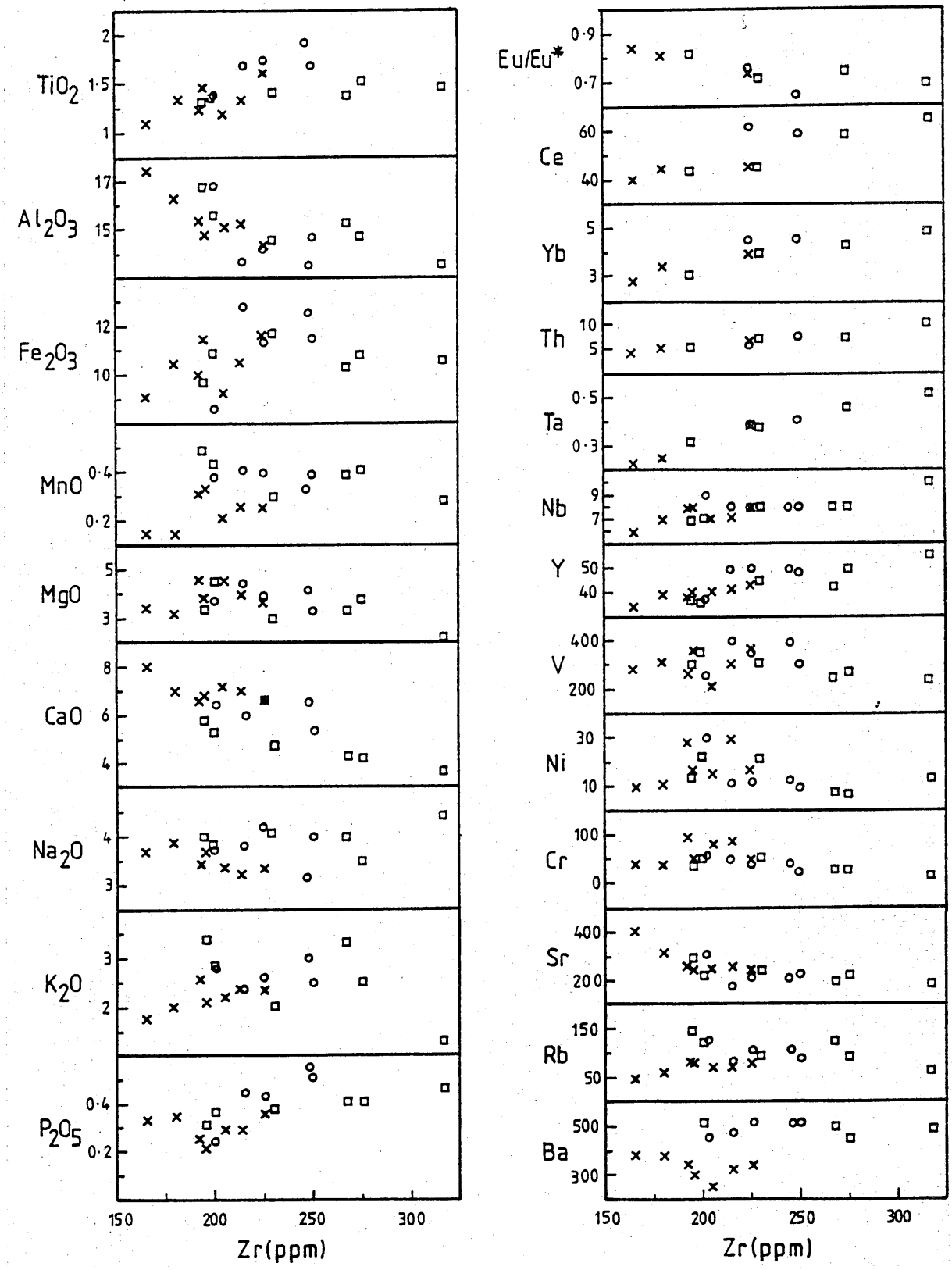

Figure 3.6

Variation diagrams for the La Negra Formation using Zr as the fractionation index. O = Lower Group: × = middle group: □ = upper group. See text for discussion.

Table 3.1 Comparison between the La Negra Formation, a high alumina basalt from Antuco, southern Chile, and two ensialic marginal basin lavas

	8088 La Negra	Bustamante Hill[a]	Puente Piedra[b]	801[c] Antuco
SiO_2	53.81	52.23	49.31	53.23
TiO_2	1.10	0.99	0.84	0.80
Al_2O_3	17.49	16.38	17.93	21.52
Fe_2O_3	9.12[d]	3.64	4.31	-
FeO	-	7.26	4.57	5.66[e]
MnO	0.15	0.22	0.16	0.18
MgO	3.38	3.84	5.79	3.22
CaO	8.03	8.48	8.14	9.70
Na_2O	3.67	2.55	3.25	3.87
K_2O	1.73	2.23	2.08	0.49
P_2O_5	0.33	0.34	0.11	0.06
Rb	48	94	51	20
Sr	402	502	514	470
Ba	385	-	432	150
Y	34	36	26	-
Zr	165	137	71	-

(a) Bustamante Hill analysis from Levi et al. (1982)

(b) Puente Piedra analysis from Atherton et al. (1983)

(c) Antuco analysis from Lopez-Escobar et al. (1977)

(d) Total iron as Fe O

(e) Total iron as FeO

petrographic evidence that plagioclase is the dominant, and often only, phenocryst phase. The behaviour of Fe_2O_3, MgO, Cr and Ni on the one hand and TiO_2 and V on the other attest to the lack of major influence of olivine and clinopyroxene, and titanomagnetite respectively during low pressure fractional crystallization. Moreover, the positive correlation between Fe* (total iron as Fe^{2+}) and Fe*/Mg and the lack of variation in SiO_2 with increasing Fe*/Mg indicate tholeiitic fractionation trends (Figure 3.7). Low concentrations of MgO, Cr and Ni, however, militate against the lavas being in equilibrium with likely mantle compositions, and imply considerable fractionation involving olivine and clinopyroxene. This probably occurred primarily at depth, perhaps accompanied by minor plagioclase, prior to the final plagioclase dominated fractionation. If the liquid prior to low pressure fractionation lay close to the Di-Fo-An cotectic at high pressure (5 - 10 kbar) and was suddenly injected into a lower pressure magma chamber, then, given the expansion of the An phase volume with decreasing pressure, the resulting liquid would be capable of crystallizing only plagioclase. This in turn may have led to the observed tholeiitic low pressure fractionation trends. The presence, especially in the middle group of lavas (Section 3.2) of higher modal percentages of ferromagnesian minerals, suggests that low pressure fractionation of these phases did take place, but they were always subordinate to plagioclase. As mentioned earlier (Section 3.2) there is textural evidence for disequilibrium between various phases and the melt, and the scatter of data for MgO, Ni, Cr and Fe_2O_3 may reflect small degrees of accumulation and/or loss of olivine and clinopyroxene.

There is no systematic variation of any chemical parameter with height in the volcanic pile at Punta Ampa, although the lavas of the

middle group tend to have lower concentrations of incompatible elements and higher concentrations of Al_2O_3, CaO and Sr. Immobile incompatible element ratios (e.g. Zr/Nb) nonetheless are fairly constant throughout, implying derivation from a homogeneous source region with respect to these elements. The ratios of incompatible LILE (e.g. Rb/Ba), however, vary randomly, indicating the operation in the source of a process (or processes) which can fractionate LILE but leave the HFSE unaffected. (An alternative possibility, that those random variations are due to subsolidus alteration processes is discussed in Section 3.6). Furthermore, the general coherence of the variation diagrams at the same degree of fractionation for the different lava groups suggests that the same gross process was operative throughout. The inference from this lack of systematic variation with stratigraphy yet overall chemical unity is that melts at depth were periodically injected into lower pressure magma chambers (where they further fractionated), and were replaced by fresh batches of melt from a mantle source which was homogeneous with respect to HFSE. The number of flows erupted from any one higher level magma chamber is uncertain as it was not possible to sample every flow. It is apparent, however, that even within the larger groupings of the flows there must have been several injections of magma.

The minimum overall degree of fractionation involved during the higher level differentiation can be estimated using elements which are highly incompatible in this magma system, such Zr, Hf, P, Th, Ta and Nb. Taking samples 8088 and 8077 as being the least and most evolved respectively of the basaltic andesites (165 and 249 ppm Zr) the latter can be derived by 34% fractional crystallization from the former. These figures are further supported by moderately incompatible elements such as K_2O, Ba and Ce, assuming that plagioclase is the only crystallizing

phase. The addition of a little clinopyroxene makes little difference to the conclusions. If one assumes either 35% or 40% fractionation then the appropriate bulk K_D for Sr varies from 2.25 - 2.05, values entirely plausible for plagioclase crystallization in basic rocks (Arth, 1976; Lopez-Escobar et al., 1977; Cox et al., 1979). The degree of fractionation from a parental, primary mantle-derived magma is unknown, the extent of evolution being dependent upon several variables including the initial mantle concentration of a chosen element, the modal mineralogy of the source, the P, T, P_{H_2O}, P_{O_2}, conditions under which the source melts, the residual mineralogy, the degree and type of melting, the phase composition(s) of the fractionating assemblage(s), and the precise values for mineral/melt distribution coefficients and how these vary in multivariant space. (Confidence in the accuracy of the whole rock concentration is assumed). Choosing a highly incompatible element alleviates some of these problems, but the degrees of melting and crystallization remain unknown. However, an attempt to characterise the nature of the mantle-derived magma prior to low pressure fractional crystallization can be made if one assumes (somewhat arbitrarily) that this parental liquid had no Eu anomaly, and that to achieve this condition phases were added to sample 8088 (the least fractionated sample) in the relative proportions to those therein observed (i.e. $plag_{0.87}$, $cpx_{0.1}$, $opx_{0.01}$, $ol_{0.01}$, $mt_{0.01}$). The K_D's of Arth (1976) were used for all elements considered except Nb(Ta), Zr(Hf), Y and Ti (Pearce and Norry, 1979), and Tb which was estimated by linear interpolation between Gd and Dy from Arth (op. cit.); all K_D's are presented in Table 3.2. It was found that 50% fractional crystallization. was required to remove the Eu anomaly. Major elements were calculated assuming the same extract which produced 34% fractional cystallisation. between samples 8088 and 8077. The resulting composition is very similar to many of the high alumina basalts from southern Chile (Lopez-Escobar et al., 1977); high Al_2O_3, and CaO, moderate K_2O, LREE enriched

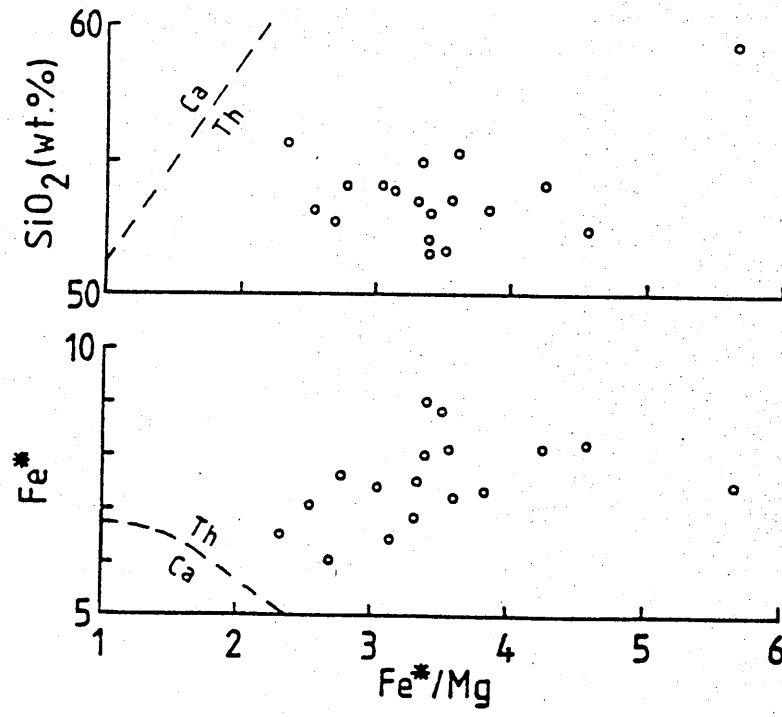

Figure 3.7

Fe*/Mg - Fe* and Fe* and Fe*/Mg - SiO_2 diagrams for the La Negra Formation illustrating the tholeiitic fractionation trends. Field boundaries are from Miyashiro (1973). Fe* = Total iron as Fe^{2+}.

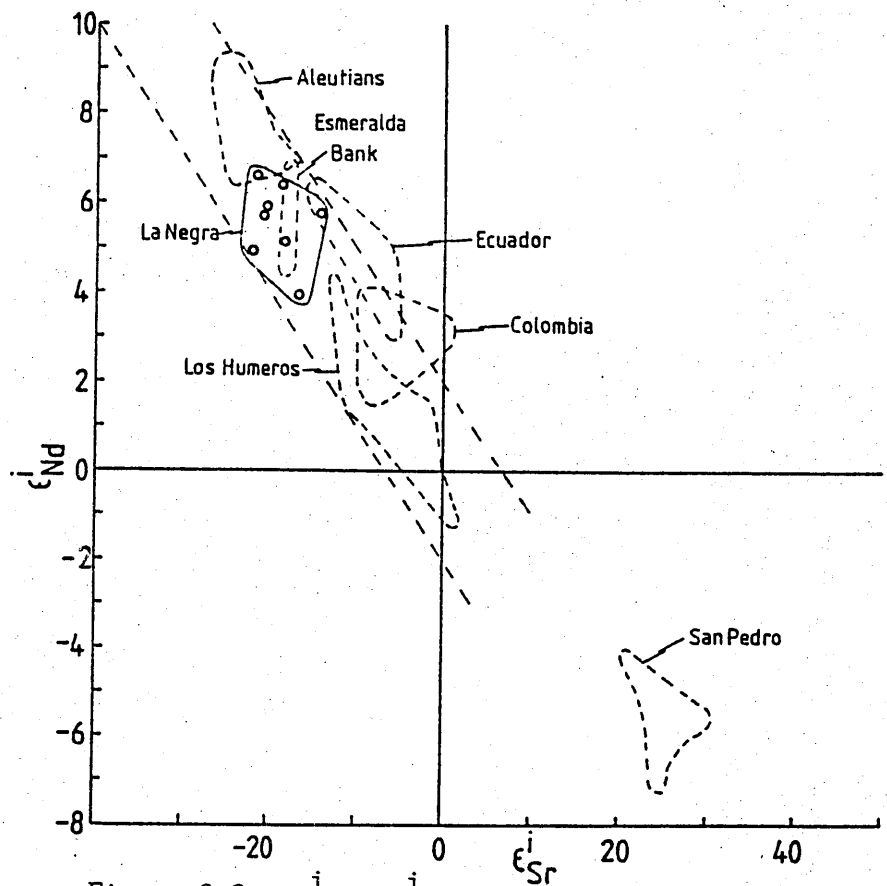

Figure 3.8 ε^i_{Sr} - ε^i_{Nd} diagram for the La Negra Formation. Data for the Aleutians; McCulloch and Perfit (1981); Morris and Hart (1983); White and Patchett (1984): Esmeralda Bank; Stern and Bibee (1980): Los Humeros; Verma (1983): Colombia; James and Murcia (1984): Ecuador and San Pedro (this work, Chapter 7).

Table 3.2 Distribution coefficients used in calculating the parental liquid to sample 8088

	Plag	Cpx	Opx	Ol	Mt
Rb	0.071	0.031	0.022	0.0098	0.01
Sr	1.83	0.12	0.017	0.014	0.01
Ba	0.23	0.026	0.013	0.0099	0.01
Y	0.03	0.5	0.2	0.01	0.2
Zr(Hf)	0.01	0.1	0.03	0.01	0.1
Nb(Ta)	0.01	0.1	0.15	0.01	0.4
Th	0.01	0.01	0.01	0.01	0.01
Ce	0.12	0.15	0.024	0.0069	0.01
Nd	0.081	0.31	0.033	0.0066	0.01
Sm	0.067	0.50	0.054	0.0066	0.01
Eu	0.34	0.51	0.054	0.0068	0.01
Tb	0.057	0.645	0.12	0.0087	0.05
Yb	0.067	0.62	0.34	0.014	0.2

Table 3.3 Comparison between the parental liquid to sample 8088, a high alumina basalt, low K tholeiite and MORB.

	La Negra parental liquid	Antuco[a]	Low K[b] tholeiite	MORB[c]
SiO_2	53.62	53.23	54.05	49.91
TiO_2	0.53	0.80	0.72	1.17
Al_2O_3	20.18	21.52	17.36	14.09
Fe_2O_3	6.73[d]	-	3.34	2.46
FeO	-	5.66[e]	6.35	8.14
MnO	0.08	0.18	0.17	0.17
MgO	3.59	3.22	5.21	8.15
CaO	10.57	9.70	9.95	11.89
Na_2O	3.40	3.87	2.37	2.21
K_2O	0.96	0.49	0.38	0.07
P_2O_5	0.16	0.06	0.09	0.14
Rb	25	20	4.9	1
Sr	611	470	241	83
Ba	222	150	116	38
Y	18	-	21	23
Zr	84	-	37	57
Nb	3.1	-	0.56	6
Ta	0.12	0.40	-	0.24
Th	2.41	2.00	-	0.22
Hf	2.15	1.70	0.63	1.7
Ce	21.7	18.8	5.61	6.0
Nd	13.6	10.3	-	5.9
Sm	3.13	2.49	-	2.09
Eu	1.02	1.01	-	0.78
Tb	0.47	-	-	0.50
Yb	1.56	1.60	1.28	2.14

(a) Antuco high alumina basalt (Lopez-Escobar et al., (1977)
(b) Low K tholeiite average for S.W Pacific (Ewart, 1982)
(c) MORB 409 - 2 63°N (Wood et al., 1979)
(d) Total iron as Fe_2O_3
(e) Total iron as FeO

$((Ce/Yb)_N \sim 3.5)$ and (by definition in this case) negligible Eu anomalies. It is not typical of island arc tholeiites or MORB (Table 3.3).

3.5 Isotopic characteristics

Initial Sr isotope ratios (i.e. at 186.5 Ma) vary from 0.70292 - 0.70346 (ε^i_{Sr} = -22.1 to -14.3), and show no correlation with differentiation index or stratigraphic position. The uniform values are low and imply negligible contamination by the continental crust during fractionation (Taylor, 1980; Hawkesworth, 1982; Hawkesworth et al., 1982). Initial Nd isotope ratios range from 0.512600 - 0.512739 (ε^i_{Nd} = +3.90 to +6.62) with all but one sample lying between ε^i_{Nd} = +4.48 and +6.62. The lavas all plot on or close to the mantle array in the depleted quadrant of an ε_{Sr}- ε_{Nd} diagram (Figure 3.8) similar to many Recent lavas from the Andes (Hawkesworth et al., 1979a; Stern and Futa, 1982; Hickey et al., 1984; James and Murcia, 1984; this study, Chapter 7) and to many other circum-Pacific arcs (e.g. DePaolo and Wasserburg, 1977; Stern and Bibee, 1980; Stern, 1981; McCulloch and Perfit, 1981; Verma, 1983). They were clearly derived from a source region with depleted time-integrated isotopic characteristics. This is in marked contrast to the Recent volcanics at this latitude (Chapter 7), and to the central Andes in general which show high $(^{87}Sr/^{86}Sr)_i$ and low $(^{143}Nd/^{144}Nd)_i$ (Hawkesworth et al., 1982; James, 1982). This could imply (i) that there has been a gross change in the isotopic characteristics of the mantle source region since the Jurassic (be this temporal and/or geographical); (ii) that the Recent lavas are derived by extensive crustal contamination of mantle-derived magmas with a depleted signature similar to La Negra; (iii) that the isotopic characteristics of material released

from the subducting slab have changed; (iv) that the variation is a combination of the end member possibilities.

3.6 Alteration effects.

As mentioned in Section 3.2 the La Negra volcanic pile has undergone burial metamorphism in the more porous tops and bottoms of flows, and along sedimentary and tuffaceous intercalations. There are several pieces of evidence to indicate that the geochemistry of the more massive flow-centres has not been substantially altered by this process. Firstly, the age presented in Section 3.3 of 186 Ma corresponds with faunal ages obtained from marine sedimentary intercalations in the formation near Antofagasta; if there had been significant mobilization of either Rb or Sr, or if there had been large scale interaction with a fluid of differing Sr isotopic composition then one would have expected the isochron systematics to have been drastically upset. Secondly, the rocks exhibit coherent trends on variation diagrams; again the effects of significant burial metamorphism would be expected to scatter the data, particularly the alkali, and alkaline earth elements. (The high Ba contents of 8092 and 8097 may be due to some alteration; it is significant that these rocks come from high in the pile at Punta Ampa close to the point above which extensive greenschist alteration is prevalent). Thirdly, the petrography indicates no albitization of plagioclase phenocrysts and there is little evidence of epidote growth. It is concluded that post-eruption alteration has had little effect on the geochemistry of the rocks studied in this formation.

3.7 Tectonic environment

The MORB normalised plot of the La Negra volcanics (Figure 3.4) emphasises the enrichment of LILE over HFSE. Such patterns are

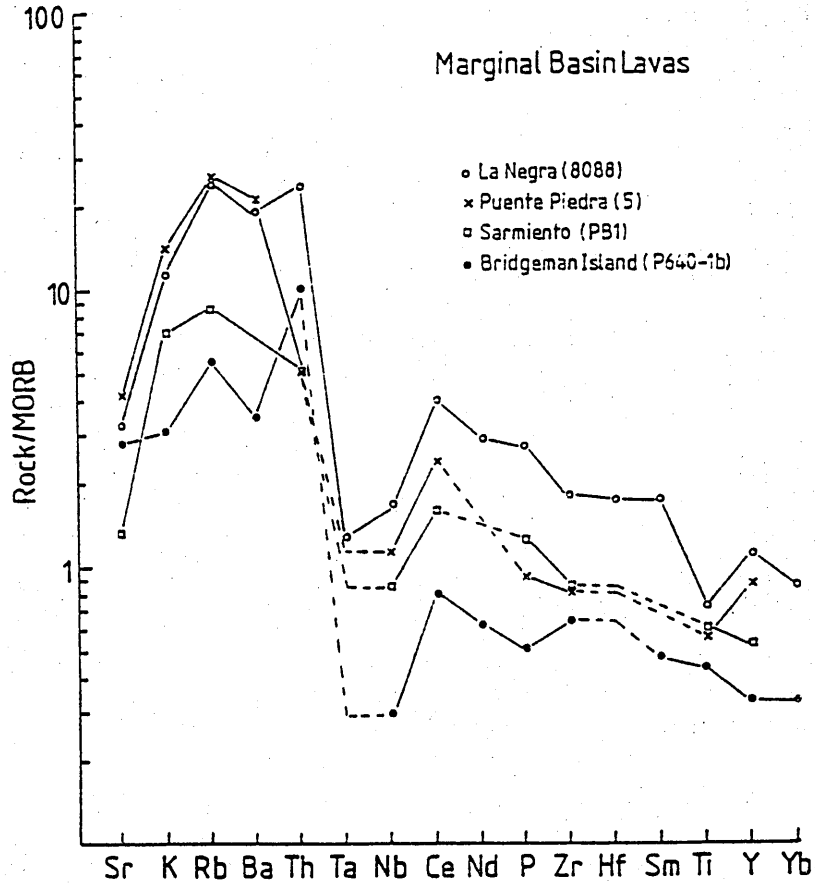

Figure 3.9

MORB normalised plot of the La Negra Formation (8088) compared to marginal basin lavas. Note that the latter also have depletions of Ta and Nb compared to LILE. Data sources: Sarmiento; Saunders et al. (1979): Puente Piedra; Atherton et al. (1983): Bridgeman Island; Weaver et al. (1979).

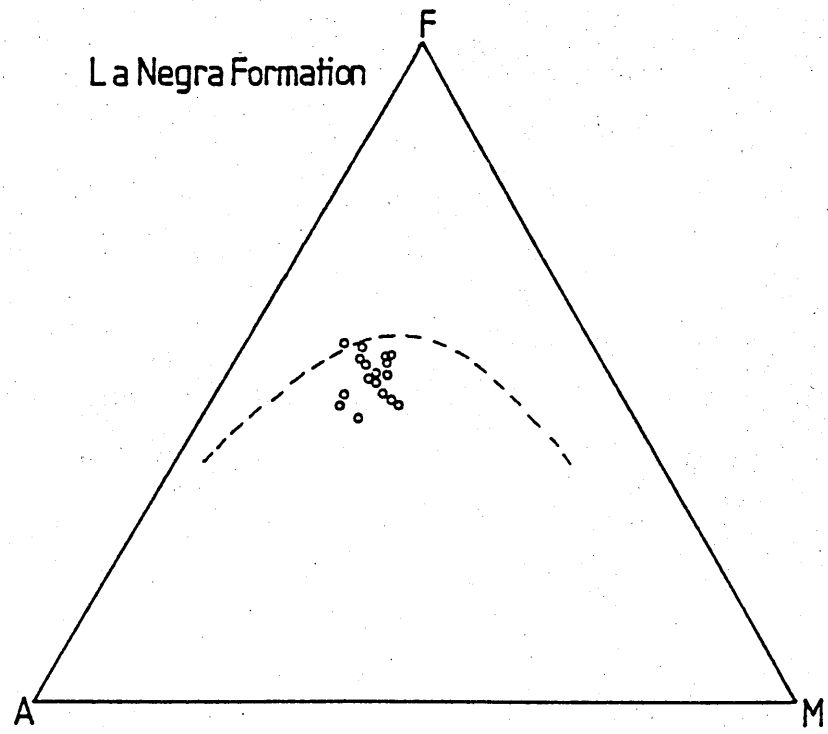

Figure 3.10

AFM diagram for the La Negra Formation

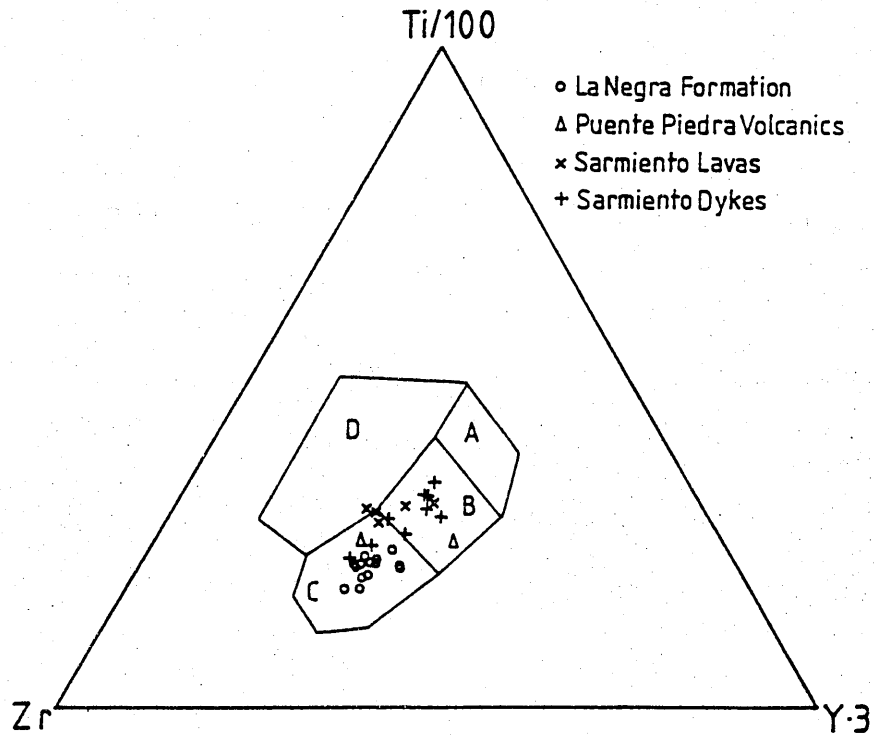

Figure 3.11

Ti-Y-Zr discriminant diagram for the La Negra Formation and other marginal basin igneous rocks. Data sources: Puente Piedra; Atherton et al. (1983): Sarmiento; Saunders et al. (1979). Field boundaries from Pearce and Cann (1973). A = Low K Tholeiites, B = Low K Tholeiites, Calc-alkali basalts, ocean floor basalts, C = Calc-alkali basalts, D = Within plate basalts.

characteristic of subduction-related magmas (Hawkesworth, 1982; Pearce, 1982; Hole et al., 1984) though ensialic marginal basin lavas may also display these features (e.g. Bransfield Strait (Weaver et al., 1979); Sarmiento, S. Chile (Saunders et al., 1979); Huarmey Basin, Peru (Atherton et al. 1983) and the review by Saunders and Tarney (1984); Figure 3.9). The low value for Sr and the overall elevated level of the pattern when compared to those for other arcs (Pearce, 1983) is due to the extensive fractional crystallization which for incompatible elements merely translates the curve higher and does not alter its fundamental shape. The high Th/Ta, Ce/Ta and Zr/Nb ratios are also more typical of island arcs than continental arcs (Pearce, 1983). On an AFM diagram the lavas fall in the calcalkaline field (Figure 3.10) and likewise on a Ti-Y-Zr plot (Pearce and Cann, 1973; Figure 3.11), similar to other marginal basin magmas.

The critical question regarding the La Negra Formation is whether the lavas, erupted in an extensional regime, presumably through fissures, represent an arc or a marginal basin setting. In these areas it appears that the subduction zone component of destructive margins is inherited by the magmatism behind the arc particularly during the initial stages of spreading. Thus, in the 'Rocas Verdes' of southern Chile the lavas of the Sarmiento ophiolite complex (51^{o}S: Dalziel, 1981; Dalziel et al., 1974) have slightly LREE enriched profiles, whereas those from the Tortuga complex (55^{o}S) have LREE depleted patterns (Saunders et al., 1979; Saunders et al., 1982). This difference correlates with the width of the marginal basin, the former being from a much narrower part of the basin. At the inception of back arc spreading, therefore, magmas may tap subduction-related fluids derived from the nearby descending slab. With continued spreading and basin widening the

subduction zone becomes progressively further removed from this locus of spreading, and the ensuing lavas reflect the composition of the associated unmodified mantle to a greater extent, as in the case of the Tortuga complex. (For a review of the putative mechanics of back arc spreading see Saunders and Tarney, 1984). It is interesting to note that the lavas most closely related geochemically to the La Negra Formation are the Puente Piedra volcanics from Peru, the oldest rocks in the Huarmey basin, and which are thought to represent the initial stages of back arc spreading (Atherton et al., 1983). These rocks are described as being mainly high-K, but calcalkaline and low-K tholeiites do occur (Figure 3.3). Analogous to this is the presence in the section at Punta Ampa of the calcalkaline andesite, and of low-K, calcalkaline and high-K series rocks over a wider area of the La Negra (Palacios, 1978). It is probable, therefore, that the La Negra Formation represents the first stages of marginal basin formation; in the case of northern Chile this basin aborted and mafic crust was not generated as in southern Chile.

3.8 Mass balance considerations

Utilising the mantle-normalised plot and methodology of Pearce (1983) it is possible to determine the approximate relative contributions of the subduction zone and the overriding mantle to the incompatible element geochemistry of subduction-related volcanics. Certain assumptions are paramount to this approach, most notably that the elements Ta, Nb, Zr, Hf, Y and Yb are not released from the slab during subduction as their reasonably high ionic potentials render them immobile in aqueous fluids. Furthermore, fractional crystallization of basaltic assemblages (olivine + clinopyroxene + orthopyroxene + plagioclase + magnetite) will only affect the level of the plot and not the overall shape (with the exception Ti and

Sr which are compatible in magnetite and plagioclase respectively); ratios of elements which are incompatible in the crystallizing phases also remain constant. In the calculations performed herein the technique of Pearce (op. cit.) was employed with some minor modifications.

(i) Nd was introduced into the diagrams between Ce and P_2O_5: its normalising value was taken to be 8.8 ppm.

(ii) In determining the boundary between the subduction and mantle components Ce, Nd and P were obtained by linear interpolation between Zr and Nb.

(iii) Due to the negative Ti anomalies in the plots the position of Ti for the purposes of the aforementioned boundary construction was obtained by a linear regression of Yb and Y. Sm was then determined by linear interpolation between the new Ti and Hf.

The results of these calculations are presented in Table 3.4. It is apparent that for all the rocks studied the subduction zone component contributes > 80% of all the alkalis and Th: furthermore, the range shown by each individual element of this group is very restricted. The LREE and P show a wider spread of subduction zone contribution with each element having a comparable range of between 14-18% though at differing percentage levels, the relative contributions decreasing in the order Ce > Nd > P > Sm. A significant subduction zone influence in the Sr content of the La Negra Formation might also be expected, but this cannot be determined directly from the whole rock analysis due to the compatible behaviour of Sr in plagioclase. It is possible, however, to obtain an approximation to this contribution by considering the liquid calculated in Section 3.3 (Table 3.3) in which the effects of low pressure fractionation have been removed. If it is assumed that prior to this stage Sr behaved incompatibly then the subduction zone contribution of Sr can be

Table 3.4 Subduction zone contributions (%) for the La Negra Formation

Sample	8077	8080	8088	8086	8084	8092	8092A	8097	8098
K	86	87	86	88	85	92	85	84	68
Rb	95	96	94	94	95	97	95	96	92
Ba	91	91	91	91	87	96	89	98	89
Th	94	93	94	94	93	93	91	94	95
Ce	59	62	57	55	49	54	58	53	57
Nd	37	45	39	35	27	36	38	33	31
P	38	32	35	32	18	18	16	21	14
Sm	13	20	10	11	6	17	10	6.4	5.7

Table 3.5 Subduction zone contributions for selected elements in the parental liquid to sample 8088

Elememt	Sr	K	Rb	Ba	Th	Ce	Nd	P	Sm
%	82	87	94	93	94	59	41	31	14

ascertained. The contributions have also been determined for the same range of incompatible elements as in Table 3.4 and are presented in Table 3.5. As expected, this shows that, within the limitations of the model, the values are the same as for sample 8088 (the whole rock from which the parental liquid was derived). The subduction zone contribution of Sr is also high at 82%.

Figure 3.12a is a plot of ε^{i}_{Nd} against the subduction zone contribution of Nd (% Nd_{sz}). With the exception of the low $\varepsilon^{i}Nd$ sample (8086) noted earlier the lavas portray a broad negative correlation. This intersects 0% Nd_{sz} at about ε^{i}_{Nd} = +10 and 100% Nd_{sz} at about ε^{i}_{Nd} = -2. These values respectively represent the Nd isotopic composition of the overriding mantle wedge prior to the addition of the subduction zone component, and the Nd isotopic composition of the subduction zone component itself. This technique for estimating the isotopic composition of mantle and subduction zone components may be particularly valuable in oceanic arcs where the potential for crustal contamination is minimised.

Whilst these calculations can be made with isotope ratios which remain constant during equilibrium partial melting and closed system fractional crystallization problems arise when attempting to quantify elemental parameters. In particular the concentrations of ultra-incompatible elements increase by $\sim 1/F$ during partial melting (F = proportion of melt formed), and again by about 1/F during fractional crystallization (F = fraction of melt remaining); therefore estimates have to be made as to the effects of these respective processes. This is a problem fraught with uncertainities as outlined earlier (Section 3.4). Nonetheless reasonable assumptions and constraints can be made, and a

Figure 3.12 a.

ε^{i}_{Nd} against $\%Nd_{SZ}$ for the La Negra Formation. The ε^{i}_{Nd} value of the mantle source is where $\%Nd_{SZ} = 0$ (i.e. $\varepsilon^{i}_{Nd} \sim +10$); the ε^{i}_{Nd} value of the subduction zone component is at $\%Nd_{sz} = 100$ (i.e. $\varepsilon^{i}_{Nd} \sim -2$). See text for discussion.

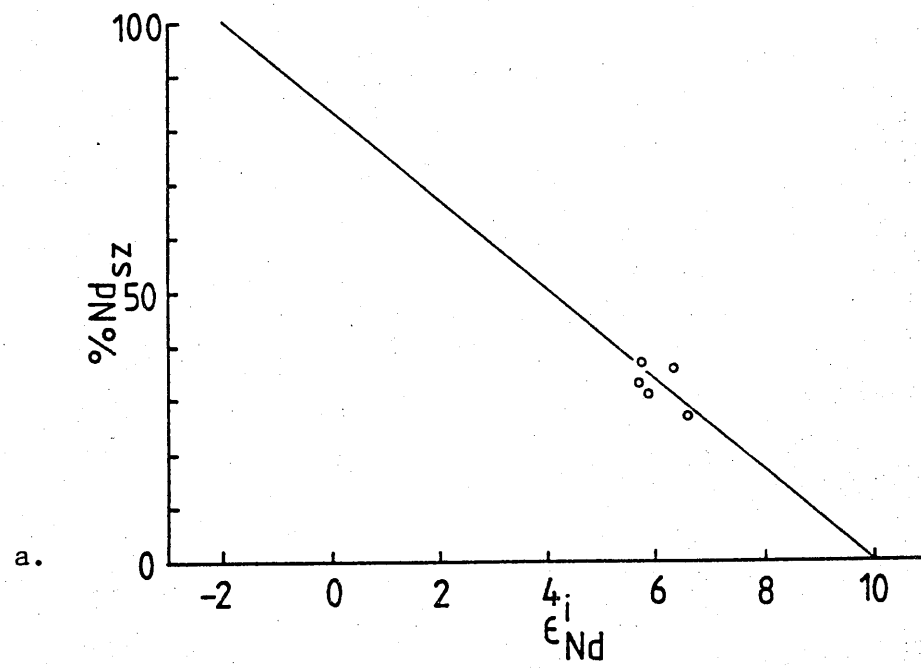

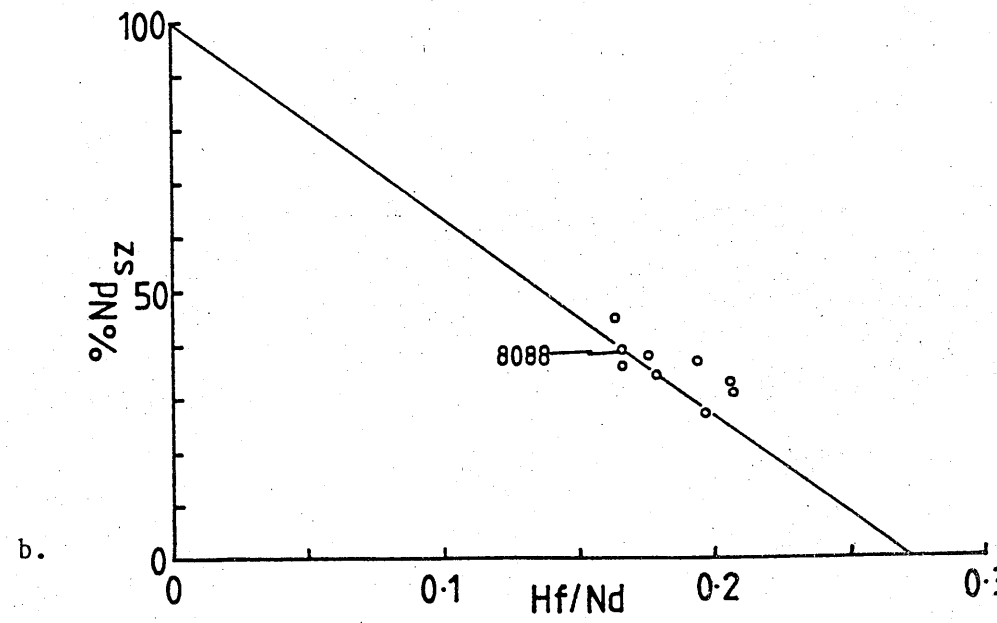

Figure 3.12 b.

Hf/Nd - $\%Nd_{sz}$. The Hf/Nd ratio of the mantle source is constrained to be where a line from Hf/Nd = 0, $\%Nd_{sz}$ = 100 through any point intersects $\%Nd_{SZ} = 0$. A line through sample 8088 is illustrated.

range of likely concentrations calculated for each element for any given stage in the procedure. One technique available for minimizing some of the limitations is to monitor ratios of elements which have similar bulk distribution coefficients in both melting and fractionating assemblages as these should remain essentially constant.

The problem of elemental concentrations in the overriding mantle prior to subduction can be addressed by considering a ratio such as Hf/Nd. If the magma from which a lava was generated were wholly derived from material released from the slab then it would have an Hf/Nd ratio of 0 (as no Hf is released from the slab) and Nd_{sz} = 100%. Conversely if a magma were wholly derived from the mantle with no slab input then its Hf/Nd ratio will closely reflect that in the source (given the slight differences in bulk K_D between Hf and Nd in basaltic phase assemblages) and Nd_{sz} = 0%. In Figure 3.12b Hf/Nd is plotted against the percentage of Nd from the subduction zone (% Nd_{sz}) producing an anticorrelation intecepting the $\%Nd_{sz}$ axis at 100% Nd_{sz} and Hf/Nd = 0. Extrapolating this line to $\%Nd_{sz}$ = 0 gives the value of Hf/Nd in the mantle prior to the addition of the subduction zone component. Assuming a mantle concentration for Hf the Nd concentration can thus be determined. It is alternatively possible to construct a series of lines by simple interpolation between Hf/Nd = 0, 100% Nd_{sz} and each point of the rock suite. This produces a narrow range of Hf/Nd ratios for the mantle and thus a range in mantle Nd concentrations. Similar plots can also be constructed for other LILE involved in the subduction zone component, and a spectrum of concentrations calculated. HFSE concentrations can be calculated directly from the whole rock Hf/HFSE ratios. Concentrations determined for 8088 (high $\%Nd_{sz}$) and 8084 (low $\%Nd_{sz}$) are presented in Table 3.6 and

Table 3.6 Unmodified mantle concentrations

Sample	8084	8088	Parental liquid of 8088
Ce	1.96	1.93	1.97
Nd	1.76	1.74	1.77
Sm	0.564	0.586	0.595
Tb	0.098	0.98	0.104
Yb	0.332	0.321	0.345
Sr	-	-	24.2
K(%)	0.029	0.027	0.028
Rb	0.349	0.324	0.331
Ba	3.65	3.89	3.43
Th	0.039	0.032	0.032
P(%)	0.025	0.024	0.024
Ta	0.032	0.026	0.027
Nb	0.667	0.674	0.685
Zr	18.77	18.55	18.55
Hf[1]	0.475	0.475	0.475
Y	3.58	3.82	3.98
$(Sm/Nd)_m$	0.320	0.337	0.336

1. Hf concentration assumed

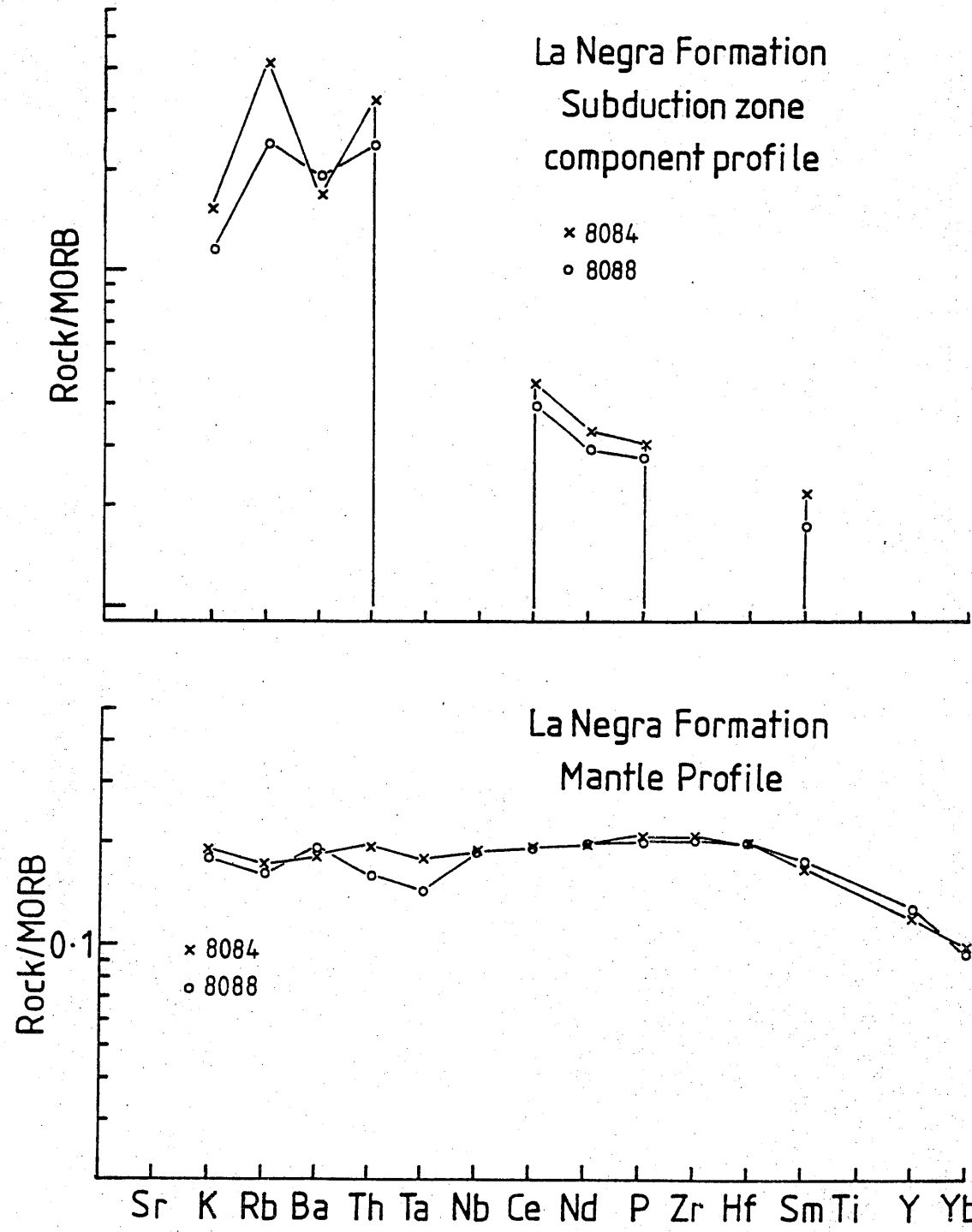

Figure 3.13

MORB normalised profile for the mantle sources of samples 8084 and 8088 calculated assuming Hf_{mantle} = 0.475 ppm (Table 3.6). The profiles of the respective subduction zone components are also shown, but these are dimensionless as absolute concentrations cannot be determined.

plotted on a MORB normalised diagram in Figure 3.13. Also shown on this diagram is the shape of the pattern for the subduction zone component, though this is dimensionless as the absolute concentrations cannot be determined. Chondrite normalised REE patterns for the sources of 8088 and 8084 are plotted in Figure 3.14. The curves for the two samples are almost coincident and show slight LREE enrichment with $(Ce/Yb)_N$ = 1.50 - 1.53. Sm and Nd, however, show more enhanced concentrations, and thus $(Sm/Yb)_N$ = 1.84 - 1.98 and $(Ce/Sm)_N$ = 0.81 - 0.82. The overall pattern has a humped appearance.

Other non slab derived HFSE (e.g. Ta, Zr, Nb) may be substituted for Hf as the numerator in these ratio plots; analogous anticorrelations are apparent and corresponding interpolations can be made regarding the respective mantle ratios. By keeping the Hf content of the mantle inviolate, and having calculated a corresponding denominator concentration in the mantle (e.g. Nd, Sm, etc.) one can further determine the concentrations of other HFSE numerators. Inter LILE ratios (e.g. Sm/Nd) of the mantle can be determined without assuming any mantle concentrations:

$$(Sm/Nd)_m = (Hf/Nd)_m/(Hf/Sm)_m$$

where $(Hf/Nd)_m$ = the Hf/Nd ratio at 0% Nd_{sz}

$(Hf/Sm)_m$ = the Hf/Sm ratio at 0% Sm_{sz}

This value can be checked for internal consistency by performing identical manipulations of other pairs of ratios (e.g. Zr/Nd and Zr/Sm). For sample 8088 the calculated $(Sm/Nd)_m$ = 0.3369 using Hf as the numerator, whereas the value based on Zr is 0.3372. It is noteworthy that despite the crude approximations of the model these results are remarkably consistent.

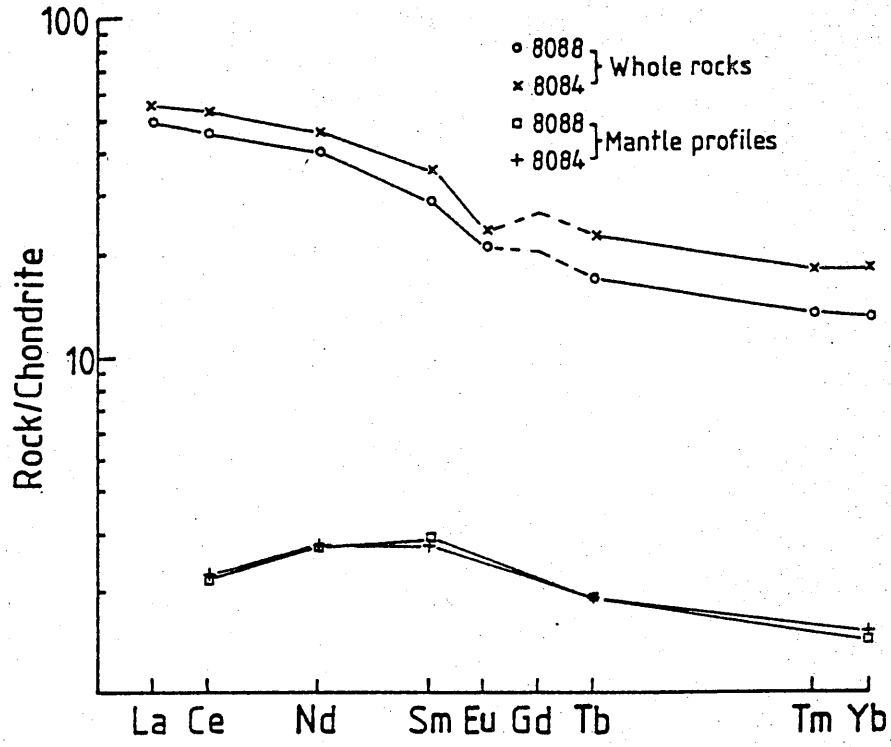

Figure 3.14

Chondrite normalised REE profiles for samples 8088 and 8084 and their computed mantle sources, assuming Hf_{mantle} = 0.475 ppm.

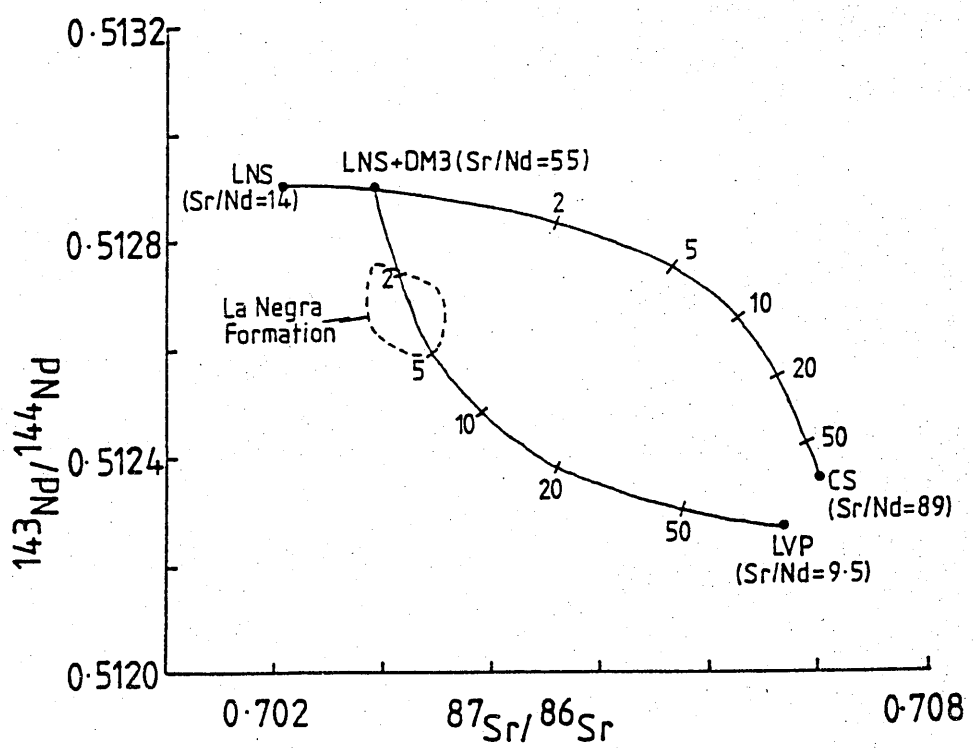

Figure 3.15

A binary mixing curve between the calculated source of the La Negra Formation (LNS) and calcareous sediment (CS) is used to illustrate the general effect of mixing LNS with a high Sr/Nd component. The binary mixing curve between a combination of LNS and a dehydrated MORB (DM3, Table 3.7) and low Sr/Nd continental detritus represented by the average Limon Verde pluton (LVP) pass through the data for the La Negra Formation. Values along the curves indicate the percentages of CS and LVP in the mixtures.

Table 3.7a End Member parameters used in mixing calculations

End Member	$^{87}Sr/^{86}Sr$	$^{143}Nd/^{144}Nd$	Sr	Nd	Sr/Nd
La Negra source (LNS)	0.70208	0.512911	24.2	1.77	13.7
Seawater[1] (S)	0.7070	0.512360	8	0.0027	2963
Calcareous sediment[2] (CS)	0.7070	0.512360	1234	13.9	88.8
Dehydrated MORB (DM1)	0.7050	0.512911	150	0	
Dehydrated MORB (DM2)	0.7050	0.512911	670	0	
Dehydrated MORB (DM3)	0.70298	0.512911	670	0	
Limon Verde Pluton (LVP)	0.70666	0.512269	284	30	9.5

1. Data from Brass (1976), Piepgras and Wasserburg (1980) and Hawkesworth and van Calsteren (1983).

2. Data sources as above and Hole et al. (1984)

Table 3.7b Results of mixing calculations

Model	Mixing Proportions	$^{87}Sr/^{86}Sr$	$^{143}Nd/^{144}Nd$	Sr	Nd	Sr/Nd
LNS + S	38% S	0.70292	0.512911	18.0	1.09	16.5
LNS + CS	0.4% CS	0.70292	0.512911	29.0	1.82	15.9
LNS + DM1	6.1% DM1	0.70292	0.512911	31.9	1.66	19.2
LNS + DM2	1.4% DM2	0.70292	0.512911	33.2	1.75	19.0
LNS + DM3	9.8% DM3	0.70292	0.512911	87.5	1.60	54.7
(LNS + DM3) + LVP	2.5% LVP	0.70315	0.512700	92.4	2.31	40.0

Similar calculations can be performed for Sr to ascertain the Sr/Nd ratio of the original mantle, but using the fractionation corrected concentrations in Table 3.3. Using Hf and Zr as the numerators yields $(Sr/Nd)_m$ = 13.7 in both cases: this value is similar to N-type MORB (Pearce, 1982; Hole et al., 1984). If regressions analogous to those used earlier for sample 8088 are performed and an original mantle concentration for Hf of 0.475 ppm is assumed then the mantle concentrations of Nd and Sr are 1.77 ppm and 24.2 ppm respectively: this in turn gives a $(Sr/Nd)_m$ ratio of 13.7, in accord with those obtained independently above. The Nd value is also consistent with that calculated directly from the whole rock analysis of 8088 (1.74 ppm; Table 3.6).

Given the constraint that the mantle endmember should lie on the mantle array (i.e. ε^i_{Sr} = -34) it is possible to characterise the subduction zone component more closely. A binary mixing curve (Vollmer, 1976; Langmuir et al., 1978) between the mantle end member and the bulk subduction zone component passing through the data for the La Negra Formation on an ε_{Sr}- ε_{Nd} diagram (Figure 3.15) constrains the Sr/Nd ratio of the latter end member to be no higher than that of the former (i.e. $\sim$14). However, many basic lavas in volcanic arcs have high Sr/Nd ratios (e.g. Lopez-Escobar et al., 1977; Hawkesworth et al., 1982), and the calculated parental liquid to sample 8088 also has a high Sr/Nd ratio (45). Consequently the introduction of the subduction zone contribution must be a multistage process involving mixing between the mantle end member and a high Sr/Nd component, followed by mixing between this hybrid and a low Sr/Nd component. There are several putative candidates for these two end members, details of which are given in Table 3.7a.

Mixing between seawater and the mantle source of the La Negra Formation is constrained by the Sr isotopic composition of the lavas to 38% seawater; however, the resultant mixture has a low Sr/Nd ratio of 16.5 (Table 3.7b). Calcareous sediments may also be involved in the initial mixing event as they, too, have high but variable Sr/Nd ratios (44 - 186, Hole et al., 1984). In this instance their involvement is limited to a maximum of 0.4%, but again the Sr/Nd ratio (15.9) is too low. Both hydrothermal alteration at ridge crests and low temperature seafloor alteration increase the $^{87}Sr/^{86}Sr$ ratios and Sr contents of MORB (Hart et al., 1974; Staudigel et al., 1981; Cohen and O'Nions, 1982) whilst the $^{143}Nd/^{144}Nd$ ratios and Nd content remain unaffected due to the low concentration of Nd in seawater. Whilst it is difficult to quantify dehydration of this subducted lithosphere it is expected that the fluid derived therefrom will have high $^{87}Sr/^{86}Sr$ ratios (> 0.705), $^{143}Nd/^{144}Nd$ ratios (ε_{Nd} = +10) and Sr contents (>150 ppm) and low Nd contents ($\sim$0) resulting in a high Sr/Nd ratio. Mixing of a maximum of 6.1% of this dehydration product (DM1, Table 3.7b) with the mantle source of the La Negra Formation raises the $^{87}Sr/^{86}Sr$ ratio to that of the lavas, but only results in an Sr/Nd ratio of 19.2. Raising the Sr content of the dehydration product to 670 ppm still only yields a Sr/Nd ratio of 19.0. Only if the Sr isotopic composition of the "altered" MORB is very close to that of the La Negra lavas can the Sr/Nd ratio of the mixture be raised sufficiently (DM3, Table 3.7b). It thus appears that this part of the subduction zone component is not readily identifiable with anything in the slab itself, and that its source must be in the overriding mantle itself. The subduction process, therefore, is the "catalyst" for generating the overabundance of Sr. The problem of reconciling relatively high Sr

contents with low $^{87}Sr/^{86}Sr$ ratios has also been noted in the Marianas (Hole et al., 1984) and in Baja California and southernmost Chile (Rogers et al., in press).

To lower the Nd isotopic composition of the hybrid to that of the lavas of the La Negra Formation requires the introduction of a component with a low Sr/Nd ratio and $\varepsilon^{186}_{Nd} \sim -2$ (to be in accord with the subduction zone component identified earlier). The average composition of the Limon Verde pluton at 186 Ma fulfils the specified criteria (Table 3.7a), and thus may be mobilised within the subduction zone. Its involvement is constrained to about 2.5%.

3.9 Summary and Conclusions

Field relationships, and geochemical studies of the La Negra Formation at Punta Ampa indicate the following conclusions:

(a) The lavas were erupted through fissures in an extensional environment to produce very thin flows, some of which are demonstrably subaqueous. The volcanic pile accumulated as imbricate sheets with a possible eastwards dip. Rb-Sr geochronology yields a Liassic age of 186 Ma, in agreement with palaeontological evidence from marine sedimentary intercalations.

(b) The geochemistry of the Formation at Punta Ampa consists mostly of high K calcalkaline basaltic andesites which have experienced pronounced low pressure plagioclase-dominated fractional crystallization. Correction for this process indicates that the parental liquid was similar to the high alumina calcalkaline basalts from southern Chile; MgO, Cr and Ni

contents imply earlier fractionation of olivine and clinopyroxene. The isotope geochemistry indicates that the lavas were derived from a source with time-integrated depleted characteristics. There is no evidence that crustal contamination played a significant role in the genesis of the lavas.

(c) More than 80% of Sr, K, Rb, Ba and Th, 50 - 60% Ce, and lesser amounts of Nd, P and Sm reflect the process of subduction. Using plots of these proportions against HFSE/LILE, and assuming an original mantle concentration for the HFSE in question, deductions can be made concerning elemental concentrations in the mantle prior to modification by the subduction zone component. Evaluation of the Nd isotopes with respect to the proportion of Nd from the subduction zone reveals that the mantle component had $\varepsilon^{186}_{Nd} \sim +10$ and that the subduction zone component had $\varepsilon^{186}_{Nd} = -2$. To satisfy Sr/Nd criteria the addition of the subduction zone contribution must be a multistage process involving the early addition to the mantle host of a high Sr/Nd component (possibly derived from within the mantle itself) and a later addition of a low Sr/Nd component: subducted detritus from the Limon Verde pluton is a suitable candidate.

(d) Whilst the lavas have a volcanic arc signature their morphology and their chemical similarity to the marginal basin Puente Piedra volcanics in Peru suggest that they too were erupted in an analogous tectonic setting. This contrasts with the view of Palacios (1978) who considered that they represented an island arc assemblage. If the La Negra Formation does represent an ensialic back arc basin then the arc itself has been removed; regional geological considerations suggest that it has been thrust under the continental margin.

CHAPTER 4

JURASSIC PLUTONISM

4.1 Introduction

The volcanic pile of the La Negra Formation is intruded by a large granite batholith elongated north-south and composed of several discrete entities. Rocks of the Toco Formation also suffered intrusion during the same episode in the Sierra de la Cruz (Figure 4.1). Several plutonic bodies were investigated in the present study, and each will be considered with respect to field relations and petrography, geochronology and geochemistry in order to elucidate their petrogenesis and to highlight similarities and differences between the intrusions.

4.2 Field Relations and Petrography

4.2.1 Gatico Pluton

Thirty kilometres south of Tocopilla the rocks forming the coastal escarpment comprise a granitic pluton which ranges in composition from quartz gabbro, through quartz diorite and quartz monzodiorite to granite (Figure 4.2). The intrusion of this pluton resulted in hornfelsing of the La Negra Formation for a distance of about 500 m, and the development of a mottled texture therein due to the growth of quartz. This contact metamorphism implies that the pluton was hot relative to the country rock. Abundant screens of hornfelsed lava are found close to the contact suggesting a stoping mode of intrusion. A component of shearing during emplacement is also evident from the gneissic texture of certain areas which contain blocks of lava and coarse-grained pluton. Aplite and pegmatite veins cut the lavas. It is unclear whether the lavas had already been tilted and/or had an original depositional dip prior to intrusion.

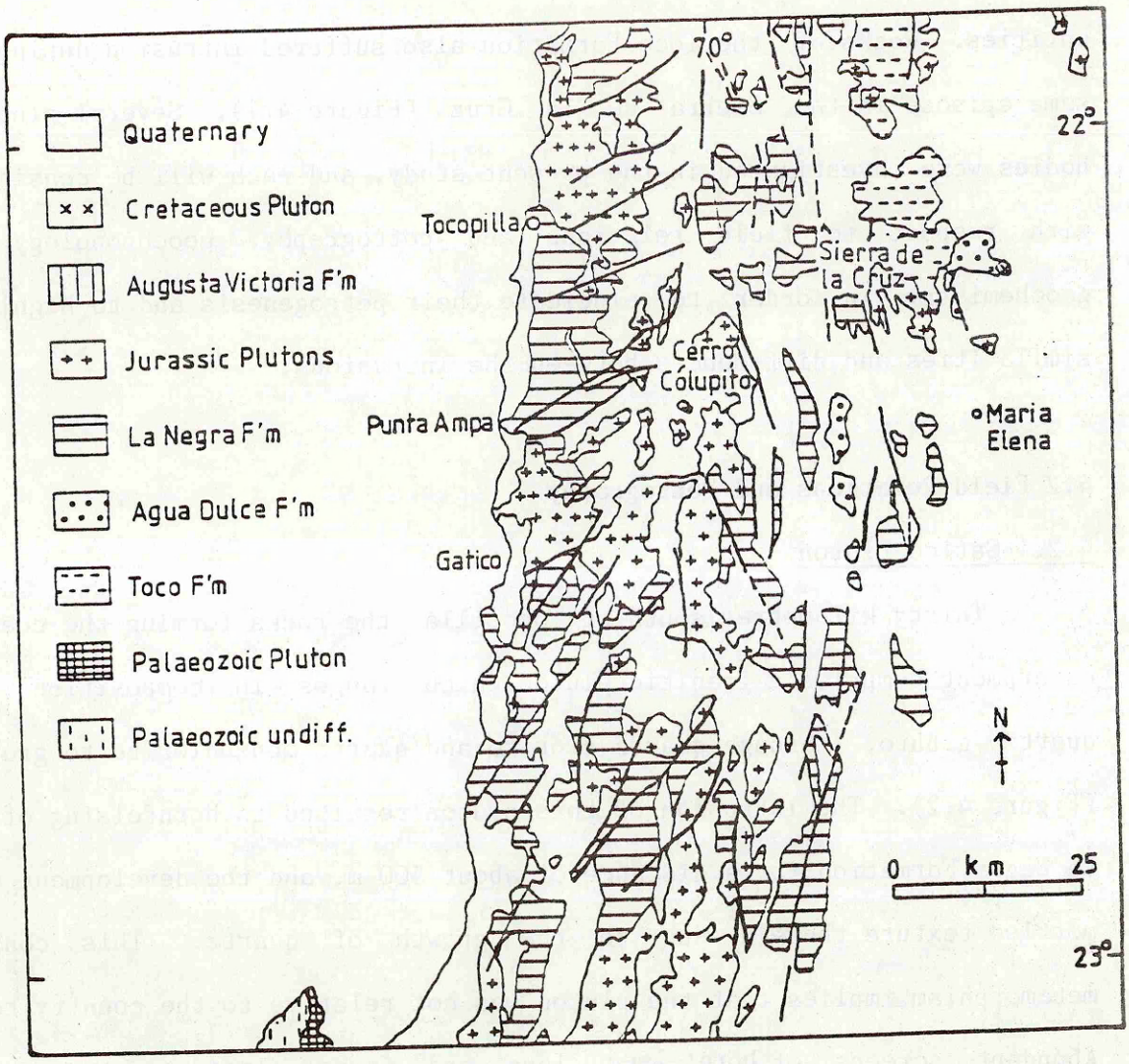

Figure 4.1

Generalised geological map showing the location of Jurassic plutons studied in this work (after Servicio Nacional de Geologia y Mineria, 1980).

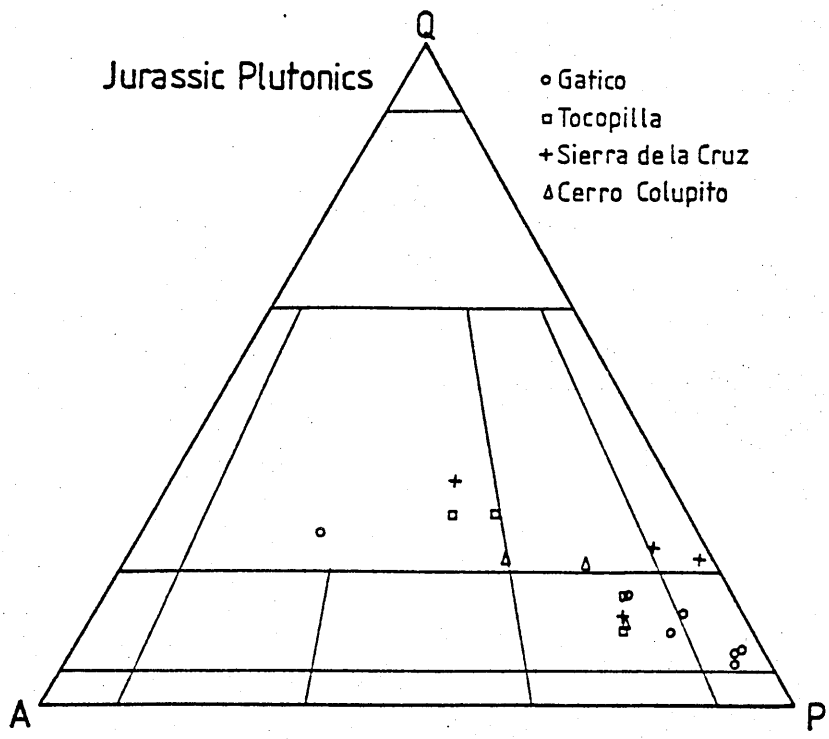

Figure 4.2

Modal QAP diagram for the Jurassic plutons

a.

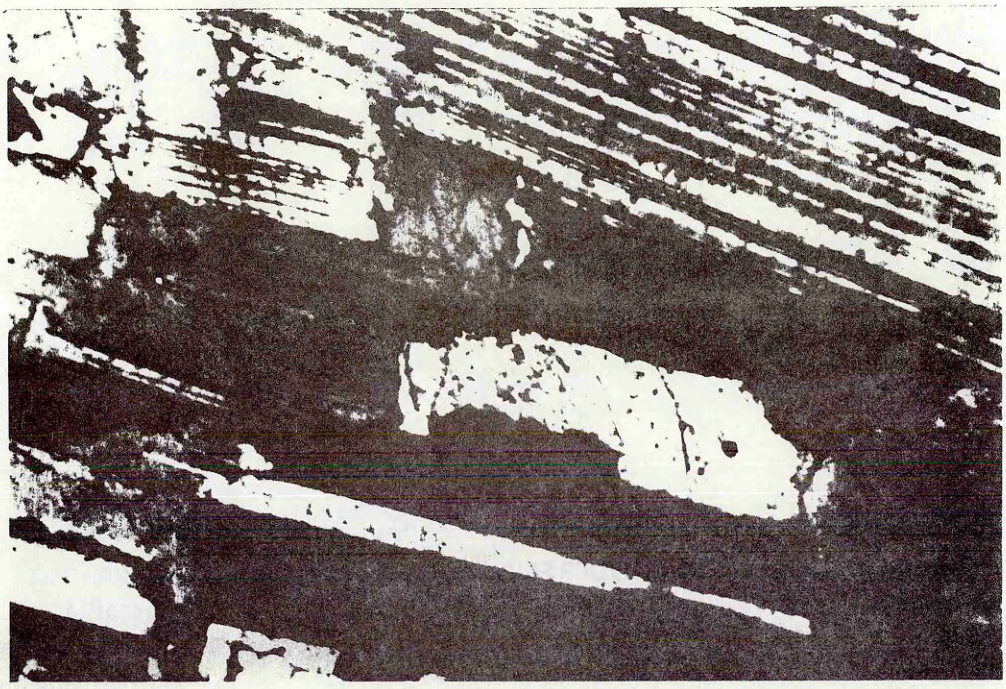

b.

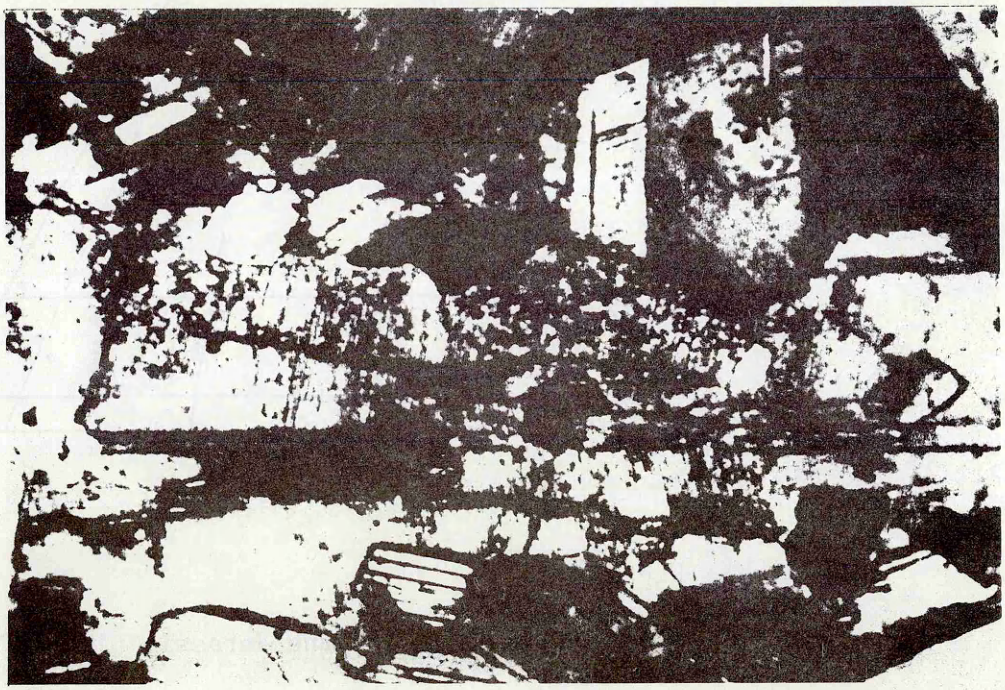

Plate 4.1a. Igneous lamination defined by plagioclase in quartz diorite (8062) with euhedral clinopyroxene (bottom right) and interstitial potassium feldspar (black) and quartz (cream).
XP. Field of view 3.47 mm.

Plate 4.1b. Herringbone twinned clinopyroxene in quartz diorite (8062).
XP. Field of view = 3.47 mm.

a.

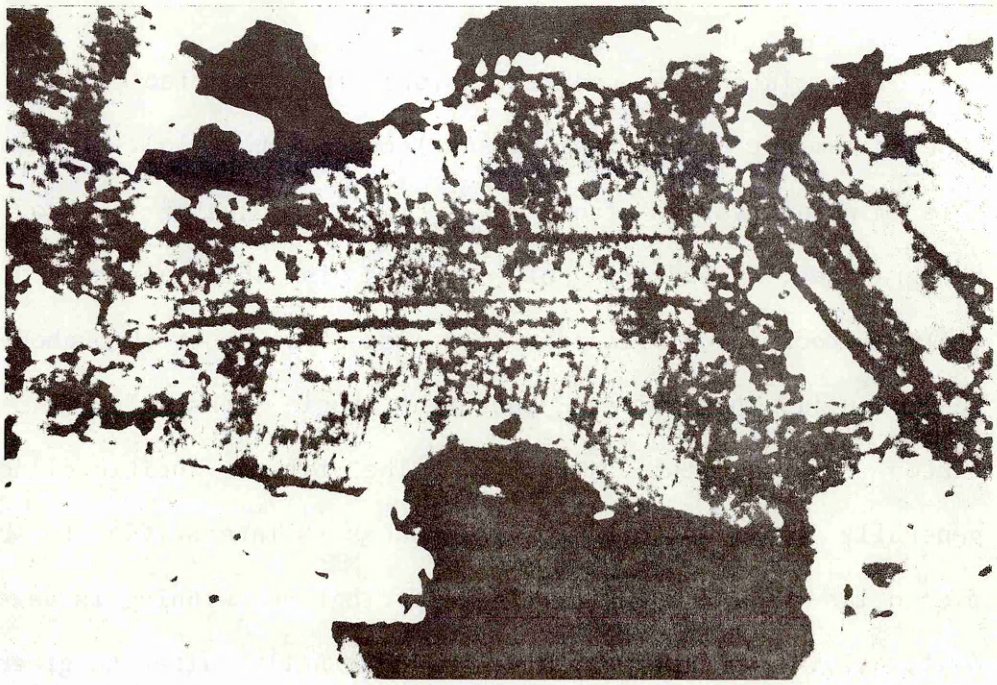

b.

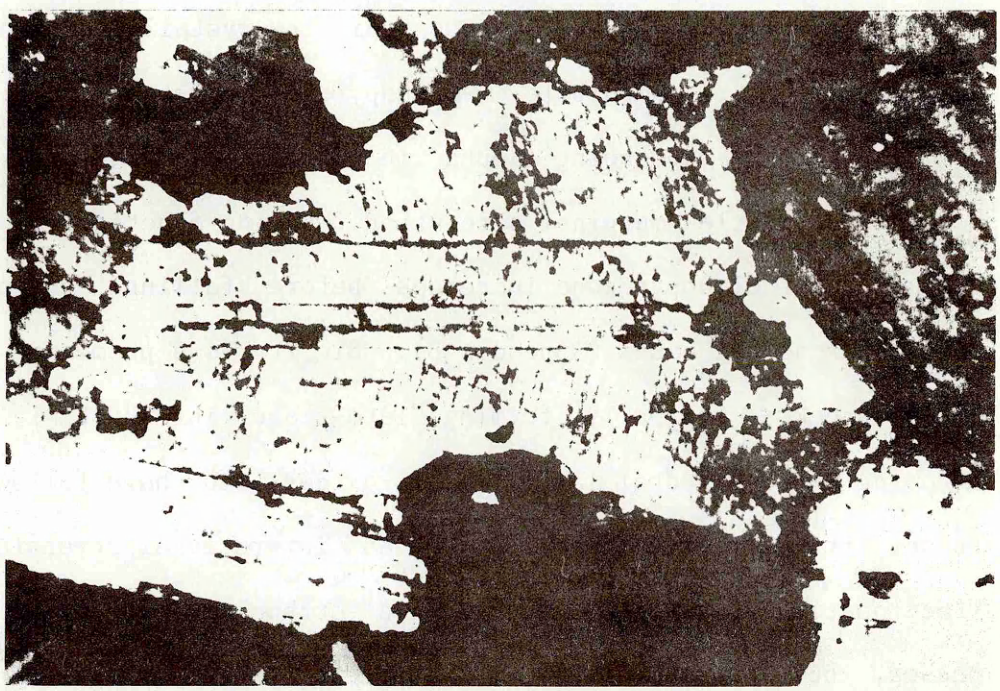

Plate 4.2a. Quartz diorite (8062) containing herringbone twinned clinopyroxene (pale brown - centre), orthopyroxene (very pale brown - right), biotite (orange), Fe-Ti oxides (black), plagioclase and quartz (colourless).
PPL. Field of view 3.47 mm.

Plate 4.2b. As above but note low birefringent orthopyroxene, twinned plagioclase and interstitial quartz (white).
XP. Field of view = 3.47 mm.

The pluton is coarsely crystalline, most facies displaying slight igneous lamination of plagioclase laths (Plate 4.1a). The composition of this mineral varies from An_{60} in the quartz gabbro to An_{20} in the granites. Weak zoning of crystals is only apparent in the more evolved rocks. Plagioclase has a euhedral habit throughout the pluton, being usually the earliest phase to begin crystallizing. Most of the pluton contains two pyroxenes. The first, augitic clinopyroxene, is generally euhedral, though in places is interstitial to early formed plagioclase. In the basic facies herringbone twinning is developed (Plates 4.1b, 4.2). The crystals tend to marginally alter to green actinolite; where this is more extensive in some of the more evolved rocks it is difficult to distinguish between this recrystallized amphibole, and primary, magmatic amphibole. Orthopyroxene crystallized simultaneously with augite, the two being found in intimate association. It, too, has suffered a little marginal alteration. During fractionation the modal proportion of clinopyroxene increases before falling, whereas that of orthopyroxene decreases (Appendix B). Biotite is a prominent phase within these rocks, initially forming late-stage interstitial plates, but becoming more euhedral later. Fe-Ti oxides, too, have followed a similar trend. Primary amphibole appears as interstitial crystals late in the fractionation sequence. Quartz and orthoclase are both interstitial phases, but increase in modal proportions with fractionation at the expense of plagioclase, the colour index remaining fairly constant. Accessory phases comprise apatite (in all but the most basic rocks) and trace amounts of zircon and tourmaline in the evolved facies. Partial melting textures similar to those found in the Loch Doon pluton in Scotland (Tindle and Pearce 1983) are displayed in the granites, namely the generation of tiny acicular apatite crystals, and of blebs of

clinopyroxene within plagioclase crystals.

Joints within the pluton have acted as conduits for later mineralizing fluids which have coated their walls in chlorite, actinolite, plagioclase, and occasionally copper minerals. Acidic dykes have also exploited these fractures, and they, too, are frequently mineralized.

4.2.2 Tocopilla Pluton

The coastal escarpment immediately to the north and east of Tocopilla is composed of intrusive rocks, here termed the Tocopilla pluton. Two distinct facies are present: the first, outcropping furthest north and east from Tocopilla comprises quartz monzogabbros - granites; the second, occurring closer to the town consists of highly potassium metasomatized pink rocks, for which the field term "monzonite" will be used. Gradations between the two were observed in the vicinity of Quebrada Barriles (which cuts the escarpment above Tocopilla), thus implying that they are part of one pluton rather than two separate magma pulses (Figure 4.2).

The monzonites are generally strongly porphyritic (Plate 4.3a) with phenocrysts of plagioclase, clinopyroxene, amphibole, and (rarely) quartz. This texture becomes less pronounced as one moves north, grading into an equigranular texture (Plate 4.3b), and thence into quartz monzodiorites in Quebrada Barriles. Plagioclase phenocrysts are generally extensively potassium metasomatized, being completely pseudomorphed by turbid orthoclase. Fresh crystals may be found with core compositions being uniform and ranging from An_{38} - An_{45}; individual crystals may show limited normal zoning from An_{45} - An_{30}. Potassium feldspar pseudomorphs after plagioclase occur in the groundmass. Clinopyroxene is

a.

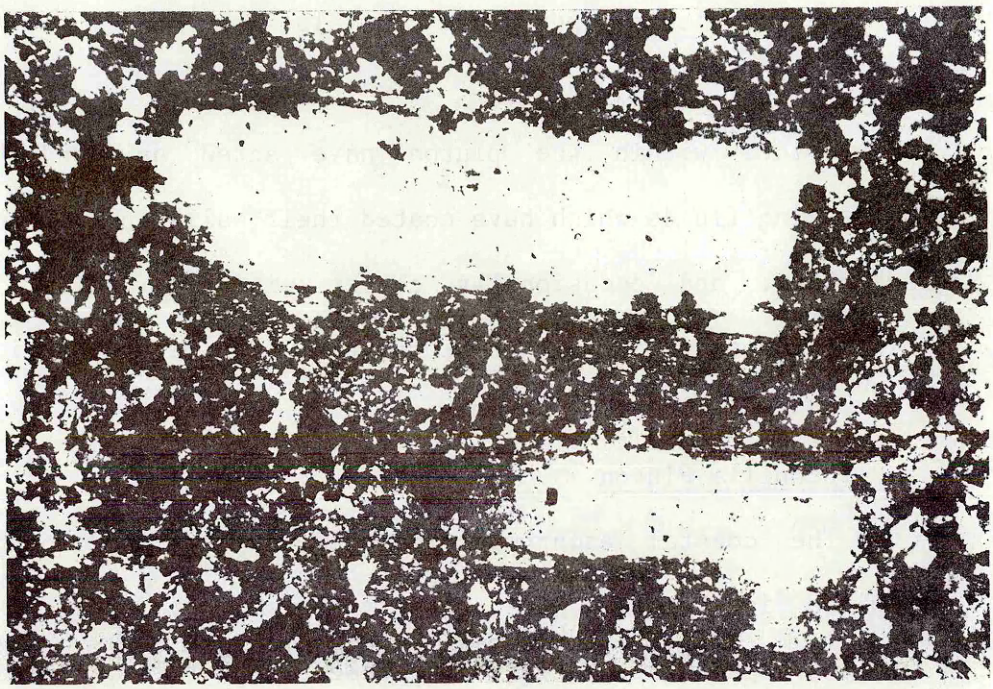

b.

Plate 4.3a. Porphyritic monzonite (81077) with "phenocrysts" of plagioclase set in groundmass of quartz (colourless), potassium feldspar (brown), oxides (black) and chlorite (green). PPL. Field of view = 3.47 mm.

Plate 4.3b. Equigranular monzonite (TOC3) containing quartz (clear), potassium feldspar (brown and grey) and clinopyroxene (moderate birefringence). Relict twinning is discernible in some feldspars.
XP. Field of view = 3.47 mm.

a ubiquitous phase in these rocks, but it, too, has undergone extensive alteration, typically to an amorphous dirty brown amphibole plus oxides, which in turn may break down to chlorite. Towards the centre of the intrusion the alteration is more of a conversion to oxide, and amphibole is poorly developed; this suggests that this region had a lower water content than its surrounds. Orthopyroxene is only found in the most basic of the monzonites. It alters to oxide, sometimes pervasively. Amphibole, as mentioned above, takes various guises as a replacement of pyroxene. The secondary nature is not always apparent, and in some cases phenocrysts of amorphous brown amphibole rimmed by oxide occur; however, comparing these with rocks in which the alteration texture is evident implies that these amphiboles are also secondary. The only convincing primary amphibole is found in the more equigranular monzonites. Occasionally the style of alteration is different with green/brown phenocrysts of (presumably) amphibole rimmed by fresher clinopyroxene. Fe-Ti oxides form small sporadic phenocrysts, but are most commonly related to ferromagnesian breakdown. The groundmasses of the monzonites are composed principally of quartz and potassium feldspar which may develop a graphic texture. Typically, however, they form small plates or rounded grains. Orthoclase frequently pseudomorphs both plagioclase phenocrysts and groundmass crystals. Pyroxene is a rare groundmass phase. Accessory minerals are apatite and rare sphene. Biotite is notably absent.

The unmetasomatized parts of the pluton are meso-leucocratic and medium grained. Plagioclase is the most abundant mineral ranging in composition from An_{56} - oligoclase with individual crystals being only weakly zoned. Propyllitic alteration is minimal, but in the vicinity of the monzonites is more extensive. Clinopyroxene began crystallizing after plagioclase, but is still usually euhedral. It is generally fresh,

though may alter marginally to actinolite; this is not as pervasive as in the monzonites. Orthopyroxene is rare and forms small euhedral crystals in clots with other ferromagnesians; it appears to be pre-clinopyroxene. Dark green magmatic amphibole occurs as an interstitial phase usually contemporaneous with biotite to which it may marginally alter. Biotite forms the dominant mafic mineral in the majority of these rocks occurring as interstitial plates; it often contains sparse inclusions of tiny zircons. Fe-Ti oxides form euhedral grains, poikilitically enclosed by other ferromagnesians, with which they tend to clot. Orthoclase generally displays poikilitic plates though in places may be pre-biotite and amphibole. Quartz is interstitial in all but the most evolved rocks where it is an early crystallizing phase. Accessory minerals include nearly ubiquitous early crystallizing apatite, rare zircons, interstitial sphene, and tourmaline.

The main feature of this pluton is the identification of the two main rock types, the monzonites in the south and the unmetasomatized rocks to the north. There is also the possibility that elevation also plays an important role here. In general the monzonites are found on high ground south of Quebrada Barriles and in the upper part of the Quebrada: to the north of the quebrada only localities along the base of the coastal escarpment were sampled for access reasons, thus creating the possibility that the high peaks of this area are also monzonitic. Thus, either way the monzonites have stewed in a potassium rich fluid which was concentrated in the southern part and perhaps at high levels of the intrusion. In the more equigranular facies the metasomatism must have been late in the crystallization history, but in the porphyries only a few large crystals had grown before the potassium alteration ensued. (A similar conclusion was also reached by Ambrus (1977) for the potassium

metasomatized diorites at El Abra). The alteration is thus magmatic, syn-crystallization auto-metasomatism rather than subsolidus and post-consolidation. No biotization was observed. Small copper deposits have been worked within the monzonites (Ferraris and Di Biase, 1978) attesting to more severe alteration on a local scale.

4.2.3 Cerro Colupito Pluton

Inland from the coastal escarpment the Cordillera de la Costa consists of isolated hills or north-south elongate ranges rising from a surface of recent gravels. One prominent range (Cerros de Colupito) culminates at its northern extremity in the peak of Cerro Colupito. Observed rock types range from quartz monzodiorite - granite (Figure 4.2), though there may be more evolved or basic facies towards the centre of the massif which was not investigated. All are leucocratic and reasonably fine grained, plagioclase laths at 1.5 mm long being the largest crystals. These sometimes impart a mild porphyritic texture to the rocks. Early crystallizing plagioclase varies in composition from An_{38} in the most basic to An_{20} in the most acid rocks: individual crystals may display weak concentric zoning. Sodic overgrowths may jacket more calcic or turbidly altered cores. Although no pyroxene is observed its former presence is suggested by the texture of the amphibole; this forms ragged, colourless-pale yellow/green mats, often fibrous, speckled with Fe-Ti oxides. These may also undergo further marginal alteration to chlorite (Plate 4.4). Primary biotite is present only in the most basic rock type as plates. Fe-Ti oxides form small euhedral crystals, but are most often associated with pyroxene breakdown. Quartz and orthoclase are both interstitial though the former crystallized first; granophyric intergrowths may be extensive. Trace phases include apatite and sphene.

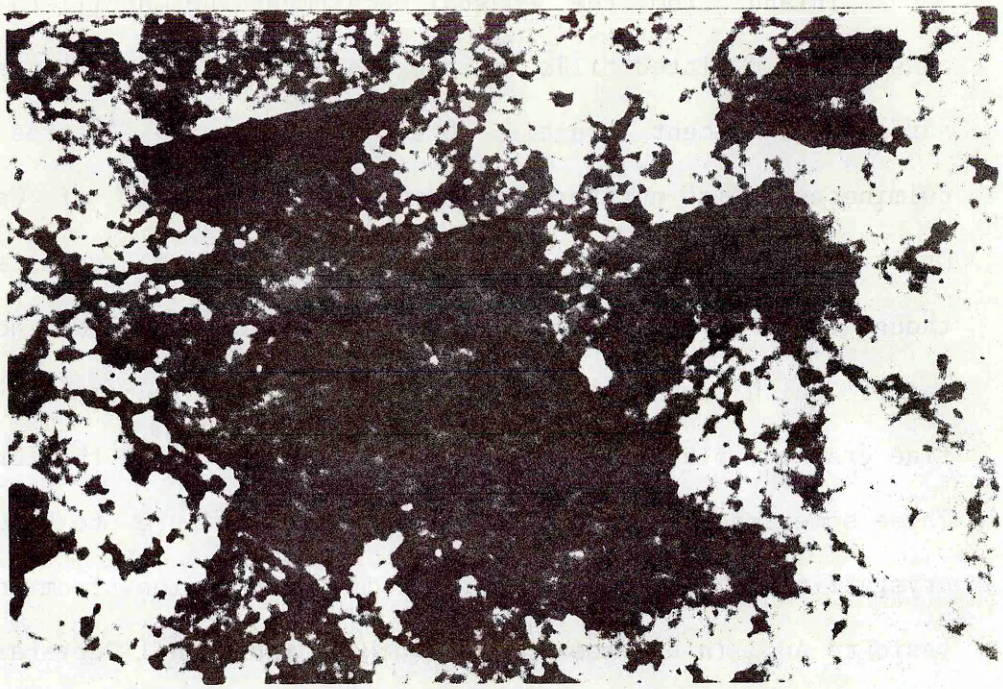

Plate 4.4. Breakdown of amphibole (dirty brown) to chlorite (green) and biotite (orange/brown) in quartz monzodiorite (81094).
PPL. Field of view = 3.47 mm.

4.2.4 Sierra de la Cruz Pluton

The Sierra de la Cruz is cited 15 km to the north of Maria Elena and about 45 km to the east of Tocopilla (Figure 4.1). As mentioned in Sections 2.5 and 3.3 the pluton cuts rocks of the Toco Formation, and probably also the La Negra Formation, causing extensive hornfelsing. Large screens of hornfelsed sediment suggest a stoping mechanism of intrusion. Further evidence for this comes from the presence of rounded melanocratic autoliths, which locally are quite numerous. These probably represent early formed facies of the intrusion which crystallized against the margins but which were subsequently reincorporated into the magma as stoping proceeded. The rounded, mafic nature of these autoliths reflects varying degrees of assimilation of the felsic phases by the parent magma. (A detailed study of autoliths and assimilation has been performed by Tindle and Pearce (1983) for the Loch Doon pluton in Scotland). The rock types range from quartz monzodiorite, through tonalite to granite (Figure 4.2); all are medium-coarse grained.

Plagioclase compositions show little variation, ranging from sodic andesine-oligoclase; weak concentric zoning may be present. The ferromagnesian minerals tend to form clots. Generally the most abundant of these phases is dark green hornblende which has a dominantly interstitial habit. Biotite has a similar paragenesis, the two phases crystallizing together. Clinopyroxene is developed at the expense of amphibole and biotite in the more leucocratic facies; elsewhere it is found in only minor quantities. Quartz and orthoclase both form large interstitial poikilitic plates; in the granites the former becomes an early crystallizing phase. Accessory phases include Fe-Ti oxides, apatite and rarely sphene and zircon.

The pluton is cut by a series of dykes, striking N-NNW which also intrude the Toco Formation (Section 2.5). These fall into broadly three categories:

i) Highly acidic fine grained varieties consist mainly of rounded quartz grains with interstitial pale brown biotite, set in a matrix of finely divided oxide, quartz, and potassium feldspar.

ii) Strongly plagioclase phyric microandesites have phenocrysts of plagioclase, clinopyroxene, oxide and rare orthopyroxene and olivine. Plagioclase varies from An_{50} - An_{57} with weak normal and concentric zoning; the crystals are usually fresh though sericitization is apparent in a few crystals. Clinopyroxene forms subordinate glomeroporphyritic masses, commencing crystallization after plagioclase. Olivine and orthopyroxene are both altered to serpentine and rimmed by oxide granules.

iii) Sparsely phyric microandesites containing albitized plagioclase, pyroxenes which may be converted to pumpellyite or chlorite, specular oxide and fine grained quartz.

The slight chilled margin to several of these dykes suggests that the pluton was cool prior to their emplacement. Their orientation is parallel to the major structural trends of the Mesozoic-Recent evolution of the Cordillera. As mentioned in Section 1.6 the eastern flank of the Cordillera de la Costa descends gradually into the Pampa del Tamarugal by a sequence of poorly defined north-south trending faults, and it may be that these fractures, or their earlier equivalents were exploited by these magmas. The exact timing of the dyke emplacement is unknown.

4.3 Geochronology

The four plutons discussed above have been subject to a whole rock Rb-Sr geochronological study. Isochron diagrams are shown in Figure 4.3. A seven point isochron for the Gatico pluton yielded an age of 158 $\pm$ 6 Ma with an initial $^{87}Sr/^{86}Sr$ ratio of 0.7033$\pm$1 (ε^{i}_{Sr} = -17.3). The Tocopilla pluton produced a twelve point errochron with an age of 155 $\pm$ 13 Ma and an initial $^{87}Sr/^{86}Sr$ ratio of 0.7039$\pm$2 (ε^{i}_{Sr} = -9.1). A four point errochron for the Sierra de la Cruz intrusion gave an age of 156$\pm$32 Ma with an initial $^{87}Sr/^{86}Sr$ ratio of 0.7041$\pm$5 (ε^{i}_{Sr} = -5.6). The Sierra de la Cruz pluton was ascribed to the Permian by Ferraris (1978) even though it lies considerably to the west of the Palaeozoic intrusive belt; the 1:1,000,000 geological map of Chile (Servicio Nacional de Geologia y Mineria), however, shows the Sierra de la Cruz to be Mesozoic. The current study supports the latter view, and confirms the temporal relationship with the middle Jurassic coastal batholith and stratigraphic position with respect to the lower Jurassic La Negra Formation. The pluton at Cerro Colupito did not give a sufficient spread in Rb/Sr ratios to yield a meaningful age. Its spatial proximity to other plutons of the Cordillera de la Costa suggests that it, too, is likely to belong to the same period of magmatism, and consequently has been assigned an age of 155 Ma.

The ages obtained in this study for the plutons of the Cordillera de la Costa at 22°S form a tight grouping between 155 - 158 Ma. They agree well with Pb/α dates spanning 150 - 159 Ma reported by Ferraris (1978) and Ferraris and Di Biase (1978) for intrusions between Antofagasta and Tocopilla, although it is difficult to establish which individual

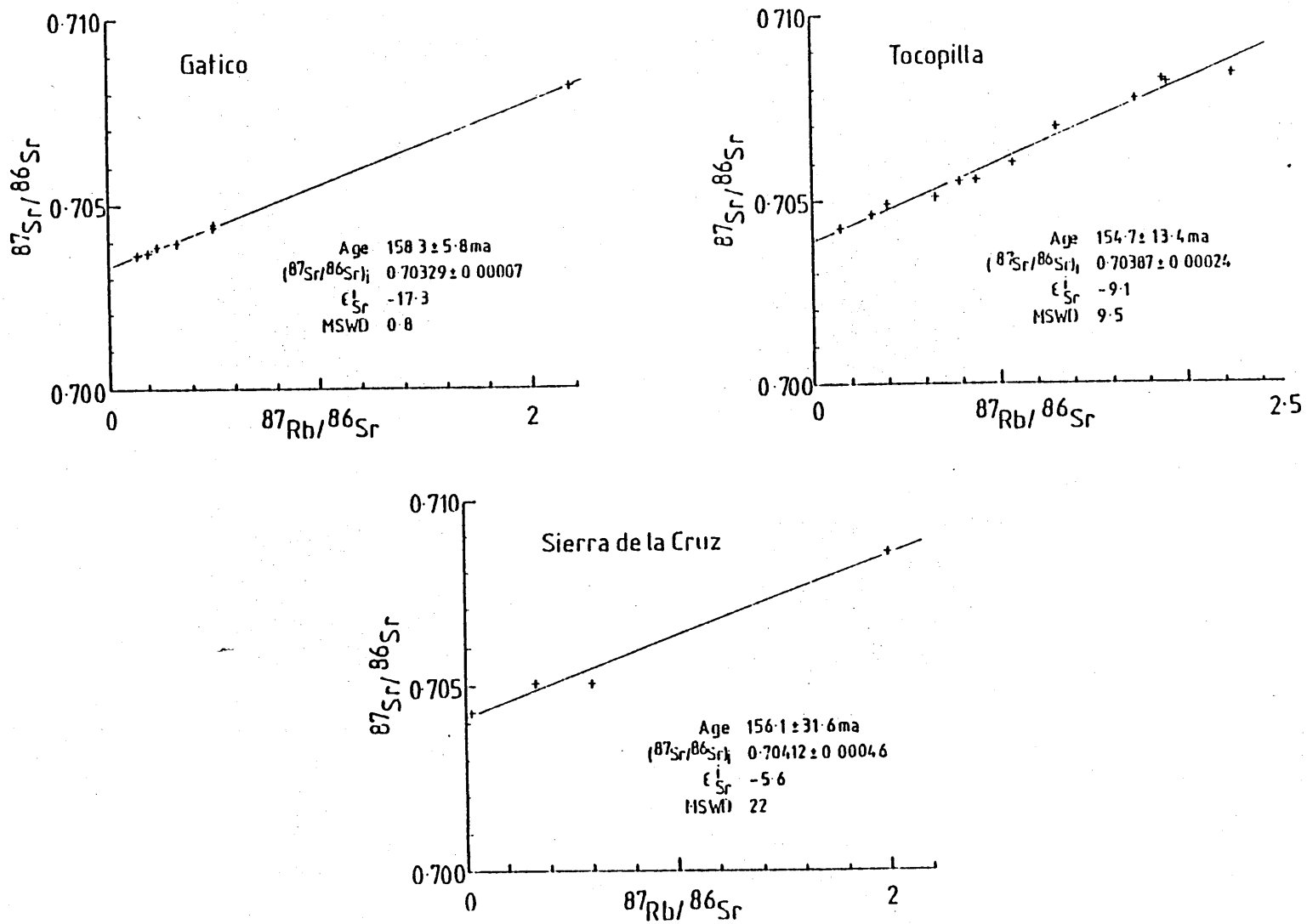

Figure 4.3 Rb - Sr whole rock isochron diagrams for the Gatico, Tocopilla and Sierra de la Cruz plutons.

plutons were dated as, on the relevant geological maps, the ornamentation of the intrusions to which the dates are ascribed indicate supposed Palaeozoic, Jurassic and Cretaceous units. Farrar et al. (1970), Quirt (1972), Zentilli (1974), McNutt et al. (1975), Ulrickson (1979) and Berg et al. (1983) presented both Rb-Sr and K-Ar ages between 147 - 160 Ma for the coastal batholith between 25^{o}-29^{o}S, and Jurassic dates have also been extracted from coastal intrusions between 31^{o} - 36^{o}S (Caminos et al., 1982; Drake et al., 1982).

4.4 Major and trace element variations

Harker variation diagrams for the four Jurassic plutonic complexes studied are shown in Figure 4.4. The restricted number of samples for the Cerro Colupito and Sierra de la Cruz intrusions makes them of more limited use, but nonetheless they do illustrate their behaviour relative to those of the Gatico and Tocopilla plutons.

4.4.1 Gatico Pluton

The Gatico pluton displays a wide range in SiO_2 from 53.1-65.0%. The variation diagrams show trends for all elements. There are anticorrelations for CaO, Al_2O_3, MnO, MgO, Sr, Cr and Ni, thus supporting the petrographic evidence for plagioclase, clinopyroxene and orthopyroxene being early crystallizing phases and controlling fractionation trends. All other elements increase with increasing SiO_2. The depletion in the most evolved facies of TiO_2, V and Fe_2O_3 on the one hand, and Y and Zr on the other indicate that titanomagnetite and zircon respectively became crystallizing phases (Figure 4.5); this again is borne out by the petrography. K_2O, Rb, Ba and P_2O_5 increase throughout implying that biotite, potassium feldspar and apatite did not influence

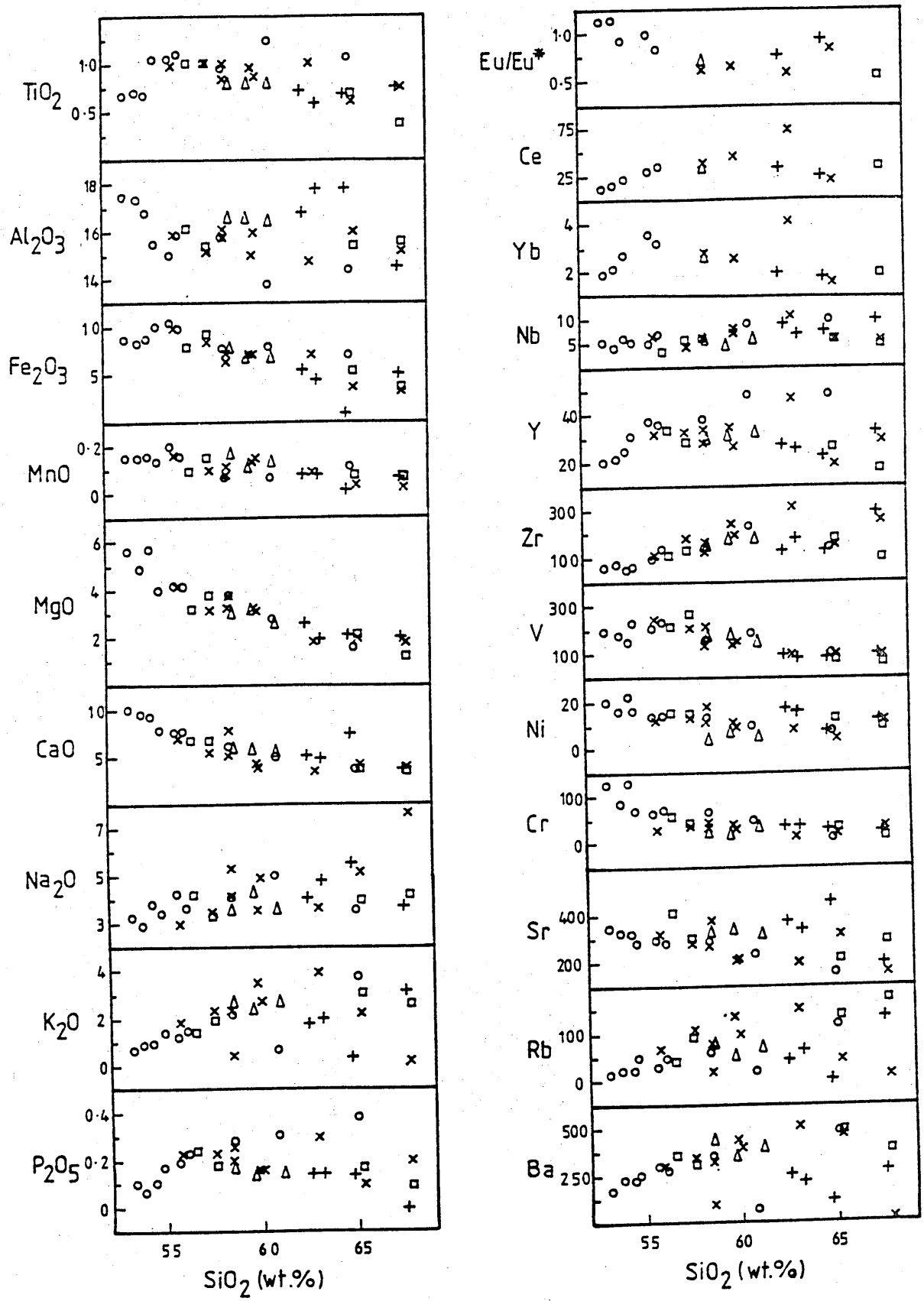

Figure 4.4

Harker variation diagrams for selected elements from the Jurassic plutons. O = Gatico, □ = Tocopilla, × = Tocopilla monzonites, + = Sierra de la Cruz, Δ = Cerro Colupito.

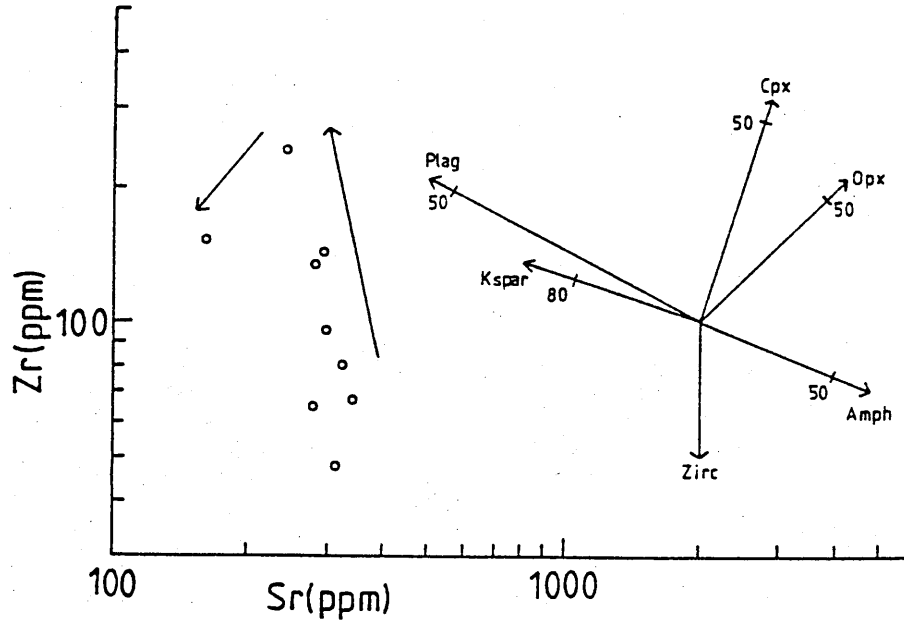

Figure 4.5 Sr - Zr diagram for the Gatico pluton: arrows indicate the fractionation path of the intrusion. Rayleigh fractional crystallization vectors show the effects of removing selected phases: numbers along vectors indicate the percentage of liquid remaining. Distribution coefficients from Arth (1976) and Pearce and Norry (1979).

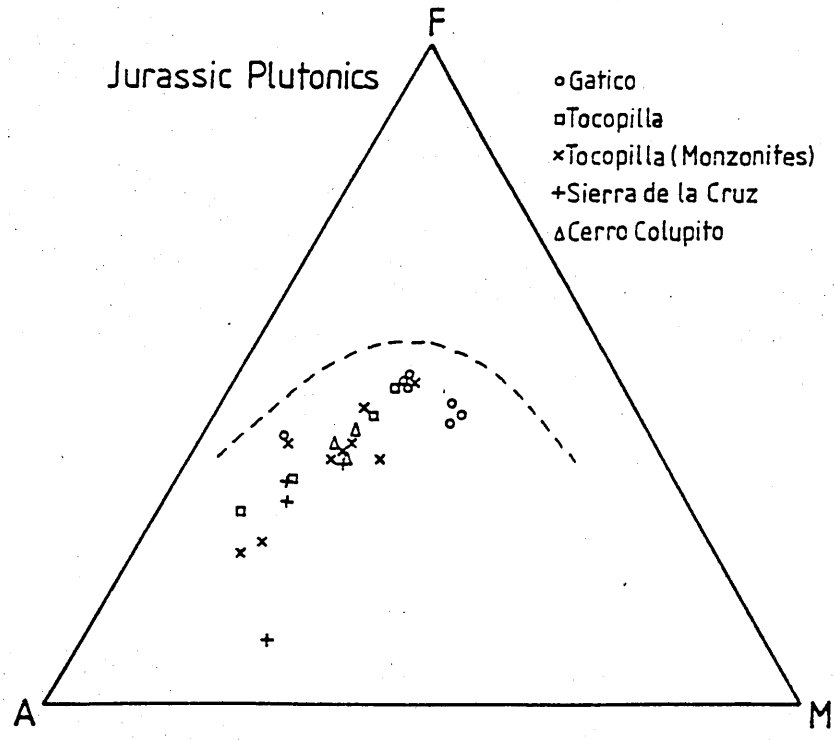

Figure 4.6

AFM diagram for the Jurassic plutons.

liquid trends. The behaviour of Na_2O is due to the lower anorthite content of plagioclase in the granite. The intrusion follows a calcalkaline trend on an AFM diagram (Figure 4.6) showing a little early iron enrichment.

The pluton is slightly LREE enriched (Figure 4.7a) with $(Ce/Yb)_N$ = 1.86 - 2.76; Ce_N and Yb_N vary between 17.3 - 45.0 and 8.5 - 16.1 respectively and both increase with fractionation. The most basic rocks have small positive Eu anomalies (Eu/Eu* = 1.12 - 1.14), but this becomes slightly negative as fractionation proceeds (Figure 4.4). It is possible that these positive anomalies reflect the nature of the parental liquid, but they may also represent plagioclase accumulation. Crystallization in granitic magmas rarely produces a clear cut distinction between liquids and cumulates and most bodies may thus be regarded as crystal "mushes" composed of "cumulus" crystals and trapped interstitial melt (McCarthy and Groves, 1979). Consequently a high proportion of "cumulus" plagioclase crystals may impart a positive (or less negative) Eu anomaly upon a specific rock. This is indeed the case with the Gatico pluton where the samples with positive Eu/Eu* have the highest proportions of cumulus plagioclase crystals; with further plagioclase removal from the liquid a negative anomaly develops, the magnitude of which may be tempered by accumulation.

4.4.2 Tocopilla Pluton

The Tocopilla pluton has a continuum of SiO_2 from 55.7 - 67.8% with both monzonitic and unmetasomatised facies roughly encompassing this range. In general both facies follow the same fractionation trends (Figure 4.4) though the coherence of these varies from element to element. TiO_2, Fe_2O_3, MgO, MnO, CaO, P_2O_5, Cr, Ni, V and

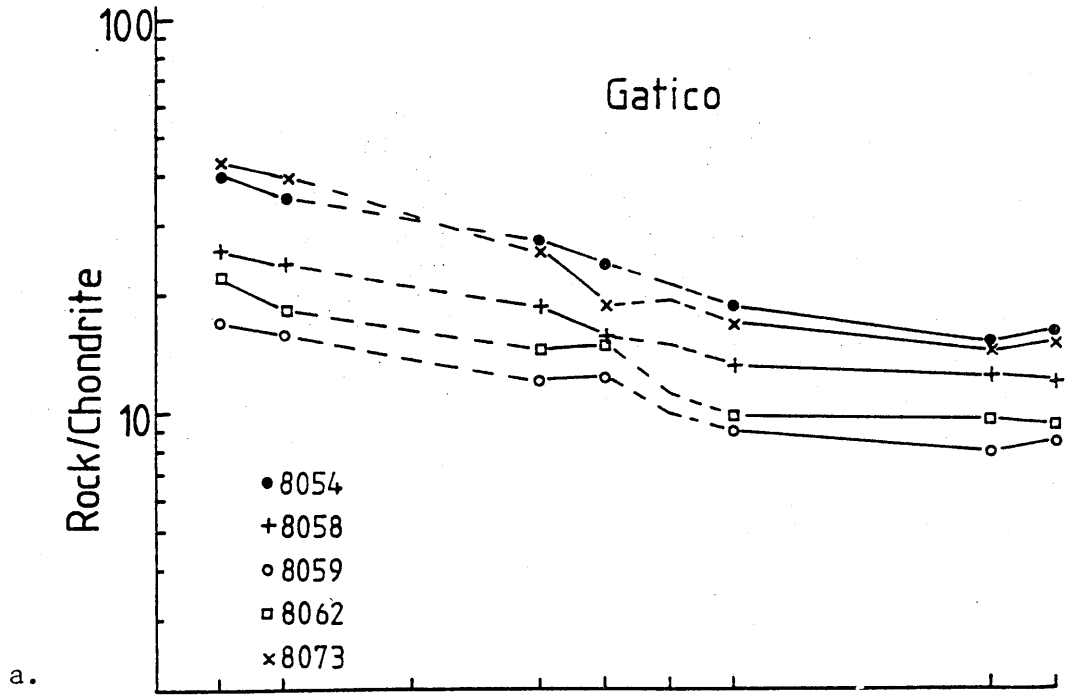

a.

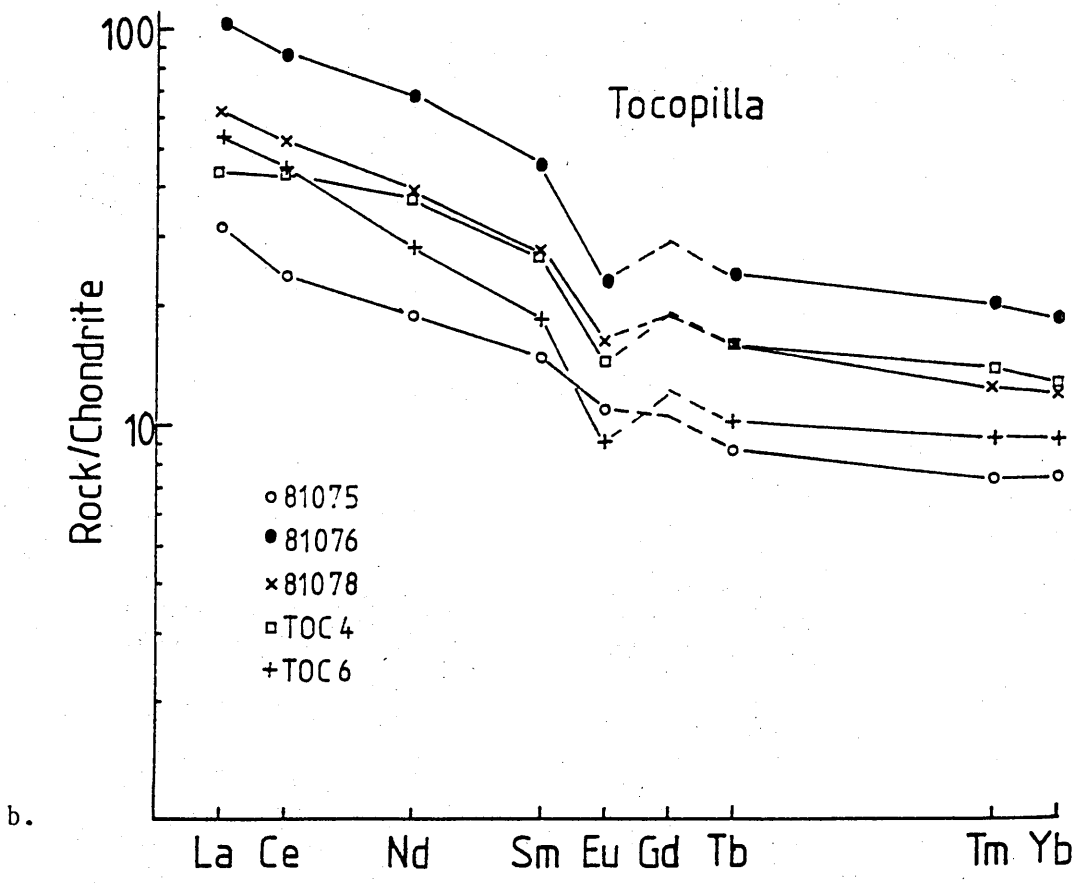

b.

Figure 4.7

Chondrite normalised REE diagrams for (a) Gatico, (b) Tocopilla, (c) Colupito, (d) Sierra de la Cruz.

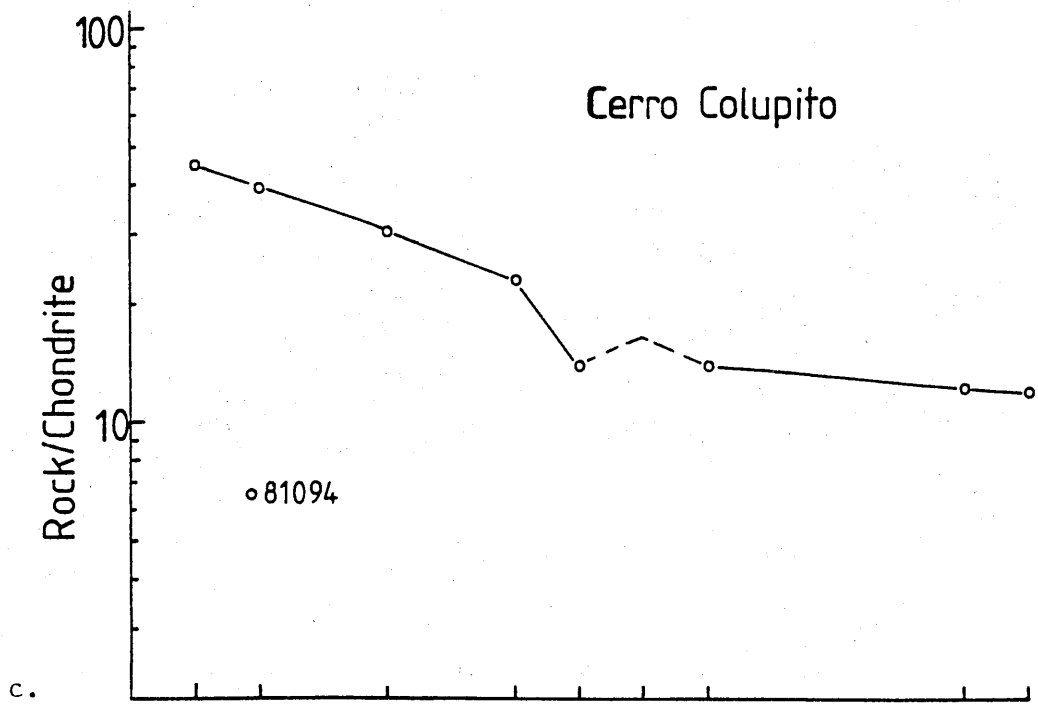

c.

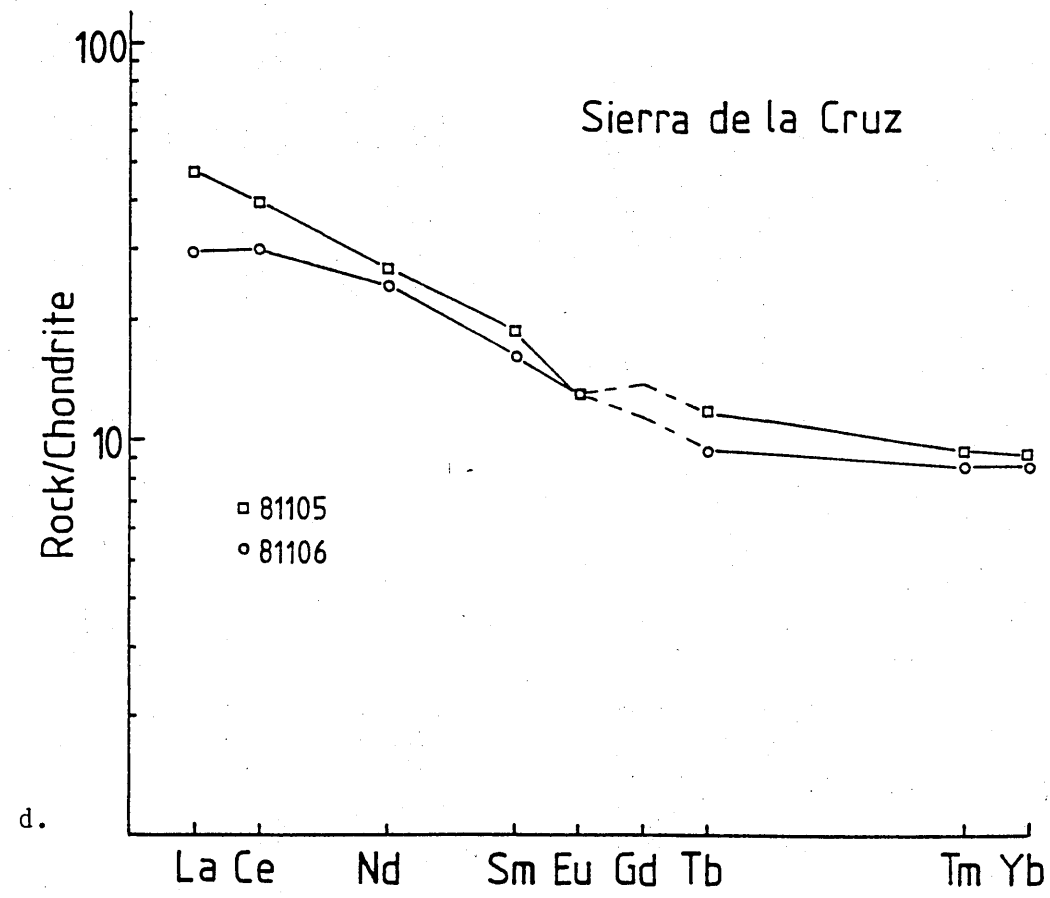

d.

Figure 4.7 (continued)

Sr decrease with increasing SiO_2; K_2O, Ba, Zr, Nb and Ce increase slightly, and Y and Yb are constant, before dropping in the evolved rocks: Al_2O_3 and Na_2O remain essentially constant. These variations are consistent with the removal of plagioclase along with pyroxenes, titanomagnetite and a little apatite. The decrease in K_2O and Ba, and Zr and Hf suggests that potassium feldspar and zircon respectively were early crystallizing phases in acidic rocks; the behaviour of Y and Yb could also imply some amphibole removal, but the zircon fractionation noted above could easily account for this (Hanson, 1978). The fractionation scheme presented above creates a problem in that orthoclase and amphibole always appear as interstitial phases and thus should not control liquid compositions. Therefore, either the fractionation mechanism is more complex, perhaps involving elemental diffusion out of trapped interstitial melt, or that the concentations are controlled by volatile fluxing. The depletion of Ce, Ta and Nb in the most acid rocks may be attributable to the removal of minor phases such as allanite or sphene in very small quantities (Tindle and Pearce, 1981) and/or to the presence of a vapour phase into which these elements partition. Certain parts of the pluton in both monzonites and granitoids show pronounced depletions of K_2O, Rb and Ba which are not correlated with any mineralogical effects; again this may be due to local volatile control.

It is apparent from Figure 4.4 that while some elements (e.g. MgO, TiO_2 and V) show tight trends, those of the alkalis are more diffuse. It is likely that this is mostly caused by the potassium metasomatism which, for instance has decreased the Sr content of the monzonites relative to the unmetasomatised facies. The coherence of the Rb-Sr isotope systematics implies that the metasomatic fluids had an almost

identical $^{87}Sr/^{86}Sr$ ratio to the main magma body, and thus were probably derived from within that body. This correlates well with the textural evidence presented in Section 4.2.2 that the alteration was magmatically derived rather than subsolidus and from an external source.

The Tocopilla pluton is LREE enriched (Figure 4.7.b) with $(Ce/Yb)_N$ = 3.1 - 4.7 and Ce_N and Yb_N varying between 43.2 - 85.7 and 9.36 - 18.6 respectively. As already mentioned the REE concentrations firstly increase and then fall; this is shown in Figure 4.7b by the sequence of samples TOC4, 81078, 81076, TOC6. Coupled with this is a generally increasing negative Eu anomaly. Sample 81075 is not readily accommodated within this framework as it has lower REE contents, the lowest $(Ce/Yb)_N$ and the smallest Eu anomaly (Eu/Eu^* = 0.86), but a reasonably high SiO_2 content (65.4%) which falls between 81076 and TOC6. Two possibilities present themselves. Firstly the sample is the only monzonite which has large quartz phenocrysts, and thus it is possible that the SiO_2 value has been enhanced by quartz accumulation. The concentrations of many trace elements and the small Eu anomaly in the sample also appear to be consistent with a less evolved nature. Alternatively extensive plagioclase accumulation would lead to lower contents of REE and other elements, a more positive Eu anomaly and higher concentrations of Sr, CaO and Na_2O. However, plagioclase "phenocrysts" constitute less than 10% of the rock, and therefore would be insufficient to generate the observed trend. In addition some other samples show a more "cumulate" nature, yet do not portray similar REE patterns. Consequently it is concluded that the geochemistry of this sample reflects quartz accumulation.

In a similar manner to the Gatico pluton the Tocopilla pluton

follows a calcalkaline trend on an AFM diagram (Figure 4.6) though the latter lies closer to the alkalis apex in accordance with its more evolved elemental concentrations.

4.4.3 Cerro Colupito

The limited data available regarding the Cerro Colupito pluton show a restricted SiO_2 range between 58.6 - 61.1%. One sample (Figure 4.7c) shows LREE enrichment with $(Ce/Yb)_N$ = 3.26, Ce_N = 39.7, Yb_N = 12.2, and a moderate negative Eu anomaly (Eu/Eu* = 0.69). The data points are broadly concordant with similarly evolved rocks from the Tocopilla Pluton.

4.4.4 Sierra de la Cruz pluton

Data were obtained on four samples from the Sierra de la Cruz pluton. SiO_2 ranges from 62.7 - 67.6% and implies that the pluton is a little more evolved than the others in the Cordillera de la Costa; although this may be due to sampling bias the rocks were collected from geographically diverse locations. The pluton is LREE enriched with $(Ce/Yb)_N$ = 3.5 - 4.3; Ce_N = 29.5 - 47.1, Yb_N = 8.6 - 9.1 and Eu/Eu* = 0.81 - 0.94 (Figure 4.7d).

4.5 Isotopic characteristics

Sr isotope analyses were performed on a large number of rocks from the Jurassic plutons for geochronological purposes, and Nd isotopes were obtained on selected samples thereof.

Initial Sr isotope ratios for the Gatico pluton vary from 0.70322 - 0.70339 (ε^{i}_{Sr} = -18.4 to -15.9) and initial Nd isotopes from 0.512740 - 0.512772 (ε^{i}_{Nd} = +5.93 to +6.55). The initial

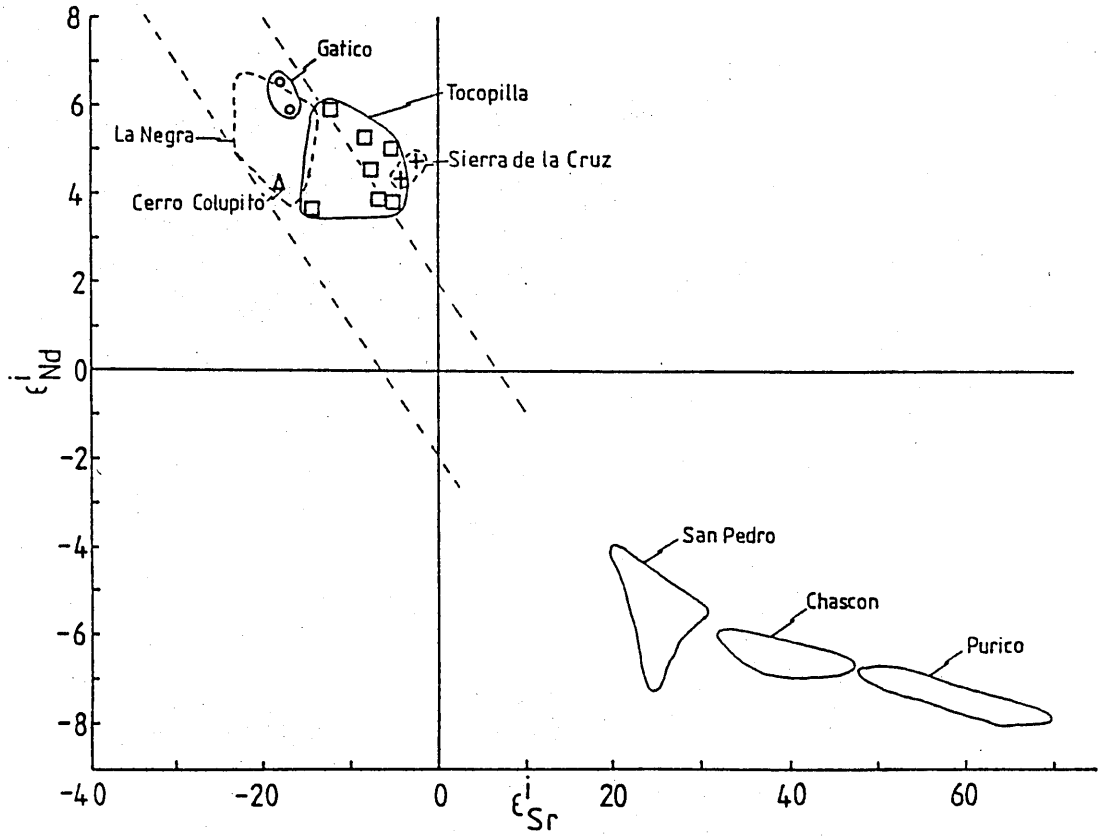

Figure 4.8

ε^i_{Sr} - ε^i_{Nd} diagram for the Jurassic plutons. The positions of the Jurassic La Negra Formation (Chapter 3), and the Recent volcanics from San Pedro (Chapter 7) and Purico-Chascon (Hawkesworth et al., 1982) are shown for comparison.

$^{87}Sr/^{86}Sr$ ratios of the Tocopilla pluton show a little more scatter but nevertheless form a coherent group ranging from 0.70351 - 0.70415 (ε^{i}_{Sr} = -14.3 to -5.2); associated initial $^{143}Nd/^{144}Nd$ ratios span 0.512601 - 0.512743 (ε^{i}_{Nd} = +3.71 to +5.89). Assuming an age of 155 Ma for the Cerro Colupito pluton initial $^{87}Sr/^{86}Sr$ ratios vary between 0.70322 - 0.70343 (ε^{i}_{Sr} = -18.3 to -14.8), and a single Nd isotope analysis yields an initial $^{143}Nd/^{144}Nd$ = 0.512659 (ε^{i}_{Nd} = +4.26). The granitoids of the Sierra de la Cruz show some scatter in their initial Sr isotope ratios from 0.70373 - 0.70433 (ε^{i}_{Sr} = -11.1 to -2.6); initial $^{143}Nd/^{144}Nd$ are 0.512664 - 0.512682 (ε^{i}_{Nd} = +4.39 to +4.74).

All the plutons plot in the depleted quadrant of an ε_{Sr} - ε_{Nd} diagram (Figure 4.8) on or close to the mantle array indicating derivation from a source with time-integrated isotopic depletion relative to 'bulk Earth', similar to the La Negra Formation, but again in stark contrast to the Recent volcanics at this latitude (Hawkesworth et al., 1982; Section 7.4.3).

4.6 Petrogenesis

As all the plutons studied were essentially intruded contemporaneously and in geographic proximity one may have expected them to have similar geochemical characteristics. Indeed all of the plutons follow similar fractionation trends; for instance the Tocopilla pluton continues the evolutionary path of the basic parts of the Gatico pluton. Significant differences are, however, noted in that the evolved facies of the latter contain higher concentrations of P_2O_5, TiO_2 and Y than the former suggesting less apatite, magnetite and amphibole control

in the Gatico pluton; this may be a function of relatively lower oxygen fugacities in this intrusion. Both the Cerro Colupito and Sierra de la Cruz intrusions have slightly higher CaO, Al_2O_3 and Sr contents than the Tocopilla pluton at similar SiO_2 levels, reflecting increased plagioclase accumulation. All the plutons have high ratios of LILE/HFSE and alkalis/LREE indicative of subduction related magmas (Pearce, 1982).

There is no systematic increase of incompatible element concentrations (e.g. K_2O) as has been observed in certain volcanic arcs (Whitford et al., 1979; Roobol et al., 1976), but there are changes in certain immobile inter-element ratios. For instance the Hf/Ta ratio, which one would expect to be reasonably constant within a suite due to the general incompatibility of these elements during fractionation (at least until zircon becomes a crystallizing phase), shows distinct variations between plutons with Gatico having the highest ratio and the Sierra de la Cruz the lowest (Figure 4.9). This variation is not simply perpendicular to the present trench, as there are differences between the Gatico and Tocopilla plutons which are along strike from each other.

The REE patterns also show variations between the intrusions. Whilst $(Tb/Yb)_N$ ratios are fairly constant $(Ce/Sm)_N$ ratios are much lower in the Gatico pluton than in the others (Figure 4.10). This presents a number of possibilities regarding magmagenesis. Firstly, if the source of the magma for all of the plutons had flat $(Tb/Yb)_N$ then, assuming a constant subduction zone contribution, that of the Gatico pluton must have been more LREE depleted than the others, or that the parental magma was derived by higher degrees of partial melting. Secondly, if the source had a higher $(Tb/Yb)_N$ then hornblende must be

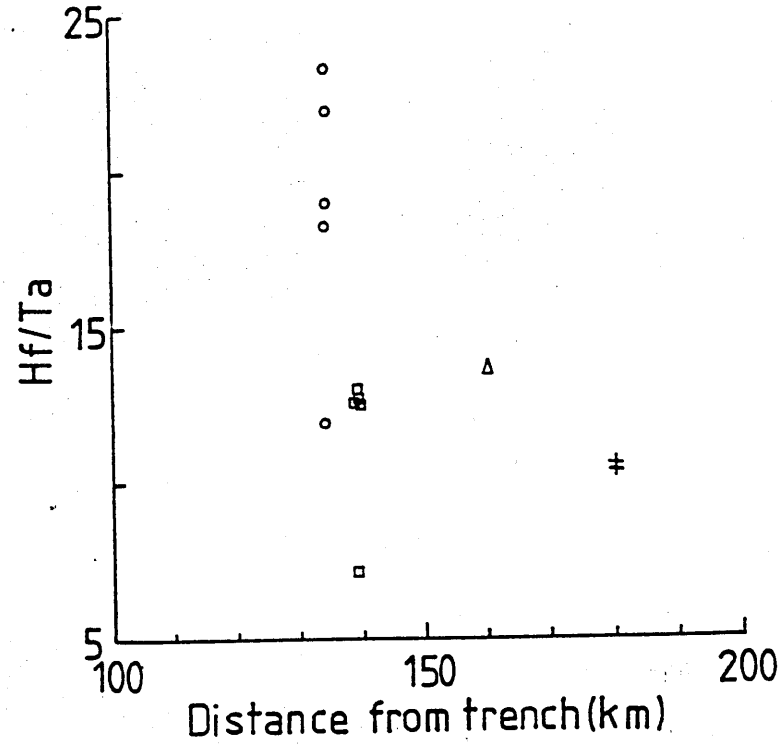

Figure 4.9

Hf/Ta against distance from the present day trench to illustrate the more depleted trace element signature of the Gatico pluton relative to the other Jurassic intrusions. ○ = Gatico, □ = Tocopilla, Δ = Cerro Colupito, + = Sierra de la Cruz.

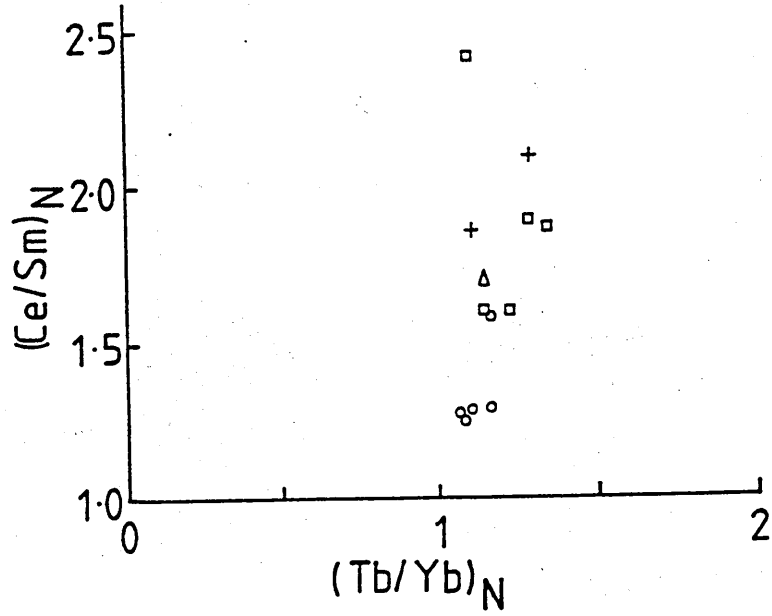

Figure 4.10

$(Ce/Sm)_N$ - $(Tb/Yb)_N$ diagram illustrating the lower LREE enrichment of Gatico relative to the other Jurassic plutons, whilst all have similar flat HREE profiles. Symbols as in Figure 4.9.

incorporated into the residue during partial melting to depress the middle REE relative to the HREE; again Gatico must represent a more LREE depleted source or a higher degree of partial melting.

The concept of sources with differing degrees of enrichment is substantiated by the isotope systematics where all four plutons plot in discrete fields on or near the mantle array (Figure 4.8). It is thought unlikely that crustal contamination processes have been instrumental in determining the relative positions of these fields due to the constancy of initial isotope ratios with differentiation indices. It may also be argued that the Tocopilla pluton contains more of a subduction zone contribution (which has a high $^{87}Sr/^{86}Sr$ and a low $^{143}Nd/^{144}Nd$) than the Gatico pluton, but this is difficult to reconcile with the latter's more depleted trace element characteristics which are considered to be independent of the subduction process, coupled with the more depleted isotope systematics. Furthermore, whilst the compatibility of P_2O_5 in all except the Gatico pluton (where it is incompatible) may reflect a smaller subduction zone contribution of P to the latter, it is also consistent with higher P_2O_5 contents in the mantle sources of the other intrusions prior to subduction and subsequent earlier P_2O_5 saturation in magmas derived therefrom.

The isotope systematics are consistent with a petrogenesis by remelting the lavas of the La Negra Formation, but the field relations showing the granites intruding the lava pile negate this, unless the lava pile is very thick. Also the REE content of the lavas is much higher than in the Gatico pluton necessitating phase assemblages which retain all these elements being present in the residue whilst a large volume of magma was produced. This mechanism is considered highly unlikely.

4.7 Summary and Conclusions

During the middle Jurassic a number of granitic plutons were emplaced in the Cordillera de la Costa cutting the pre-existing Toco and La Negra Formations. These plutons show no systematic age variation with geographical position. The pluton at Tocopilla displays two distinct facies which grade into one another, the distribution of the "monzonites" being controlled by height and/or lateral position within the pluton. The other plutons do not exhibit this alkali metasomatism, but the presence of tourmaline in some rocks and the juxtaposition against the La Negra Volcanics suggests that they were intruded at high levels. All the plutons are dominated by plagioclase removal, though a "cumulate" nature is noted in certain samples by petrographic textures and positive Eu anomalies. Apatite, amphibole and magnetite played a lesser role in the Gatico pluton than in the others probably reflecting a drier magma (lower P_{H_2O}), and original source characteristics. Crystallization in all involved an in situ differentiation mechanism.

Major elements follow similar calcalkaline trends, analogous to the Peruvian batholith (McCourt, 1981) and may be interpreted as representing derivation from a common magma source. However, trace elements and isotopic data do not support major crustal contamination in their petrogenesis, and highlight differences between the plutons which are best interpreted in terms of derivation from a heterogeneous mantle source.

CHAPTER 5

SEDIMENTATION AND VOLCANISM AROUND CERRITOS BAYOS

5.1 Introduction

The area between the Pampa del Tamarugal and Calama, bounded on the south by the Sierra Limon Verde, consists of the Cerros de Montecristo, the Cerros de Guacate and the easterly extension of the Pampa del Tamarugal, the Pampa Limon Verde and Pampa del Indio Muerto (Figure 5.1). This region is composed of Jurassic and Cretaceous sedimentary, volcanic and plutonic rocks overlain by Quaternary gravels. This chapter considers the sedimentary and volcanic sequences whereas the following chapter describes the intrusive rocks along with other plutons of Cretaceous age.

5.2 Jurassic Marine Sedimentation at Cerritos Bayos (Cerritos Bayos Formation)

Many of the small hills rising out of the Pampa Limon Verde are formed of marine sediments of Sinemurian - Kimmeridgian age. They disconformably overlie the fluvial sediments and volcanics of the Agua Dulce Formation, and rest unconformably on the Limon Verde schist belt and plutonics. The area has been described by Biese (1961) and Baeza (1976), and the reader is referred to these works regarding detailed stratigraphy and faunal content. Briefly three marine cycles were recognised. The first commenced with a marine transgression in the Sinemurian which initially deposited calcarenites, cherty lutites and glauconitic sands. These were succeeded by a sequence of fossiliferous limestones, sometimes bituminous. The transgression appears to have been diachronous across this sector of Chile, reaching Moctezuma to the east of the Sierra Limon Verde in the Pleinsbachian (implying that the Sierra Limon Verde had a low relief at the onset of the Jurassic), and Caracoles, 40 km to the

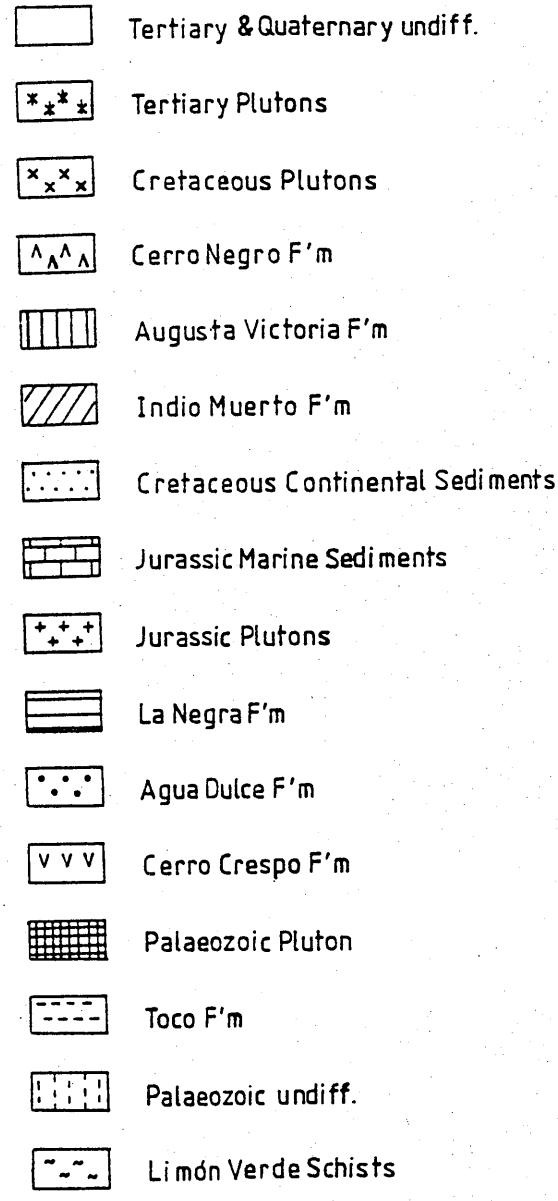
Tertiary & Quaternary undiff.
Tertiary Plutons
Cretaceous Plutons
Cerro Negro F'm
Augusta Victoria F'm
Indio Muerto F'm
Cretaceous Continental Sediments
Jurassic Marine Sediments
Jurassic Plutons
La Negra F'm
Agua Dulce F'm
Cerro Crespo F'm
Palaeozoic Pluton
Toco F'm
Palaeozoic undiff.
Limón Verde Schists

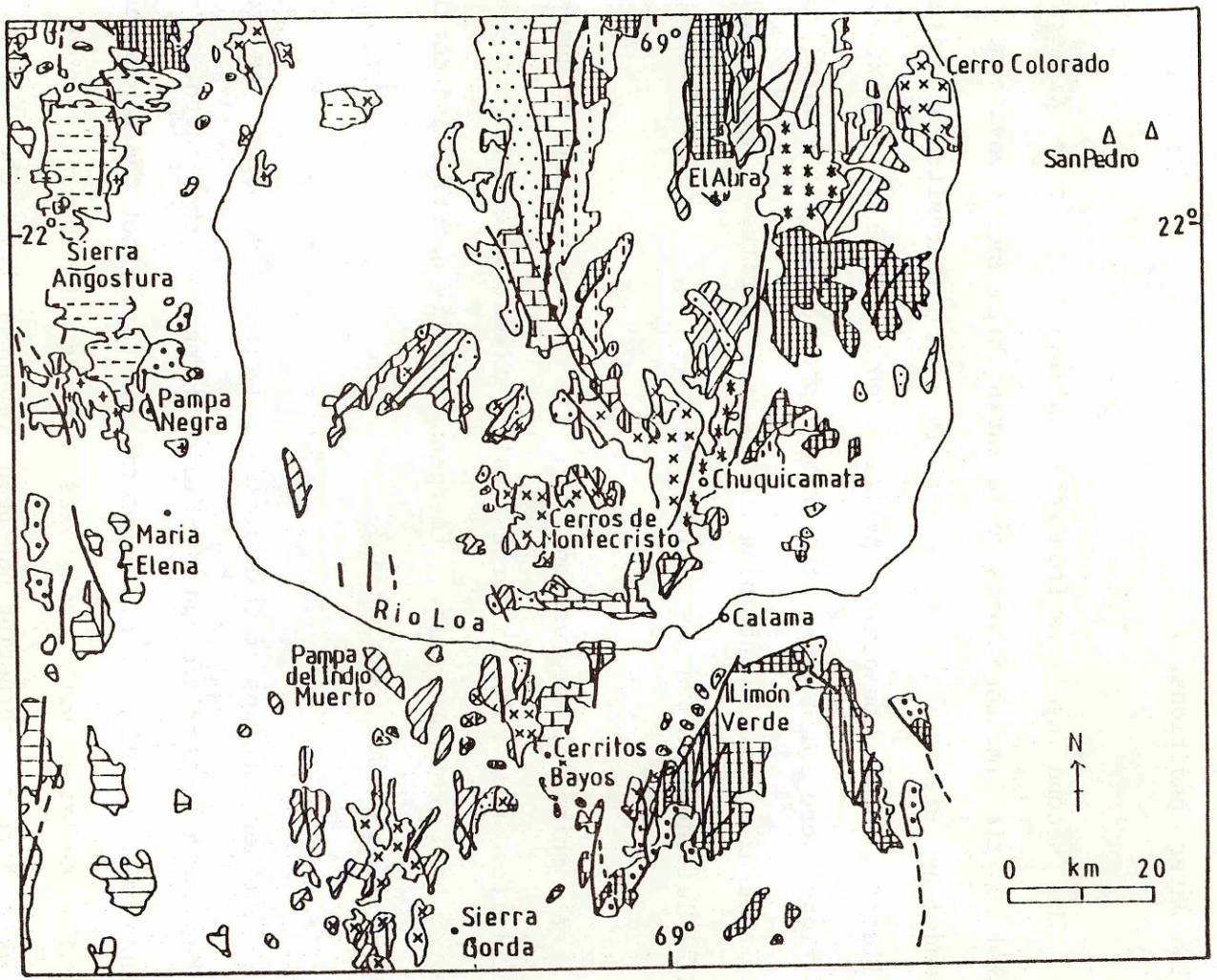

Figure 5.1

Geological map depicting areas of Jurassic-Cretaceous sedimentation and volcanism around Cerritos Bayos (after Servicio Nacional de Geologia y Mineria, 1980). Key on facing page.

south-east, in the Bajocian. Shallow water conditions prevailed until the upper Bajocian when there was a period of emergence; conglomerates in the upper Bajocian may have formed in response to a (relatively) rising landmass. Bathonian sediments are absent from Cerritos Bayos, though limestones and gypsum beds are present at Caracoles, representing very shallow water conditions.

The second cycle is from the Callovian - lower Kimmeridgian. Initial oolitic limestone banks representing high energy environments were succeeded by quieter calcilutite deposition. Calcarenites and bituminous calcilutite, some containing pyrite and representing anoxic bottom conditions, were followed by a further shallowing of the water, and the deposition of arenites containing continental detritus. Gypsum beds were finally laid down in the lower Kimmeridgian.

A third transgression in the Kimmeridgian produced more calcarenites and unfossiliferous calcilutites: water conditions at this time may have been brackish. Emergence finally occurred and continental sedimentation ensued (Section 5.3).

Further outcrops of this Jurassic marine succession are found in the Cerros de Montecristo and the Sierra Moreno to the north, and in a linear belt to the south. The formation throughout the region has been strongly deformed with fold axes running predominantly north-south. Westerly directed thrusting has been reported from the Sierra Moreno (Ferraris, 1978).

5.3 Continental sediments of Cerritos Bayos

Conformably overlying the marine lutites of Kimmeridgian age in the northern Cerros de Guacate and near Cerritos Bayos is a sequence of orange and purple quartzo-feldspathic, fine - medium grained sandstones and siltstones about 600 m thick. In both sections these dip between 50° - 80° to the west concordant with the underlying lutites. Higher up the clastics become interbedded with andesitic lavas of the Indio Muerto Formation (Section 5.4), and thin, reddened coarsely conglomeratic horizons may occur. The clasts in these conglomerates, which range in size up to 25 cm, are usually sub-rounded, and mainly composed or arenites and andesites from lower in the succession. Also to the north-west of Cerro Crespo on the western margins of the Sierra Limon Verde there are isolated hillocks of these arenites and conglomerates intercalated with thin andesite units; these have a faulted eastern contact with the Palaeozoic batholith of the main massif.

In view of their stratigraphic position above the Kimmeridgian the continental-type deposits have been assigned to the Tithonian by Biese (1961) and to the Tithonian - Neocomian by Baeza (1976). It is notable that marine sedimentation subsequently never returned to this part of Chile: the implications of this for uplift and crustal thickening are considered in Chapter 8.

Indio Muerto Formation

5.4.1 Introduction

Lying to the west of Cerritos Bayos is a gently westwards sloping region, the Pampa del Indio Muerto, forming the eastern margin of the Pampa del Tamarugal, with sporadic hillocks rising 30 - 50 m from its

surface (Figure 5.1). In the east close to the Antofagasta - Calama road these are composed of sediments of presumed Lower Cretaceous age (Section 5.3), monzonitic intrusives (Section 6.2.2), and lavas, but further north and west only the lavas may be found dipping gently westwards. (However, to the north of Sierra Gorda, further granitoids have limited exposure). Similar lavas are found to the south of Caracoles - the Quebrada Mala Formation of Montaño (1976).

The lavas are assumed to be of Lower Cretaceous age (∿ 130 Ma) as they overlie and are intercalated with continental sediments of this age (Section 5.3). They are thus not contemporaneous with the Lower Jurassic La Negra Formation in the Cordillera de la Costa (Chapter 3) as suggested by Baeza (1976) and Palacios (1978).

5.4.2 Petrography

All the lavas of this formation are porphyritic (10-30%) with plagioclase usually comprising 80 - 90% of the total phenocryst content. In one flow immediately above the continental conglomerates the plagioclase crystals attain a length of more than 20 mm. There is ubiquitous albitization and sericitization of the plagioclase, though this is very variable, in some flows the crystals are completely replaced, and may even be saussuritized, whereas in others only the cores may be slightly altered. Fresh plagioclase compositions are remarkably uniform around An_{52}, but normally zoned crystals may exhibit variation from An_{52} in cores to An_{40} at the margins. Magnetite is an almost universal phenocryst phase though its concentration varies considerably. Crystals are generally less than 0.2 mm across, but larger allotriomorphic mats are sometimes found. Augitic clinopyroxene is a common phenocryst, absent only in the more evolved flows. Its usual habit is as fresh, small

a.

b.

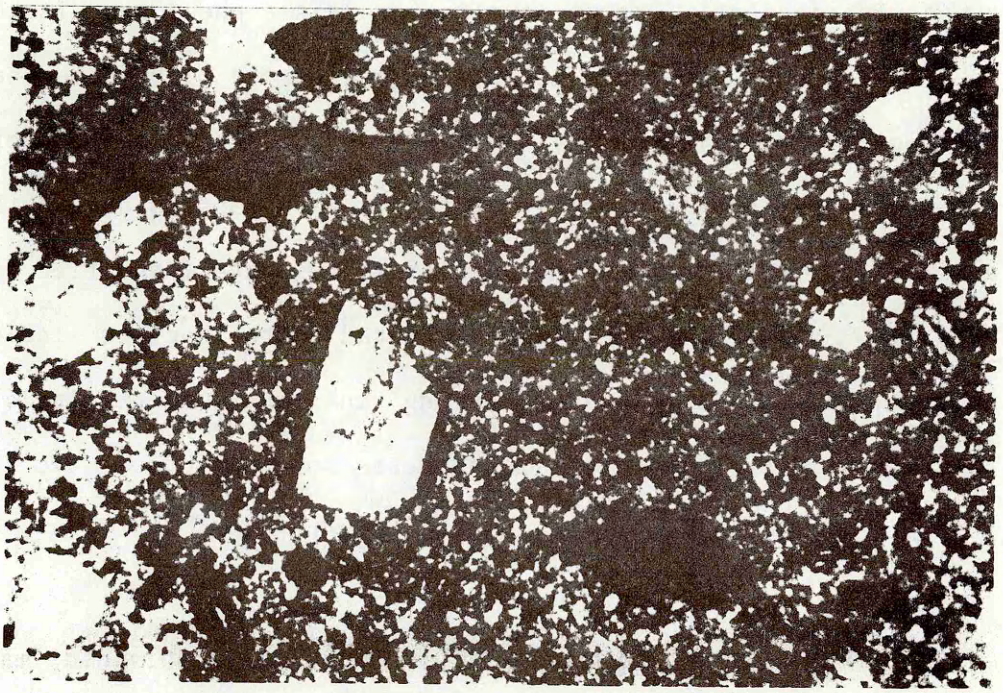

Plate 5.1a. Phenocrysts of clinopyroxene (colourless) and Fe-Ti oxides in andesite (81055).
PPL. Field of view 2.23 mm.

Plate 5.1b. Phenocrysts of plagioclase (colourless) sphene rimmed by oxide (dark brown) and amphibole (brown) in dacite (81054).
PPL. Field of view = 3.47 mm.

(less than 0.5 mm) idiomorphic and hypidiomorphic crystals forming glomeroporphyritic aggregates (Plate 5.1a). Some flows show extensive alteration to epidote whilst in others an amouring rim of iron oxides has prevented further degradation. Olivine is a notable phase in contrast with its virtual absence from the La Negra Formation. However, it is generally altered to iron oxide, either marginally and along cracks, or, in extreme cases, being completely pseudomorphed. Rarely, one finds crystals of olivine with rims of orthopyroxene, which could be due to down temperature resorption of olivine. Orthopyroxene is a rare phase, and when present is completely serpentinized and heavily corroded. Amphibole is found in the dacites as small, idiomorphic and hypidiomorphic phenocrysts which are sometimes zoned. It never exceeds 5% of the total phenocryst content. Quartz is also found as a phenocryst in these evolved rocks. The occasional coexistence of quartz and olivine may be due to the rimming of the latter by iron oxides, thus preventing resorption: the composition of the olivine is difficult to assess due to the degree of alteration, but Baeza (1976) claims to have identified fayalite-rich crystals. Other phenocrysts restricted to the dacites include sphene, biotite, and apatite, all occurring in minor quantities (Plate 5.1b). Evidence of a metamorphic paragenesis for the former two minerals as suggested by Baeza (op. cit.) was not observed.

Groundmasses contain ubiquitous finely divided magnetite and plagioclase microlites, frequently albitized. These microlites sometimes give rise to a trachytic texture. Ferromagnesian minerals are extensively chloritized; quartz grains occur in the evolved lavas. Almost all the groundmasses have suffered haematite staining. In some of the eastern flows quartz veining is prominent, presumably related to the silicic alteration which affected the intrusives of Cerritos Bayos

(Section 6.2.2).

5.4.3 Major and trace element variations

The lavas of the Indio Muerto Formation show a range in SiO_2 content from 51.7 - 67.9% though some of these values are probably enhanced by post consolidation quartz veining. The samples analysed define a high K calcalkaline series on a K_2O - SiO_2 diagram, and span a much broader compositional range than the La Negra Formation (Figure 5.2). None of the lavas can be considered primary mantle melts as Cr (<46 ppm), MgO (<4.34%) and Ni (<22 ppm) are all too low. There are trends of decreasing TiO_2, Al_2O_3, Fe_2O_3, MnO, MgO, CaO, Co, Sr and V, increasing Na_2O, K_2O, Ba, Rb, Th, Zr, Hf, Ta and Nb, and roughly constant Y (excluding sample 81054) with increasing SiO_2. P_2O_5 contents remain constant but fall in the dacites, and Cr and Ni have a nebulous distribution. All the samples are LREE enriched (Figure 5.3) with $(Ce/Yb)_N$ extremely uniform between 4.5 and 5.0; Ce_N and Yb_N range from 60.9 - 93.6 and 12.1 - 20.5 respectively, both positively correlated with SiO_2. The magnitude of ubiquitous negative Eu anomalies (Eu/Eu^* = 0.94 - 0.45) increases with fractionation. The exception to these geochemical characteristics is sample 81054 which has a much more fractionated REE pattern with $(Ce/Yb)_N$ = 10.3, Ce_N = 37.5 and Yb_N = 3.64. Coupled with this are low concentrations of Zr, Hf, Ta, Nb, Ba, Rb, Sr and Th; major elements (including K_2O) continue the trends defined by the other samples.

The lavas also display trace element features typical of subduction related magmatism, viz. high ratios of LILE/HFSE and alkalis/LREE, and relative depletions of Ta and Nb (Figure 5.4), though as outlined in

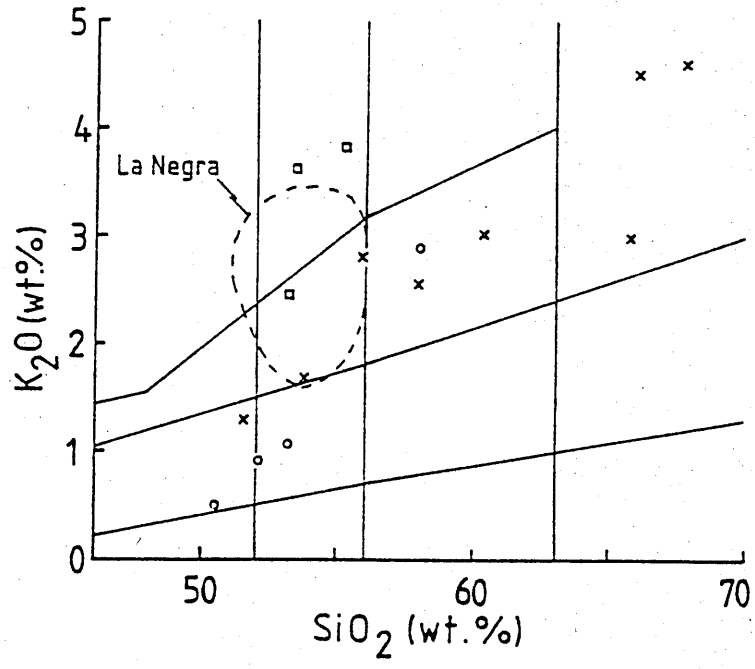

Figure 5.2

K_2O - SiO_2 diagram for the lavas of the Indio Muerto Formation (×) and the Augusta Victoria Formation (□ - high K group: o - low K group). The field of the La Negra Formation is shown for comparison. Field boundaries from Peccerillo and Taylor (1976).

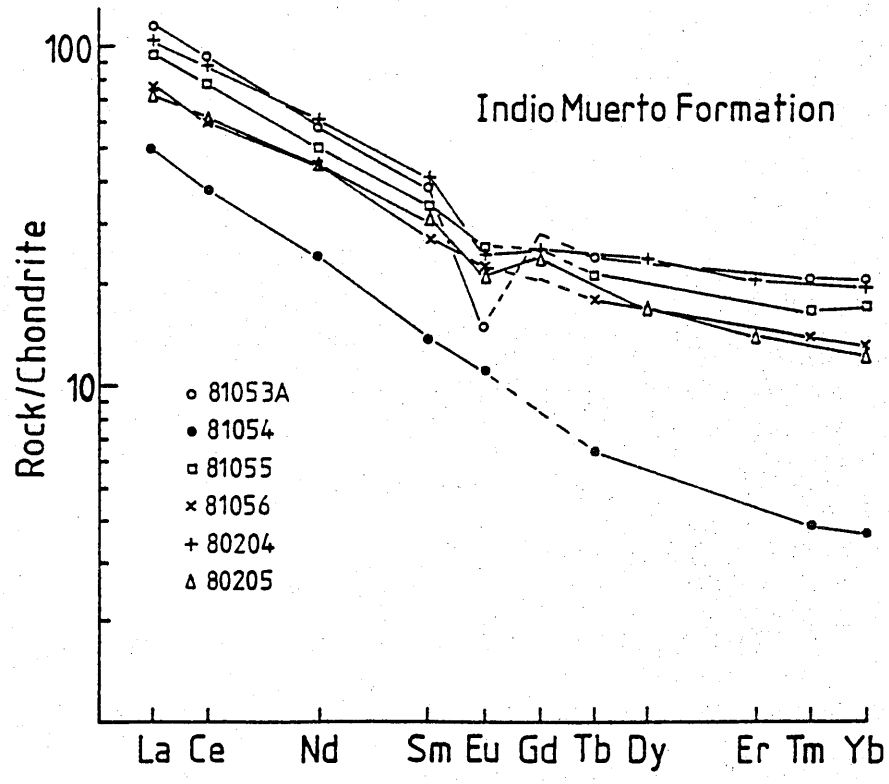

Figure 5.3

Chondrite normalised REE plot of the Indio Muerto Formation.

Section 3.7 these do not necessarily represent a volcanic arc environment, but can be associated with retro arc marginal basins.

5.4.4 Isotope Geochemistry

Sr isotopes were determined on four samples of the Indio Muerto Formation and Nd isotopes on two of these. An age of 130 Ma was assumed on the basis of the Formations' relationships with Lower Cretaceous sediments (Section 5.4.1). The Sr isotope data produce a range of initial $^{87}Sr/^{86}Sr$ ratios from 0.70220 to 0.70534 (ε^{i}_{Sr} = -33.3 to +11.3) which show no correlation with other geochemical parameters, even when sample 81054 is omitted. Initial $^{143}Nd/^{144}Nd$ ratios are 0.512396 and 0.512499 (ε^{i}_{Nd} = -1.50 and +0.51).

5.4.5 Discussion

It was noted earlier that the lavas of the Indio Muerto Formation had undergone post eruptive alteration. Geochemically its effects can be seen most notably in the random variations in ε^{i}_{Sr}. Furthermore, sample 81053A, which has been laced by quartz veins, also has high concentrations of Rb and Th which give pronounced spikes on the MORB normalised plot (Figures 5.4). The coherence of the REE and HFSE data (Figures 5.3 and 5.4) suggests that these have been unaffected by the alteration processes, and thus provide a basis for petrogenetic evaluation.

The major and trace element data are generally similar to other high K andesite suites from continental margins (Ewart, 1982) except that the Indio Muerto Formation has very low concentrations of MgO, Cr and Ni and lower Sr, CaO and Al_2O_3 contents. The fractionation trends

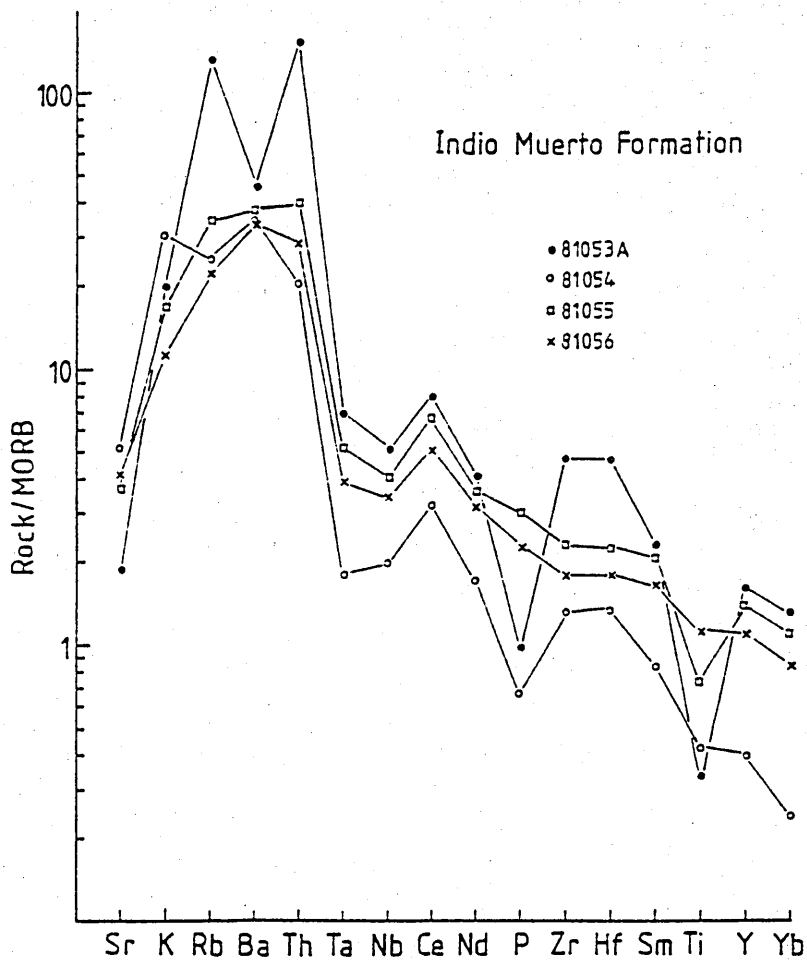

Figure 5.4 MORB normalised plot of the Indio Muerto Formation. Fractionation of apatite is apparent in samples 81053A and 81054 by the pronounced negative P anomalies.

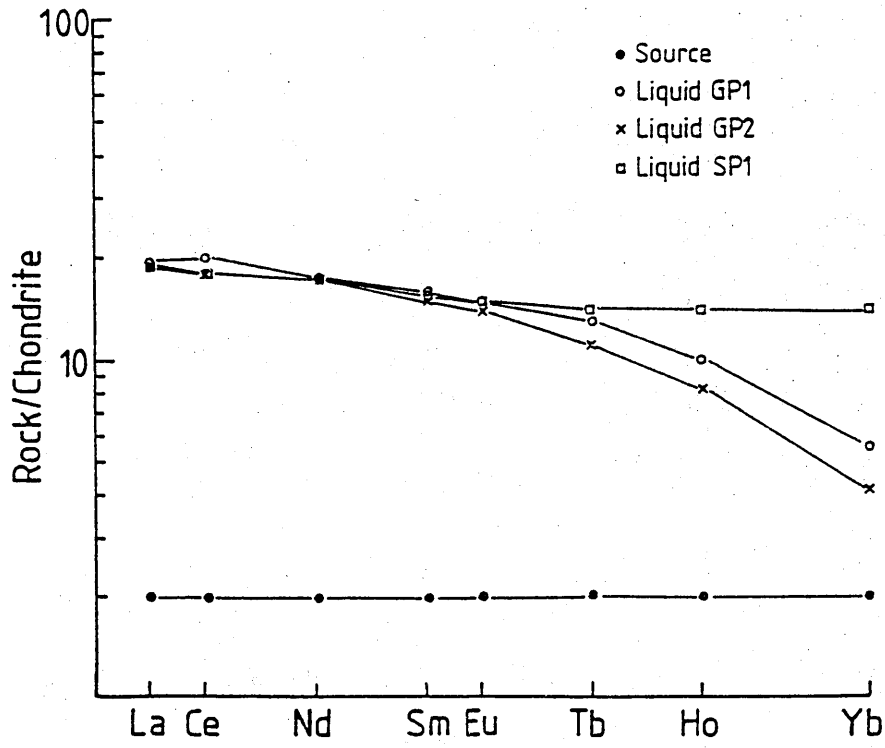

Figure 5.5 REE modelling of mantle melting to illustrate the effects of residual garnet in liquids derived from garnet peridotite (GP1 and GP2) when compared to that derived from spinel peridotite (SP1). See Table 5.1 for modelling parameters. All sources have (arbitrarily) 2 x chondrite abundances: degree of melting = 10%.

Table 5.1a Phase compositions of sources and liquids used in illustration of 10% mantle melting

Phase	Solid	Liquids GP1	GP2	Phase	Solid	SP1
Ol	0.55	0.1	0.4	Ol	0.55	0.2
Cpx	0.10	0.4	0.1	Cpx	0.25	0.6
Opx	0.25	0.1	0.4	Opx	0.20	0.2
Gt	0.10	0.4	0.1			

Table 5.1b Distribution coefficients used (Frey et al., 1978b)

	Ol	Cpx	Opx	Gt
La	0.0005	0.02	0.0005	0.004
Ce	0.0008	0.04	0.0009	0.021
Nd	0.0013	0.09	0.0019	0.087
Sm	0.0019	0.14	0.0028	0.217
Eu	0.0019	0.16	0.0036	0.320
Tb	0.0019	0.19	0.0059	0.700
Ho	0.0020	0.195	0.0089	1.4
Yb	0.0040	0.20	0.0286	4.03

are broadly consistent with an overall fractionation scheme involving removal of plagioclase, olivine, pyroxene and titanomagnetite, and in the more evolved rocks (e.g. 81053A) apatite, as portrayed by the pronounced negative P anomaly of this sample in Figure 5.4. Rayleigh fractionation modelling for incompatible HFSE (Zr and Hf) indicates that 23% fractional crystallization is needed to move from 81056 (basic) to 81055 (intermediate). There are, however, differences between the lavas, even excluding the anomalous sample 81054. For instance the Hf/Ta ratio of 81053A (9.0) is higher than those of 81055 and 81056 (6.0); this difference is too great to be produced by either equilibrium partial melting as both elements have K_D's approaching zero during mantle melting or by fractional crystallization as neither sphene nor zircon is seen as a phenocryst phase in the lavas in question. Consequently the variation is probably due to trace element heterogeneities in the source region. A further implication of this is that the lavas are the products of discrete batches of melt from a variety of mantle sources.

Sample 81054 shows pronounced HREE depletion suggesting that garnet was an important phase in its genesis (Figure 5.5 and Table 5.1). As this is not a phenocryst phase in the rock it is considered that the low concentrations of Yb and Y are governed by partial melting processes. If 81054 were derived from the same source as the other samples but by a lower degree of partial melting in which garnet was residual, then the concentrations of Ce, Zr, Hf, Nb and Ta should be the highest of the suite; this is obviously not the case as these elements are relatively depleted in 81054. Consequently the observed geochemistry requires a source in which garnet is stable at high degrees of melting and/or a source which is depleted in the aforementioned elements and still retains garnet in the residue during partial melting. A notable feature of the

REE pattern is the absence of a Eu anomaly given the evolved natue of the rock and the presence of plagioclase phenocrysts. Coupled with this is a high concentration of Sr which, taken together, may be indicative of high Sr contents and a positive Eu anomaly in the source, plagioclase accumulation or contamination by a crustal melt dominated by plagioclase breakdown. With regard to the latter two possibilities one might also expect CaO or Na_2O to be high, which is not the case. Furthermore, the rock is no more plagioclase phyric than other members of the Formation. On balance, therefore, it is thought that the geochemical features of 81054 reflect source characteristics and partial melting processes rather than upper crustal processes.

Crustal contamination effects are difficult to model due to the disruption of the Sr isotope systematics and LILE abundances by the alteration discussed above. The variation in initial Nd isotope ratios may be attributable to crustal contamination with the more evolved rock having the lower ε^{i}_{Nd} value, in line with the AFC models of DePaolo (1981).

5.4.6 Tectonic setting

The rocks of the Indio Muerto Formation present a similar problem to those of the La Negra Formation (Chapter 3) as regards tectonic setting. Whilst the trace element geochemistry indicates subduction related volcanism it cannot distinguish between material actually erupted in the arc or within the back arc basin when both display calcalkaline characteristics. However, it has been argued earlier (Chapter 3) that the Lower Jurassic La Negra Formation may represent marginal basin volcanics thus indicating that this part of South America had a history of extensional tectonics prior to the eruption of the Indio Muerto Formation.

Moreover, there is a scarcity of pyroclastic material within the Formation, and the post-Middle Jurassic dykes which cut the Sierra de la Cruz pluton (Chapter 4) on the eastern margin of the Cordillera de la Costa may have been feeders to a Cretaceous arc which has since been eroded away. The presence of Cretaceous marginal basin sequences in Peru (Atherton et al., 1983) and Central Chile (Levi et al., 1982) render it highly plausible that a similar scenario existed in northern Chile.

5.5 Augusta Victoria Formation

5.5.1 Field relations

The Cerros de Montecristo, 15 km to the west of Chuquicamata (Figure 5.1) are composed of Jurassic marine sediments and upper Jurassic/lower Cretaceous continental sediments overlain by a sequence of tuffs, lavas and volcaniclastics, and intruded by a granitic pluton. The volcanic succession was equated by Ferraris (1978) with the Augusta Victoria Formation, defined by Garcia (1967) near the railway station of the same name on the Antofagasta to Salta line south of the area of the present transect. In the study area the formation is dominated by tuffs and volcaniclastics: the lavas are generally less than 5m thick and probably represent distal deposits. The whole sequence dips at 10^{o} - 15^{o} away from the granite suggesting that locally, at least, dips are controlled by updoming associated with intrusion. Close to the intrusion much of the sequence is hornfelsed and haematite stained: the tuffs and volcaniclastics are most strongly affected. This formation may be coeval with the Cerro Negro Formation (Section 5.6) though the lavas of the latter are much more evolved. Both formations, however, have a predominance of pyroclastics.

5.5.2 Petrography

The lavas themselves are porphyritic basalts, basaltic andesites and andesites. Ubiquitous phenocrystal plagioclase is often fresh, and generally forms idiomorphic - hypidiomorphic laths less than 1 mm long; its composition varies from An_{65-70} in the basalts to An_{45} in the andesites, some crystals exhibiting weak normal and concentric zoning. Evidence for disequilibrium between crystal and melt and for multistage growth is apparent in partially resorbed phenocrysts, and zones of melting being jacketed by idiomorphic overgrowths (Plate 5.2a). Augite occurs in glomeroporphyritic aggregates; it is susceptible to alteration to green chlorite, but rimming by fine granules of oxide armours it against further decay. Olivine is a rare phase forming rounded crystals with oxide rims. Amphibole is present in parts of the succession though it is extensively pseudomorphed by oxide due to water loss on eruption: basaltic hornblende may be seen to form during this process. Some amphibole also rims clinopyroxene cores. Fe-Ti oxides are present in all the lavas though it is often difficult to distinguish from the corroded, pseudomorphed amphibole. Groundmasses have intersertal and intergranular textures, and consist of fine plagioclase microlites, finely divided oxides and a brown iron rich mesostasis. Occasionally small clinopyroxenes are found though these are often corroded.

5.5.3 Geochronology

Five lavas from the Augusta Victoria Formation gave a whole rock Rb-Sr age of 105 $\pm$ 19 Ma with an initial $^{87}Sr/^{86}Sr$ ratio of 0.7043 $\pm$ 3 (ε^{i}_{Sr} = -4.3) (Figure 5.6). Two of the samples have been strongly altered, but nonetheless the remaining three yield an age which is analytically indistinguishable from that given above. Huete *et al.* (1977) have dated rhyolites by K-Ar from the Sierra del Medio (Peña

a.

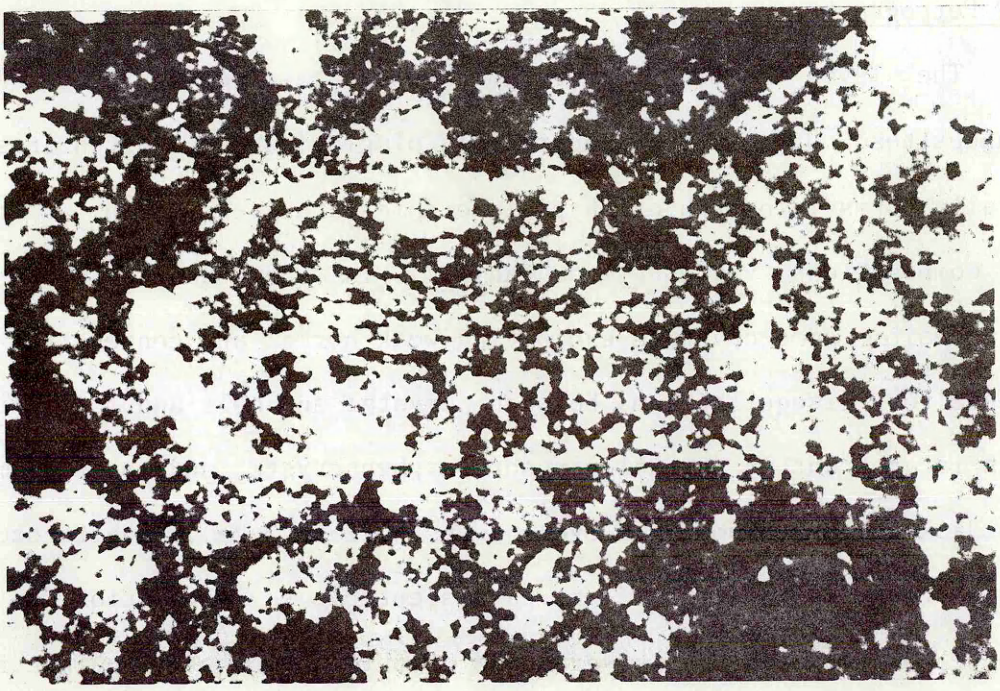

b.

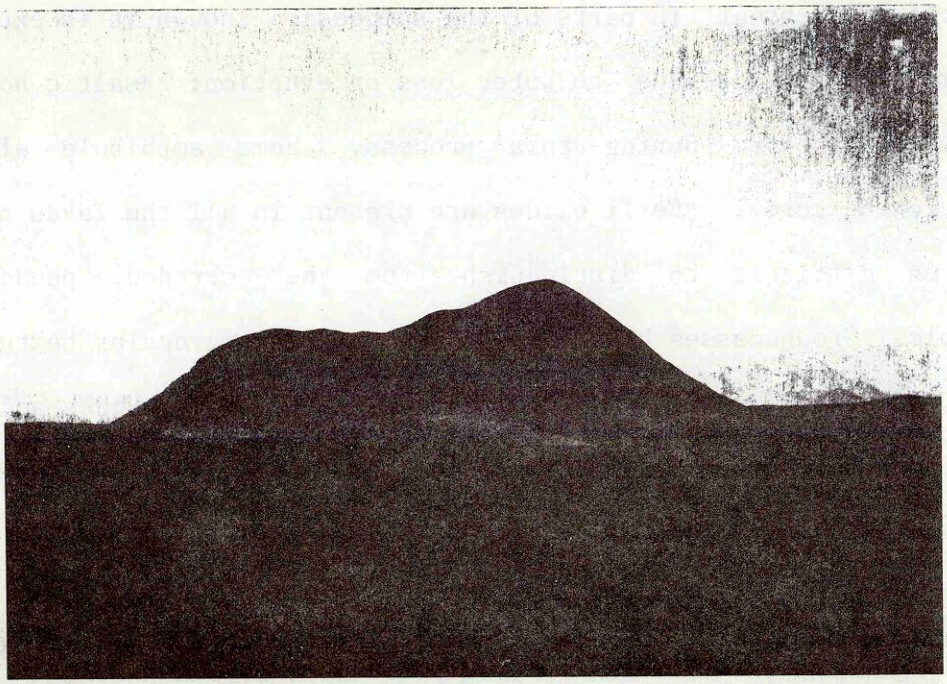

Plate 5.2a. Multistage growth of plagioclase in andesite (81135).
PPL. Field of view 3.47 mm.

Plate 5.2b. Hill on the Pampa Limon Verde composed of tuffs and lavas of the Cerro Negro Formation.

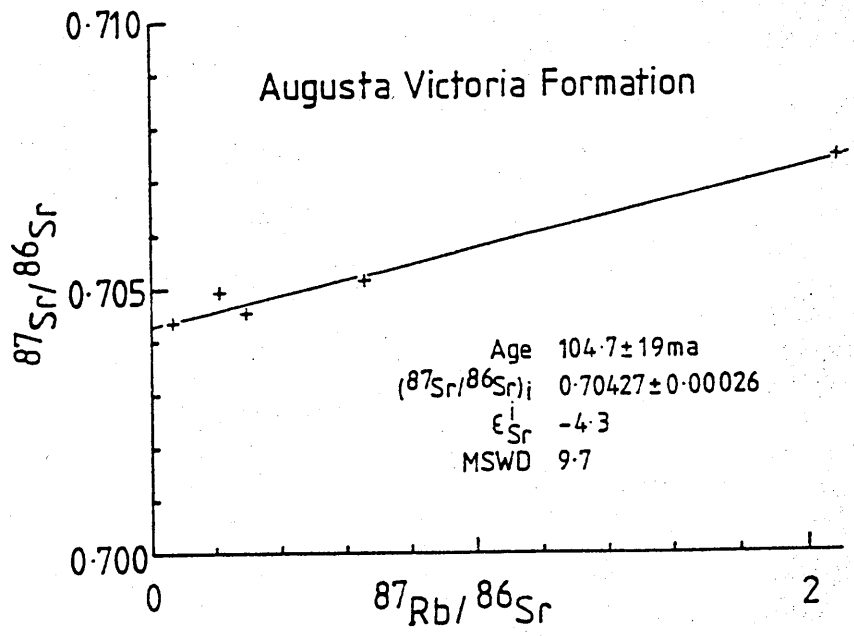

Figure 5.6

Rb - Sr whole rock isochron diagram for the Augusta Victoria Formation.

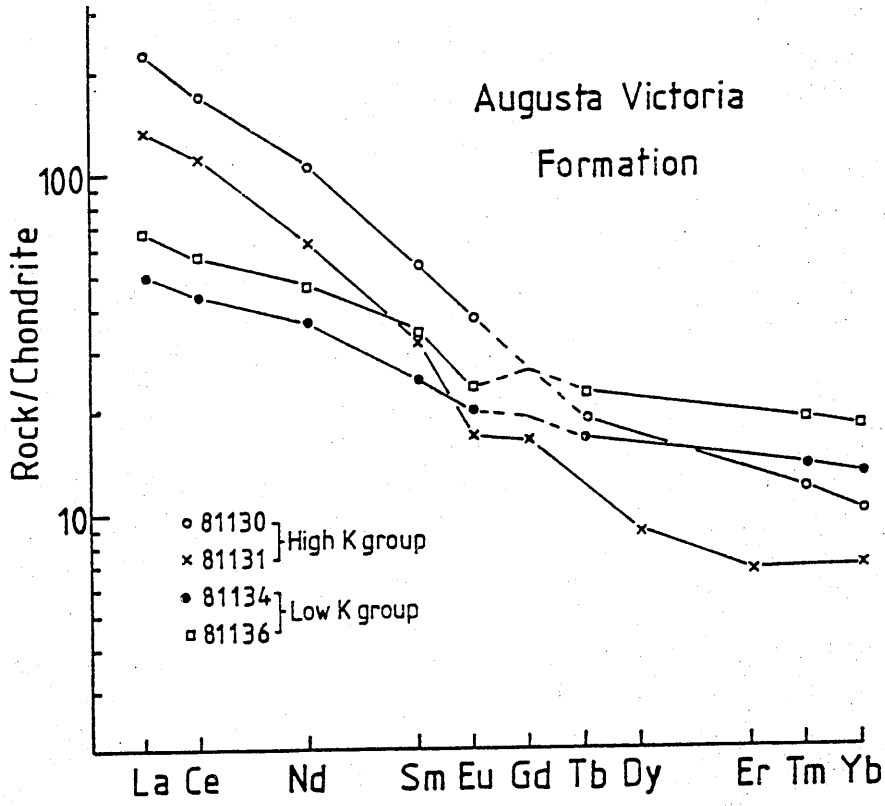

Figure 5.7

Chondrite normalised REE plot of the Augusta Victoria Formation.

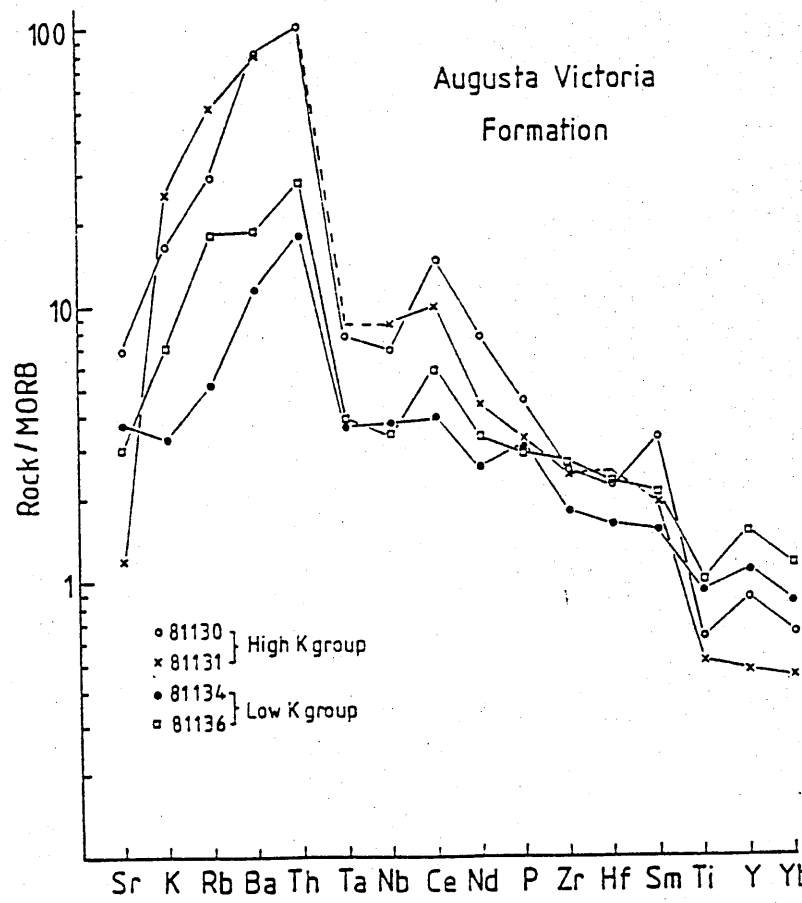

Figure 5.8

MORB normalised plot of the Augusta Victoria Formation.

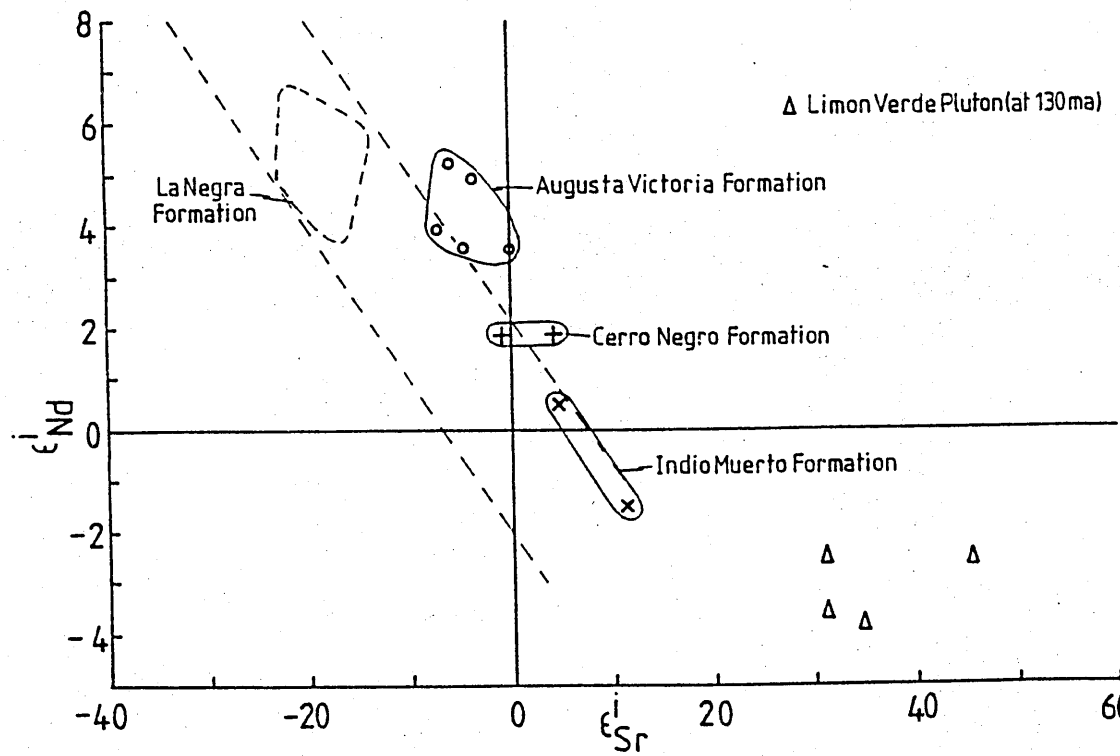

Figure 5.9 $\varepsilon^i_{Sr} - \varepsilon^i_{Nd}$ diagram for the Cretaceous volcanic rocks. The position of the Limon Verde pluton at 130 Ma is also shown.

Morada Formation of Maksaev (1978)) to the northeast at 109 - 114 Ma, and basalts of comparable ages (100 - 117 Ma) are also reported in a K-Ar study from 27°S by McNutt et al. (1975).

5.5.4 Geochemical characteristics

The analysed lavas show a restricted range in SiO_2 between 50.5 - 58.0%, and have low Cr (< 62 ppm), Ni (<28 ppm) and MgO (<5.6%). Two separate groupings are defined on a K_2O - SiO_2 diagram (Figure 5.2). The one is a high K trend of shoshonites and high K basaltic andesites, whereas the other follows a trajectory from basalt through basaltic andesite to high K andesite, similar to that shown by the Indio Muerto Formation. This division into two groups is also apparent when other elements are considered. The higher K group has higher concentrations of Nb, Ta, Rb, Ba, Th, Na_2O, P_2O_5 and LREE, and lower CaO, HREE, Y, TiO_2 and V for a given Zr content: Sr is highly variable. The differences amongst the REE are clearly seen in Figure 5.7 where the higher K rocks have $(Ce/Yb)_N$ = 16.2 - 16.9 compared to 3.2 - 3.5 for the lower K group. The MORB normalised diagram (Figure 5.8) shows that the lavas have a subduction related signature with high ratios of alkalis/HFSE and alkalis/REE, but that in certain samples from both groups the Ce/Ta ratio is close to that of N-type MORB (56), though the elemental concentrations are considerably higher than MORB.

5.5.5 Isotope Geochemistry

Initial ε_{Sr} values (i.e. at 105 Ma) vary from -7.0 to +0.10, though the fresher samples define a narrower range from -7.0 to -4.9. The total span in ε^{i}_{Nd} is +3.6 to +5.2, the altered lavas being indistinguishable from the others. These parameters indicate that the lavas were derived from a source with time-integrated depleted isotopic

characteristics (Figure 5.9). The extension of the Augusta Victoria Formation field on Figure 5.9 to high ε^{i}_{Sr} values may be a function of the alteration - a hypothesis substantiated by the highly variable Sr concentrations - yet there is no dramatic increase in ε^{i}_{Sr} as in the case of the Indio Muerto Formation. The position of the lavas on this diagram is therefore close to where they would have been before alteration.

5.5.6 Discussion

Consideration of the REE profiles in Figure 5.7 suggests that the major difference between the two rock groups may be due to variations in the degree of partial melting. Thus the higher K series (samples 81130 and 81131) could be generated by a lower degree of partial melting of the same source than the lower K group (81134 and 81136); the fractionated HREE of the former ($(Tb/Yb)_N$ = 1.82 - 1.88) point to garnet being a residual phase (Figure 5.5). This would also be consistent with the higher incompatible element concentrations and lower Y of the higher K group. There are, however, a number of objections to this explanation. Firstly the high K group itself was not generated from a single source; sample 81130 is slightly more basic than 81131, yet has higher REE contents and a smaller negative Eu anomaly (Eu/Eu^* = 0.88 compared to 0.71). Consequently those two samples are not related by fractional crystallization of the observed plagioclase dominated phenocryst assemblage. Secondly there is a wide range in Zr/Nb ratios with the higher K group varying from 6.6 - 9.5, and the lower K rocks spanning 12.5 - 20.2. This variation may potentially reflect amphibole fractionation from the high K (amphibole phyric) group leaving the residual liquids (the low K (non-amphibole phyric) group) with higher Zr/Nb ratios (Pearce and Norry, 1979). However the rocks of the former group contain more Zr than

most of the latter, and so it is impossible to move from one group to the other by fractional crystallization. Furthermore, crystallization in the latter group would also have to incorporate apatite to explain its lower P_2O_5 contents; this phase is not observed in the rocks and there are no pronounced depletions of P on the MORB normalised plot (Figure 5.8). The large variation in Zr/Nb within the low K group also cannot be explained by fractional crystallization of the observed phenocryst assemblages. Consequently, it is envisaged that the lavas were injected as discrete batches from geochemically distinct source regions, the more enriched ones, at least, being in the garnet stability field.

Crustal contamination is believed to have played a minimal role in the petrogenesis of the Augusta Victoria Formation. There are no correlations between initial isotope ratios and indices of differentiation as would be expected if AFC processes were operative (DePaolo, 1981; Menzies et al., 1983) or inverse correlations, at least in the most basic rocks, if contamination were analogous to that observed in the Deccan (Cox and Hawkesworth, 1984) or Skye (Thirlwall and Jones, 1983).

Calculations can therefore be made as in Section 3.8 to determine the subduction zone contributions for various elements and elemental profiles for the mantle sources. Table 5.2 shows that generally large proportions (>50%) of K, Rb, Ba, Th and lesser proportions of Ce, Nd, P and Sm (<60%) are in the subduction zone component. MORB normalised profiles for the unmodified mantle sources of samples 81130, 81134 and 81136 (Table 5.3) are shown in Figure 5.10. Whilst the lower concentrations of Y and Yb for sample 81130 (high K group) are probably due to the high K_D of these elements relative to Hf in residual garnet the differences between the low K group samples show that 81134 was

Table 5.2 Subduction zone contributions for the Augusta Victoria Formation

Sample	81130	81131	81132	81134	81136
K	56	67	62	0	49
Rb	75	84	83	30	80
Ba	91	90	86	68	81
Th	93	-	-	80	87
Ce	61	28	-	16	34
Nd	38	0	0	0	9
P	20	0	0	28	1.4
Sm	50	24	37	4	0

Table 5.3 Unmodified mantle concentrations for the Augusta Victoria Formation

Sample	High K 81130	Low K 81134	81136
Ce	5.12	3.96	2.78
Nd	3.72	2.81	2.28
Sm	0.493	0.598	0.586
Tb	0.088	0.106	0.101
Yb	0.197	0.347	0.334
K(%)	0.098	0.060	0.047
Rb	1.33	0.897	0.620
Ba	13.6	9.10	6.14
Th	0.127	0.088	0.063
P(%)	0.039	0.033	0.026
Ta	0.125	0.081	0.059
Nb	2.15	1.59	1.02
Zr	20.4	19.8	20.6
Hf[1]	0.475	0.475	0.475
Y	2.33	4.03	3.82

1. Hf concentration assumed.

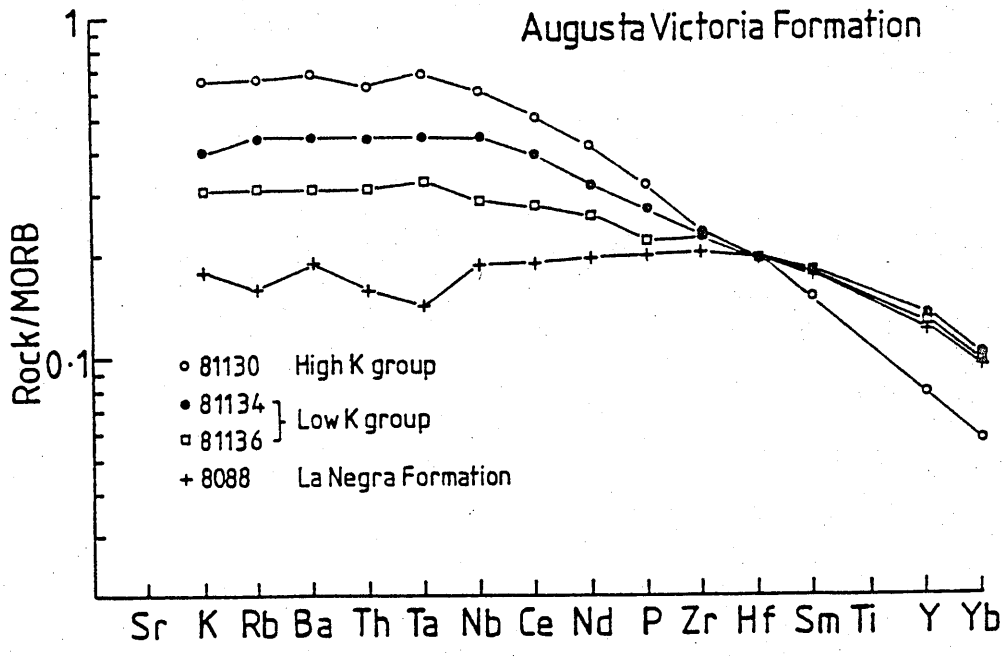

Figure 5.10

MORB normalised plots of the calculated unmodified mantle sources for the Augusta Victoria Formation assuming Hf mantle = 0.475 ppm (Table 5.3). The calculated source for the La Negra Formation is shown for comparison.

derived from a slightly more enriched source than 81136, Both sources, however, are enriched relative to that of the La Negra Formation (Section 3.8).

5.6 Cerro Negro Formation

5.6.1 Introduction

In the foothills of the north-western margins of the Sierra Limon Verde, as well as there being outcrops of the schist belt and Triassic-Jurassic succession, there are also several exposures of intercalated lavas, tuffs and clastic sediments forming prominent hills such as Cerro Negro, which rises about 300 m above the level of the Pampa Limon Verde. This unit probably overlies the basal Jurassic, though the actual contact is not observed among the multitude of hillocks protruding through the pampa surface.

5.6.2 Petrography

One major hill in this area consists of dacite-rhyolite tuffs and occasional andesitic - dacitic lavas, with sediments being absent (Plate 5.2b). The tuffs contain both lithic and crystal fragments. Examples of the former include quartzite aggregates derived from the schist belt, lavas and other tuffs, while the overall crystal content comprises quartz, plagioclase, alkali feldspar, biotite, amphibole, pyroxene, magnetite and apatite. In some tuffs different generations of plagioclase are present as evidenced by their relative degrees of alteration and resorption, and an origin involving some form of magma mixing is implied. All the crystals are highly resorbed and fractured, and are supported by fine grained, quartz-rich, crystalline matrices which have often been extensively haematised.

Many of the lavas have suffered extensive alteration with groundmasses largely converted to calcite. Others have experienced milder modification; olivines are iddingsitized, pyroxenes are resorbed, and rimmed and speckled with finely divided oxide, and plagioclase is very turbid. The groundmasses of these lavas consist of plagioclase microlites with an almost trachytic texture, and chloritized ferromagnesian minerals. The freshest lavas are dacites with zoned sodic plagioclase, quartz, biotite, amphibole, and a little potassium feldspar and magnetite. Amphibole is often rimmed by oxide due to water release on eruption.

The occurrence of a large lava pile at this locality as opposed to a mainly sedimentary sequence at Cerro Negro (below) led Baeza (1976) to infer that there had been a volcanic centre here. No evidence for subvolcanic-structures was found in this area during the present study, though the distribution of rock types does indicate the closer proximity of an eruptive edifice.

The section at Cerro Negro is composed predominantly of reddened coarse sandstones and conglomerates, with rare intercalated tuffs and lavas. Solid outcrop is sparse and there are many gaps in the section. The conglomerates contain rounded clasts of quartz, alkali feldspar, ferromagnesian minerals, chert, assorted lavas and sediments ranging up to 15 cm in diameter. Many of the sandstones are micaceous, muscovite being the predominant sheet silicate. Several of these units have a carbonate rich matrix, perhaps indicative of subaerial dehydration of the sand. The presence of muscovite flakes implies that the succession is younger than the schist belt, as this is the only unit hereabouts containing this mineral. (Of course, the relative deformation state would lead one to the same conclusions as to their relative ages). More importantly the

occurrence of chert clasts, similar to those found in the basal Jurassic marine sequence suggests a post lower Jurassic age. In view of the completely marine nature of the Cerritos Bayos Formation and the continental affinities of the basal Cretaceous, these rocks are also assigned to the Cretaceous. Baeza (1976) correlates them with the Upper Cretaceous Quebrada Seca Formation of Montaño (1976) from the Carcaoles region, 50 km to the south.

5.6.3 Geochemical characteristics

As the geochemistry of the tuffs of the Cerro Negro Formation reflects a mixture of juvenile material and lithic fragments, and as there are few lavas in the pile there is little data pertaining to magma compositions. Nonetheless the freshest dacite (81020) has high alkali/HFSE and LREE/HFSE ratios (Ce/Ta = 126), and shows a subduction related geochemical signature (Figure 5.11). The dacite is LREE enriched with a high $(Ce/Yb)_N$ (15.8) due to the low HREE (Yb_N = 3.3; Figure 5.12), which suggests that garnet was a residual phase during partial melting. The lack of a large negative Eu anomaly is perhaps surprising in view of the evolved composition and the plagioclase dominated phenocryst assemblage. A dacitic crystal tuff (81019) has very similar REE characteristics implying that it was derived by a similar process. It also has an almost identical MORB normalised plot to the dacite, but with a pronounced P depletion in keeping with the presence of apatite phenocrysts. A feature of most of the igneous rocks of this formation is their high Sr concentrations, up to 1541 ppm in an altered andesite, and 929 ppm in sample 81020. If these rocks have evolved by fractional crystallization of, mainly, plagioclase then the original concentrations must have been even higher: alternatively plagioclase accumulation would elevate the Sr levels, and also raise the Eu contents

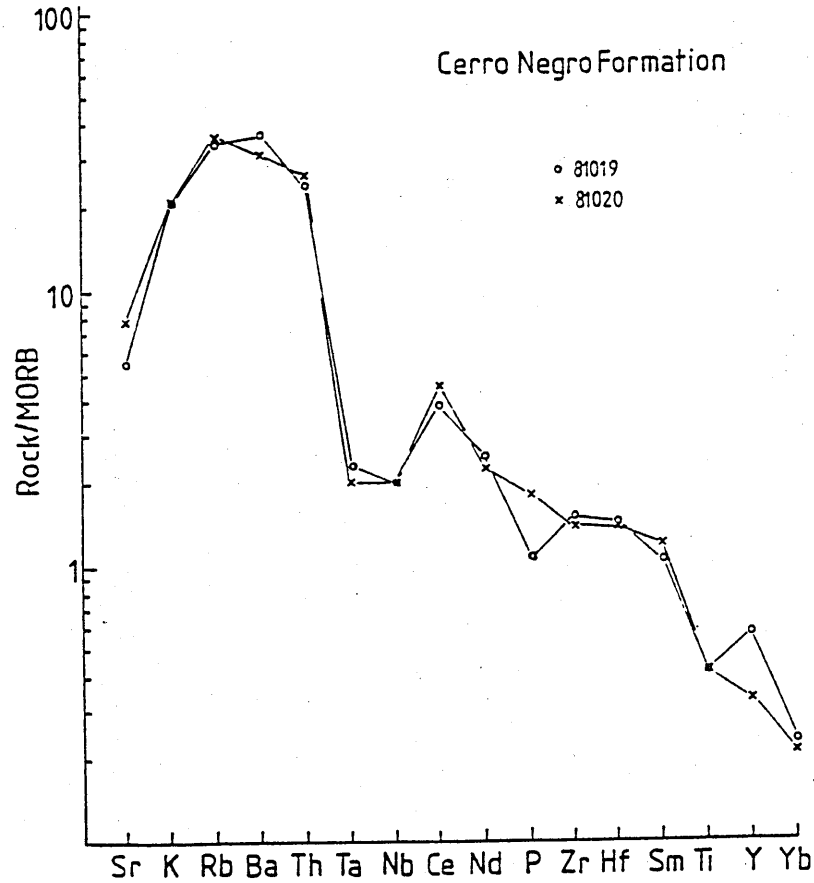

Figure 5.11

MORB normalised plot of the Cerro Negro Formation.

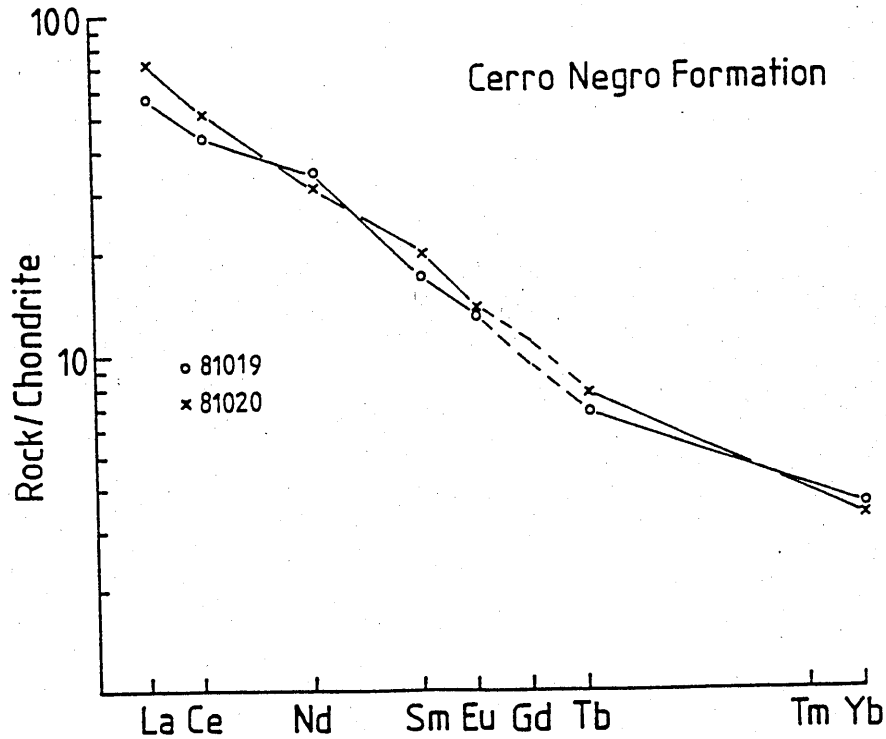

Figure 5.12

Chondrite normalised REE plot of Cerro Negro Formation.

which may explain the lack of negative Eu anomalies.

Sr and Nd isotopes were determined on two samples; the dacite (81020) and a crystal tuff (81019). Given that the age of the Cerro Negro Formation is unclear, there is uncertainty regarding the calculation of initial isotope ratios. If an upper Cretaceous date is assumed ($\sim$70 Ma) the ε^{i}_{Sr} = -0.7 to +4.3 and ε^{i}_{Nd} = +1.85 to +1.88; an age of 80 Ma has little effect on these values: ε^{i}_{Sr} = -2.3 to +2.9 and ε^{i}_{Nd} = +1.98 for both samples. They thus plot between the Indio Muerto and Augusta Victoria Formations on an ε_{Sr} - ε_{Nd} diagram (Figure 5.7), and represent derivation from a time-integrated isotopically depleted source.

5.7 Summary

The Jurassic succession of the Cerritos Bayos area is one of marine sedimentation comprising a number of shallowing cycles separated by transgressions. Locally gypsum beds were formed during periods of shallowest water conditions. This contrasts markedly with the Jurassic of the Cordillera de la Costa where the thick volcanic sequence of the La Negra Formation was extruded in the Lower Jurassic (Chapter 3) and was later intruded by calcalkaline plutonics (Chapter 4).

Continental sedimentation ensued in the uppermost Jurassic and/or basal Cretaceous when conglomerates and arenites were laid down. Intercalated with and succeeding the sediments are the calcalkaline lavas of the Indio Muerto Formation. These show a wider compositional range than the La Negra Formation, and, coupled with the geochronological and stratigraphic relationhips, are therefore not thought to be the lateral equivalents as postulated by Palacios (1978). Predominantly pyroclastic

volcanism accompanied by basic lavas ensued around 105 Ma. These lavas - the Augusta Victoria Formation - are also calcalkaline, but were derived from a variety of variably trace element enriched sources. Further continental sedimentation and intermediate-acidic mainly pyroclastic volcanism occurred in the upper Cretaceous to produce the Cerro Negro Formation.

Overall, therefore, the Jurassic and Cretaceous stratigraphy around Cerritos Bayos represents a transition from marine to continental sedimentation, and towards more pyroclastic volcanism. All the volcanics are subduction related, though whether they represent actual arc material or retro arc eruptions is unclear. Certainly the Jurassic marine sequence was laid down in shallow waters behind the contemporaneous arc to the west, whichever tectonic scenario one accepts for the La Negra Formation, and was probably bounded to the east by a low lying and periodically submerged landmass. During the Jurassic and Cretaceous it is apparent that the locus of observable magmatic activity shifted to the east. This could have been due to a shallowing of the angle of the subduction zone, to erosion of the western edge of the continental margin, or to cooling and stabilization of the overriding mantle wedge beneath the present day Cordillera de la Costa, thus necessitating a deeper, more easterly, source of magma generation, assuming a constant dip of the Benioff zone.

CHAPTER 6

CRETACEOUS PLUTONISM

6.1 Introduction

In a similar manner to the Jurassic plutons, those of Cretaceous age mainly form a north-south oriented linear belt (Figure 6.1); this zone, however, is sited to the east of the Pampa del Tamarugal, through the Cerros de Montecristo and Cerritos Bayos. Isolated stocks occur further west such as in the Pampa Negra to the east of the Sierra de la Cruz; the granitic belt to the north of Sierra Gorda is also ascribed to this phase of plutonism (Ferraris, 1978). Plutonic rocks occur in the Sierra del Medio to the east, including Cerro Colorado, though this belongs to an intrusive episode at the Cretaceous/Tertiary boundary (Section 6.3.4). Four complexes are described in the following sections: their modal mineralogy is presented in Appendix B.

6.2 Field relations and petrography

6.2.1 Cerros de Montecristo

The general geology of the Cerros de Montecristo, to the west of Chuquicamata, was outlined in the previous Chapter. These hills are mainly formed of a granitic pluton, the composition of which varies from quartz monzodiorite through granodiorite to granite (Figure 6.2), with the more evolved rocks lying to the north-west. The intrusion is mostly fine-medium grained, but coarser facies do occur. The intrusion of this pluton seems to have been passive as no stoped blocks, screens or roof pendents were observed in the vicinity of the host lavas and volcaniclastics of the Augusta Victoria Formation.

Plagioclase is always an early crystallizing phase, sometimes

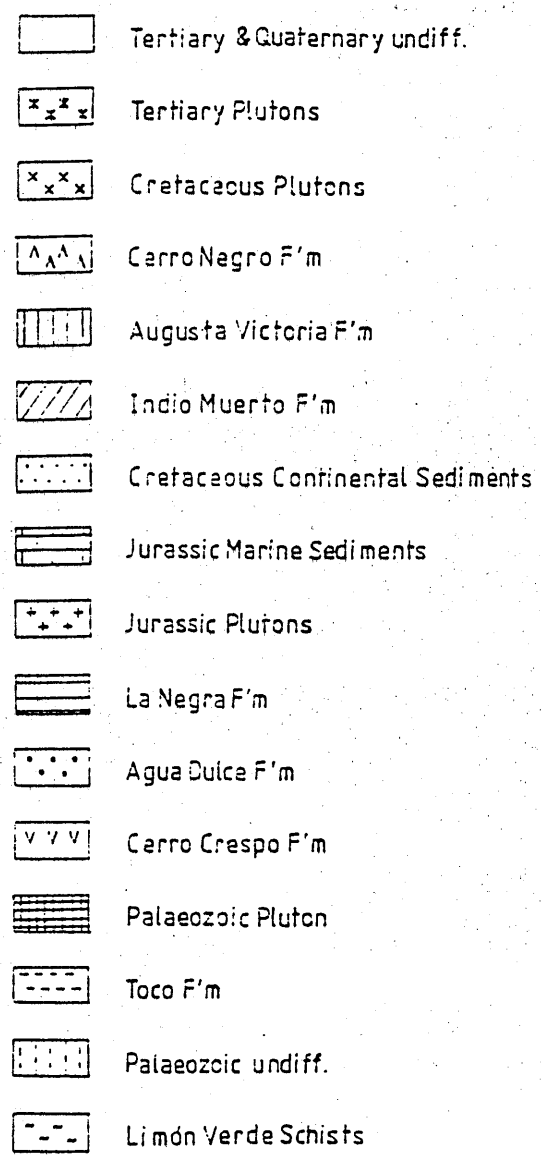
Tertiary & Quaternary undiff.
Tertiary Plutons
Cretaceous Plutons
Carro Negro F'm
Augusta Victoria F'm
Indio Muerto F'm
Cretaceous Continental Sediments
Jurassic Marine Sediments
Jurassic Plutons
La Negra F'm
Agua Dulce F'm
Cerro Crespo F'm
Palaeozoic Pluton
Toco F'm
Palaeozoic undiff.
Limón Verde Schists

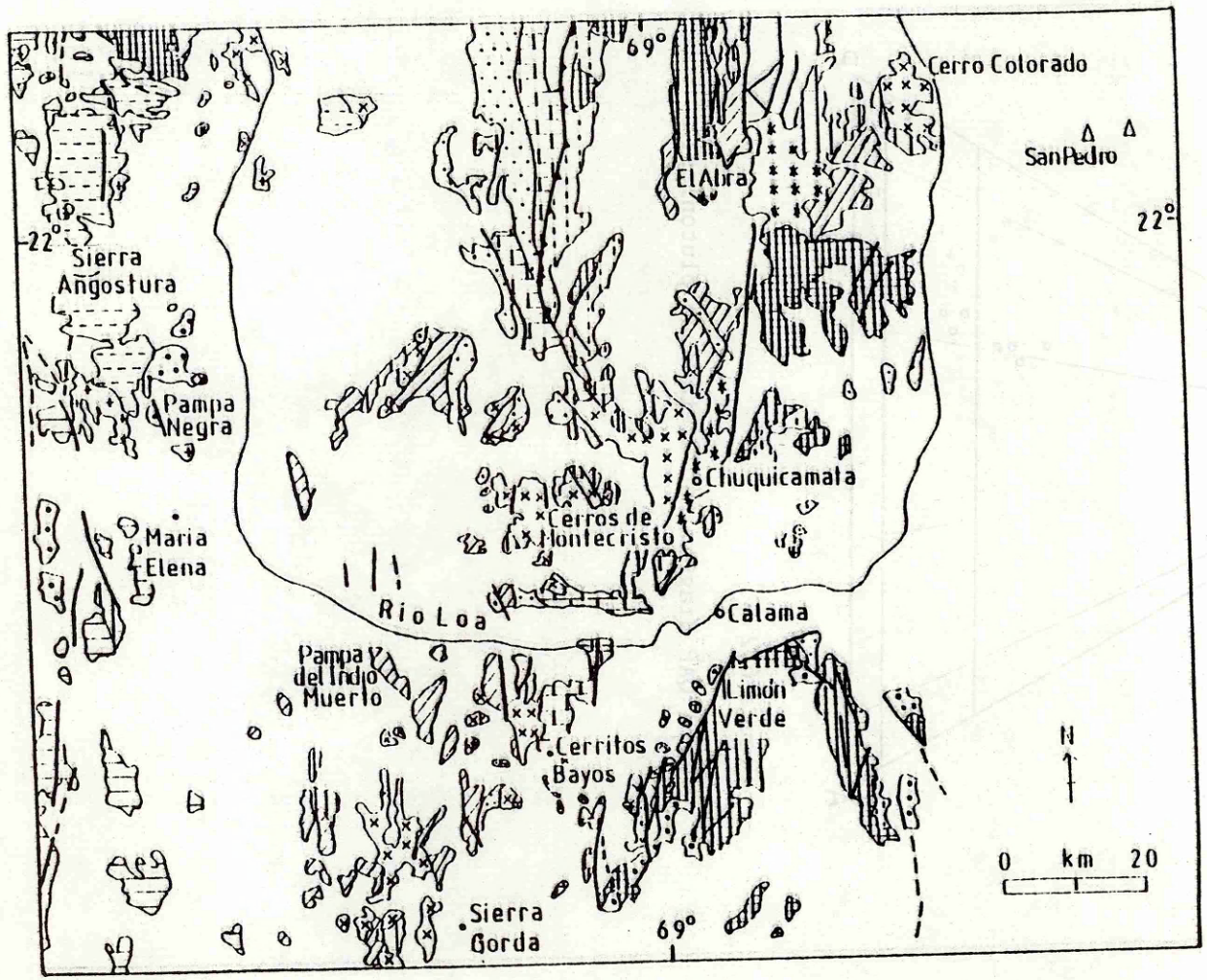

Figure 6.1 Generalised geological map showing the location of Cretaceous plutons described in this study (after Servicio Nacional de Geologia y Mineria, 1980). Key on facing page.

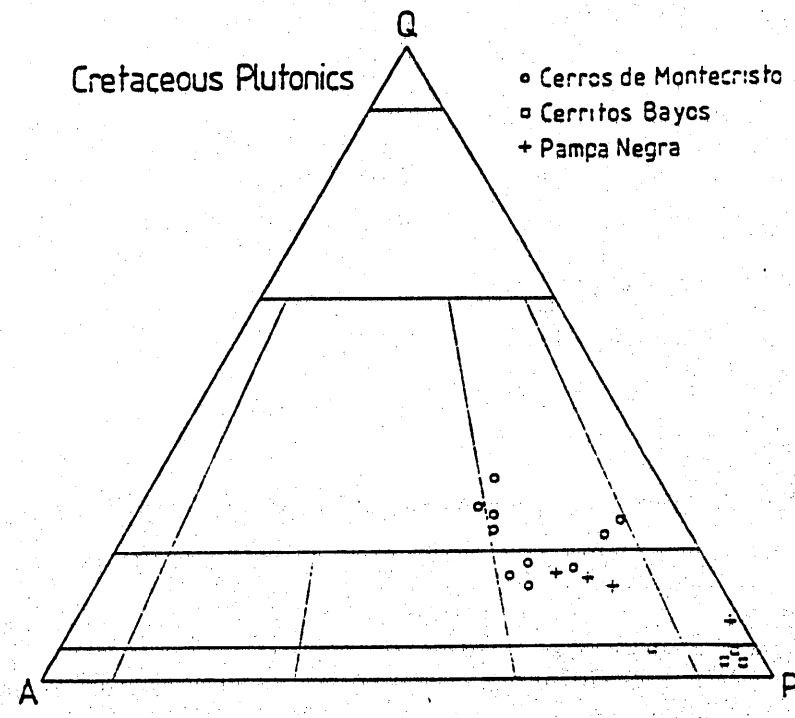

Figure 6.2

Modal QAP diagram for Cretaceous plutonics.

exhibiting concentric zoning. Cores have a uniform composition of about An_{32} - An_{38}, though some zoned crystals have albitic margins: sericitization is minimal. Augite occurs as euhedral-subhedral crystals in all the more primitive rocks, but began to crystallize after plagioclase; inclusions of the one may be found within the other. Margins are often corroded, and there is ubiquitous alteration to mainly fibrous amphibole and iron oxides, or, more rarely, into biotite or epidote; relict fresh cores are frequently observed. Amphibole is present in two forms: firstly as a fibrous replacement of clinopyroxene, and secondly as dark green, pleochroic hornblende. In this latter paragenesis it can occur either as small interstitial crystals or as larger more euhedral grains, poikilitically enclosing apatite and zircon. Marginal alteration to chlorite or biotite is evident in places. Clinopyroxene and hornblende may be found together, with the latter being interstitial to the former. Biotite is present throughout as interstitial plates, occasionally poikilitic to plagioclase, clinopyroxene, apatite, zircon, and Fe-Ti oxides. It sometimes alters at the margins to chlorite and iron oxides. Biotite is also found as an alteration product of clinopyroxene or hornblende, but in these cases has a more amorphous habit. Orthoclase is generally interstitial, but in some of the granodiorites small euhedral-subhedral crystals appear in addition to the usually anhedral grains and poikilitic plates. Turbid alteration of the mineral increases with fractionation but nowhere is it extreme. Quartz remains interstitial throughout the pluton. Fe-Ti oxides have three parageneses, namely as early crystallizing and interstitial crystals, and as a breakdown product of ferromagnesian minerals. Given that the mafic minerals have a tendency to clot together 'primary' oxide is not always distinguishable from 'secondary' oxide. There are several minor phases present in the intrusion. Apatite is ubiquitous as small euhedral crystals which may be

included in clinopyroxene, biotite and hornblende. Sphene occurs as rare, small interstitial crystals: Zircon is present in the more evolved rocks as tiny inclusions within biotite and hornblende. Its apparent absence from rocks with between 61 - 64% SiO_2 may be an artefact of the thin sections available due to its trace abundances.

Several pieces of evidence indicate that localised partial melting has occurred within the pluton. Some of the granodiorites contain small, resorbed, melanocratic enclaves with prominent biotite and plagioclase. As in the Sierra de la Cruz pluton (Section 4.2.4) these were probably earlier crystallized facies of the pluton which have been assimilated back into the main body of the magma. Plagioclase crystals locally show several stages of growth, the different periods being separated by glassy blebs formed around the margins of the original crystal: in some cases the cores may be turbidly altered while the rims are fresh (Plate 6.1a). Plagioclase sometimes contains round blebs of clinopyroxene with associated small needles of apatite. Similar textures have been interpreted by Tindle and Pearce (1983) as being due to incipient partial melting. This texture develops into one where zones of melting, 3-4 mm wide are generated. These areas contain large crystals of plagioclase, clinopyroxene, oxide and orthoclase all undergoing fragmentation, small blebs of mafic material, and acicular crystals of apatite and plagioclase set in a matrix predominantly composed of orthoclase (Plate 6.1b).

Ten km to the WNW of the Cerros de Montecristo the batholith is again exposed on a small ridge rising from the pampa. Here the mineralogy resembles that of the evolved granodiorites described above, though it is a little coarser grained.

a.

b.

Plate 6.1a. Turbid cored plagioclase in granodiorite (81139). XP. Field of view = 2.76 mm.

Plate 6.1b. Zone of melting in granodiorite (81140) containing laths of plagioclase, blebs of birefringent clinopyroxene and opaque oxides; larger crystals on the margins of the zone include plagioclase (twinned) clinopyroxene (orange) and biotite (orange/green).
XP. Field of view = 3.47 mm.

a.

b.

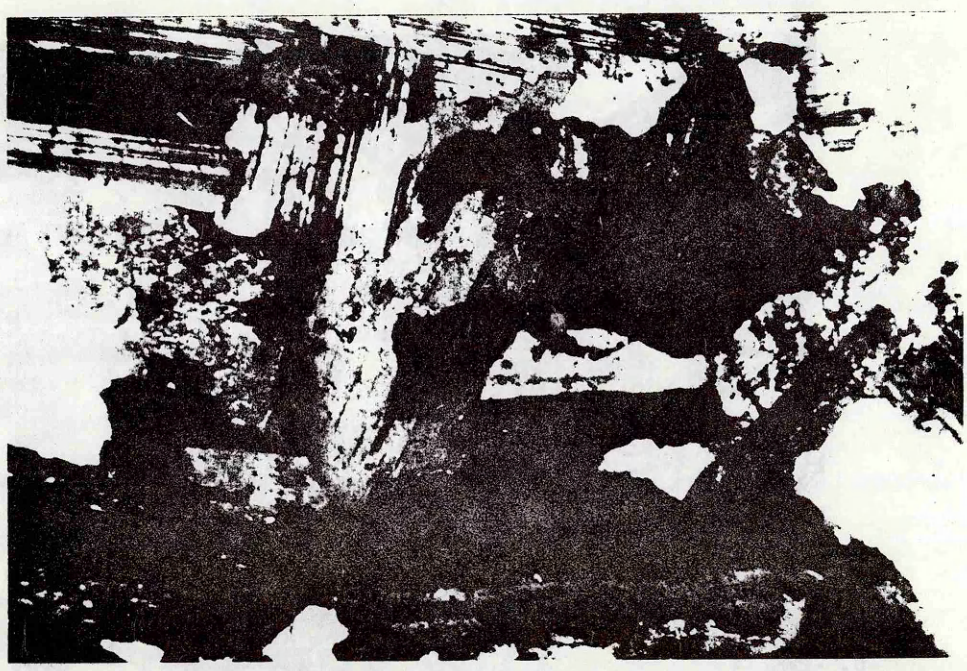

Plate 6.2a. Diorite (81051) containing biotite (orange), Fe-Ti oxides (black) clinopyroxene (brown - centre and left), orthopyroxene (brown - bottom left) plagioclase, quartz and potassium feldspar (colourless), and apatite (grey - above large clinopyroxene).
PPL. Field of view = 3.47 mm.

Plate 6.2b. As above, but note euhedral orthopyroxene (in extinction) and plagioclase, and interstitial white quartz and potassium feldspar.
XP. Field of view = 3.47 mm.

6.2.2 Cerritos Bayos Pluton

The hills to the south of Estacion Cerritos Bayos and the southern part of the Cerros de Guacate consist of an intrusive complex which cuts the Jurassic marine Cerritos Bayos Formation (Section 5.2) and the lavas of the Indio Muerto Formation (Section 5.4). Isolated outcrops occur to the west in the hillocks on the eastern margin of the Pampa del Indio Muerto, and Baeza (1976) has noted a faulted contact against the Sierra Limon Verde pluton in the east. He also described a concentric lithological zonation from granite and alkaline granite around Cerritos Bayos, to syenite in the Cerros de Guacate, and passing out into monzonite in some isolated peripheral outcrops. However, it is apparent that most of this pluton has suffered extensive potassium metasomatism and silicification, and thus the names applied as above do not reflect primary mineralogy. As with the Tocopilla Pluton (Section 4.2.2) the field term "monzonite" will be used to describe those rocks showing the effects of this alteration.

Mineralogically the freshest part of the pluton is to the south of Estacion Cerritos Bayos where coarse-grained mesocratic-leucocratic gabbros, diorites and monzodiorites are found (Figure 6.2; Plate 6.2). Plagioclase is the major early crystallizing phase in these rocks ranging from An_{43} - An_{55} in core composition: individual crystals sometimes display weak normal and concentric zoning. A mild igneous lamination texture also develops. Augite, the most abundant ferromagnesian mineral, is generally an early crystallizing phase, but in places is interstitial to plagioclase. Neutral coloured when fresh, it sometimes alters to pale green fibrous amphibole. Orthopyroxene is a rare phase crystallizing contemporaneously with clinopyroxene but after plagioclase, of which it contains inclusions. Biotite occurs as

interstitial plates with inclusions of Fe - Ti oxides, augite, and (rarely) zircon. The opaque oxides form large subhedral crystals as well as more specular grains generated by the breakdown of augite. All the ferromagnesians tend to clot. Quartz and orthoclase occur in minor quantities as interstitial grains and larger plates; the latter mineral may develop a microperthitic texture. Accessory phases include ubiquitous euhedral apatite (up to 0.5 mm in length), interstitial sphene, and rare zircon.

Surrounding this fresh region the pluton has undergone extensive alteration. Firstly, a late magmatic alkali metasomatism has albitized plagioclase and then converted it into turbid potassium feldspar to produce pink "monzonites". This alteration has also had a major effect on the ferromagnesians: clinopyroxene is transformed into fibrous amphibole, and amphibole is oxidised and occasionally broken down into biotite. Often, however, the original mineralogy of these crystals is indeterminate. As at Tocopilla the basic facies still retain a more equigranular texture whereas the more evolved rocks assume a porphyritic texture with phenocrysts of early crystallized plagioclase, ferromagnesians, and rarely orthoclase. The groundmasses of these porphyritic monzonites are composed of fine grained crystalline aggregates of quartz and orthoclase with some albite, Fe-Ti oxides and altered mafic minerals; quartz and orthoclase may also form pools. Apatite, tourmaline, and allanite are rare accessory phases.

Locally a second style of alteration is evident, producing a highly recrystallized white rock with speckles of limonite. This is composed of an irregular mass of quartz and albite. The latter forms tiny laths, almost like microlties, and larger "phenocrysts" up to 2 - 3 mm in length

which are partly sericitized; the former is generally very finely divided, but may exhibit larger, rounded grains and pools. The limonite spots are ragged and may be pseudomorphs after pyrite. The timing of this silicification is unknown but it would appear to be post consolidation as some of the monzonites are cut by very fine quartz veins. The localized nature of this alteration implies that it may be controlled by minor faults.

A late magmatic alteration in the Cerros de Guacate centred on Alcaparrosa was very intense. Here, because of the arid climate, unusual minerals, mainly anhydrous iron sulphates such as jarosite, copiapite and coquimbite are preserved.

6.2.3 Pampa Negra Stock

Between the Pan American highway and the Sierra de la Cruz (Figure 6.1) there outcrops a sequence of lavas and sediments belonging to the Agua Dulce Formation (Section 2.8). These have been intruded by a small, medium-fine grained, subcircular stock of Cretaceous age. The composition of the stock ranges from quartz gabbro-quartz monzodiorite (Figure 6.2).

As in the Cerros de Montecristo plagioclase forms mildly zoned euhedral crystals. Core compositions vary from An_{58} - An_{40}, the more calcic varieties being in the basic rocks. Although the crystals may poikilitically enclose clinopyroxene and Fe - Ti oxides, in general plagioclase commenced crystallizing first. Sericitization is again minimal. Orthopyroxene is found in the most basic facies where it began crystallizing after plagioclase but before clinopyroxene. It is slightly altered to pale yellow/green cummingtonite. Augite is found throughout the sequence and as usual it breaks down to fibrous amphibole (which in

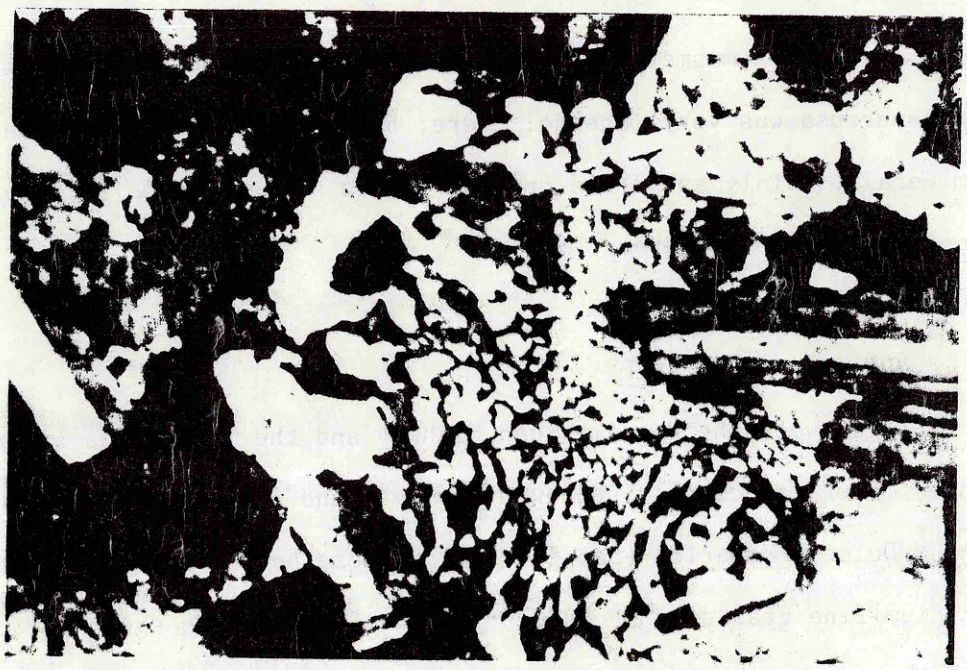

Plate 6.3. Granophyric intergrowth in quartz monzodiorite (81089).
XP. Field of view = 3.47 mm.

turn may alter to biotite) and fine granular oxide. Fe - Ti oxides have a subhedral habit, crystallizing after the aforementioned phases. They also form during augite alteration but these crystals are smaller and more amorphous. Biotite is a minor phase, having an interstitial habit, and being frequently converted to chlorite. It does, however, enclose small zircons in the most evolved rocks. In the basic rocks orthoclase forms rare interstitial crystals; further along the fractionation scheme its abundance increases, first developing a granophyric intergrowth with quartz, and then becoming more euhedral (while still retaining its two previous habits). Quartz is an early crystallizing phase in the more evolved rocks; in these the granophyric intergrowth may also become extensive (Plate 6.3).

6.2.4 Cerro Colorado Pluton

The Cerro Colorado pluton lies on the west bank of the Rio Loa on the eastern edge of the Sierra del Medio. It has been studied in detail by O'Callaghan (unpublished data). Briefly the pluton intrudes a sequence of clastic and volcaniclastic sediments intercalated with lavas of basic-intermediate compositions which have been domed upwards by the intrusion. In the south-west the contact between the pluton and its roof is strongly sheared and mineral segregation into quartzo-feldspathic and mica-rich layers has occurred. Epidote, albite and potassium feldspar have also grown in veins and as stringers throughout the pile indicating extensive metasomatic alteration of the country rock. The pluton consists of two facies; a main gabbro group and a monzonitic suite, the two generally separated by a fault. The gabbro is coarse grained and dominated by euhedral labradorite which displays igneous lamination: this is intergrown with acicular euhedral olivine. Later crystallization involved Fe - Ti oxides and clinopyroxene together with plagioclase.

Interstitial biotite and orthoclase account for 25 - 30% of the rock. Ubiquitous minor phases include apatite, Fe - Ti oxides and rare sphene. In the south-east part of the pluton layering is apparent within the gabbro; leucocratic olivine-plagioclase layers alternate with more melanocratic pyroxene - biotite - orthoclase - apatite layers.

The monzonitic facies is finer grained than the gabbro. Close to the gabbro it is simply a finer grained equivalent, though lacking the plagioclase fabric and forming an equigranular mass of olivine - clinopyroxene - plagioclase - orthoclase and biotite. Towards the east olivine is replaced by greenish blue amphibole and orthopyroxene and eventually the rocks become a felted mass of amphibole, orthoclase and quartz with large poikilitic biotites.

6.3 Geochronology

Whole rock Rb-Sr geochronological studies have been performed on the four plutons discussed above, the results of which are shown in Figure 6.3. A nine point errochron for the Cerros de Montecristo intrusion yielded an age of 102 $\pm$ 23 Ma with an initial $^{87}Sr/^{86}Sr$ ratio of 0.7041 $\pm$ 3 (ε^{i}_{Sr} = -6.8). Farrar et al. (1970) have dated plutons by K-Ar of this age at about 27°30'S and Drake et al. (1982) reported K-Ar ages of 118 to 82 Ma in central Chile between 32° - 34°S. A four point isochron for the Pampa Negra stock gave an age of 79 $\pm$ 15 Ma with an initial $^{87}Sr/^{86}Sr$ ratio of 0.7042 $\pm$ 2 (ε^{i}_{Sr} = -5.7). A six point isochron for the Cerro Colorado pluton produced an age of 66 $\pm$ 24 Ma and an initial $^{87}Sr/^{86}Sr$ ratio of 0.7039 $\pm$ 2 (ε^{i}_{Sr} = -10.2). This agrees closely with the K-Ar ages given by Baker (1977a) of 62.2 $\pm$ 2.4 Ma, and Huete et al. (1977) of 65.1 $\pm$ 1.8 Ma for the same pluton.

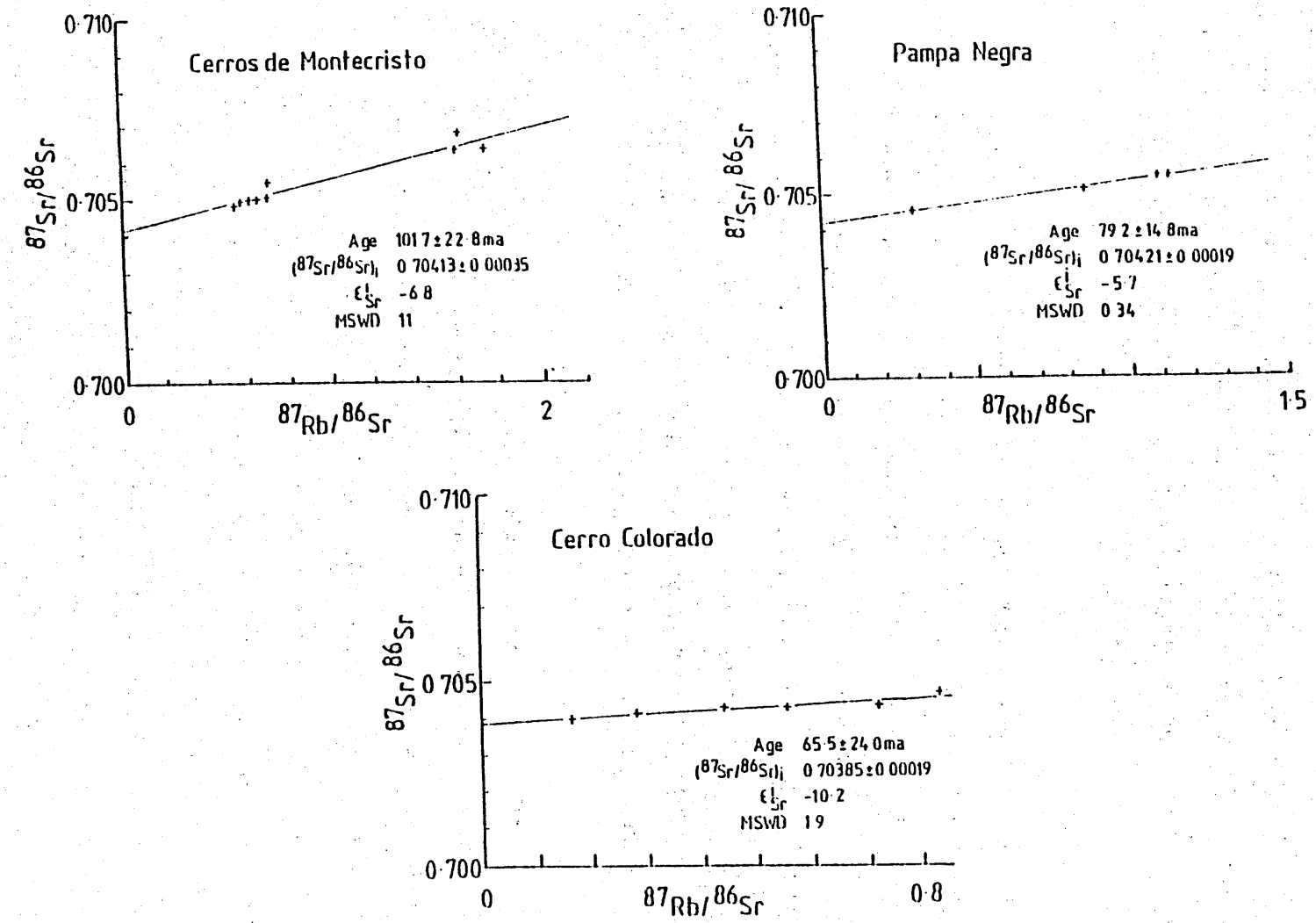

Figure 6.3

Rb - Sr whole rock isochron diagrams for the Cerros de Montecristo, Pampa Negra and Cerro Colorado plutons.

Similar dates have been reported by Huete et al. (op. cit.) for other intrusions in the Sierra del Medio. McNutt et al. (1975) obtained K-Ar dates of 60.4 and 66.6 Ma between 27°24' - 28°20'S, and Drake et al. (1982) give K-Ar ages of 62 and 65 Ma between 32° - 36°S. The large errors in the ages given above for the Pampa Negra and Cerro Colorado plutons reflect the restricted variation in whole rock Rb/Sr ratios within these bodies.

The pluton at Cerritos Bayos produced a complete scatter on an isochron diagram. As was noted in Section 6.2.2 the pluton has undergone post consolidation silicic alteration, and this has obviously disrupted the Rb-Sr systematics. The pluton, however, cuts the lavas of the Indio Muerto Formation, and thus has a maximum age of post lower Cretaceous (∿130 Ma); consideration of its position some 25 km to the south of the Cerros de Montecristo suggests it should be assigned to the same intrusive episode as the Cerros de Montecristo pluton at about 100 Ma.

6.4 Geochemistry and Petrogenesis

Harker variation diagrams for the Cerros de Montecristo and Pampa Negra intrusions and for the least altered parts of the Cerritos Bayos pluton are shown in Figure 6.4. It is noticeable that the former pluton is more evolved than either of the other two. The limited data for the latter two intrusions offers few constraints for quantitative modelling, but their geochemical trends can be compared to those of the Cerros de Montecristo. For most elements the vectors defined by the more basic Pampa Negra stock are continued by the rocks of the Cerros de Montecristo; the trends for the Cerritos Bayos pluton are more diffuse, particularly for the alkalis, indicating that although the rocks appear petrographically fresh, certain chemical mobility has occurred. For the

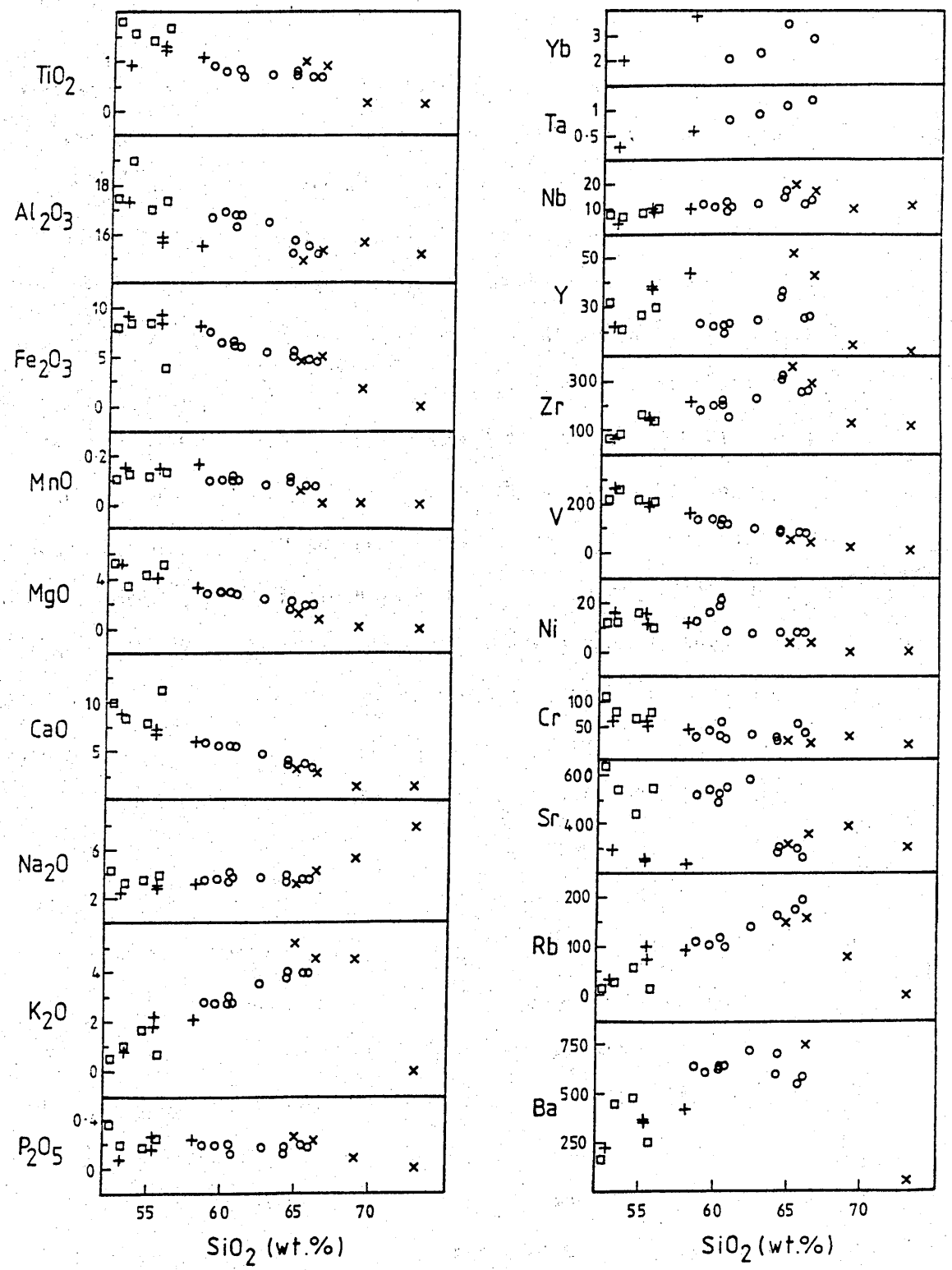

Figure 6.4

Harker variation diagrams for selected elements from the Cretaceous plutons. O = Cerros de Montecristo, □ = Cerritos Bayos, × = Cerritos Bayos monzonites, + = Pampa Negra.

Cerros de Montecristo a calcalkaline trend is followed on an AFM diagram (Figure 6.5).

The most noticeable differences between the Cerros de Montecristo and Pampa Negra intrusions are in their Sr, Y and Yb contents, with the former having much higher Sr (520 ppm compared to 240 ppm) and lower Y (23 ppm compared to 44 ppm) at approximately the same SiO_2 content. The variation in Sr content could be attributable to higher degrees of plagioclase accumulation in the Cerros de Montecristo, but both plutons contain about the same proportions of euhedral plagioclase, and portray similar trends for CaO, Na_2O and Eu/Eu*. Even allowing for scatter, the Sr data for Cerritos Bayos are also distinctly higher than those for Pampa Negra, and similar to the Cerros de Montecristo. It thus appears that the Sr variation is a function of differing concentrations in parental magmas rather than of crystallization history. The low Y content of the Cerros de Montecristo pluton may be due to greater amphibole crystallization than in the Pampa Negra stock, or to a higher proportion of residual hornblende during partial melting.

Chondrite normalised REE patterns (Figure 6.6) show that the Cerros de Montecristo pluton has a much higher $(Ce/Sm)_N$ ratio (2.33 - 2.49) than the Pampa Negra stock (1.56 - 1.70) whilst their $(Tb/Yb)_N$ ratios have coincident ranges (1.05 - 1.36 for the former and 1.15 - 1.21 for the latter). Absolute LREE abundances are also higher for the Cerros de Montecristo with Ce_N = 64.5 - 75.1 compared to 23.8 - 56.1 for the Pampa Negra pluton. Both plutons have negative Eu anomalies (Eu/Eu* = 0.66 - 0.56 and 0.98 - 0.58 respectively), which increase in magnitude with fractionation, reflecting plagioclase and potassium feldspar control (Figure 6.7). Whilst the REE for the Pampa Negra intrusion are broadly

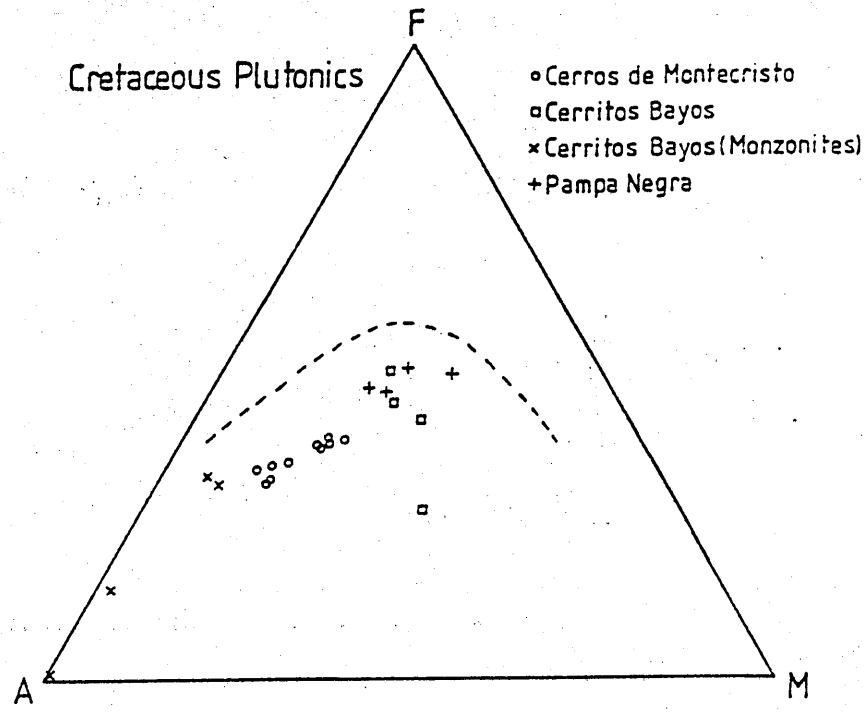

Figure 6.5

AFM diagram for Cretaceous plutons.

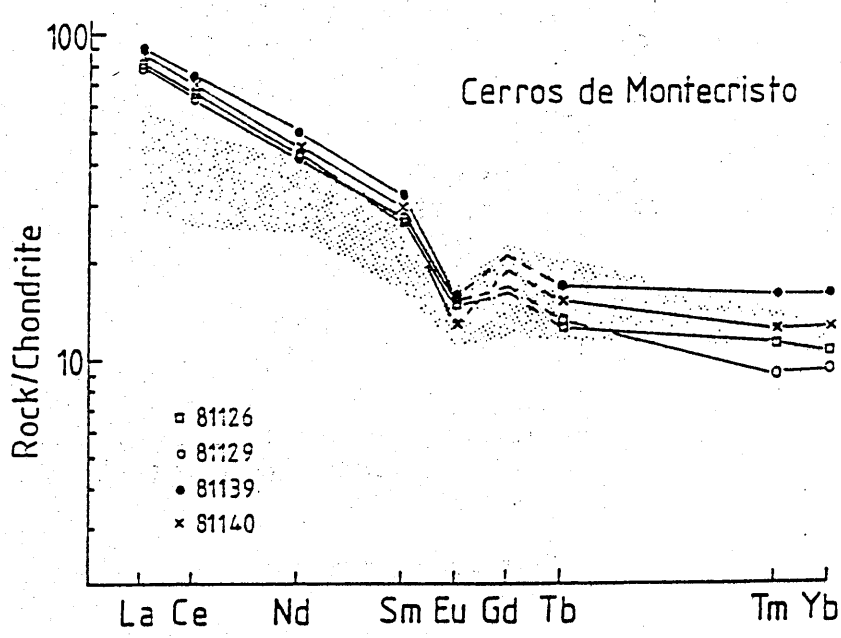

Figure 6.6

Chondrite-normalised REE plot for the Cerros de Montecristo, Pampa Negra and Cerro Colorado plutons. The shaded area on the former depicts the range for Cretaceous intrusions from central Chile (Lopez-Escobar et al., 1979).

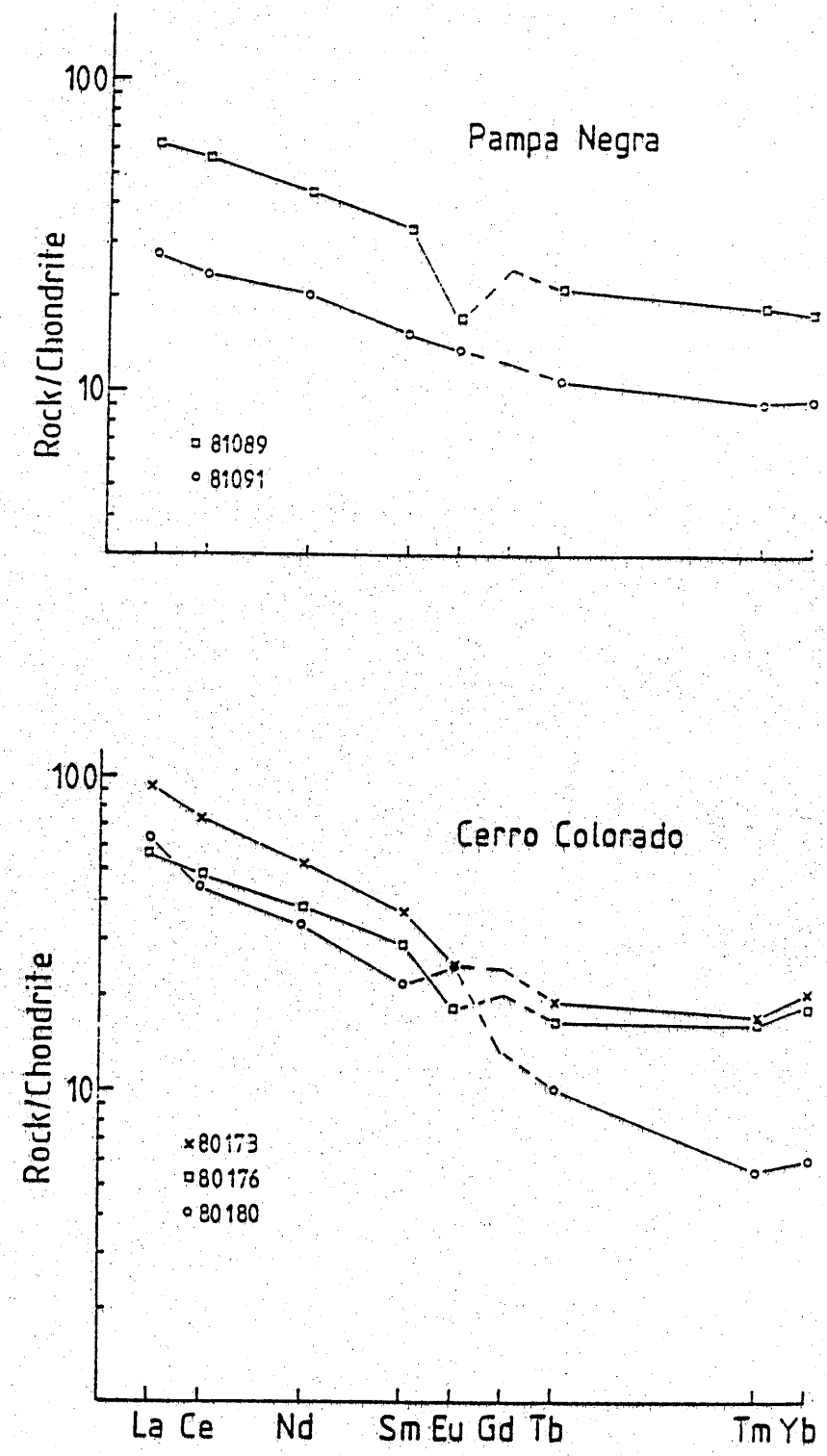

Figure 6.6 (continued)

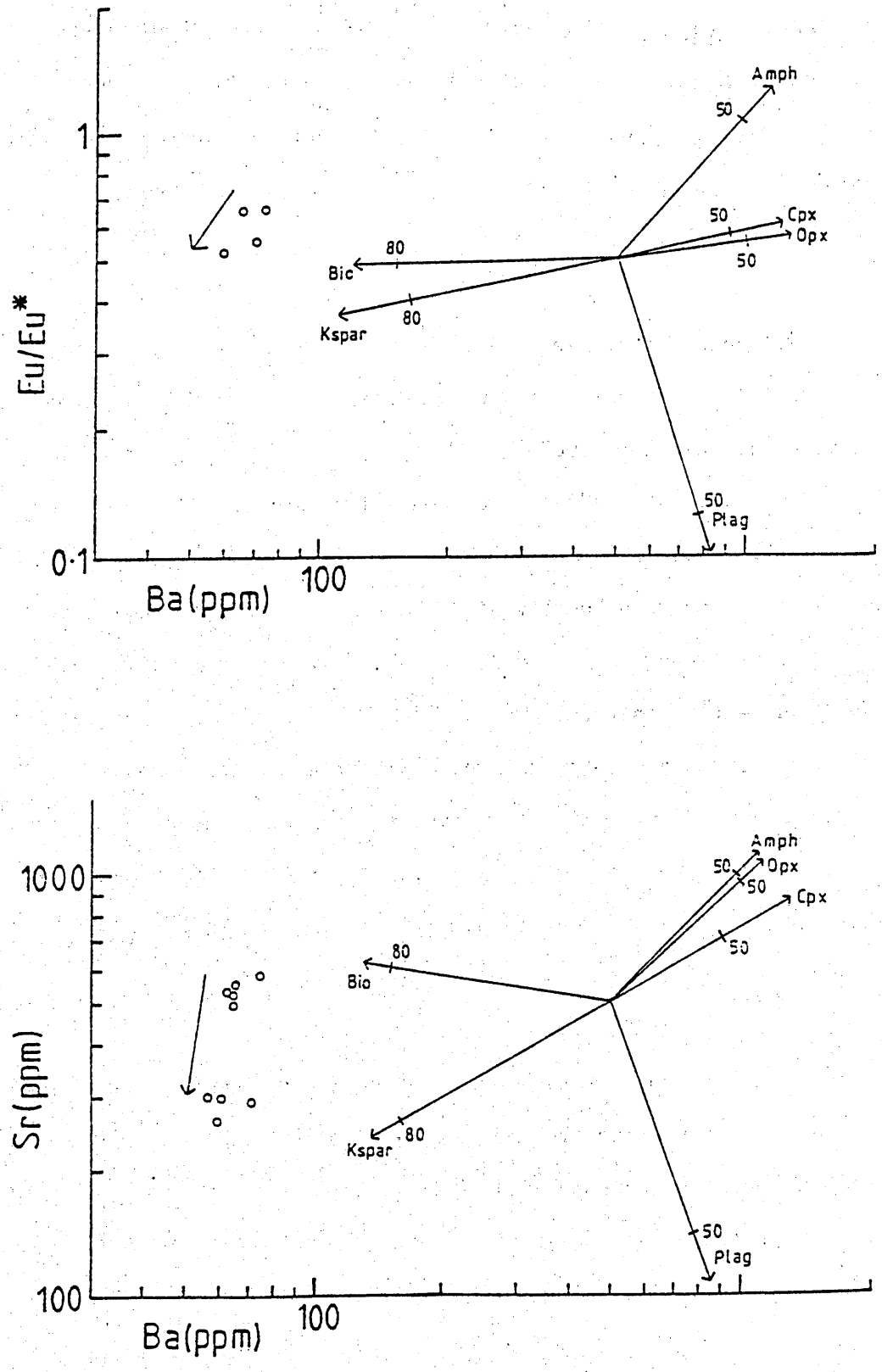

Figure 6.7

Ba - Sr and Ba - Eu/Eu* variation diagrams for the Cerros de Montecristo pluton: arrows indicate fractionation trends. Rayleigh fractional crystallization vectors show the effects of removing selected phases: numbers along vectors indicate the percentage of liquid remaining. Distribution coefficients. from Arth (1976).

coincident with those of the Cretaceous batholith in central Chile (Lopez-Escobar et al., 1979), the Cerros de Montecristo have significantly higher LREE concentrations (Figure 6.6). There is no evidence within the Cerros de Montecristo, Cerritos Bayos or Pampa Negra intrusions for a high Nb magma such as forms the high-K group of the Augusta Victoria Formation.

O'Callaghan (unpublished data) has found that at Cerro Colorado the main gabbro is chemically rather homogeneous with SiO_2 ∿56% and with high concentrations of Ba (900 - 1000 ppm), Rb (100 ppm), Sr (∿700 ppm) and K_2O and Na_2O (∿ 4%). The monzonite series is depleted in MgO (only 1.8% at 54% SiO_2), Ni and Cr, but enriched in certain incompatible elements in keeping with the biotite - amphibole - orthoclase dominated mineralogy: K_2O rises to about 7.5% at 58% SiO_2 and then remains nearly constant; Rb, Ba and Sr all have higher concentrations in the monzonites than in the gabbro. REE profiles for three samples are given in Figure 6.6. All the patterns show LREE enrichment with $(Ce/Yb)_N$ varying between 2.6 and 7.3. Sample 80180 has strongly depleted HREE (Yb_N = 6.1) compared to the others (Yb_N = 18-20), and also has a positive Eu anomaly (Eu/Eu* = 1.39).

Sr isotope analyses were obtained on a wide range of samples, from which a selection was made for Nd isotopes. The results are presented in Appendix F and in Figure 6.8. Initial $^{87}Sr/^{86}Sr$ ratios for the Cerros de Montecristo vary from 0.70384 - 0.70451 (ε^i_{Sr} = -1.0 to -10.4) and initial $^{143}Nd/^{144}Nd$ ratios from 0.512597 - 0.512611 (ε^i_{Nd} = +1.71 to +1.99). The same parameters for Cerritos Bayos are 0.70420 - 0.70660 (ε^i_{Sr} = -5.4 to +28.7) and 0.512621 - 0.512662 (ε^i_{Nd} = +2.26 to +2.94):

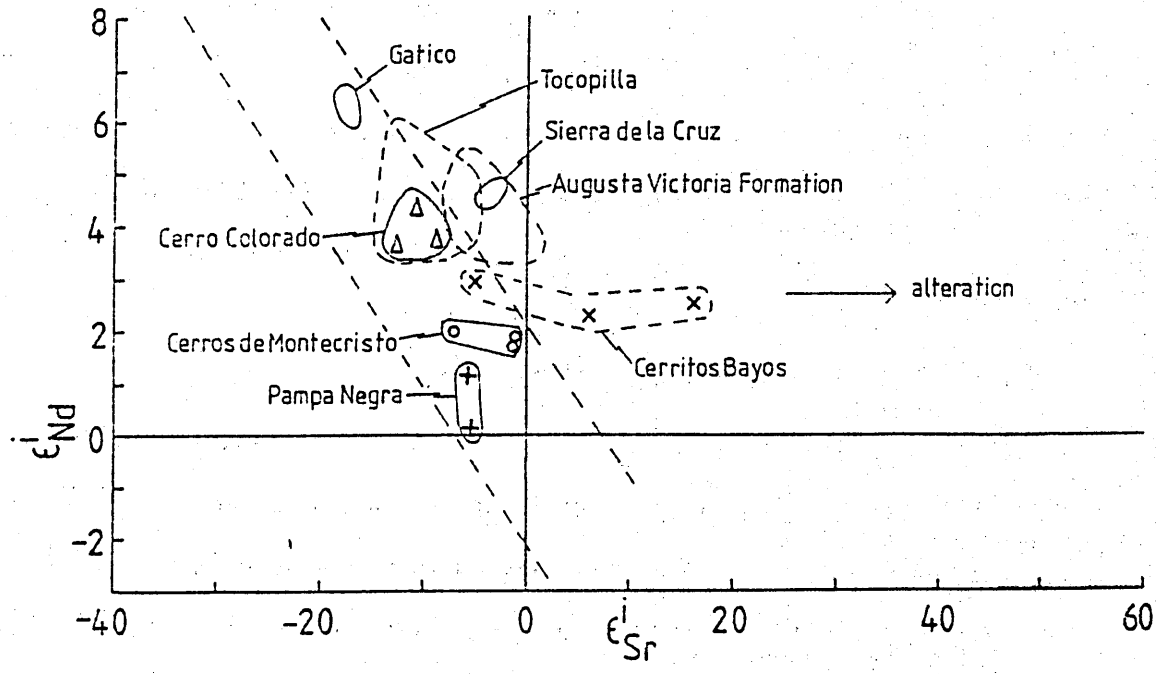

Figure 6.8

ϵ^i_{Sr} - ϵ^i_{Nd} diagram for the Cretaceous plutons. The positions of the Augusta Victoria Formation and the Jurassic plutons (Gatico, Tocopilla and Sierra de la Cruz) are shown for comparison. The effects of alteration are noticeable at Cerritos Bayos where ϵ^i_{Sr} extends to high values but ϵ^i_{Nd} is nearly constant.

the large spread of the initial Sr isotope ratios reflects the alteration processes which have affected this pluton, and which have disturbed the elemental concentrations discussed above even in the petrographically fresher rocks. The Nd isotope systematics, however, define a narrow range, and are thus probably unmodified by the alteration. Analyses from the Pampa Negra stock show little variation with initial $^{87}Sr/^{86}Sr$ ratios of 0.70417 - 0.70425 (ε^{i}_{Sr} = -5.1 to -6.2) and initial $^{143}Nd/^{144}Nd$ ratios of 0.512546 - 0.512597 (ε^{i}_{Nd} = +0.15 to +1.15). The Cerro Colorado pluton also forms a tight grouping in both isotope systems with initial $^{87}Sr/^{86}Sr$ ratios of 0.70372 - 0.70397 (ε^{i}_{Sr} = -9.3 to -12.8) and initial $^{143}Nd/^{144}Nd$ ratios of 0.512742 - 0.512779 (ε^{i}_{Nd} = +3.63 to +4.36). The four plutons define discrete fields on Figure 6.7, but all plot on or close to the mantle array in the depleted quadrant, similar to the Jurassic plutons from this transect (Section 4.5). Compared to the Cretaceous Augusta Victoria Formation (Chapter 5) the rocks from the Cerritos Bayos and Cerros de Montecristo plutons have slightly lower ε^{i}_{Nd}. However, both initial Sr and Nd isotope ratios do not vary with fractionation, and thus there is no prima facie reason to consider that either pluton has undergone any crustal contamination during crystallization.

The isotope geochemistry of the Pampa Negra stock provides a more complex picture. If one considers that the source for this pluton was the same as that of the nearby Jurassic Sierra de la Cruz pluton (Section 4.5) then in the period from 156 - 79 Ma the $^{143}Nd/^{144}Nd$ ratio of the source would need to have been reduced from 0.51267 (the ratio for the Sierra de la Cruz pluton) to 0.51257 (the average ratio for the Pampa

Negra stock). This cannot have taken place by *in situ* evolution of the source, and so some degree of crustal contamination seems necessary. The method of contamination, however, is problematical as the more basic rock has the lower ε^{i}_{Nd} value, thus precluding simple AFC processes. This style of contamination nonetheless has been reported from the Deccan in India (Mahoney *et al.*, 1982; Cox and Hawkesworth, 1984) and from Skye in Scotland (Thirlwall and Jones, 1983).

The rocks from Cerro Colorado have the most depleted isotope systematics; they appear to have crystallized with minimal crustal interaction. This isotopic signature contrasts markedly with the enriched recent lavas from San Pedro just across the valley of the Rio Loa (Hawkesworth *et al.*, 1979a; Section 7.4.3), the differences representing fundamentally different mantle characteristics beneath the two areas (Chapter 8).

6.5 Summary

Emplacement of granitic plutons during the Cretaceous occurred at three main times: at about 100 Ma in the Cerros de Montecristo and at Cerritos Bayos; at 79 Ma on the western margins of the Pampa del Tamarugal (Pampa Negra); and at 66 Ma in the Sierra del Medio (Cerro Colorado). The locus of intrusion does not follow a simple unidirectional migration with time as described by Farrar *et al.* (1970) further south in Chile. The Cerro Colorado pluton is unique amongst the intrusions studied in this transect in having olivine, and also in being highly potassic. The other plutons follow calcalkaline trends with fractionation controlled by plagioclase + clinopyroxene + Fe Ti oxides; amphibole is an important phase in the Cerros de Montecristo pluton, whereas orthopyroxene is present in the more basic facies of the Cerritos Bayos and Pampa Negra

intrusions. Late-stage alkali metasomatism and post consolidation silicification have affected the Cerritos Bayos pluton disturbing the Sr isotope systematics and the concentrations of alkali trace elements, though Nd isotope systematics are unaffected.

Consideration of the isotope systematics of these intrusions suggests that the Cerros de Montecristo, Cerritos Bayos and Cerro Colorado have tapped isotopically distinct sources, whilst the Pampa Negra Pluton may have undergone a complex crustal contamination history.

CHAPTER 7

TERTIARY-RECENT PLUTONISM AND VOLCANISM

7.1 Introduction

Details of the Tertiary-Recent evolution of this section of the Andes have been given by Hollingworth and Rutland (1968), Baker (1977a), Maksaev (1978) and Ramirez and Huete (1981). As part of this study chemical and isotopic analyses were performed on one of the plutons at the El Abra porphyry copper deposit, and on six lavas collected by M.C.W. Baker at this latitude from Chile and Bolivia. The samples from the north Chilean volcanoes analysed for Sr isotopes by Francis et al. (1977) and for Nd isotopes by Hawkesworth et al. (1979a) have been reanalysed along with five more lavas from Volcan San Pedro. In addition the isotopic composition of the lavas from Ecuador which were analysed by the above authors has also been redetermined, and are reported here for comparison with north Chile.

7.2 El Abra Pluton

7.2.1 Field Relations

The El Abra porphyry copper deposit is located in the Sierra del Medio, 40 km to the north of Chuquicamata. The geology of the area has been described by Ambrus (1977). Briefly the oldest rocks of the complex are those forming the unmineralized "Southern Granodiorite" which is exposed in the southern part of the area. This is cut by the main mineralized pluton (the El Abra Diorite), and by other dykes and stocks. A late intrusion, the Pajonal Diorite is also unmineralized. The centre lies just to the east of a major north-south trending fault - the West Fissure; the mines at Chuquicamata and Quebrada Blanca (to the north) also lie close to this fault, and it is therefore thought to have influenced

the distribution of mineralization (Ambrus, 1977).

7.2.2 Petrography

The rocks used in this study come from the medium-coarse grained Southern granodiorite. Compositions range from quartz monzodiorite-granite (Figure 7.1). Plagioclase is soda rich throughout, and is sometimes weakly zoned. Overgrowths of either plagioclase or orthoclase may develop around early crystallized plagioclase: occasionally these jackets may be separated from the core by a zone of melting. Crystals are generally fresh, with only a little propylitic alteration on some margins. In the granites plagioclase becomes partially interstitial and a little antiperthite is found. Orthoclase is interstitial, frequently forming poikilitic plates enclosing plagioclase, biotite and apatite. Large perthite crystals form in the granites, and microcline occurs in late stage aplite dykes. Quartz has a very variable grain size, ranging from large ($\sim$2 mm) poikilitic plates to fine granules. Biotite and actinolite are the main ferromagnesian phases. The former is normally subhedral, crystallizing after amphibole, though in the most evolved rocks it forms interstitial flakes. Marginal alteration is rare. In the basic rocks actinolite replaces clinopyroxene, relict cores of the latter being evident; subsequently amphibole supersedes pyroxene as the early crystallizing phase, before becoming interstitial. The amphibole itself may alter slightly to biotite. Clots of biotite, amphibole and Fe-Ti oxides are common. Accessory phases include zircon, sphene and ubiquitous early crystallizing apatite; all these are depleted or absent in the granites.

7.2.3 Geochronology

A three point whole rock Rb-Sr isochron for the Southern

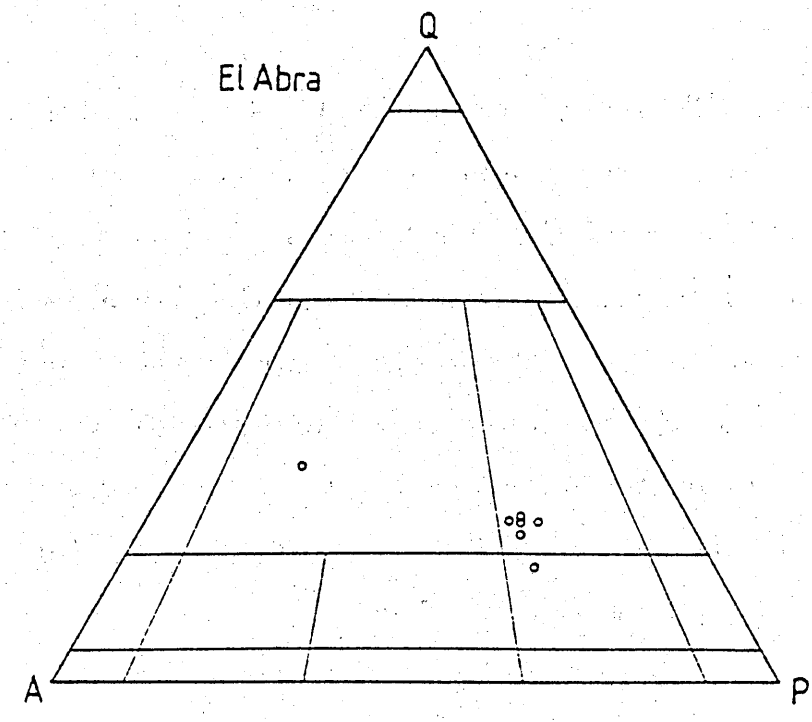

Figure 7.1

Modal QAP diagram for the El Abra pluton.

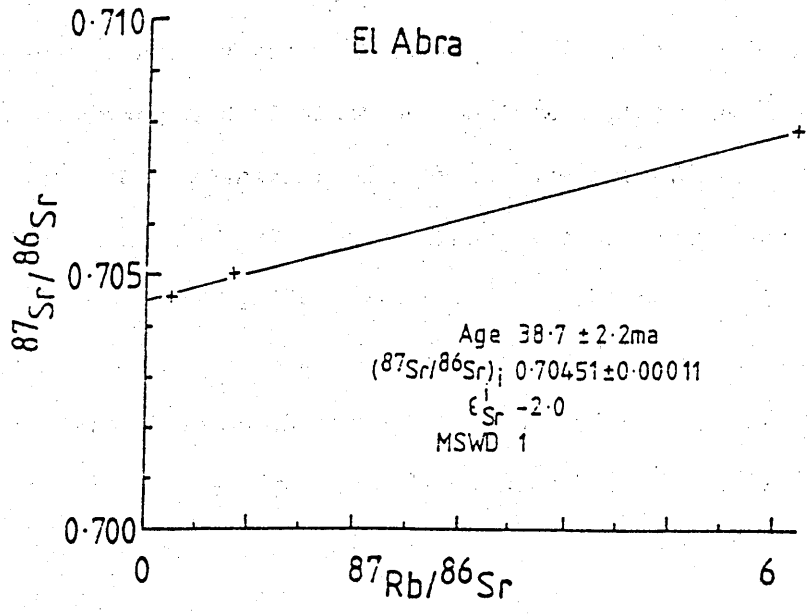

Figure 7.2

Rb - Sr whole rock isochron diagram for the El Abra pluton.

Granodiorite at El Abra yielded an age of 38.7 ± 2.2 Ma with an initial $^{87}Sr/^{86}Sr$ ratio of 0.7045 ± 1 (ε^{i}_{Sr} = -1.99) (Figure 7.2). The date is close to the K-Ar biotite age of 34.5 ± 0.5 Ma reported by Ambrus (1977) from the same pluton, though this author concluded that the biotite chosen was probably an alteration product, and hence gave a slightly younger age than that of the crystallization of the pluton. The Fortuna granodiorite at Chuquicamata also belongs to this same period of intrusive activity having given Pb/α ages of 35-40 Ma (Thomas, 1969) and a K-Ar age of 35 ± 1 Ma (Ambrus, 1977).

7.2.4 Geochemistry

The Southern Granodiorite at El Abra shows a wide range in SiO_2 content (65.4 - 78.2%), but the samples taken cluster at either end of this range. If the Rb concentration is used as a fractionation index (Figure 7.3) it is seen that there are negative correlations with Al_2O_3, MnO, CaO, Na_2O, P_2O_5, Sr and Ni indicating fractionation dominated by plagioclase, apatite and pyroxene/amphibole. Zr, Hf and Y initially rise, and then fall in the evolved compositions due to zircon control. The behaviour of Ba indicates that alkali feldspar was an important phase in the granite and aplite, but the continued increase in K_2O implies either some volatile influx of K or loss of Ba from the system. Unusually, TiO_2 and V do not show continuous negative correlations, and only decrease in the acid rocks; this suggests that magnetite was not a major crystallizing phase which may be due to a low P_{O_2} in the magma.

REE diagrams are given in Figure 7.4. The rocks are all strongly LREE enriched with $(Ce/Yb)_N$ = 8.1 - 12.4; Ce_N = 50.2 - 73.5 and Yb_N = 4.4 - 10.0: the relative enrichment in LREE is thus primarily

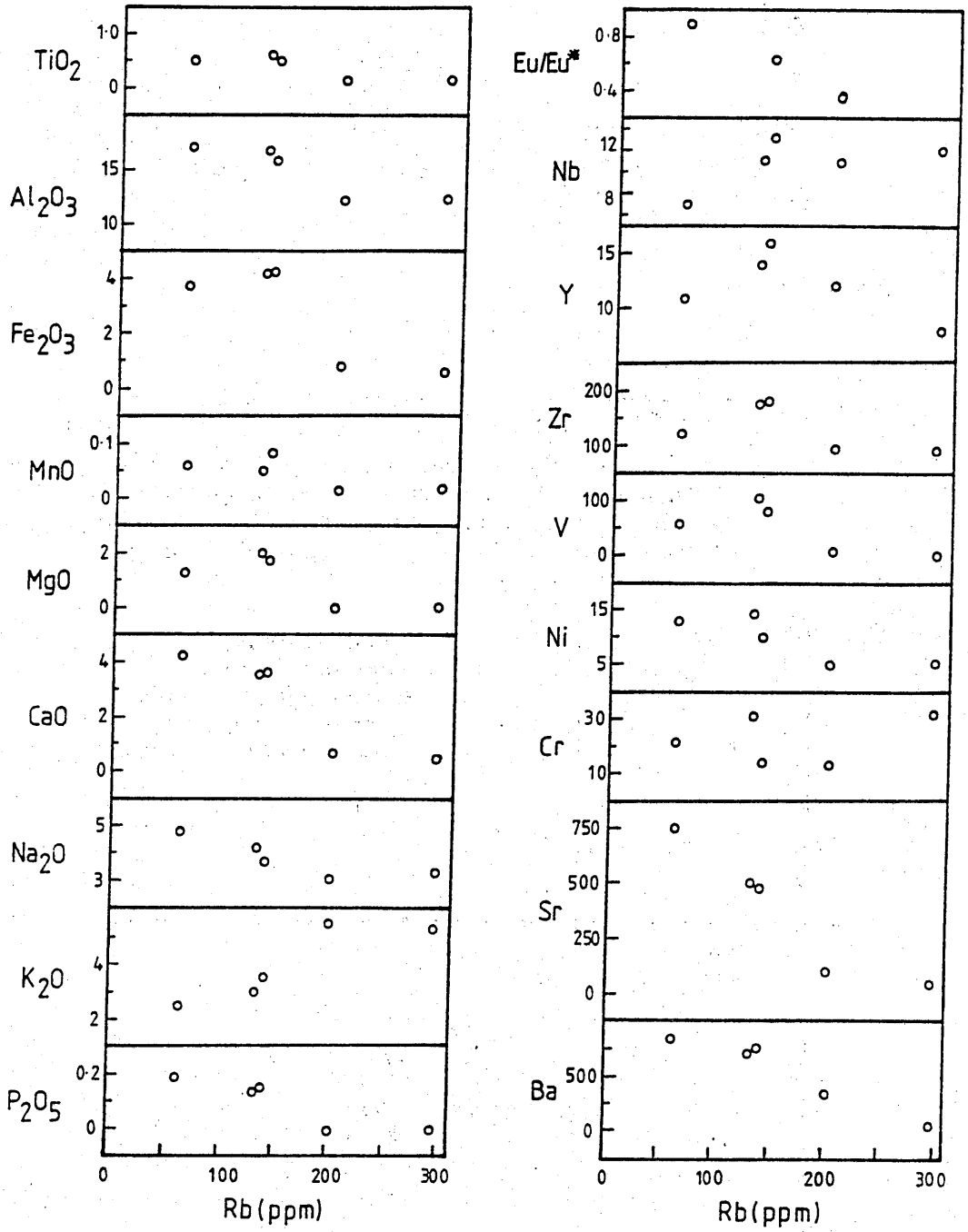

Figure 7.3

Variation diagrams for the El Abra pluton using Rb as the index of differentiation.

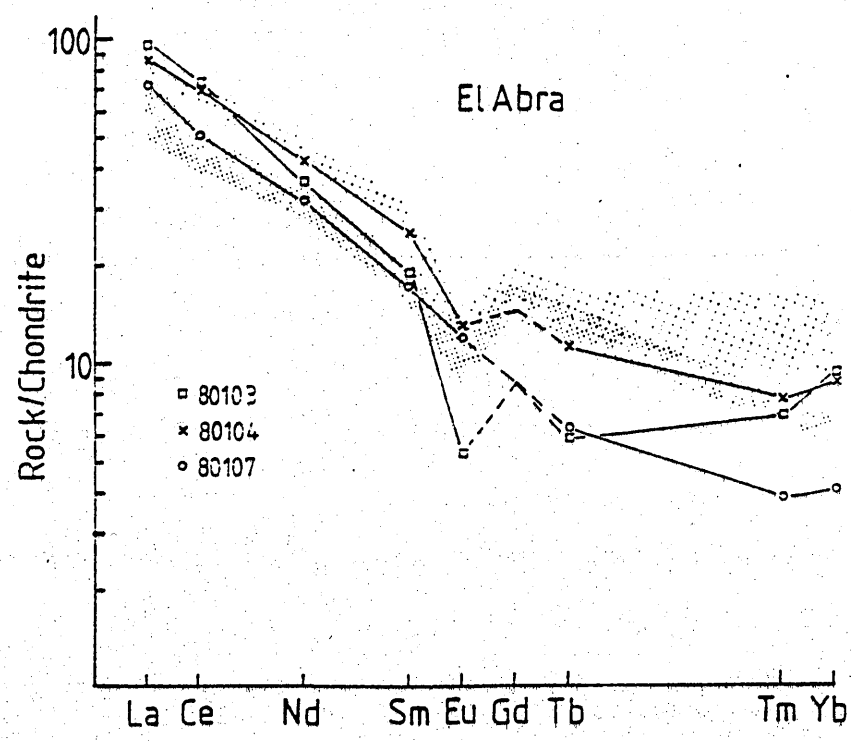

Figure 7.4 Chondrite normalised REE diagram for the El Abra Pluton. Also shown are ranges for the Cerros de Montecristo pluton (Chapter 6) (:::) and for Tertiary plutons from 33°-34°S (▒); (Lopez-Escobar et al., 1979)

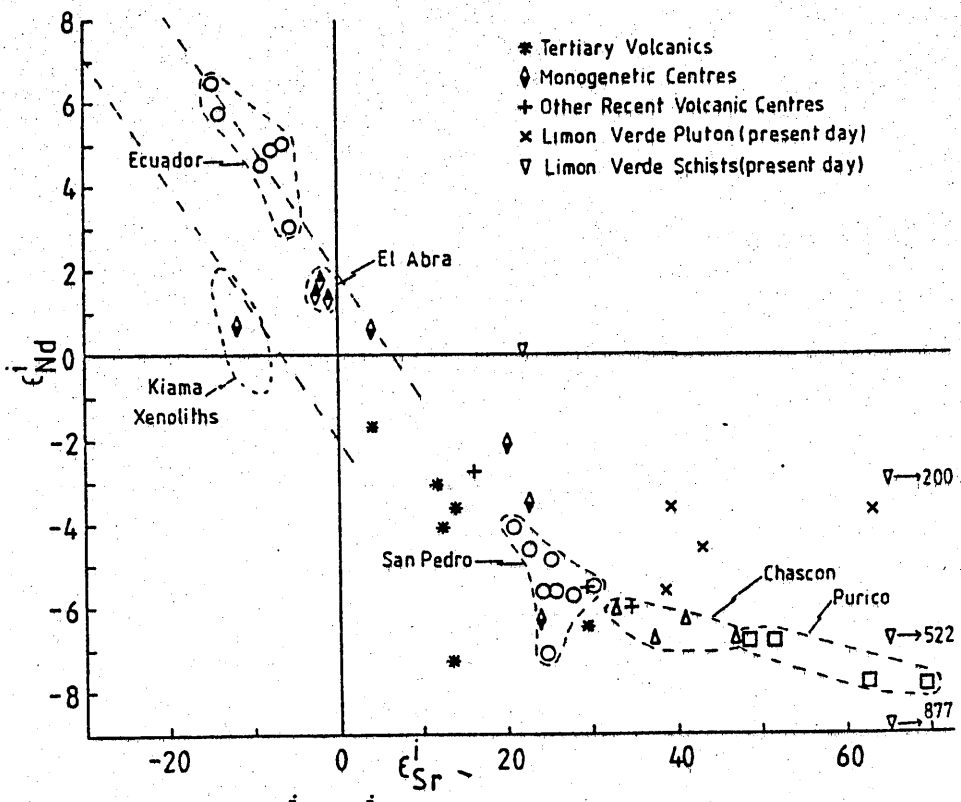

Figure 7.5 ε^i_{Nd} - ε^i_{Sr} diagram for Tertiary-Recent igneous rocks from northern Chile and Ecuador. Data for Purico and Chascon from Hawkesworth et al. (1982). Present day values for the Limon Verde schists and the Palaeozoic Limon Verde pluton are shown to highlight their unsuitability as contaminants for the Recent volcanics. The field of Kiama xenoliths (Menzies and Wass, 1983) is shown for comparison with the alkali basalt (B1) from Bolivia. See text for discussion.

due to depletion of the HREE. The concentrations of the REE tend to increase with fractionation though the behaviour of the middle REE in the granite (80103) is probably controlled by extensive removal of apatite. Negative Eu anomalies become more marked due to continuous feldspar fractionation with Eu/Eu* = 0.89 - 0.36.

Sr and Nd isotopes were determined on three samples of the pluton. Initial $^{87}Sr/^{86}Sr$ ratios vary between 0.70447 - 0.70457 (ε^{i}_{Sr} = -2.7 to -1.2) and initial $^{143}Nd/^{144}Nd$ ratios from 0.512659 - 0.512683 (ε^{i}_{Nd} = +1.34 to +1.81). All these form a tight cluster and plot in the depleted quadrant of an ε_{Sr}- ε_{Nd} diagram (Figure 7.5).

7.2.5 Discussion

MORB normalised plots (Pearce, 1982) for two granodiorites are given in Figure 7.6. These show patterns characteristic of subduction-related magmatism with high alkali/Nb and LREE/Nb ratios. The depletion of phosphorous in the more evolved rock (80104) is caused by earlier fractionation of apatite leaving the residual liquid poor in P_2O_5; this is borne out by the aforementioned low modal abundance of apatite in the more acidic facies. The low levels of HREE in the most basic rock (80107) and the high $(Ce/Yb)_N$ ratio imply that garnet was a residual phase during the partial melting which generated the magma from which the pluton crystallized. The REE pattern contrasts with that shown by the Cretaceous pluton of the Cerros de Montecristo (Section 6.4) which had low $(Tb/Yb)_N$ ratios and higher $(Yb)_N$ values; their variation is, however, similar to that portrayed by Upper Tertiary granitoids from 33°-34°S in Chile (Lopez-Escobar et al., 1979). Ranges for these two groups of intrusives are also shown on Figure

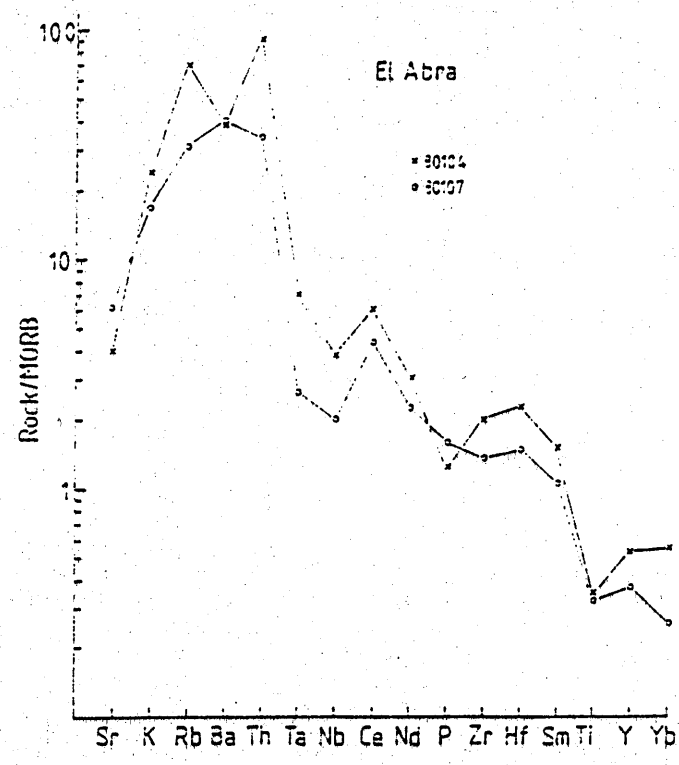

Figure 7.6 MORB normalised diagram for two granitoids from El Abra.

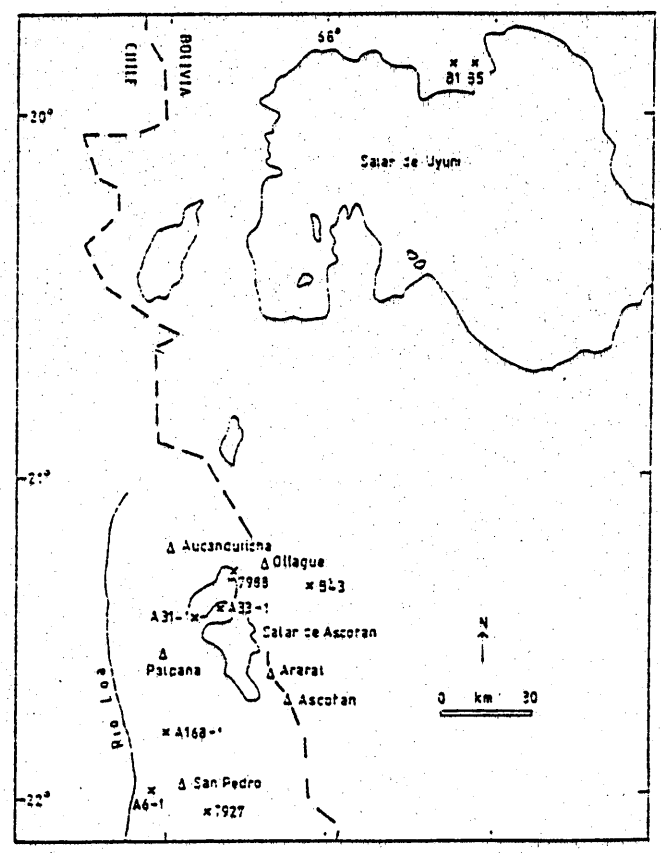

Figure 7.7

Sketch map showing the location of the Tertiary volcanics, monogenetic centres, analysed from the Western Cordillera near San Pedro.

7.4. The low HREE contents of the latter were also ascribed to residual garnet by Lopez-Escobar et al. (op. cit.).

The depleted isotope characteristics of the El Abra pluton show little variation even though SiO_2 varies considerably (65.4-77.4%). There is, therefore, no prima facie evidence to indicate that there has been any contamination en route through the crust, and thus the observed isotope ratios may well reflect those in the mantle source (i.e. $\varepsilon^i_{Sr} = -2$ and $\varepsilon^i_{Nd} = +1.15$).

7.3 Tertiary Volcanics

Six samples collected by M.C.W. Baker were chosen for analysis to provide coverage of the period between the intrusion of the El Abra pluton (38.7 Ma) and the Recent volcanics: the lavas investigated give K-Ar ages from 15.2 - 2.5 Ma (Baker, 1977b; Baker and Francis, 1978). Furthermore the specimens were selected to give a wide geographic distribution, thus extending the region of sampling into Bolivia (Figure 7.7).

The lavas range from basaltic andesites to dacites and broadly follow a calcalkaline trend (though this is not to imply that the lavas are cogenetic). Moderate levels of MgO (3.8-6.2%) and Ni (41-79 ppm) in the more basic rocks imply fractionation of olivine and probably clinopyroxene, though no Cr data are available. REE were determined on the three more basic rocks (Figure 7.8). The samples are all LREE enriched with $(Ce/Yb)_N = 4.0 - 7.2$, $Ce_N = 35.5 - 61.3$ and $Yb_N = 7.1 - 9.1$: negative Eu anomalies are small with $Eu/Eu^* = 0.80 - 0.85$.

Initial ε_{Sr} values range from +4.1 to +29.3 whilst ε^i_{Nd}

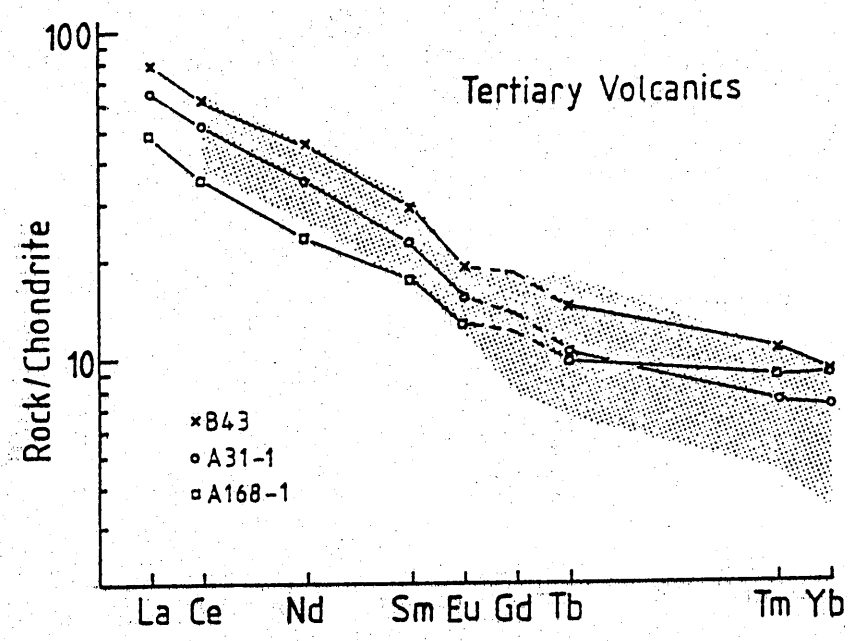

Figure 7.8

Chondrite normalised REE diagram for Tertiary volcanics. Also shown is the range for San Pedro lavas - data from Thorpe et al. (1976).

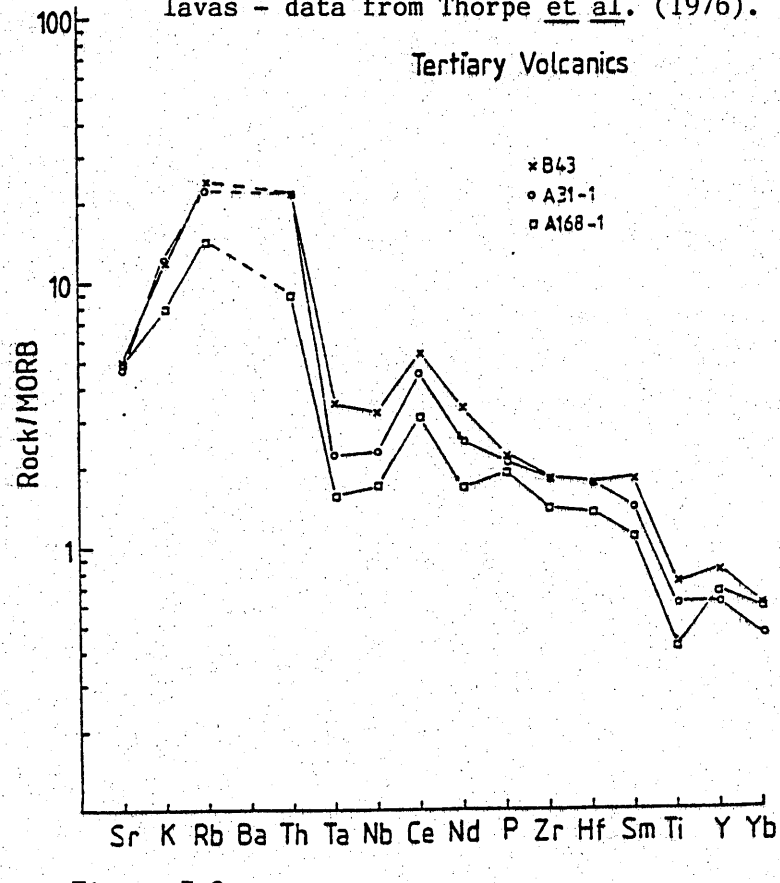

Figure 7.9

MORB normalised plot for Tertiary volcanics.

varies from -1.65 to -7.22. The two Bolivian samples (B5 and B43) have higher ε^{i}_{Sr} and lower ε^{i}_{Nd} than their Chilean counterparts. All the samples plot in the bottom right hand quadrant of the ε^{i}_{Sr}- ε^{i}_{Nd} diagram (Figure 7.5) similar to the lavas from San Pedro (Section 7.4) and from the Purico ignimbrite centre (Hawkesworth et al., 1982). This is in contrast to the Recent volcanics from Ecuador (Section 7.4), Colombia (James and Murcia, 1984) and southern Chile (Hickey et al., 1984) and to the Mesozoic and early Tertiary rocks from this transect across the Andes (Chapters 3, 4, 5 and 6 and Section 7.2). Sample B5, however, plots on a different trend to Purico-Chascon having much lower ε^{i}_{Nd} for a given ε^{i}_{Sr}. T^{Nd}_{DM} ages for the Tertiary volcanics range from 798-1151 Ma implying that the Western Cordillera is underlain by old continental lithosphere.

A MORB normalised diagram (Pearce, 1982) for the more basic lavas is presented in Figure 7.9, which indicates that these rocks have a subduction-related signature. There is, however, a progressive enrichment in incompatible elements in these samples in passing from west (A168-1) to east (B43). Whilst this may have been attributable to higher degrees of fractional crystallization from a common parental magma, sample B43 has the lowest SiO_2 and highest MgO and Ni contents. Alternatively, the variation may be due to a smaller degree of partial melting of a homogeneous source; whilst the $(Ce/Yb)_N$ ratio of B43 (6.3) is higher than that of A168-1 (4.0) it is lower than that of A31-1 (which lies geographically between the other two) (7.2) thus precluding this simple relationship. Coupled with this increase in elemental concentrations there is also a decrease in inter HFSE ratios; Hf/Ta ratios fall from 11.5 - 6.7 and Zr/Nb ratios from 20.1 - 14.6. If the more evolved lavas are

included for comparison, (as Zr/Nb is assumed not to vary significantly during fractional crystallization of major phases) then this range is expanded to 28.3 - 13.3. Table 7.1 shows the subduction zone contributions for the more basic lavas: >74% of K, Rb and Th and <51% Ce, Nd, Sm and P are introduced as the subduction zone component. Elemental concentrations for the mantle sources are presented in Table 7.2 and their MORB normalised profiles given in Figure 7.10. Again the enrichment in incompatible elements in passing from west to east is apparent with B43 having a more enriched source. All the sources, however, are enriched relative to that of the La Negra Formation (sample 8088).

7.4 Recent Volcanism

7.4.1 Volcanic Structures

The style of present day volcanism in northern Chile can be broadly divided into four main types.

(i) Stratovolcanoes

These structures, as exemplified by San Pedro produce lavas ranging from basaltic-andesite-dacite (Plate 7.1a). The stratigraphy and geochemistry of this volcano have been extensively studied by O'Callaghan (in prep.) after the initial studies of Francis *et al.* (1974) and Roobol *et al.* (1976). Sr and Nd isotope results for San Pedro and some other nearby volcanoes have been presented by Francis *et al.* (1977) and Hawkesworth *et al.* (1979a) respectively. Thorpe *et al.* (1976), in a REE study, noted that the lavas could not be produced by a single-stage partial melting model, and that LILE source enrichment was required. Oxygen isotope data were reported by Harmon *et al.* (1981); two samples from San Pedro gave $\delta^{18}O$ values of 8.0 and

Table 7.1 Subduction zone contributions (%) for Tertiary volcanics

Sample	A31-1	A168-1	B43
K	82	80	74
Rb	90	89	86
Th	89	81	85
Ce	51	47	47
Nd	18	8	25
P	8	23	2
Sm	11	3	23

Table 7.2 Unmodified mantle concentrations for the Tertiary volcanics

Sample	A31-1	A168-1	B43
K(%)	0.038	0.035	0.053
Rb	0.512	0.469	0.764
Th	0.054	0.050	0.073
Ta	0.045	0.041	0.071
Nb	0.922	0.885	1.26
Ce	2.52	2.40	3.21
Nd	2.08	2.01	2.48
P(%)	0.027	0.025	0.029
Zr	18.6	18.4	18.4
Hf[1]	0.475	0.475	0.475
Sm	0.469	0.508	0.518
Y	2.08	2.95	2.74
Yb	0.181	0.291	0.230

1 Hf concentration assumed.

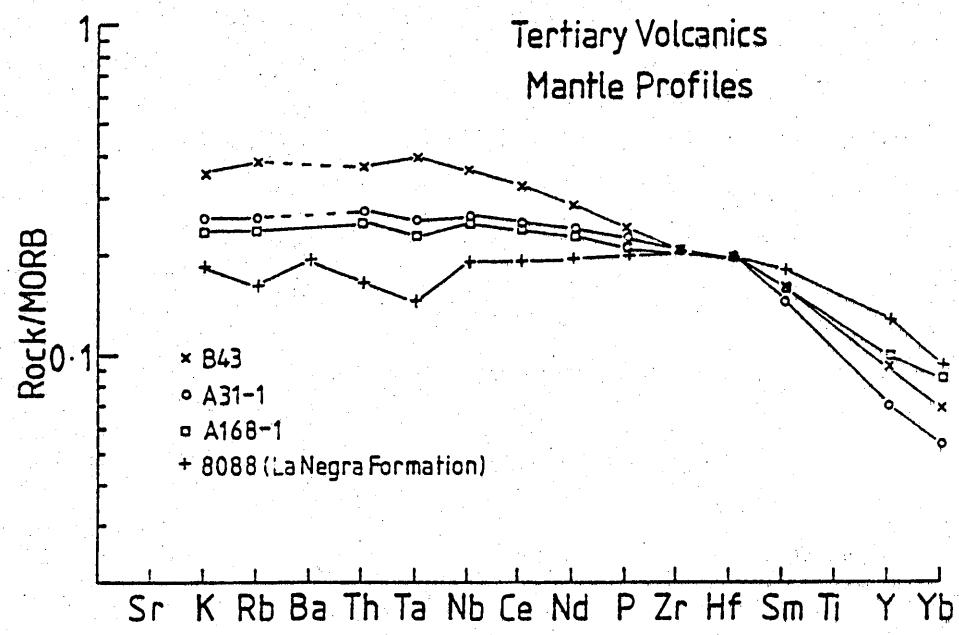

Figure 7.10

MORB normalised profiles for the mantle sources of the Tertiary volcanics assuming Hf mantle = 0.475 ppm (Table 7.2). The enrichment of these sources relative to that of the La Negra Formation (8088) is apparent.

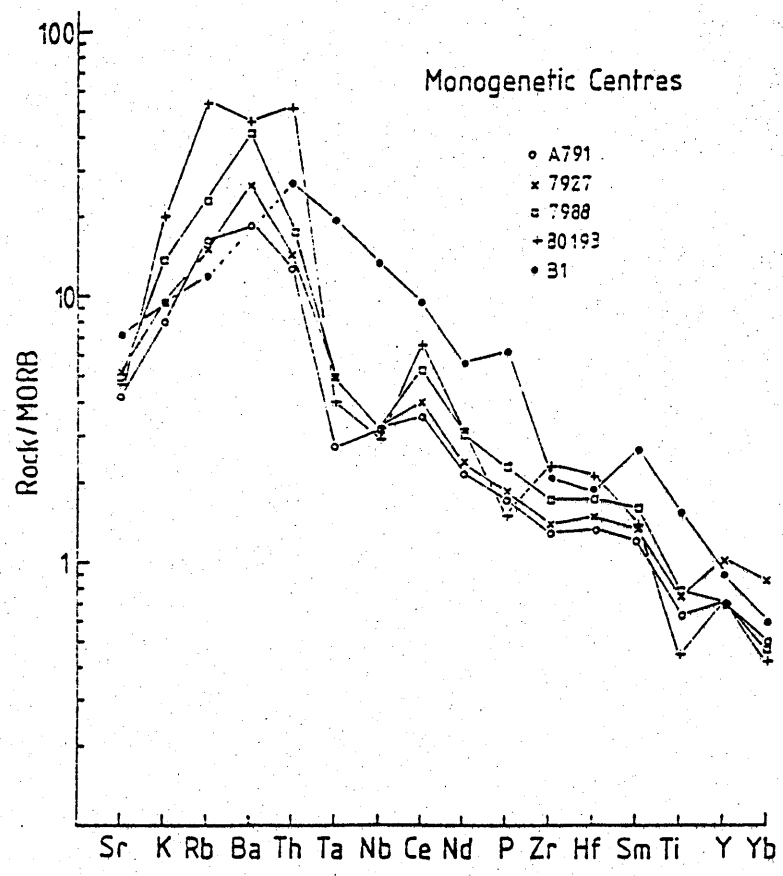

Figure 7.11

MORB normalised diagram for the monogenetic centres. All have a subduction related signature except B1 which has a marked intraplate component.

a.

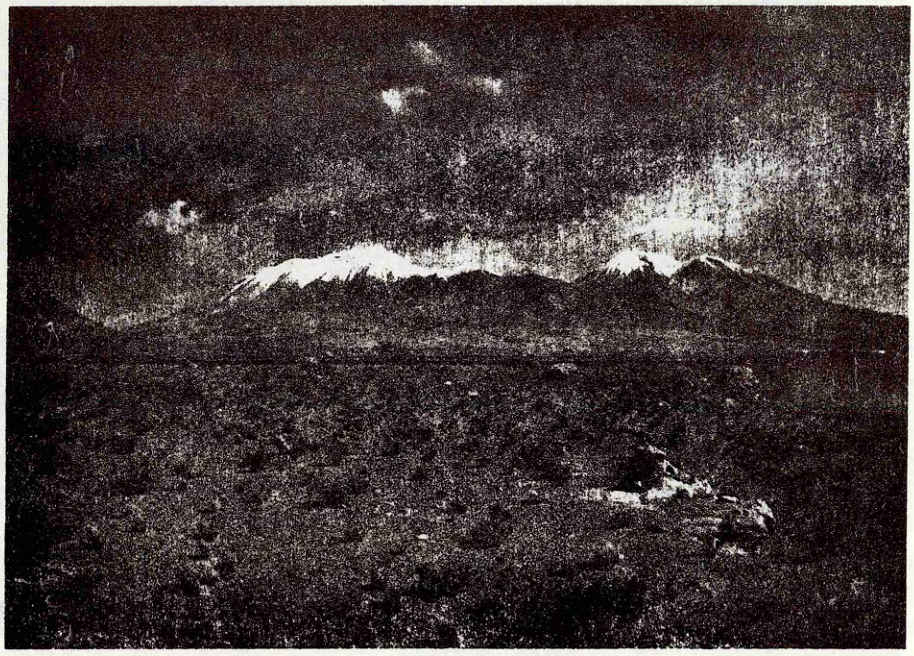

b.

Plate 7.1a. San Pablo (left) and San Pedro (right) from the north.

Plate 7.1b. The basaltic andesite maar ring of Cerro Overo.

a.

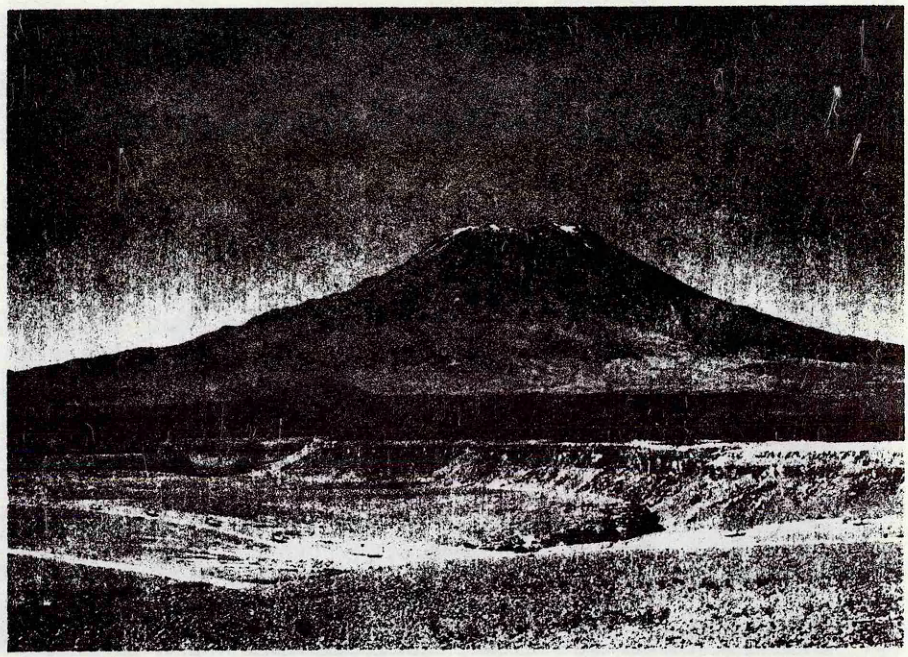

b.

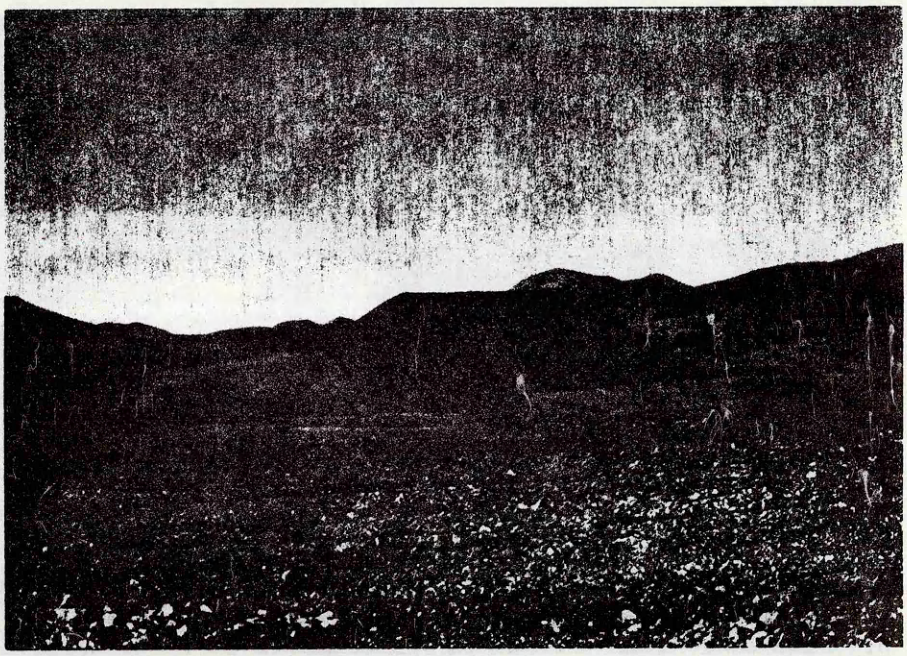

Plate 7.2a. San Pedro with the scoria cone of La Poruña at its base from the south-west. Note the large flow from the cone. The cliffs in the foreground are composed of an ignimbrite sheet which has been incised by the Rio Loa.

Plate 7.2b. La Poruña from the south.

8.4%. one from San Pablo was 8.5%. and one from another volcano 10.8%.. Pb isotope analyses have been done on five dacites; $^{206}Pb/^{204}Pb$, $^{207}Pb/^{204}Pb$ and $^{208}Pb/^{204}Pb$ values range from 18.63-18.72, 15.61-15.63 and 38.52-38.68 respectively, showing no correlation with SiO_2 (Harmon et al., 1984).

San Pedro was originally a simple stratocone which erupted basaltic andesites; this underwent caldera collapse, producing both airfall and pyroclastic flow deposits. Post caldera activity consists of a thin veneer of andesite lavas, and thicker dacite domes and flows. The whole rock trace element and mineral chemistry require a model of late stage magma mixing to generate the observed trends (L.J. O'Callaghan, pers. comm., 1984).

(ii) Monogenetic Centres

Structures of this type, experiencing only one or a few eruptions are varied in their morphologies, but are uncommon. Their products are dominantly basaltic andesites and of small volume. At the western foot of San Pedro is the small scoria cone of La Poruna about 150 m high (Plate 7.2). This has produced several small flows and one large flow to the west. A similar cone, Porunita (7988), is found at the foot of Volcan Ollague (Figure 7.7). Immediately to the south of San Pedro a basaltic maar deposit has been erupted in a small salar, Ojo de San Pedro (7927) (Figure 7.7). Further to the south there is another maar ring, Cerro Overo (A791; Plate 7.1b). This is a basaltic andesite containing phenocrysts of olivine and clinopyroxene; plagioclase only forms small needles in the groundmass. Parts of this rock contain dacite xenoliths; whilst the contact between these and the host is often sharp, partially fused xenoliths have been noted (Thorpe et al., 1984). The dacites

are here thought to be upper crustal, entrained in the magma during its forceful eruption. About 20 km south-west of Calama, on the immediate north side of the Calama-Antofagasta road, is a small hill, Cerro Isla (80193), composed of a single dacite flow. This contains phenocrysts of olivine, clinopyroxene, plagioclase and magnetite; the groundmass consists of olivine, magnetite and brown glass. Given the fresh nature of the rock, an upper Tertiary or Recent age is inferred.

The monogenetic centres erupt the most basic material found in the Central Andes. A detailed study of these may provide the most direct information regarding the nature of mantle source regions beneath the Western Cordillera, and in this respect Sr and Nd isotope analyses have been performed on some of those mentioned above. Major, trace element and REE analyses for three samples (Cerro Overo (A791), Porunita (7988) and Chiar Kkollu (B1)) have been published in Thorpe et al. (1984): similar analyses for Ojo de San Pedro (7927) were provided by L.J. O'Callaghan.

(iii) Ignimbrite Shields

Although ignimbrite sheets of Upper Tertiary-Recent age are aerially extensive in the Central Andes (Baker and Francis, 1978), their sources are not well constrained. It has been postulated that some may originate from fissures in south-west Bolivia (Baker, 1977a; Kussmaul et al., 1977), or that the salars on the Andean crest are located in calderas, marking the locus of ignimbrite eruption (Roobol et al., 1976). This genetic relationship between ignimbrites and calderas has been demonstrated in Bolivia (Francis et al., 1981) and in Cerro Galan, Argentina (Francis et al., 1983). A further centre for eruption is the ignimbrite shield complex of Purico. This

has been described by Francis et al. (1984) and geochemically modelled by Hawkesworth et al. (1982). The complex consists of a gently inclined apron of ignimbrite surmounted by a number of andesite and dacite domes forming a roughly elliptical locus of activity. It is thought that this may represent the margins of a small caldera which is filled by the ignimbrite. The youngest ignimbrite is 1.38 Ma, and some of the domes are probably only a few thousand years old (Francis et al., 1984). Ignimbrites from 22-23°S have been analysed isotopically by Thorpe et al. (1979) and Hawkesworth et al. (1982). Those from 23°S have ε^{i}_{Sr} = +55.9 to +60.4 and ε^{i}_{Nd} = -5.72 to -7.30, whereas one from 22°S has distinctly different values with ε^{i}_{Sr} = +7.0 and ε^{i}_{Nd} = -3.24. The products of these structures are generally highly evolved; they are either the result of crustal anatexis or of advanced degrees of contamination of a more basic mantle derived melt.

(iv) Dacite Domes and Lavas

These structures are relatively minor, but occur over wide areas. As mentioned above they are erupted on the Purico shield volcano around a probable ring fracture. Further examples are found on the more mature statovolcanoes such as San Pedro and Aucanquilcha. Domes also form individual entities, for instance the Chanca dome to the north-east of San Pedro: the huge (24 km^3) Chao lava flow 35 km to the south of San Pedro is also of dacitic composition (Guest and Sanchez, 1970).

7.4.2 Geochemistry of the monogenetic centres

Three of the monogenetic centres studied (Cerro Overo (A791), Porunita (7988) and Ojo de San Pedro (7927) have SiO_2 in the range 50.7-56.2%; L.J. O'Callaghan (pers. comm.) considers the low SiO_2

content (50.65%) of Ojo de San Pedro to be due to desilicification on eruption into a small salar, though the remainder of the geochemistry appears unaffected. Cerro Isla (80193) is a dacite according to the classification of Peccerillo and Taylor (1976) whilst Chiar Kkollu (B1) (Figure 7.7) is an alkali basalt (Thorpe et al., 1984). The first four aforementioned rocks all have a subduction-related signature (Figure 7.11) with depletions of Nb and Ta relative to the LILE. The negative P anomaly for 80193 is due to a small amount of apatite fractionation. In contrast B1 has a humped pattern similar to within-plate alkali basalts (Pearce, 1982); its low LILE/Ta ratios are uncharacteristic of destructive plate margin magmas. This signature may reflect the rock's eruption behind the currently active arc (Figure 7.7). Chondrite normalised REE patterns are shown in Figure 7.12. All the samples are LREE enriched with B1 having the highest levels of REE. For the subduction related rocks $(Ce/Yb)_N$ varies from 3.58-11.70; Ce_N from 40.5-76.6 and Yb_N from 6.55-12.9. There are ubiquitous negative Eu anomalies though these are uniformly small (Eu/Eu^* = 0.84-0.85). These patterns, with the exception of B1, generally fall within the range reported for San Pedro (Figure 7.11: Thorpe et al., 1976). The low concentrations of HREE and the fractionated $(Tb/Yb)_N$ ratios are indicative of garnet being a residual phase during partial melting (Thorpe et al., 1976). As also noted by the above authors and by Dostal et al. (1977) an over-abundance of LILE precludes petrogenesis by a single-stage partial melting event of garnet peridotite, and a mechanism involving fluxing of the mantle by hydrous fluids derived from the subducting oceanic lithosphere is required.

Subduction zone contributions for A791, 7927 and 7988 are given in Table 7.3. Whilst there is a greater contribution for the alkali elements

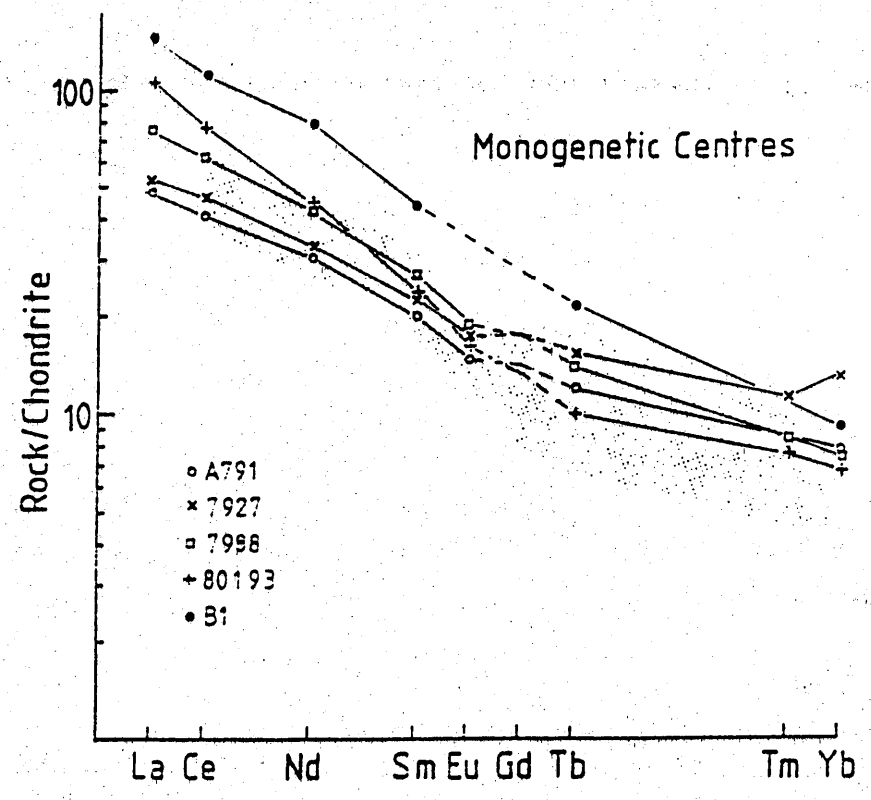

Figure 7.12

Chondrite normalised REE diagram for the monogenetic centres. The range of variation for San Pedro is also shown (Thorpe et al., 1976).

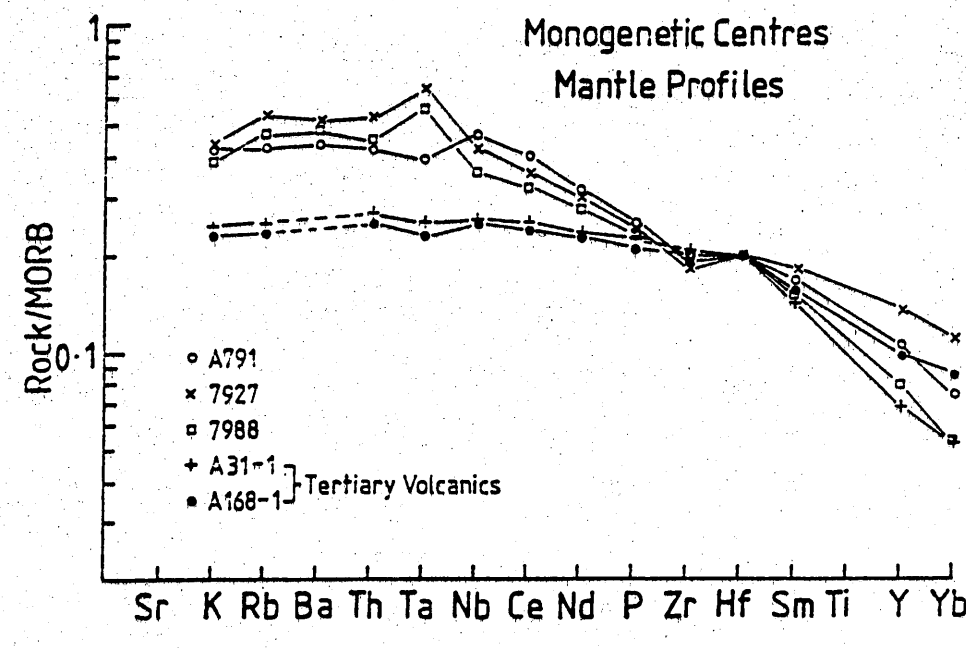

Figure 7.13

MORB normalised profiles for the mantle sources of the Monogenetic centres assuming Hf_{mantle} = 0.475 ppm (Table 7.4). These sources are compared with those for the Tertiary volcanics.

Table 7.3 Subduction zone contributions (%) for Monogenetic centres

Sample	A791	7927	7988
K	65	65	75
Rb	82	73	82
Ba	84	85	90
Th	77	72	77
Ce	23	33	47
Nd	0	3	18
P	0	0	8
Sm	7	0	17

Table 7.4 Unmodified mantle concentrations for the Monogenetic centres

Sample	A791	7927	7988
K(%)	0.062	0.066	0.058
Rb	0.855	1.07	0.937
Ba	8.72	10.4	9.58
Th	0.085	0.105	0.091
Ta	0.071	0.116	0.101
Nb	1.63	1.45	1.24
Ce	4.00	3.54	3.18
Nd	2.78	2.62	2.43
P(%)	0.030	0.029	0.028
Zr	17.1	16.4	17.7
Hf[1]	0.475	0.475	0.475
Sm	0.552	0.594	0.497
Y	3.12	4.09	2.38
Yb	0.251	0.375	0.181

1 Hf concentration assumed

compared to the LREE and P, they are all generally lower in comparison to those of the Tertiary volcanics (Table 7.1). Calculated source profiles are shown in Table 7.4 and Figure 7.13. At comparable degrees of HREE depletion the monogenetic centres have more enriched profiles than the Tertiary volcanics (Figure 7.13).

Cerro Overo (A791), Ojo de San Pedro (7927) and Porunita (7988) all yield ε_{Sr} and ε_{Nd} values close to those of San Pedro (Figure 7.5). Whilst these three have similar ε_{Sr} (20.1-23.7) Porunita, like sample B5 from Bolivia (Section 7.3), and 80012 from San Pedro (Section 7.4.3), has a low ε_{Nd} value.

Cerro Overo, by implication from its mineralogy and morphology, is unlikely to have resided for long in the upper crust where plagioclase would be expected to be a liquidus phase. Furthermore, the magnesian composition of the olivines in the sample (Fo_{88-89} (L.J. O'Callaghan, pers. comm., 1984)) implies that the transit time from the mantle to the surface has been short. It is in upper crustal domains that high Rb/Sr, and hence high time-integrated $^{87}Sr/^{86}Sr$ ratios occur. However, if the magma has traversed this region very quickly then there can have been little opportunity for contamination. The presence of partially fused dacitic xenoliths (Thorpe et al., 1984) need only be a function of the eruptive mode, and does not necessarily imply digestion in a long lived upper crustal magma chamber. Consequently it is thought that Cerro Overo (A791) represents an uncontaminated basaltic andesite and that its isotopic characteristics are those of the mantle source region; these are $^{87}Sr/^{86}Sr$ = 0.70612 (ε_{Sr} = +20.1) and $^{143}Nd/^{144}Nd$ = 0.512536 (ε_{Nd} = -2.03). Whilst one cannot, of course, unequivocably extrapolate these values to the whole of the north Chilean

mantle, the occurrence of such mantle, coupled with the generally observed isotopic base level in the region of $^{87}Sr/^{86}Sr$ ratios of 0.7056-0.7060 and $^{143}Nd/^{144}Nd$ ratios of $\sim$0.51254 leads to the conclusion that it is most likely that Cerro Overo type mantle is present beneath San Pedro and the other volcanoes in this area.

The andesite from Cerro Isla (80193) has much more depleted isotopic characteristics than either San Pedro or the three monogenetics discussed above. It has $^{87}Sr/^{86}Sr$ = 0.70498 (ε_{Sr} = +4.0) and $^{143}Nd/^{144}Nd$ = 0.512674 (ε_{Nd} = +0.66). These values, however, compare closely with the initial ratios of the Cretaceous volcanics of the Augusta Victoria Formation which were erupted in this area ($^{87}Sr/^{86}Sr$ = 0.70408-0.70458; $^{143}Nd/^{144}Nd$ = 0.512687-0.512774 : Section 5.5.5), given a slight increase in $^{87}Sr/^{86}Sr$ in the source over $\sim$ 100 Ma. The Nd data imply a very low Sm/Nd ratio in the source since the Cretaceous, though if Cerro Isla is contaminated slightly by old continental crust this ratio may be a little higher. Either way, the results from Cerro Isla indicate that there are heterogeneities in the mantle beneath northern Chile, and that towards the west it is more depleted than in the east in the active cordillera.

B1, the alkali basalt from Chiar Kkollu in Bolivia, has an $^{87}Sr/^{86}Sr$ ratio of 0.7041 (Thorpe and Francis, 1979a); these authors consider this to be representative of the sub-Andean mantle in the central Andes, and that all rocks with higher ratios are contaminated. The possibility that the Sr isotopic composition may have been reduced by contamination is not discussed. This ratio has been re-determined in the course of this study and yields a $^{87}Sr/^{86}Sr$ ratio of 0.70386

(ε_{Sr} = -11.9); the $^{143}Nd/^{144}Nd$ ratio = 0.512679 (ε_{Nd} = +0.76) (Figure 7.5). The latter value contrasts sharply with the results from Ecuador which have comparable $^{87}Sr/^{86}Sr$ ratios and places the sample below the mantle array. The petrogenesis of rocks plotting in this position has frequently been modelled in terms of contamination by old, Rb-depleted granulitic crust (e.g. Carter et al., 1978). This, of course, would necessitate a mantle source with even more depleted ε_{Nd}, or conversely, with higher ε_{Sr} so that in either case the mantle end member sat on the mantle array. There is, however, no unequivocal evidence to indicate that this sample has in fact undergone contamination. Menzies and Wass (1983) reported Sr and Nd isotope data for amphibole/apatite pyroxenite xenoliths in a SiO_2 undersaturated host dyke from Kiama in New South Wales which plotted in a similar position to B1 on an ε_{Sr}-ε_{Nd} diagram (Figure 7.5). They argued that these isotopic characteristics represented a time integrated response to the influx of CO_2 rich fluids into the local depleted mantle ~100 Ma ago, rather than crustal contamination. As mentioned in the previous Section B1 does not have a subduction-related trace element pattern, and so it is therefore possible that a segment of the sub-Andean mantle has remained immune from the subduction and enrichment processes which has been operative hereabouts for several hundred million years; alternatively this sample could be derived from asthenosphere below the subcontinental lithosphere. Either way, CO_2 rich fluids may have been involved in its petrogenesis.

7.4.3 Isotope Geochemistry of San Pedro

Sr and Nd isotope data for San Pedro and other north Chilean volcanoes have been presented by Francis et al. (1977) and Hawkesworth et al. (1979a, 1982), but in view of the variation in results for the

E. and A. Sr standard reported by the former these were reanalysed in the present study. Furthermore, the Nd analyses (performed at Leeds University) have also been repeated to ensure consistency with other Andean data generated at the Open University. Likewise, those Ecuadorian samples used in the study by Hawkesworth et al. (1979a) have been reanalysed for both Sr and Nd isotopes. The new results are presented in Appendix F together with those for an additional five samples from San Pedro. Those for Ecuador have $^{87}Sr/^{86}Sr$ ratios of 0.70365-0.70429 (ε_{Sr} = -14.9 to -5.8) and $^{143}Nd/^{144}Nd$ ratios of 0.512797-0.512970 (ε_{Nd} = +3.06 to 6.44).

$^{87}Sr/^{86}Sr$ ratios for San Pedro vary from 0.70616-0.70681 (ε_{Sr} = +20.7 to +29.9) though this range is extended to 0.70711 (ε_{Sr} = +34.1) if sample 283 from the older San Pablo is included. $^{143}Nd/^{144}Nd$ ratios span 0.512431-0.512279 (ε_{Nd} = -4.08 to -7.04). Samples 200 and 482 are from nearby volcanoes (see Thorpe et al., 1976 Table 1 for details); these have $^{87}Sr/^{86}Sr$ ratios of 0.70671 and 0.70583 (ε_{Sr} = +29.3 and +16.0) and $^{143}Nd/^{144}Nd$ ratios of 0.512355 and 0.512499 (ε_{Nd} = -5.56 and +2.75) respectively (Figure 7.5). The trend of decreasing ε_{Nd} with increasing ε_{Sr} overlaps exactly with the more depleted part of the Chascon array if the San Pablo sample is included. Nonetheless there is also a subvertical trend on Figure 7.5 defined by sample 80012. This is similar to the vector defined by the Bolivian sample (B5) noted in Section 7.3. If this is interpreted as a contamination trend then the contaminant is at least 674 Ma old if it were derived from a chondritic source, and assuming it has an average crustal Sm/Nd ratio of 0.19, or 1149 Ma if the source were to be comparable to depleted mantle. It is also clear from Figure 7.5 that the rocks of the Palaeozoic Limon Verde pluton (Section 2.4) are

unable to act as the sole contaminant of the San Pedro, Chascon or Purico lavas as they do not have sufficiently unradiogenic Nd isotope systematics. Similar arguments apply to the majority of samples from the Limon Verde schist complex.

7.5 Summary

It is clear that there are several types of volcanic structure found in the Western Cordillera of northern Chile, each with its own lithological assemblage and petrography. Whilst most are related to subduction there must be subtle differences influencing their petrogeneses such as mantle composition, local crustal structure, the amount and mechanism of crustal contamination, and the degree of magma mixing.

The brief study of the five monogenetic centres from northern Chile and Bolivia indicate that the sub-Andean mantle is heterogeneous on a scale of tens of kilometres. The geochemistry of Cerro Overo (A791) implies the existence of isotopically enriched mantle sources, without the need to resort to crustal contamination models. More depleted mantle sources, however, do exist as shown by Chiar Kkollu in Bolivia (B1), though this has tapped a source unrelated to subduction.

CHAPTER 8

TRANS CORDILLERAN VARIATIONS

8.1 Introduction

The preceding chapters have described individual volcanic formations and igneous intrusions and interpreted the geochemistry of each in general isolation from the other units. This chapter considers the transverse geochemical and geochronological variations displayed by the transect when viewed as a whole. The conclusions of the earlier work have sometimes provided petrogenetic constraints for each of the units within which any large scale models must be compatible. In view of the uncertainties regarding palaeo-trench positions and palaeo-inclinations of the Benioff Zone, transverse variations are portrayed as the distance in kilometres perpendicular to the present day Peru-Chile trench.

8.2 Age variations

Considering only the evolution of this transect since the Jurassic, there has been a general eastwards migration of the locus of igneous activity (Figure 8.1) in accord with the findings of Farrar et al. (1970) from 26-29 ^{o}S in Chile. This has not, however, been totally systematic: for instance the Pampa Negra pluton (79 Ma) was intruded further west than the Cerros de Montecristo and Cerritos Bayos plutons ($\sim$100 Ma), and the pluton at El Abra (39 Ma) is 15 km west of Cerro Colorado (66 Ma). Moreover, as noted by McNutt et al. (1975) and Kussmaul et al. (1977) there has been a westwards migration of activity during the past 5 Ma. Present day activity spans a broad front from Calama in the west ($\sim$ 260 km from the trench) to Chiar Kkollu in Bolivia ($\sim$ 410 km). The observed age progression is in contrast to that reported for the Antarctic Peninsula (Saunders et al., 1980) where

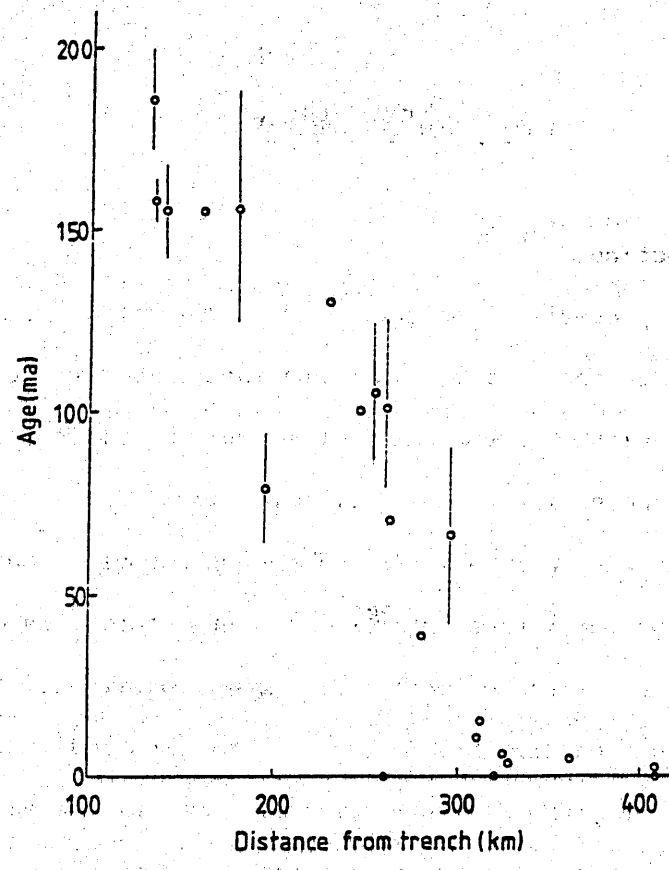

Figure 8.1

Plot of distance from the present day trench versus age for the various rock units in the transect. Errors on the ages (2σ) are shown.

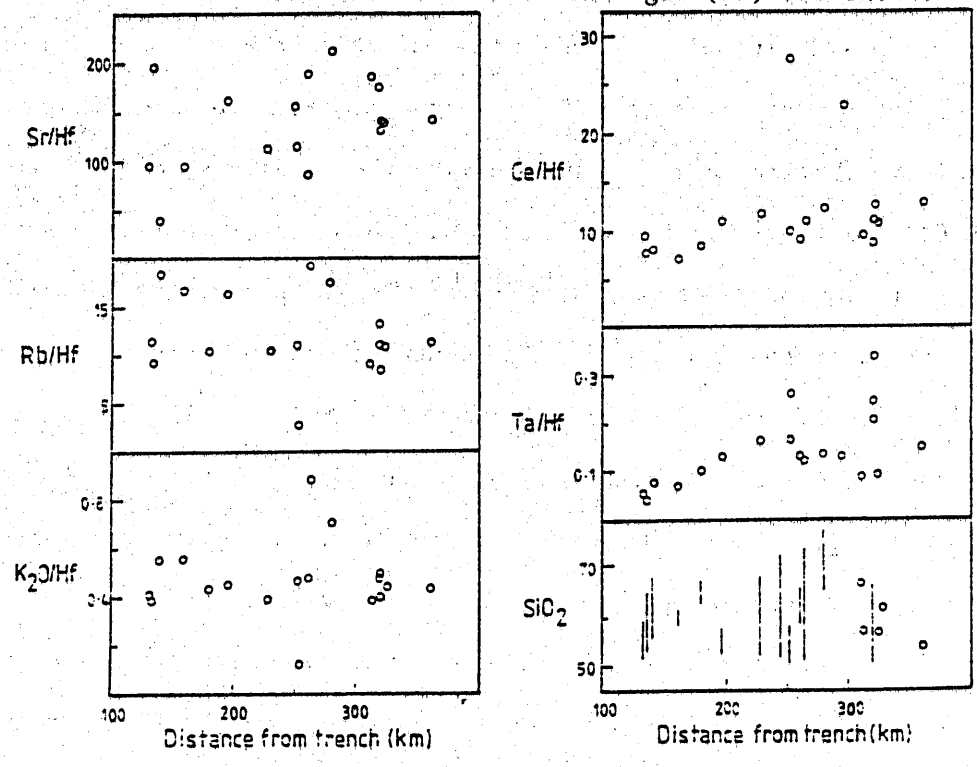

Figure 8.2

Plot of distance from the present day trench against the concentrations of selected elements in the most basic rocks of each unit studied normalised against Hf. The range in SiO_2 for each unit is also shown. See text for discussion.

magmatism has migrated westwards towards the trench since ∿ 185 Ma.

8.3 Elemental variations

Variations in incompatible element abundances across Recent arcs have been documented by several authors (e.g. Jakeš and White, 1972; Whitford et al., 1979). These studies have noted increases in LILE and some HFSE (e.g. Nb, Zr and Hf) at a given degree of fractionation with increasing depth to the Benioff Zone (h) within an arc (the K-h relationship of Dickinson and Hatherton (1967) and Hatherton and Dickinson (1969)): HREE and Y concentrations sometimes decrease with increasing h (Gill and Gorton, 1973) or remain constant (Whitford et al., 1979). Furthermore, it has been postulated that the oldest lavas erupted in an arc are low K tholeiites, but that as the arc matures so calcalkaline and shoshonitic material is produced (e.g. Jakeš and White, 1969; Jakeš and Gill, 1970; Ringwood, 1974). Thus there is a spatial as well as a temporal control on magma compositions. In the Pliocene-Recent volcanics of northern Chile and S.W. Bolivia Roobol et al. (1976) reported increasing K_2O, Rb, Y and Th and decreasing Sr in passing from west to east across the Cordillera. Dostal et al. (1977) noted an increase in K_2O, Rb, Ba, Sr and Zr content for a given SiO_2 value across the Andes between 26° and 29°S. Thus Jurassic-Eocene rocks outcropping near the present day coast were said to have island-arc affinities, whilst the Miocene-Quaternary lavas further east were compared to calcalkaline suites from continental margins. Shoshonitic rocks were reported furthest from the trench. This zoning, however, has a time span of about 160 Ma, and so is not strictly analogous to the Dickinson and Hatherton model which covers essentially contemporaneous volcanic rocks. Dostal et al. (op. cit.) do not indicate whether there is any petrological or geochemical variation across the volcanic belt in lavas of

the same age. However, it is interesting to note that the overall gross trends are operative over such a long time interval, which suggests that spatial control on volcanism is a more important factor than the temporal control in determining the geochemical composition.

Selected elemental variations across the Andes at 22°S are shown in Figure 8.2 where the most basic rock in each suite is normalised against Hf as this element shows little variation across the cordillera in rocks of similar composition, and is incompatible in both mantle melting and low pressure fractional crystallization processes. There are notable overall increases in Sr, Ta and Ce with increasing distance from the present day trench: Rb and K show no pronounced trends either way. Suites also do not become more SiO_2 rich.

8.4 Arc Maturity

Brown (1982) used a plot of calc-alkali ratio ($CaO/(Na_2O+K_2O)$) against SiO_2 as an index of arc maturity. Granitoids from immature arcs are found to be calcic (i.e. have an alkali lime index of > 61), whereas those from arcs of increasing maturity have lower values of this index and can eventually become alkali-calcic (51-56) or even alkalic (<51). The data for the plutonic complexes studied in this work are plotted on Figure 8.3. It is seen that the plutons are all calcalkaline, but that there is no progression with time towards more alkali-calcic compositions even though the arc is maturing: indeed the youngest pluton, El Abra, has the highest alkali lime index. Superimposed on this idealistic trend of increasing arc maturity are variations induced by the regional stresses operative at the time of intrusion. Brown (1982) indicates that extensional regimes yield alkali-calcic magmas whereas compressional ones produce calcalkaline rock suites. Thus the variation

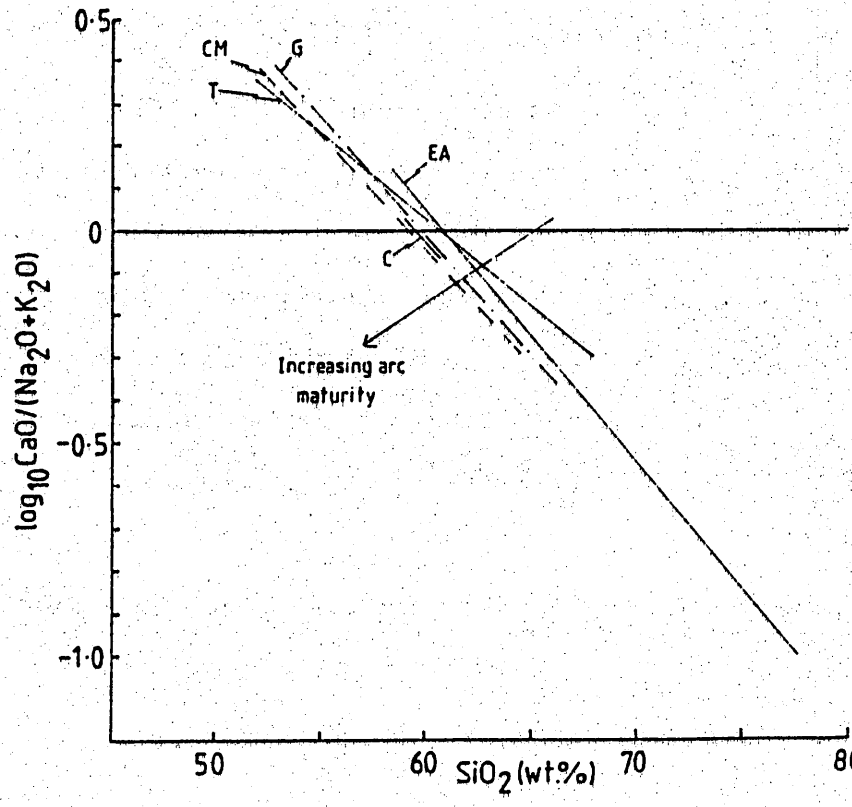

Figure 8.3

Plot of calc-alkali ratio against SiO_2 showing the trends defined by the various plutonic suites of the transect. G = Gatico (158 Ma): T = Tocopilla (154 Ma): C = Cerro Colupito (155 Ma): CM = Cerros de Montecristo (102 Ma): EA = El Abra (39 Ma). The trend for increasing arc maturity is taken from Brown (1982). Note the overall lack of variation shown by the plutons despite their considerable age differences.

seen in Figure 8.3 may reflect temporal changes in the stress configuration which dominate over the effects of increasing maturity of the arc.

8.5 Isotopic Variations

Figure 8.4 shows the variation in ε^{i}_{Sr} and ε^{i}_{Nd} for rocks of the Andean orogeny with increasing distance from the present day trench. ε^{i}_{Sr} increases progressively eastwards, though Cerro Colorado (295 km) has lower values than the Cretaceous volcanics and plutonics further west. There is also a sharp rise between Cerro Colorado and the Tertiary-Recent volcanics to the east. The spread of ε^{i}_{Sr} to high values for the Cerritos Bayos pluton is due to post-consolidation hydrothermal alteration (Chapter 6). ε^{i}_{Nd} decreases gradually away from the trench as far as Cerro Colorado, though the lower values for the contaminated Pampa Negra pluton (195 km) and the Indio Muerto Formation (229 km) are notable deviants. To the east of Cerro Colorado ε^{i}_{Nd} drops dramatically to the negative values of the Upper Tertiary and Recent volcanics.

Figure 8.5a shows the Sr isotopic evolution of this transect over the last 270 Ma. The diagram can be divided into two parts, namely the Palaeozoic and the Jurassic-Recent (Andean orogeny). The Palaeozoic rocks of the Limon Verde have higher initial $^{87}Sr/^{86}Sr$ ratios (0.70703-0.70831), and it has been argued earlier (Section 2.4) that these represent contamination of basic mantle-derived magmas with more radiogenic continental crust prior to high level fractionation. At the beginning of the Jurassic (or even in the late Triassic further south (McNutt et al., 1975)) there was a switch in the locus of magmatism westwards to the present day Cordillera de la Costa with the eruption of

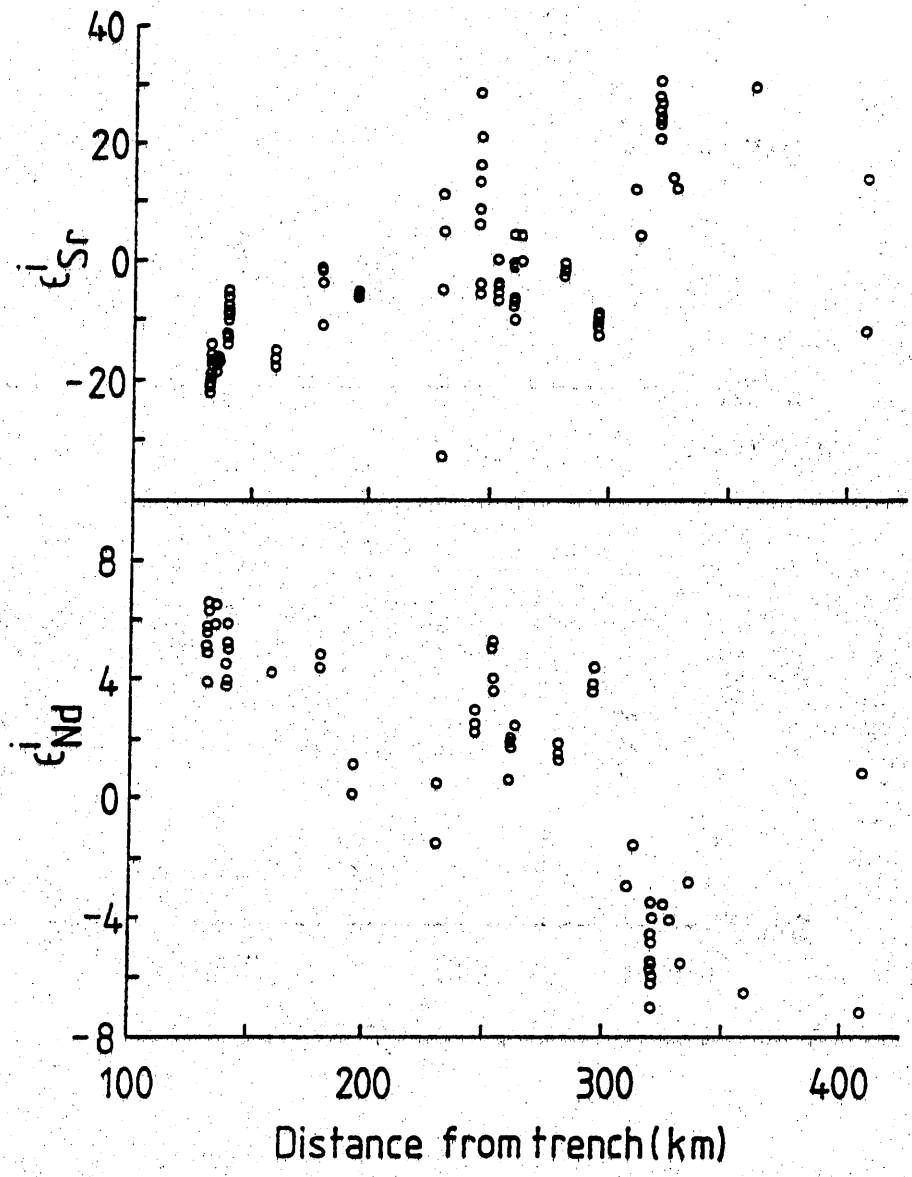

Figure 8.4

Variation in ε^i_{Sr} and ε^i_{Nd} with increasing distance from the trench. Both ε^i_{Sr} and ε^i_{Nd} tend sharply to more enriched values at distances greater than $\sim$ 300 km.

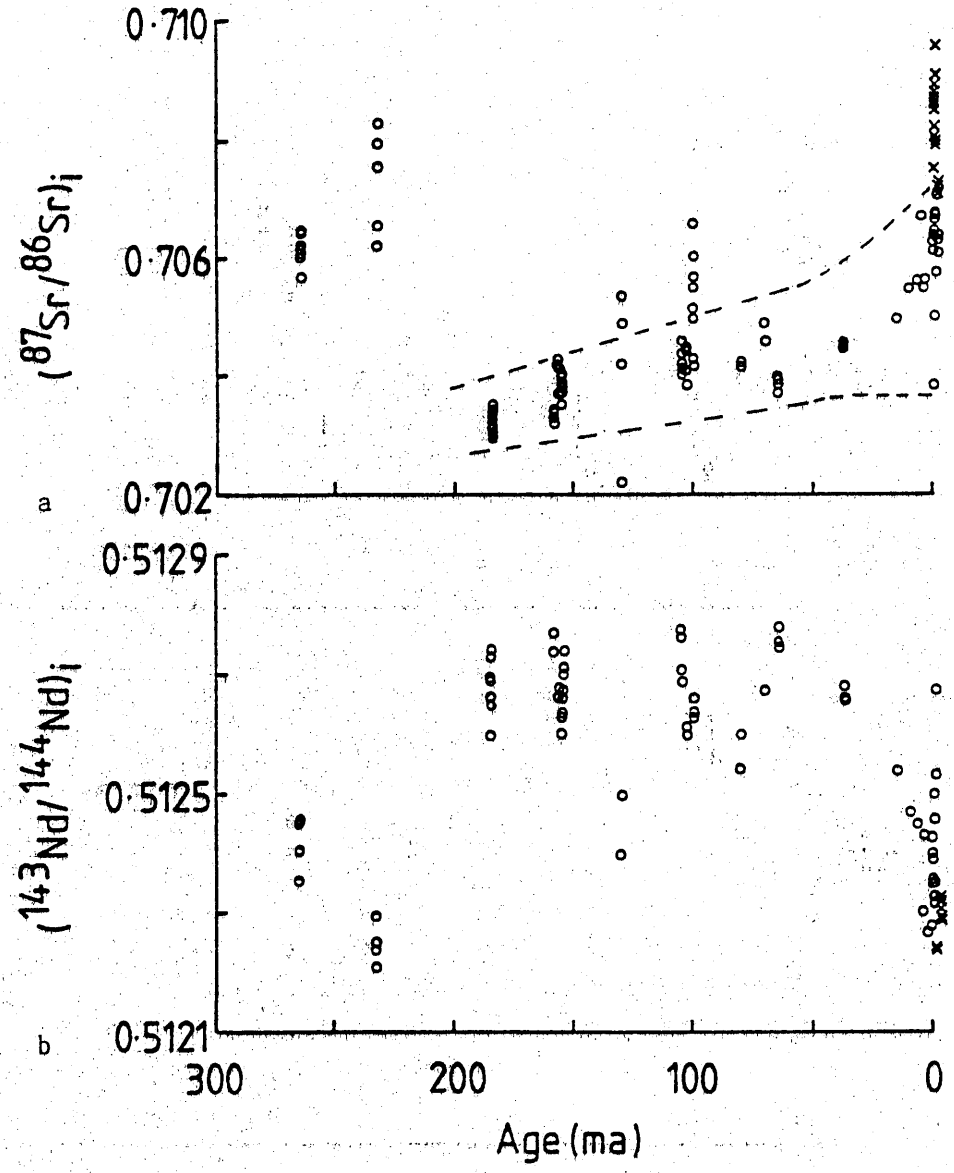

Figure 8.5

Sr and Nd isotope evolution diagram for the Andes at 22°S since 270 Ma ago. Note the transition between the "Hercynian" orogenic suite of the Palaeozoic and the "Andean" orogenic rocks from the Jurassic-Recent Data for Purico-Chascon from Hawkesworth et al. (1982) (x) The dashed lines on the Sr evolution diagram represent the region of essentially uncontaminated rocks.

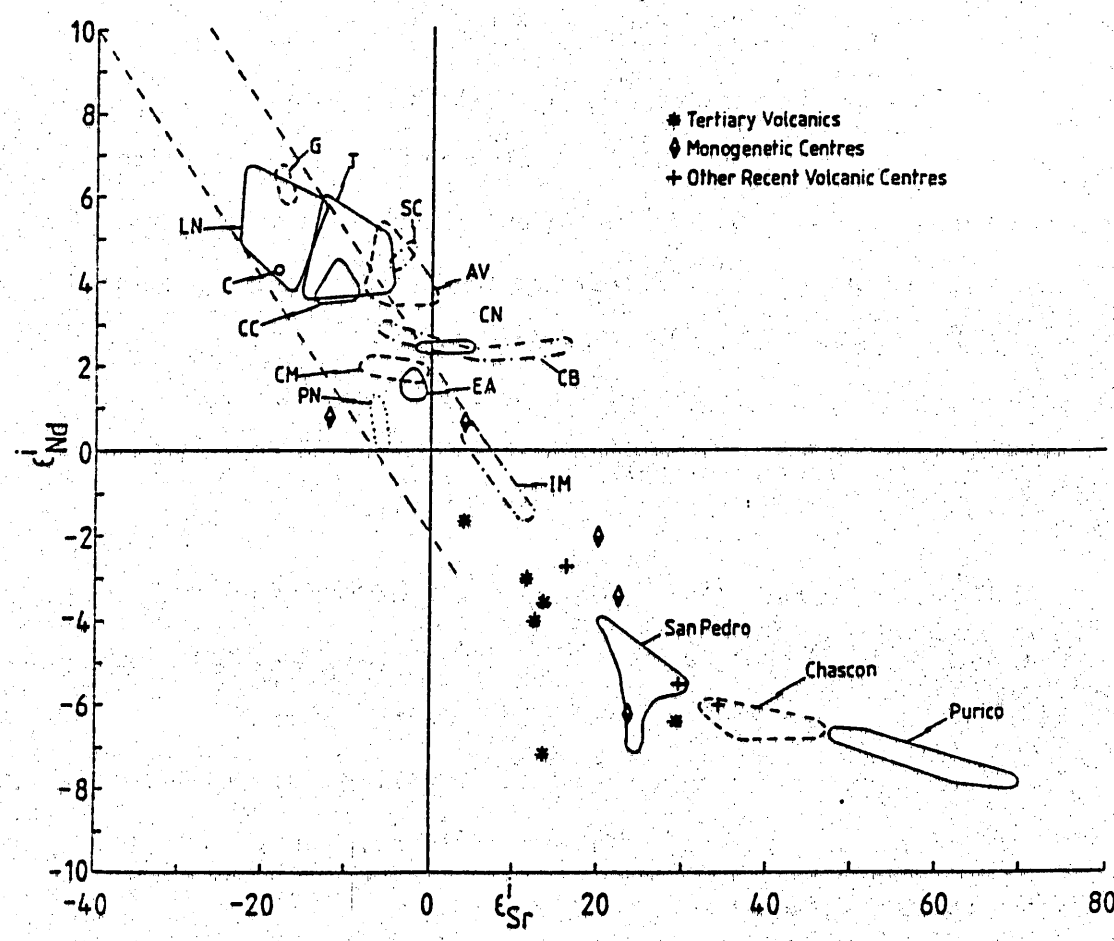

Figure 8.6

ϵ^i_{Sr} - ϵ^i_{Nd} diagram for the north Chilean Andes since 186 Ma. Names of units are given beside each field. LN = La Negra: G = Gatico: T = Tocopilla: C = Cerro Colupito: SC = Sierra de la Cruz: IM = Indio Muerto: AV = Augusta Victoria: CM = Cerros de Montecristo: CB = Cerritos Bayos: CN = Cerro Negro: PN = Pampa Negra: CC = Cerro Colorado: EA = El Abra. Note the overall migration through time towards more enriched isotopic compositions. See text for discussion.

the La Negra Formation. This has low initial $^{87}Sr/^{86}Sr$ ratios (0.70292-0.70347), in marked contrast to the earlier units. Since the Jurassic there has been a general progressive increase in the initial ratios with a sharp rise to the Recent volcanics of San Pedro and Purico-Chascon (Hawkesworth et al., 1982). The rise, however, has not been uniform: variations exist within the Jurassic batholith at ∿155 Ma, and Cerro Colorado (66 Ma) has lower values than the earlier Cretaceous suites. McNutt et al. (1975) reported Sr isotope variations from a transect between 26-29°S. Rocks aged 191-137 Ma have lower ratios of 0.7023-0.7035. Subsequent to 125 Ma the initial ratios rise progressively to 0.7077in Recent andesites.

In sympathy with the Sr isotope results, there are analogous variations in Nd isotopes (Figure 8.5b). Again the Palaeozoic rocks form a distinct entity having much lower initial $^{143}Nd/^{144}Nd$ ratios than the Jurassic rocks. From the Jurassic to the end of the Cretaceous these ratios are generally almost constant, whence there is a pronounced drop to the present day.

The time independent covariation of initial Sr and Nd isotopes is best seen on a plot of ε^{i}_{Sr} against ε^{i}_{Nd} (Figure 8.6). All the pre-Upper Tertiary data have depleted Nd isotope systematics (except for the Indio Muerto Formation); unaltered samples tend to have depleted ε^{i}_{Sr}. The data show a general migration towards more 'enriched' compositions with time, although, as noted earlier, Cerro Colorado is more depleted than the Cerros de Montecristo; Pampa Negra and the Indio Muerto Formation have low ε^{i}_{Nd} due to crustal contamination. The Upper Tertiary-Recent volcanics plot in the bottom right hand quadrant (except B1 and 80193; Section 7.4.2), with

Purico-Chascon defining a flat-lying trend and San Pedro possibly two trends, the first an extension of Purico, and the second towards lower ε_{Nd} for a given ε_{Sr} (Section 7.4.3).

8.6 Discussion

8.6.1 Introduction

There are several potential explanations for the observed isotopic trends.

(i) A progressive increase with time in the amount of upper crustal contamination experienced by mantle derived melts (from a homogeneous source).

(ii) A progressive increase of the subduction zone component of the magmas, since it could have high $^{87}Sr/^{86}Sr$ and low $^{143}Nd/^{144}Nd$ ratios.

(iii) The composition of the material introduced as the subduction zone component could have changed with time.

(iv) The mantle wedge is chemically zoned, being progressively more enriched and perhaps older towards the east.

8.6.2 Subduction zone contributions

Using MORB normalised plots (Pearce, 1982) and the methodology of Pearce (1983) one can assess the relative contributions of the subduction zone component and the overriding mantle wedge to a given magma. These calculations have been performed for the La Negra Formation and the Augusta Victoria Formation. Table 8.1 compares the ranges of percentages of the subduction zone component for different elements from the Jurassic-Recent.

Table 8.1 Percentage subduction zone contributions for various elements from the Jurassic-Recent

Element	Jurassic	Cretaceous	Tertiary	Recent
K	88 - 92	0 - 69	74 - 82	65 - 75
Rb	92 - 97	30 - 84	86 - 90	73 - 82
Ba	87 - 98	68 - 91	-	84 - 90
Th	91 - 95	80 - 93	81 - 89	72 - 77
Ce	49 - 62	16 - 61	47 - 51	23 - 47
Nd	27 - 45	0 - 38	8 - 25	0 - 18
Sm	6 - 20	50 - 37	37 - 50	0 - 17
P	14 - 38	0 - 28	2 - 23	0 - 8

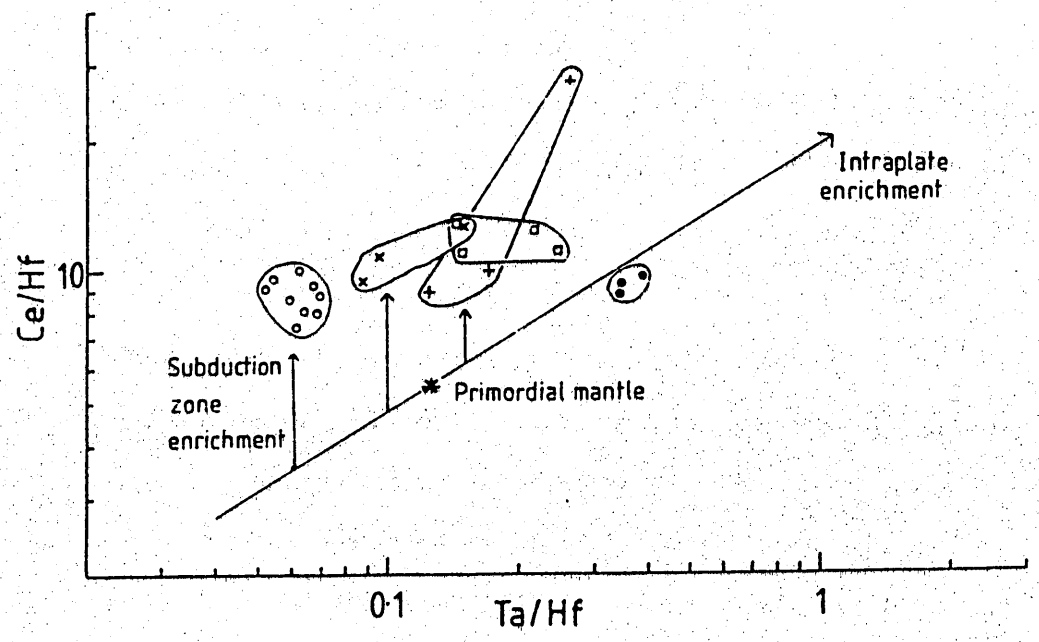

Figure 8.7

Ta/Hf - Ce/Hf diagram showing the overall decrease in the proportion of the subduction zone component with time for the uncontaminated volcanic formations in the transect. O = La Negra Formation (186 Ma), + = Augusta Victoria Formation (105 Ma), × = Tertiary Volcanics, □ = Monogenetic centres, ● = San Pedro. Vectors for intraplate enrichment and subduction zone enrichment are shown. Data for the "mantle array" from Wood et al. (1979) and White et al. (1979). Primordial mantle from Wood (1979).

It is clear from Table 8.1 that for all the elements considered there is a decrease in the proportion of material derived from the subduction zone from the Jurassic-Recent: most importantly Nd shows a decrease from 27-45% to 0-18%. This can be seen diagrammatically in Figure 8.7 where intraplate enrichments merely move data along the 'mantle array' whereas the introduction of a subduction zone component increases the Ce/Hf ratio but not the Ta/Hf ratio. Thus the vertical displacement above the 'mantle array' of subduction related rocks is dependent on the proportion subduction zone derived Ce in those rocks. Whereas Pearce (1982) used Yb as the denominator in his plots showing subduction zone and intraplate enrichments, in view of the evidence from several of the studied suites that garnet was a residual phase during melting, Yb was not utilised as both intraplate enrichment and small degrees of partial melting can increase ratios such as Ta/Yb. Instead, Hf is used as the denominator for the reasons outlined in Section 8.3; in addition Hf is also considered not to be introduced in the subduction zone component. For the Andean lavas the vertical displacement above the 'mantle array' generally decreases with time, again indicating progressively lower proportions of the subduction zone component. Consequently if this component has low ε_{Nd} then the trend to lower ε^{i}_{Nd} with time (Figure 8.6) is unlikely to be caused by changes in the proportion of the subduction zone component.

If the nature of the material comprising the subduction zone component has changed with time then the more recent components must have contained progressively older material to produce the observed trends. The possibilities that either subducted continental detritus or pelagic sediments could reflect this hypothesis are now considered in turn.

This part of the Andes lies in the Atacama Desert which receives essentially zero rainfall: most of the drainage is into internal basins or to the east of the Andean crest. Between Arica (on the Peruvian frontier) and Antofagasta there are few rivers cutting across the Cordillera de la Costa, and those that do are small. Geomorphological studies (Galli-Olivier, 1967; Baker, 1977a; Mortimer et al., 1977) have shown that this climatic regime has been operative for at least 20 Ma. Furthermore, Kulm et al. (1977) noted that the continental margin in the region contains few sedimentary basins or benches. Whilst this may be taken as evidence that continental-derived sediments are continuously being subducted (James, 1978) it is more likely that the trench is devoid of sediment due to the climate and physiography of the coastal regions. Moreover, no unequivocally old continental crust has been found on the coast in this part of Chile, the nearest being the 2.0 Ga Arequipa Massif in Peru (Shackleton et al., 1979). Thus erosion and subduction of old continental crust in the form of detritus is not a plausible mechanism for producing the observed variation.

An alternative hypothesis is that the isotopic composition of pelagic sediments on the Nazca Plate has changed with time. However, whilst the Sr isotopic composition of seawater (with which pelagic sediments are in equilibrium) has fluctuated slightly with time there is no progressive increase as required by the Andean data. Moreover, due to the short residence time of Nd in the oceans, the Nd isotope ratios reflect local terrigenous input, and thus the same problems as for the subduction of terrigenous clastics are encountered.

8.6.3 Crustal contamination

If one advocates a crustal contamination model to explain the

isotopic variation with time, then all of the Upper Tertiary-Recent volcanics must be more contaminated than all of the earlier rocks; assuming a mantle-derived end member with approximately uniform values and a similar crustal contaminant. The timing of the sudden rise in $(^{87}Sr/^{86}Sr)_i$ and concomitant drop in $(^{143}Nd/^{144}Nd)_i$ are coincident with the initiation of uplift of the Andean margin at about 15-20 Ma. Proponents of extreme contamination for the Recent volcanics in north Chile argue that a thicker crust leads to increased residence times of mantle derived magmas in the crust, and hence a greater opportunity for contamination (Francis et al., 1977; Harmon et al., 1984). However, McNutt et al. (1975) noted that initial $^{87}Sr/^{86}Sr$ ratios at 26-29°S continued to increase after passing over the crustal keel, and consequently dismissed that as the prime influence on the isotopic composition. Roobol et al. (1976) also dismissed crustal thickness as the major control on major and trace element geochemistry of Recent volcanics in S.W. Bolivia and north Chile as K_2O contents increased across the keel at constant SiO_2. Both of these studies imply that longitudinal variation of the magma source is the most important factor in determining the observed geochemistry.

The transition from high ε^i_{Nd}-low ε^i_{Sr} to low ε^i_{Nd}-high ε^i_{Sr} also occurs across the structural boundary defined by the Rio Loa between the Precordillera and the downfaulted Western Cordillera. Does this boundary represent a junction between contrasting geochemical domains in the mantle, differing crustal ages with older basement to the east, or increased crustal contamination upon which the variations seen by Roobol et al. (1976) are superimposed? Certainly old basement (1 Ga) was found during drilling on the Altiplano

in Bolivia (Lehmann, 1978), yet similar rocks outcrop in the Arequipa Massif of southern Peru (Shackleton et al., 1979) on the western flanks of the Cordillera. Similarly, the schists of the Limon Verde (Section 2.2) record a contribution from a component 1 Ga old. Thus it is difficult to attribute the isotopic transition to changes in basement age.

It was noted in Section 8.3 that there are few pronounced elemental trends across the Cordillera. However, Figures 8.2 and 8.7 have shown that there is an overall increase in the Ta/Hf ratio with increasing distance from the present day trench. Considering a plot of Hf/Ta against ε^{i}_{Nd} (Figure 8.8) it is apparent that the Recent volcanics, as well as being more enriched isotopically, also have lower Hf/Ta ratios. The La Negra Formation has Hf/Ta = 14.5-19.2 and ε^{i}_{Nd} = +3.90 to +6.62 whereas San Pedro has Hf/Ta = 2.6-2.9 and associated ε_{Nd} = -4.08 to -5.60. As neither Ta nor Hf is considered to be released from the subducting slab, the trend to lower, more enriched Hf/Ta ratios in Figure 8.8, therefore, cannot be produced by the subduction process. The variation is also not simply due to fractionation: certain rocks from San Pedro, the Indio Muerto Formation and the Augusta Victoria Formation all have similar SiO_2 contents to the La Negra Formation, but have much lower Hf/Ta ratios. If the trend is taken to represent increased crustal contamination since the Jurassic then the crustal contaminant must have a very low Hf/Ta ratio (< 4). Bulk assimilation of material similar to the Arequipa Massif or the 1 Ga Charcani Gneiss (James and Brooks, 1976) is unlikely as they do not have the required trace element signature (Hf/Ta = 5.2-14.2 and 4.0-13.3 respectively; Barreiro, 1982b). However, collision granites, considered to be produced by crustal anatexis, are characterised by low Hf concentrations and low Hf/Ta ratios

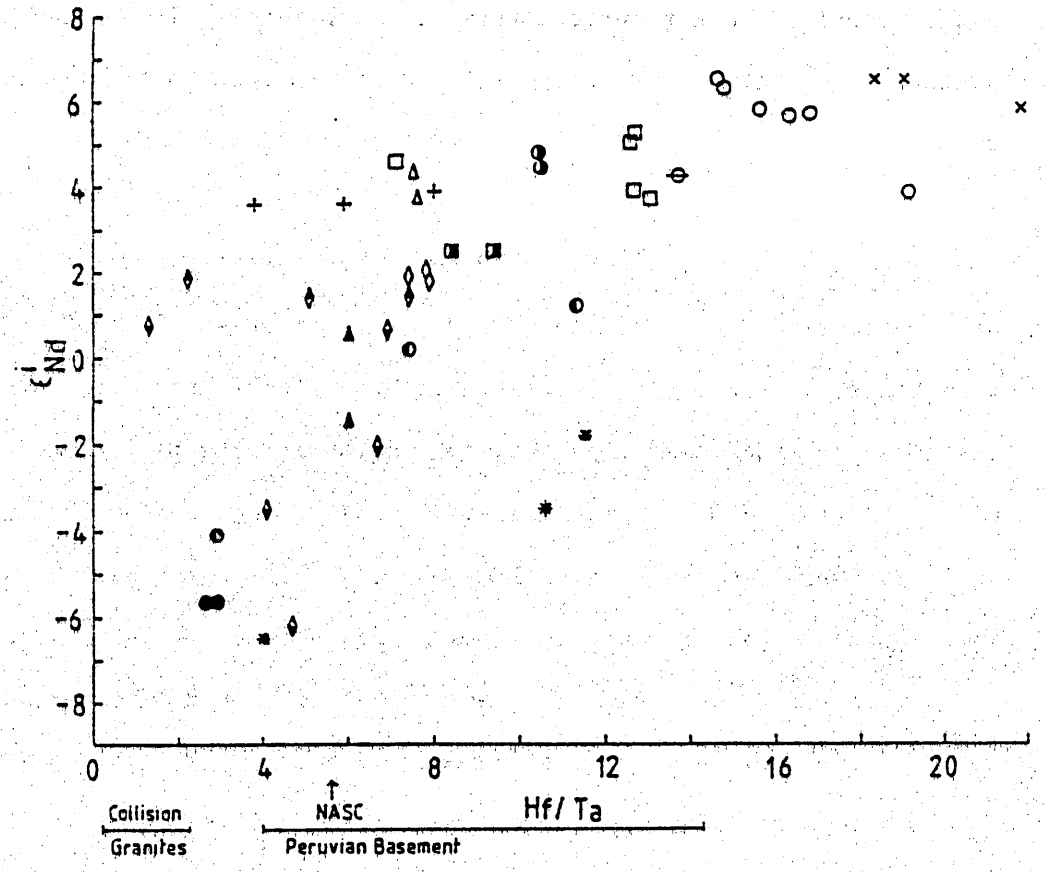

Figure 8.8

Hf/Ta against ε^i_{Nd} for rocks of the Andean orogen since (186 Ma) showing the progressive trend towards low Hf/Ta and low ε^i_{Nd}. Data for collision granites from Alderton et al. (1980), Vidal et al. (1982) and Harris et al. (in press). Peruvian basement from Barreiro (1982b). NASC (North American Shale Composite) from Gromet et al. (1984).

Key (with ages):○La Negra Formation (186): × Gatico (158): ◑ Sierra de la Cruz (156): ⊖ Cerro Colupito (155): □ Tocopilla (154): ▲ Indio Muerto Formation (130): + Augusta Victoria Formation (105): ◊ Cerros de Montecristo (102): ◐ Pampa Negra (79): ◘ Cerro Negro Formation (70): Δ Cerro Colorado (66): ◊ El Abra (39): * Tertiary Volcanics: ● San Pedro (0): ◊ Monogenetic Centres (0).

(Alderton et al., 1980; Vidal et al., 1982; Harris et al., in press). It is feasible, therefore, that the overall trend may be produced by increased crustal contamination.

Figure 8.2 showed that the Sr content of the most basic rocks tended to increase across the Cordillera. A plot of Sr against ε^{i}_{Nd} (Figure 8.9) reveals that the enrichment of Nd isotopes is paralleled by an increase in the highest Sr contents seen in rock suites. The diagram also gives generalised vectors for plagioclase-dominated fractionation, involvement of old mantle, and crustal contamination. Whilst it is unclear as to the proportion of Sr being released from the subducting slab due to the effects of plagioclase fractionation, the progressive relatively lower subduction zone contributions through time of other LILE suggests that Sr may behave similarly (Figure 8.7 and Table 8.1). Thus the trend is unlikely to reflect increasing subduction zone contributions. There is little evidence of trends indicative of crustal contamination, this only being apparent in the Indio Muerto Formation and in the Purico ignimbrite centre (Hawkesworth et al., 1982; Francis et al., 1984). Hawkesworth et al. (1982) argued that this centre was generated either by intracrustal melting or by crustal contamination of mantle derived magmas; either way the crustal input is reflected in the distinctive trend shown on Figure 8.9.

Analogous variations are also displayed on a graph of Sr against ε^{i}_{Sr} where two trends are noticeable (Figure 8.10). Firstly there is an overall trend of increasing ε^{i}_{Sr} with increasing Sr content covering all units except Purico-Chascon. Individual units show little variation in ε^{i}_{Sr} with decreasing Sr, indicating a closed system evolution. Secondly, there is a trend of

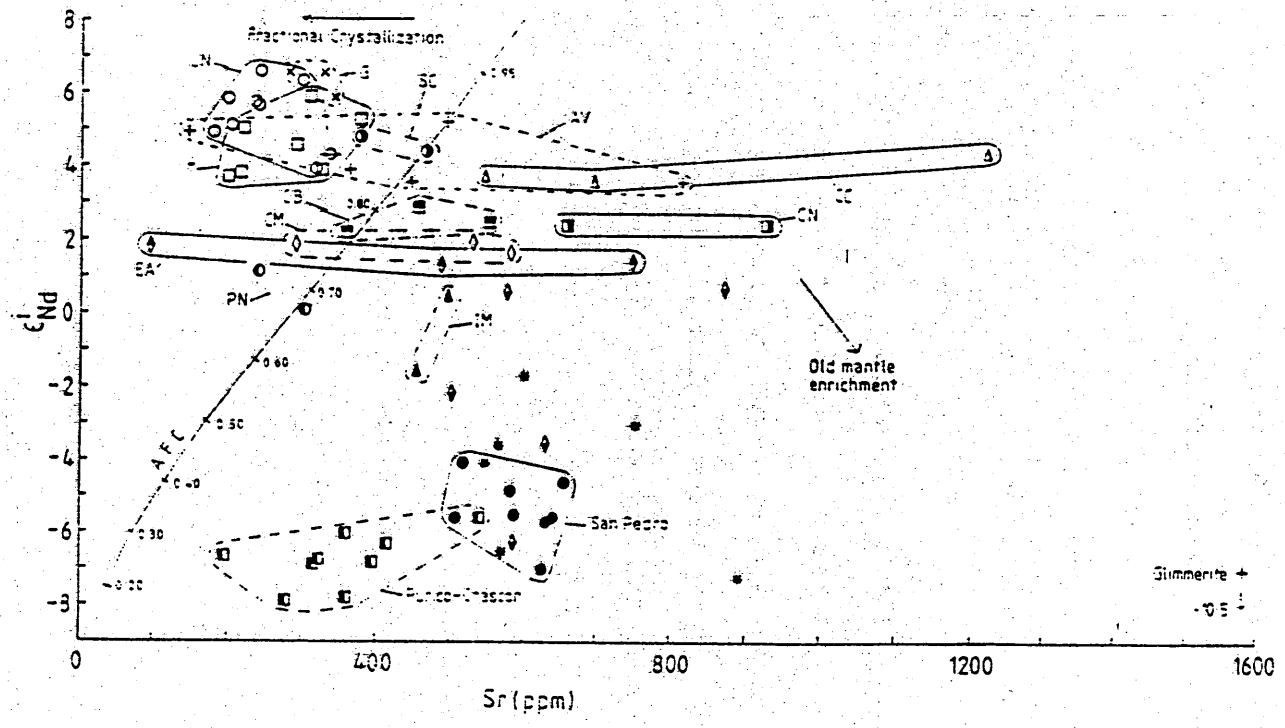

Figure 8.9

Sr against ε^i_{Nd} diagram for Jurassic - Recent rocks of the transect. Generalised vectors for closed system fractional crystallization and old mantle enrichment, and an AFC curve for old upper crustal contamination of a La Negra type mantle-derived magma are shown. Glimmerite data from Menzies et al. (in press). Numbers along AFC curve indicate fraction of magma remaining. See text for discussion. Key as for Figures 8.6 and 8.8.

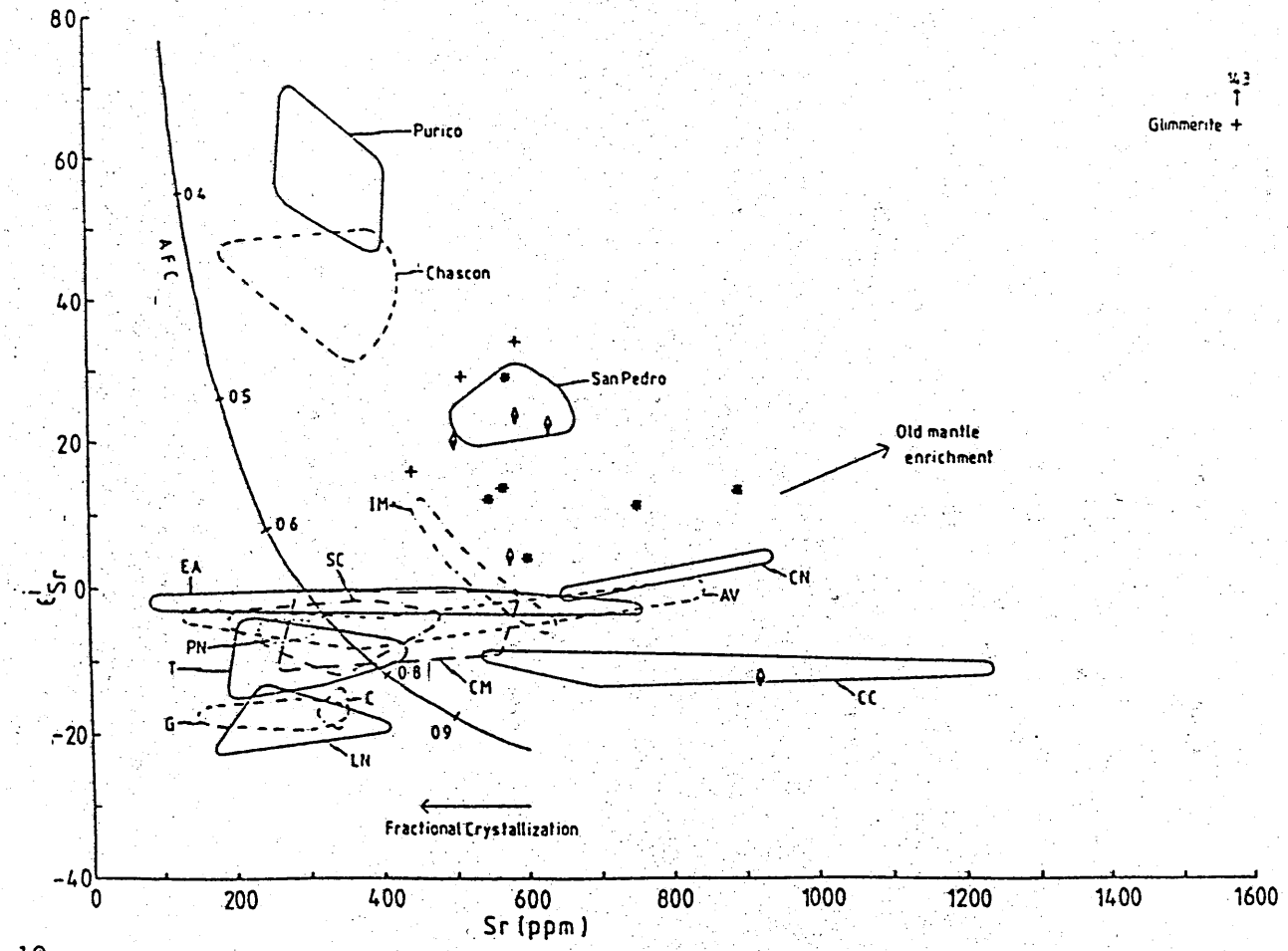

Figure 8.10

Sr against ε^{i}_{Sr} diagram for Jurassic-Recent rocks from the transect. Generalised vectors for closed system fractional crystallization, old mantle enrichment and an AFC curve for old upper crustal contamination of a La Negra type mantle-derived magma are shown. Glimmerite data from Menzies et al. (in press). Key as for Figure 8.9 except + = Other Recent Stratovolcanoes. See text for discussion.

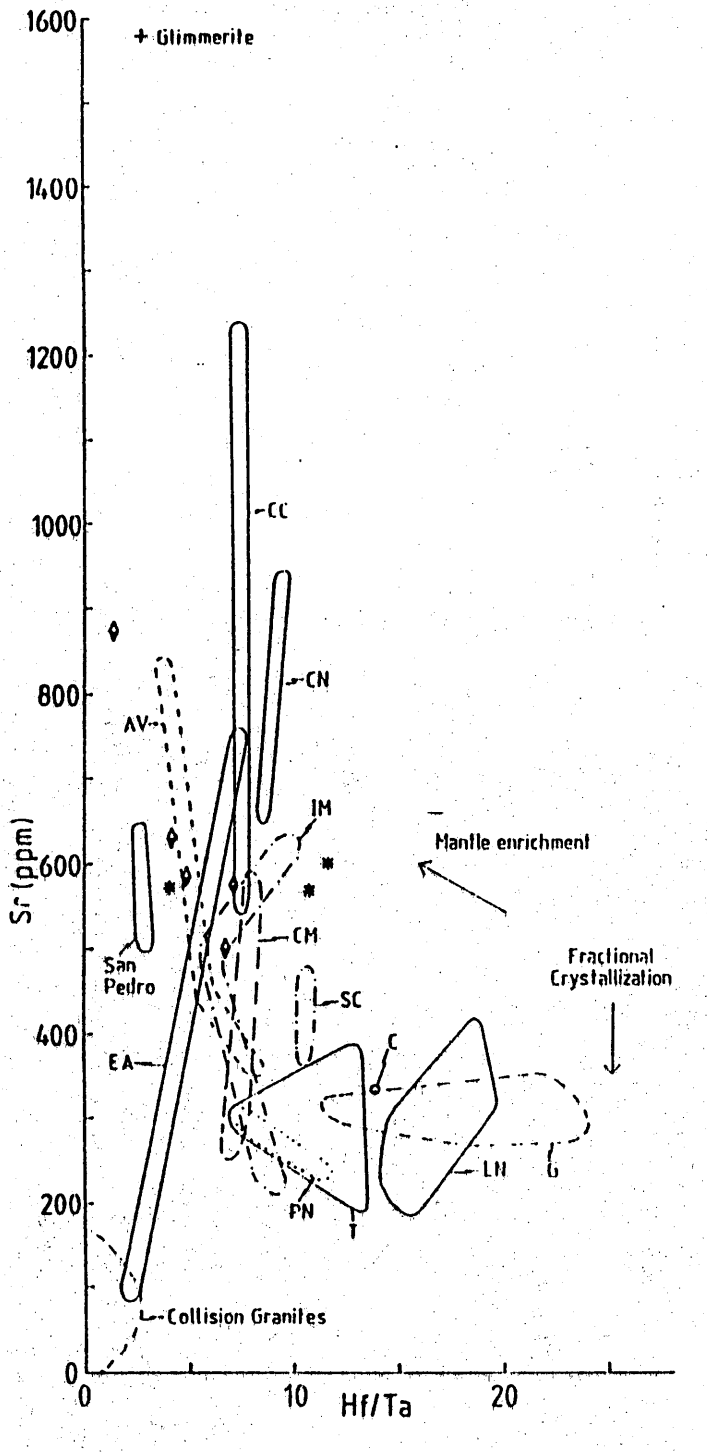

Figure 8.11

Hf/Ta - Sr diagram for Jurassic-Recent rocks from the transect. Generalised vectors for mantle enrichment and closed system fractional crystallization are shown. The trend to low Hf/Ta ratios in younger rocks (Figure 8.8) correlates with the trend to higher Sr contents (Figures 8.9 and 8.10), and not with lower Sr contents as would be expected if there were progressively increasing degrees of crustal contamination with time. The field for collision granites is from Alderton et al. (1980), Vidal et al. (1982) and Harris et al. (in press). Glimmerite data from Menzies et al. (in press). Key as for Figure 8.10.

increasing ε^{i}_{Sr} with decreasing Sr content, most clearly displayed by Purico-Chascon, but also by the Indio Muerto Formation. The diagram also shows an AFC curve for contamination of a basic mantle derived magma with a Sr isotopic composition similar to the La Negra Formation by old upper continental crust. It is apparent that the trend of increasing ε^{i}_{Sr} with increasing Sr content cannot be produced by upper crustal contamination. For this trend to be the result of lower crustal processes the contaminant must have both a high Sr content and ε_{Sr}; high Sr granulites, however, tend to have low ε_{Sr} (Rogers and Hawkesworth, 1982). Consequently, the vector defined by these Andean rocks is best interpreted as a mantle enrichment trend along which Sr exhibits incompatible behaviour. The trend towards low Hf/Ta ratios with low ε^{i}_{Nd} in Figure 8.8 is now seen to correlate with high Sr contents (Figure 8.11) and to be primarily dependent upon mantle rather than crustal processes.

In contrast, the variation in Figure 8.10 shown by Purico-Chascon and the Indio Muerto Formation closely follows that predicted by AFC contamination processes, and indicates that Sr is behaving compatibly, perforce in upper crustal environments where plagioclase is stable. These processes operate on magmas whose parental chemistry is governed by their position along the mantle enrichment trend.

8.7 The timing of mantle enrichment

The above discussion has shown that much of the geochemical variation seen in this transect can be explained by more enriched and older mantle being tapped by younger rocks further east. Such an interpretation is consistent with ideas linking the generation of enriched domains to the stabilisation of continental lithosphere after a major

thermal event (Oxburgh and Parmentier, 1978; Hawkesworth et al., 1983). To the east of the Andes there are large areas of craton, up to 3 Ga old (Wernick, 1982). As the locus of magmatism has migrated eastwards it is possible that areas within this old lithospheric mantle have been tapped. However, during the Palaeozoic there were three main phases of plutonism: at the Ordovician-Silurian boundary (Ocloyic phase of Coira et al., 1982); during the Upper Devonian-Lower Carboniferous at about 350 Ma (Eohercynian phase of Dalmayrac et al., 1980; Pitcher, 1984; Kontak et al., 1984): during the Permian which produced the Limon Verde pluton in the present transect (Section 2.4). The T^{Nd}_{DM} ages of the Upper Tertiary - Recent volcanics (excluding B1 and 80193) vary from 798-1547 Ma. The lowest T^{Nd}_{DM} age from San Pedro is 981 Ma, whereas the uncontaminated A791 has a value of 911 Ma. Thus if the source of these rocks had originally been isotopically depleted similar to MORB it must have stabilised at least ~800 Ma ago. These values decrease if less depleted sources are proposed: for instance the T^{Nd}_{CHUR} age of A791 is 236 Ma. It does not seem likely, therefore, that the sole source was lithospheric mantle which had stabilised in the Archaean or early Proterozoic, but more probably one which had evolved since the early Palaeozoic disturbances.

8.8 The role of the continental crust

The foregoing conclusions that the mantle beneath the Western Cordillera is enriched isotopically and in incompatible elements does not rule out the presence of crustal contamination in the Recent lavas of northern Chile. Variations within any one volcanic centre (e.g. San Pedro) may well be due to differing degrees of contamination. However, the mechanism of contaminaton in these volcanic centres is unclear. Recently the process of combined assimilation-fractional crystallization

(AFC; DePaolo, 1981) has become in vogue for several rock suites in the Andes (James, 1982; James and Murcia, 1984; Thorpe, 1984, Thorpe et al., 1984; Harmon et al., 1984). This mechanism requires that all the rocks ascribed to the process must belong to a common liquid line of descent, and hence that there should be correlations between fractionation indices and other chemical parameters. Such a situation was well portrayed at Craters of the Moon by Menzies et al. (1983). However, when only inter isotope trends are considered false conclusions may be drawn. Thus the subhorizontal trend for San Pedro on Figure 7.5 may be deemed to be one of contamination of a basic, mantle-derived melt similar to A791 or 7927 by old upper continental crust by an AFC mechanism. However, there are no correlations between ε_{Sr} or ε_{Nd} and fractionation indices. Consequently, whilst the trend on Figure 7.5 may represent crustal contamination, the mechanism does not conform to one of AFC (i.e. operative upon a single closed magmatic system). Furthermore, as O'Callaghan (in prep.) has noted, magma mixing processes are required to satisfy the geochemistry of San Pedro. To constrain precisely the nature and modus operandi of contamination a detailed knowledge of the stratigraphy, whole rock and mineral geochemistry of an individual centre must be ascertained, in addition to the composition of local putative crustal contaminants and uncontaminated (or less contaminated) mantle derived melts. It is envisaged that in the case of San Pedro (and, by implication, other volcanic complexes) there may be several closed system contamination trends (each, perhaps, obeying something similar to AFC behaviour) whose characteristics depend upon the contrast in chemical composition between new magma batches injected into a magma chamber and the preexisting fluid, on the physical properties governing their abilities to mix, on their residence times in these chambers, and on the availability of crustal material to act as a contaminant.

On an ε_{Sr}- ε_{Nd} diagram therefore, contamination of mantle derived magmas by old upper crustal rocks (whatever the precise mechanism) often leads to a displacement to the right of the 'mantle array' (i.e. to high ε_{Sr}), thus producing a subhorizontal trend (e.g. Purico-Chascon, Figures 7.5, 8.6). However, for small degrees of AFC contamination the trend may be subvertical giving a large variation in ε_{Nd} for little change in ε_{Sr}. Consequently these contaminated rocks can still lie close to the mantle array. In both instances, however, Sr is compatible in the crystallizing assemblages, and thus there should be negative correlations between Sr and ε_{Sr} and positive correlations between Sr and ε_{Nd} (Figures 8.9 and 8.10). This is in contrast to variations produced by mantle enrichment processes in north Chile in which Sr is incompatible and which leave data close to the 'mantle array'. These produce overall positive correlations between Sr and ε_{Sr} and negative correlations between Sr and ε_{Nd} (Figures 8.9 and 8.10).

8.9 Reasons for the eastwards migration of magmatism

Figure 8.1 showed that the locus of magmatic activity has generally migrated eastwards with time in accord with the findings of Farrar et al. (1970) for northern Chile between 26-29°S and Giletti and Day (1968) for southern Peru. Various hypotheses, all not mutually exclusive, have been proposed to account for this migration.

(i) If the position of the trench relative to the continent has remained constant through time then either:

(a) the dip of the Benioff Zone must have decreased with time (and increased again during the last 5 Ma to account for the current

westwards trend in activity), given a fixed depth of magma generation. This is not unreasonable given the variation in dip of the Benioff Zone which exists along the continental margin today (Barazangi and Isacks, 1976; Jordan et al., 1983).

or (b) the depth of magma generation has increased with time. Oxburgh and Turcotte (1970) argued that the continual underthrusting of cold oceanic lithosphere would cool the overriding continental lithosphere and thus depress the isotherms in the subduction zone. This would lead to progressively deeper zones of melting and lower degrees of partial melting with time. James (1971b) and McNutt et al. (1975) favoured this hypothesis for the central Andes.

(ii) Alternatively, given a constant arc-trench gap and a constant depth of magma generation the trench must have migrated eastwards with time. This process could either involve strike slip movements to remove the missing continent or tectonic underthrusting of the continental margin. This overall concept has been promoted by Rutland (1971), Pitcher (1978) and Atherton et al. (1983).

The studies in northern Chile have an important bearing on this problem. The lack of correlation between many incompatible elements such as K_2O and Hf at a given degree of fractionation and the distance from the present day trench (Figure 8.2) implies that the shift in the locus of magmatism is not solely due to a progressive increase in the depth of melting ((i)(b) above). It also means that the dip of the Benioff Zone has changed with time if one assumes that the trench remains fixed with respect to the continent.

Arguments against removal of the continental margin are based on

the premise that the Jurassic rocks of southern Peru and northern Chile represent island arcs (Dostal et al., 1977; Palacios, 1978). Thorpe et al. (1981) and Barreiro and Clark (1984) have argued that as the distance from the present trench to the Jurassic 'arc' is ∿ 130-150 km, comparable to that in some active island arcs (Gill, 1981), the amount of removal of the continental margin is minimal. However, if one considers that the La Negra Formation formed in an ensialic back-arc basin (Chapter 3) then the arc itself must have been removed. Further evidence for a more westerly landmass comes from the south westerly provenance of sediments in the Cretaceous Coloso Formation on the coast immediately to the south of Antofagasta (Turner et al., 1984). There are two possibilities for the mechanism of crustal removal, namely transcurrent fault motions or underthrusting (tectonic erosion) of the continental margin. Whilst the former has been postulated for the development of Colombia (McCourt et al., 1984) it is difficult to apply to northern Chile; conveniently shunting the Jurassic arc northwards is not acceptable as there are similar problems in Peru (Pitcher, 1978; Atherton et al., 1983). The most plausible explanation is that of tectonic erosion. Support for this mechanism is provided by the geophysical work of Coulbourn (1981) who studied the morphology and structure of the Peru-Chile trench between latitudes 18-23°S. He concluded that the data were consistent with the continental margin being underlain either by a wedge of deformed and dewatered sediments or by granitic fault blocks. The absence of Mesozoic-early Tertiary sediments from the trench (Rutland, 1971) argues against the accretion of sediments over a long period of time. Furthermore, Rutland (op. cit.) considered the coastal cliffs to represent a fault escarpment: indeed evidence for recent uplift is apparent here. The present course of the Rio Loa enters the sea about 70 km north of Tocopilla whereas its Plio-Pleistocene channel is now 400 m up

the coastal scarp. Similarly at Tocopilla, the valley of Quebrada Tres Puntas ends 250-300 m up the cliff. Consequently it seems probable that the 'missing' continental margin has been dragged beneath the continent by movement on fault blocks.

8.10 Crustal thickening and uplift

James et al. (1976) argued that marine strata deposited on the western flanks of the central Andes during the Mesozoic implied a crustal thickness of 30-40 km, and that since the present day crustal thickness beneath the Western Cordillera is ∿ 70 km, the crust must have doubled in thickness since the late Mesozoic. In the present study area the latest marine sediments are upper Jurassic and found near Cerritos Bayos (Chapter 5). Thus uplift of the Andes at this latitude has been operative for 130 Ma in which time the crust at Cerritos Bayos has increased in thickness to ∿ 55 km (James, 1971a, b). One cannot, however, extend this to say that the crust under the Western Cordillera (∿70 km) has doubled in thickness in that time as its thickness beneath that region in the early Cretaceous is unknown: it may already have been an uplifted block.

Major, rapid uplift only began in the Miocene (∿ 12 Ma) as documented by the geochronology of deformed ignimbrite sheets (e.g. Rutland et al., 1965; Mortimer et al., 1974; Noble et al., 1974; Baker, 1977a, b; Lahsen, 1982). The initiation of this uplift may be attributable to the switch of sea floor spreading from the Galapagos Rise to the East Pacific Rise between 10 and 6 Ma ago (Mammerikx et al., 1980). The process responsible for the uplift is usually cited as being increased amounts of mantle derived basaltic magma being emplaced into the crust (James et al., 1976; Clark and McNutt, 1982). However, if the rate of tectonic underthrusting of the continental margin were to have

increased at this time in response to regional plate realignment, then crustal thickening could have occurred without recourse to higher rates of magma generation in the mantle. The two hypotheses are not mutually exclusive. The occurrence of major ignimbrite eruptions may reflect an increased crustal contribution to magmagenesis as the raising of isotherms within the thickened crust will increasingly favour crustal anatexis and crustal contamination (Hawkesworth et al., 1982). The crustal contamination processes, however, operate on magmas which themselves are derived from mantle sources which have undergone old enrichment events, and thus have enriched isotope and trace element signatures.

CHAPTER 9

CONCLUDING REMARKS

Combined trace element and isotope studies of the geochemical evolution of a narrow transect across the central Andean cordillera have revealed several important results both for the geodynamic evolution of the central Andes and for magmagenesis at destructive plate margins in general.

1. The Rb-Sr geochronological work has provided a detailed picture regarding the ages of magmatism, both during the Andean orogeny and in the upper Palaeozoic. Data for the former reinforce the trends established further south in Chile of a general eastwards migration of the locus of magmatism with time, though some reversals are apparent. Furthermore, the essentially N-S trending batholiths and loci of volcanism of this period cut across the more NE-SW trending structures of the Palaeozoic orogen.

2. The studies have provided the first geochemical data for rocks of the Palaeozoic basement. In particular isotopic results have shown that the parental magmas were either derived from an isotopically enriched mantle source or that the petrogenesis involved crustal contamination and equilibration prior to high level fractionation. There is no evidence that the rocks represent crustal melts. The present day Sr and Nd isotope ratios of these rocks also preclude their involvement in the petrogenesis of the Recent volcanics (e.g. from San Pedro). T^{Nd}_{DM} model ages for the Limon Verde schists indicate the presence of a component at least 900 Ma old, thus providing evidence for continental lithosphere on the western flank of the Cordillera.

3. Trace element data reveal that whereas all units studied are related to subduction, there are sometimes differing magma types erupted together (e.g. Augusta Victoria Formation, Chapter 5). Furthermore, isotopic studies of essentially contemporaneous plutons from the middle Jurassic batholith reveal local heterogeneities in the mantle sources on a scale of tens of kilometres.

4. Field relations combined with geochemical studies of the lower Jurassic La Negra Formation suggest that these lavas were erupted from fissures in a marginal basin setting similar to analogous formations in Peru and central Chile. Variations in the subduction zone component of LILE in these uncontaminated lavas were assessed relative to ratios such as Hf/LILE to determine some of the geochemical characteristics of the source regions for these lavas. Analogous variations were used to estimate the Nd isotopic composition of the mantle and subduction zone components as ε^{i}_{Nd} = +10 and -2 respectively.

This formation also highlights the paradox that many basic destructive margin lavas have high Sr/Nd ratios ($\sim$ 30) yet on ε_{Sr} - ε_{Nd} diagrams fall on convex downward mixing curves between mantle and sediment end members which necessitates a lower Sr/Nd ratio in the sediment than the mantle ($<$18). For the La Negra Formation a two stage process involving the addition of a high Sr/Nd component to the mantle source to raise ε_{Sr} and the Sr/Nd ratio to that of the parental liquid to the lavas, followed by incorporation of low Sr/Nd and ε_{Nd} and high ε_{Sr} sediments similar to the Palaeozoic Limon Verde pluton at that time (186 Ma) is envisaged. The high Sr/Nd component, however, is constrained to have ε_{Sr} very close to that of the lavas, and is thus not identifiable with altered MORB, calcareous

sediments or seawater: it is possible that this component is derived from within the mantle itself, and that the subduction process acts as a catalyst.

5. Combined trace element and isotope data were used to assess the relative roles of the subduction zone, mantle and continental crust in the petrogenesis of the rocks from this transect. Isotope data show that as magmatism migrated eastwards from the present coast to the Rio Loa on the western boundary of the Western Cordillera sources became progressively more enriched, though all were still depleted relative to "bulk Earth". To the east of this boundary, however, lavas have slightly enriched isotopic characteristics and plot in the bottom right hand quadrant of an ε_{Sr}- ε_{Nd} diagram. The data also show that from 186 to 39 Ma ago magmatism tapped isotopically depleted sources, but that since 16 Ma these have become more enriched. Trace element data indicate that the proportion of the subduction zone contribution to volcanism has decreased from the Jurassic to Recent, and regional geology suggests that the nature of subducted sediment has not dramatically changed with time: thus variations in the subduction zone component are not responsible for the isotopic variations. Although subduction independent Hf/Ta ratios also become more enriched (lower) with time, crustal melts are also characterized by low values. Overall cordilleran trends of increasing ε^{i}_{Sr} and decreasing ε^{i}_{Nd} with increasing Sr content are indicative of Sr incompatibility, and as such cannot be reconciled with processes of increasing upper crustal contamination, in which Sr is compatible, of a more depleted La Negra-type source to explain the isotope data. Consequently it is considered that as magmatism has migrated eastwards it has tapped progressively more trace element and isotopically enriched, and probably older mantle source regions.

6. The increase in crustal thickness and concomitant elevation of the cordillera since the Miocene may be largely attributable to tectonic underthrusting of the continental margin. The identification of the La Negra Formation as a marginal basin implies that the Jurassic arc has been removed, and sedimentary evidence in the Cretaceous indicates a south westerly provenance. Moreover, geophysical data for the trench and continental margin do not conflict with this hypothesis. In response to this thickening crust, rising of the isotherms within the crust promotes the likelihood of crustal contamination of basaltic mantle derived magmas. The Purico-Chascon ignimbrite shield complex displays trace element and isotopic trends indicative of derivation by crustal contamination of an enriched mantle derived melt.

7. The gross isotopic variation along the Andes (summarised in Chapter 1) of depleted Sr and Nd isotope ratios in the NVZ and SVZ, but more enriched values in the CVZ is primarily a function of the degree of enrichment and age of the mantle beneath these areas rather than of greater degrees of crustal contamination of mantle derived magmas (all with similar isotopic characteristics) in the latter. Beneath the central Andes in northern Chile the mantle is older and more enriched, and has a $^{87}Sr/^{86}Sr$ ratio $\sim$0.706 and a $^{143}Nd/^{144}Nd$ ratio 0.51253 compared to $\sim$0.704 and 0.5128 in the NVZ and SVZ. The thicker crust in the central Andes, however, has permitted more crustal contamination of these enriched mantle derived magmas, thus producing the large spread to high $^{87}Sr/^{86}Sr$ ratios and low $^{143}Nd/^{144}Nd$ ratios.

8. This work has highlighted the value of and need for integrated trace element and isotope studies on both a local and regional scale in

order to assess the relative roles of crust, mantle and subduction zone, and to unravel the complexities of spatial versus temporal control in the petrogenesis of magmas at continental margins.

BIBLIOGRAPHY

Abbey,S. (1980) Studies in "standard samples" for use in the general analysis of silicate rocks and minerals. Geostand. Newslett. 4, 163-190

Aguirre,L., Herve,F. and Godoy,E. (1972) Distribution of metamorphic facies in Chile - an outline. Krystalinikum 9, 7-19

Aguirre,L., Levi,B. and Offler,R. (1978) Unconformities as mineralogical breaks in the burial metamorphism of the Andes. Contrib. Mineral. Petrol. 66, 361-366

Alderton,D.H.M., Pearce,J.A. and Potts,P.J. (1980) Rare earth element mobility during granite alteration: evidence from southwest England. Earth Planet. Sci. Lett. 49, 149-165

Allegre,C.J. and Othman,D.B. (1980) Nd and Sr isotopic relationship in granitoid rocks and continental crust development: a chemical approach to orogenesis. Nature 286, 335-342

Ambrus,J. (1977) Geology of the El Abra porphyry copper deposit, Chile. Econ. Geol. 72, 1062-1085

Arth,J.G. (1976) Behavior of trace elements during magmatic processes - a summary of theoretical models and their applications. Jour. Research U.S. Geol. Survey 4, 41-47

Arth,J.G. and Hanson,G.N. (1975) Geochemistry and origin of the early Precambrian crust of northern Minnesota. Geochim. Cosmochim. Acta 30, 325-362

Atherton,M.P. (1981) Horizontal and vertical zoning in the Peruvian Coastal Batholith. J. Geol. Soc. London 138, 343-349

Atherton,M.P., McCourt,W.J., Sanderson,L.M. and Taylor,W.P. (1979) The geochemical character of the segmented Peruvian Coastal Batholith and associated volcanics. In: Origins of Granite Batholiths: Geochemical Evidence. (Eds. M.P.Atherton and J.Tarney) Shiva Publishing, Nantwich 45-64

Atherton,M.P., Pitcher,W.S. and Warden,V. (1983) The Mesozoic marginal basin of central Peru. Nature 305, 303-306

Baeza,L. (1976) Geologia de Cerritos Bayos y areas adyacentes entre los 22°30' - 22°45' L.S. y los 68°55' - 69°25' L.W. II Region Antofagasta, Chile. Memoria de Prueba Depto. Geol. Univ. del Norte, Antofagasta 182p

Baeza,L. and Palacios,C. (1977) Series de facies metamorficas en el Paleozoico del norte de Chile. Estudios Geologicas. I.L.M., 33, No.1, Madrid

Baker,M.C.W. (1977a) Geochronology and volcanology of Upper Cenozoic volcanic activity in north Chile and southwest Bolivia. PhD thesis, Open University (unpublished) 248p

Baker,M.C.W. (1977b) Geochronolgy of Upper Tertiary volcanic activity in the Andes of North Chile. Geol. Rundsch. 66, 455-465

Baker,M.C.W. and Francis,P.W. (1978) Upper Cenozoic volcanism in the Central Andes. Ages and Volumes. Earth Planet. Sci. Lett. 41, 175-187

Baldwin,J.A. and Pearce,J.A. (1982) Discriminations of productive and non-productive porphyritic intrusions in the central Andes. Econ. Geol. 77, 664-674

Barazangi,M. and Isacks,B.L. (1976) Spatial distribution of earthquakes and subduction of the Nazca Plate beneath South America. Geology 4, 686-692

Barreiro,B.A. (1982a) Lead isotope data from Late Cenozoic volcanic rocks of the Andes. Proc. 5th Int. Conf. Geochron., Cosmochron., Isotope Geol. 16

Barreiro,B.A. (1982b) Lead isotope evidence for crust-mantle interaction during magmagenesis in the South Sandwich Island Arc and in the Andes of South America. PhD thesis, University of California (unpublished)

Barreiro,B.A. (1984) Lead isotopes and Andean magmagenesis. In: Andean Magmatism Chemical and Isotopic Constraints (Eds. R.S.Harmon and B.A.Barreiro) Shiva Publishing, Nantwich 21-30

Barreiro,B.A. and Clark,A.H. (1984) Lead isotopic evidence for evolutionary changes in magma-crust interaction, central Andes, southern Peru. Earth Planet. Sci. Lett. 69, 30-42

Bell,C.M. (1984) (Ed.) J. Geol. Soc. London 141, 781-917

Berg,K. and Breitkreuz,C. (1983) Mesozoische plutone in der nordchilenischen kustenkordillere: petrogenese, geochronologie, geochemie und geodynamik mantelbetonter magmatite. Geotekt. Forsch. 66, 1-107

Berg,K., Breitkreuz,C., Damm,K.-W., Pichowiak,S. and Zeil,W. (1983) The north-Chilean coast range - an example for the development of an active continental margin. Geol. Rundsch. 72, 715-731

Biese,W. (1961) El Jurasico de Cerritos Bayos. Inst. de Geologia Univ. de Chile, Santiago. Publ. No. 19 61p

Brass,G.W. (1976) The variation of the marine $^{87}Sr/^{86}Sr$ ratio during Phanerozoic time: interpretation using a flux model. Geochim. Cosmochim. Acta 40, 721-730

Brown,G.C. (1982) Calc-alkaline intrusive rocks: their diversity, evolution and relation to volcanic rocks. In: Orogenic Andesites and Related Rocks (Ed. R.S.Thorpe) John Wiley & Sons, London 437-461

Bruggen,J. (1950) Fundamentos de la Geologia de Chile. Inst. Geogr. Milit., Santiago 365p

Cameron,M., Bagby,W.C. and Cameron,K.C. (1980) Petrogenesis of voluminous mid-Tertiary ignimbrites of the Sierra Madre Occidental, Mexico. Contrib. Mineral. Petrol. 74, 271-284

Caminos,R., Cingolani,C.A., Herve,F and Linares,E. (1982) Geochronology of the Pre-Andean metamorphism and magmatism in the Andean Cordillera between latitudes 30°-36° S. Earth Sci. Rev. 18, 333-352

Carter,S.R., Evensen,N.M., Hamilton,P.J. and O'Nions,R.K. (1978) Neodymium and strontium isotope evidence for crustal contamination of continental volcanics. Science 202, 743-747

Case,J.E., Barnes,J., Paris Q.,G., Gonzalez I.,H. and Vina,A. (1973) Trans-Andean geophysical profile, southern Colombia. Geol. Soc. Am. Bull. 84, 2895-2904

Casertano,L. (1963) General characteristics of active Andean volcanoes and a summary of their activities during recent centuries. Bull. Seis. Soc. Am. 53, 1415-1433

Cecioni,G. and Frutos,J. (1963) Primera noticia sobre el hallazgo de Paleozoico Inferior marino en el Sierra de Almeida, norte de Chile. Palaeontology and Biostratigraphy Congress, Argentina 1, 191-207

Chong,G. (1977) Contribution to the knowledge of the Domeyko Range in the Andes of Northern Chile. Geol. Rundsch. 66, 374-404

Clague,D.A. and Frey,F.A. (1982) Petrology and trace element geochemistry of the Honolulu volcanics, Oahu: implications for the oceanic mantle below Hawaii. J. Petrology 23, 447-504

Clark,A.H. and McNutt,R.H. (1982) Interrelated arc-broadening, topographic uplift and crustal contamination of magmas in two transects of the Mesozoic-Cenozoic central Andes. Proc. 5th Int. Conf. Geochron. Cosmochron. Isotope Geol. 55-56

Clark,A.H., Mayer,A.E.S., Mortimer,C., Sillitoe,R.H., Cooke,R.V. and Snelling,N.J.T. (1967) Implications of the isotopic ages of ignimbrite flows, Southern Atacama Desert, Chile. Nature 215, 723-724

Clark,A.H., Farrar,E., Caelles,J.C., Haynes,S.J., Lortie,R.B., McBride,S.L. Quirt,G.S. and Zentilli,M. (1973) The magmatic, tectonic, and metallogenic evolution of the Central Andean mobile belt between latitudes 26° and 29° south. Conf. on Geodynamics, Int. Union Geodesy, Geophys., Lima CGD-44

Clark,A.H., Caelles,J.C., Farrar,E., Haynes,S.J., Lortie,R.B., McBride,S.L. Quirt,G.S., Robertson,R.C.R. and Zentilli,M. (1976) Longitudinal variations in the metallogenetic evolution of the Central Andes: a progress report. In: Metallogeny and Plate Tectonics (Ed. D.F.Strong) Geol. Ass. Canada Spec. Pap. No.14, 23-58

Cobbing,E.J. and Pitcher,W.S. (1972a) The Coastal Batholith of central Peru. J. Geol. Soc. London 128, 421-460

Cobbing,E.J. and Pitcher,W.S. (1972b) Plate tectonics and the Peruvian Andes. Nature 240, 51-53

Cohen,R.S. and O'Nions,R.K. (1982) Identification of recycled continental material in the mantle from Sr, Nd and Pb isotope investigations. Earth Planet. Sci. Lett. 61, 72-84

Coira,B., Davidson,J., Mpodozis,C. and Ramos,V. (1982) Tectonic and magmatic evolution of the Andes of northern Argentina and Chile. Earth Sci. Rev. 18, 303-332

Coulbourn,W.T. (1981) Tectonics of the Nazca plate and the continental margin of western South America, 18° S to 23° S. Mem. Geol. Soc. Am. 154, 587-618

Cox,K.G. and Hawkesworth,C.J. (1984) Relative contribution of crust and mantle to flood basalt magmatism, Mahabaleshwar area, Deccan Traps. Phil. Trans. R. Soc. Lond. A310, 627-641

Cox,K.G., Bell,J.D. and Pankhurst,R.J. (1979) The interpretation of igneous rocks. George Allen & Unwin, London 450p

Crozier,R.D. (1981) Chilean nitrate mining. Mining Magazine 145, 160-173

Cummings,D. and Schiller,G.I. (1971) Isopach map of the Earth's crust. Earth Sci. Rev. 7, 97-125

Dalmayrac,B., Laubacher,G., Marocco,R., Martinez,C. and Tomasi,P. (1980) La chaine hercynienne d'Amerique du sud. Structure et evolution d'un orogene intracratonique. Geol. Rundsch. 69, 1-21

Dalziel,I.W.D. (1981) Back-arc extension in the southern Andes: a review and critical reappraisal. Phil. Trans. R. Soc. Lond. A300 319-335

Dalziel,I.W.D., de Wit,M.J. and Palmer,K.F. (1974) Fossil marginal basin in the southern Andes. Nature 250, 291-294

Damm,K.-W. and Pichowiak,S. (1981) Petrolgie, geochronologie und geochemie der magmatite im Kustenkordillerensegment Taltal - Chanaral (Nordchile). Zbl. Geol. Palaont. 1, 319-332

Damm,K.-W., Pichowiak,S. and Zeil,W. (1981) The plutonism in the north Chilean coast range and its geodynamic significance. Geol. Rundsch. 70, 1054-1076

Darwin,C. (1876) Geological observations on the volcanic islands and parts of South America visited during the voyage of H.M.S. "Beagle". Smith, Elder & Co., London 647p

DePaolo,D.J. (1981) Trace element and isotopic effects of combined wallrock assimilation and fractional crystallisation. Earth Planet. Sci. Lett. 53, 189-202

DePaolo,D.J. and Wasserburg,G.J. (1976a) Nd isotopic variations and petrogenetic models. Geophys. Res. Lett. 3, 249-252

DePaolo,D.J. and Wasserburg,G.J. (1976b) Inferences about magma sources and mantle structure from variations of $^{143}Nd/^{144}Nd$. Geophys. Res. Lett. 3, 743-746

DePaolo,D.J. and Wasserburg,G.J. (1977) The sources of island arcs as indicated by Nd and Sr isotopic studies. Geophys. Res. Lett. 4, 465-468

Deruelle,B. (1982) Petrology of the Pio-Quaternary volcanism of the south-central and meridional Andes. J. Volcanol. Geotherm. Res. 14, 77-124

Deruelle,B., Harmon,R.S. and Moorbath,S. (1983) Combined Sr-O isotope relationships and petrogenesis of Andean volcanics of South America. Nature 302, 814-816

Dickinson,W.R. and Hatherton,T. (1967) Andesitic volcanism and seismicity around the Pacific. Science 157, 801-803

Dodson,M.H. (1978) A linear method for second-degree interpolation in cyclical data collection J. Phys. E: Sci. Instrum. 11, 296

Dostal,J., Zentilli,M., Caelles,J.C. and Clark,A.H. (1977) Geochemistry and origin of volcanic rocks of the Andes (26-28° S). Contrib. Mineral. Petrol. 63, 113-128

Draguicevic,M. (1962) Interpretation de las anomalias gravimetricas de las fosas marinas de Valparaiso, Antofagasta y Arica. Dep. de Geofisica, Univ. de Chile Publ. No.28

Drake,R., Vergara,R., Munizaga,F., and Vicente,J.C. (1982) Geochronology of Mesozoic - Cenozoic magmatism in central Chile, lat. 31° - 36° S. Earth Sci. Rev. 18, 353-363

El-Hinnawi,E.E., Pichler,H. and Zeil,W. (1969) Trace element distribution in Chilean ignimbrites. Contrib. Mineral. Petrol. 24, 50-62

Ewart,A. (1982) The mineralogy and petrology of Tertiary-Recent orogenic volcanic rocks: with special reference to the andesitic-basaltic compositional range. In: Andesites: Orogenic Andesites and Related Rocks (Ed. R.S.Thorpe) John Wiley & Sons, London 25-95

Farrar,E., Clark,A.H., Haynes,S.J., Quirt,G.S., Conn,H. and Zentilli,M. (1970) K-Ar evidence for the post-Palaeozoic migration of granitic intrusion foci in the Andes of northern Chile. Earth Planet. Sci. Lett. 10, 60-66

Fernandez,A., Hormann,P.K., Kussmaul,S., Meave,J., Pichler,H. and Subieta,T. (1973) First petrologic data on young volcanic rocks of SW Bolivia. Tschermaks Mineral. Petrogr. Mitt. 19, 147-172

Ferraris,F. (1978) Hoja Tocopilla. Escala 1:250,000. Carta Geologia de Chile. Inst. Invest. Geologicas No.3 32p

Ferraris,F. and Di Biase,F. (1978) Hoja Antofagasta. Escala 1:250,000. Carta Geologica de Chile. Inst. Invest. Geologicas No.30 48p

Francis,P.W., Roobol,M.J., Coward,M.P., Cobbold,P.R. and Walker,G.P.L. (1974) The San Pedro and San Pablo volcanoes of northern Chile and their hot avalanche deposits. Geol. Rundsch. 63, 357-388

Francis,P.W., Moorbath,S. and Thorpe,R.S. (1977) Strontium isotope data in andesites from Ecuador and north Chile. Earth Planet. Sci. Lett. 37, 197-202

Francis,P.W., Hammill,M., Kretzschmar,G.A. and Thorpe,R.S. (1978) The Cerro Galan caldera, north-west Argentina and its tectonic setting. Nature 274, 748-751

Francis,P.W., Thorpe,R.S., Moorbath., S., Kretzschmar,G.A. and Hammill,M. (1980) Strontium isotope evidence for crustal contamination of calc-alkaline volcanic rocks from Cerro Galan, northwest Argentina. Earth Planet. Sci. Lett. 48, 257-267

Francis,P.W., Baker,M.C.W. and Halls,C. (1981) The Kari Kari caldera, Bolivia, and the Cerro Rico stock. J. Volcanol. Geotherm. Res. 10, 113-124

Francis,P.W., O'Callaghan,L., Kretzschmar,G.A., Thorpe,R.S., Sparks,R.S.J., Page,R.N., de Barrio,R.E., Gillou,G. and Gonzalez,O.E. (1983) The Cerro Galan ignimbrite. Nature 301, 51-53

Francis,P.W., McDonough,W.F., Hammill,M., O'Callaghan,L.J. and Thorpe,R.S. (1984) The Cerro Purico Shield Complex, North Chile. In: Andean Magmatism Chemical and Isotopic Constraints (Eds. R.S.Harmon and B.A.Barreiro) Shiva Publishing, Nantwich 106-123

Frey,F.A., Chappell,B.W. and Roy,S.D. (1978a) Fractionation of rare-earth elements in the Tuolumne intrusive series, Sierra Nevada batholith, California. Geology 6, 239-242

Frey,F.A., Green,D.H and Roy,S.D.(1978b) Integrated models of basalt petrogenesis: a study of quartz tholeiites to olivine melilitites from south eastern Australia utilizing geochemical and experimental petrological data. J. Petrology 19, 463-513

Frutos,J. (1976) Levatamiento geologico de las hojas Maria Elena y Pedro de Valdivia (1:100,000) a escala 1:250,000. Inst. Invest. Geologicas (mapas ineditos)

Frutos,J. and Tobar,A. (1973) Evolution of the southern continental margin of South America. II International Gondwana Symposium, Canberra, Australia.

Galli-Olivier,C. (1967) Pediplain in northern Chile and the Andean uplift. Science 158, 653-655

Garcia,F. (1967) Geologia del Norte Grande de Chile. Simp. Geosincl. Andino, 1962. Soc. Geol. Chile Publ. 3 138p

Garcia,F., Perez,E. and Ceballos,E. (1962) El Ordovicico de Aguada de la Perdiz, Puna de Atacama, Provincia de Antofagasta. Rev. Minerales 77, 52-61

Gerlach,D.C., Frey,F.A., Hickey,R., Moreno-Rao,H. and Hildreth,W. (1983) Geochemistry of Puyehue Volcano and Cordon Caulle, Southern Andes (40.5°S). Trans. Am. Geophys. Union 64, 326

Giletti,B.J. and Day,H.W. (1968) Potassium-argon ages of igneous intrusive rocks of Peru. Nature 220, 570-572

Gill,J.B. (1981) Orogenic Andesite and Plate Tectonics. Springer-Verlag, New York

Gill,J.B. and Gorton,M. (1973) A proposed geological and geochemical history of eastern Melanesia. In: The Western Pacific Island Arcs, Marginal Seas, Geochemistry. (Ed. P.J.Coleman) University of Western Australia Press, Perth. 543-566

Green,T.H. and Ringwood,A.E. (1968) Genesis of the calc-alkaline igneous rock suite. Contrib. Mineral. Petrol. 18, 105-162

Gromet,L.P., Dymek,R.F., Haskin,L.A. and Korotev,R.L. (1984) The "North American shale composite": its compilation, major and trace element characteristics. Geochim. Cosmochim. Acta 48, 2469-2482

Guest,J.E. (1969) Upper Tertiary ignimbrites in the Andean Cordillera, Antofagasta Province, northern Chile. Geol. Soc. Am. Bull. 80, 337-362

Guest,J.E. and Sanchez,J. (1969) A large dacitic lava flow in northern Chile. Bull. Volcanol. 33, 778-790

Guinness Book of Records, 1983 (1984) Ed. N.D.McWhirter 30th Edition. Guinness Superlatives Ltd. 349p

Hamilton,P.J., O'Nions,R.K. and Pankhurst,R.J. (1980) Isotopic evidence for the provenance of some Caledonian granites. Nature 287, 279-284

Hanson,G.N. (1978) The application of trace elements to the petrogenesis of igneous rocks of granitic composition. Earth Planet. Sci. Lett. 38, 26-43

Harmon,R.S. and Barreiro,B.A. (1984) Andean Magmatism Chemical and Isotopic Constraints (Eds.) Shiva Publishing, Nantwich 250p

Harmon,R.S., Thorpe,R.S. and Francis,P.W. (1981) Petrogenesis of Andean andesites from combined O-Sr relationships. Nature 290, 396-399

Harmon,R.S., Barreiro,B.A., Moorbath,S., Hoefs,J., Francis,P.W., Thorpe,R.S., Deruelle,B., McHugh,J. and Viglino,J.A. (1984) Regional O-, Sr-, and Pb-isotope relationships in the late Cenozoic calc-alkaline lavas of the Andean Cordillera. J. Geol. Soc. London 141, 803-822

Harrington,H.J. (1961) Geology of parts of Antofagasta and Atacama provinces of northern Chile. Am. Ass. Pet. Geol. Bull. 45, 169-197

Harris,N.B.W., Pearce,J.A. and Tindle,A.G. (in press) Geochemical characteristics of collision magmatism.

Hart,S.R., Erlank,A.J. and Kable,E.J.D. (1974) Sea floor basalt alteration: some chemical and Sr-isotopic effects. Contrib. Mineral. Petrol. 44, 219-230

Harvey,P.K. and Atkin,B.P. (1981) The rapid determination of Rb, Sr and their ratios in geological materials by X-ray fluorescence spectrometry using a rhodium X-ray tube. Chem. Geol. 32, 291-301

Hatherton,T. and Dickinson,W.R. (1969) The relationship between andesitic volcanism and seismicity in Indonesia, the Lesser Antilles and other island arcs. J. Geophys. Res. 74, 5301-5310

Hausen,H. (1937) Zur kenntnis der magmengesteine der chilenischen Atacama-wuste. Neus. Jahrb. Min. Geol. und Pal., Beil Bd. 73, 151-238

Hawkesworth,C.J. (1979) $^{143}Nd/^{144}Nd$, $^{87}Sr/^{86}Sr$ and trace element characteristics of magmas along destructive plate margins. In: Origin of Granite Batholiths: Geochemical Evidence. (Eds. M.P.Atherton and J.Tarney) Shiva Publishing, Nantwich 76-89

Hawkesworth,C.J. (1982) Isotopic characteristics of magmas erupted along destructive plate margins. In: Andesites: Orogenic Andesites and Related Rocks (Ed. R.S.Thorpe) John Wiley & Sons, London 549-571

Hawkesworth,C.J. and Powell,B.M. (1980) Magma genesis in the Lesser Antilles island arc. Earth Planet. Sci. Lett. 51, 297-308

Hawkesworth,C.J. and van Calsteren,P.W.C. (1983) Radiogenic isotopes: some geological applications. In: Rare Earth Element Geochemistry. Developments in Geochemistry, 2. (Ed. P.Henderson) 375-421

Hawkesworth,C.J., O'Nions,R.K., Pankhurst,R.J., Hamilton,P.J. and Evensen,N.M. (1977) A geochemical study of island-arc and back-arc tholeiites from the Scotia Sea. Earth Planet. Sci. Lett. 36, 253-263

Hawkesworth,C.J., Norry,M.J., Roddick,J.C., Baker,P.E., Francis,P.W. and Thorpe,R.S. (1979a) $^{143}Nd/^{144}Nd$, $^{87}Sr/^{86}Sr$ and incompatible trace element variations in calc-alkaline andesitic and plateau lavas from South America. Earth Planet. Sci. Lett. 42, 45-57

Hawkesworth,C.J., O'Nions,R.K. and Arculus,R.J. (1979b) Nd and Sr isotope geochemistry of island arc volcanics, Grenada, Lesser Antilles. Earth Planet. Sci. Lett. 45, 237-248

Hawkesworth,C.J., Hammill,M., Gledhill,A.R., van Calsteren,P. and Rogers,G. (1982) Isotope and trace element evidence for late-stage intra-crustal melting in the High Andes. Earth Planet. Sci. Lett. 58, 240-254

Hawkesworth,C.J., Erlank,A.J., Marsh,J.S., Menzies,M.A. and van Calsteren,P. (1983) Evolution of the continental lithosphere: evidence from volcanics and xenoliths in southern Africa. In: Continental Basalts and Mantle Xenoliths (Eds. C.J.Hawkesworth and M.J.Norry) Shiva Publishing, Nantwich 111-138

Haynes,S.J. (1975) Granitoid petrochemistry, metallogeny, and lithospheric plate tectonics, Atacama Province, Chile. PhD thesis, Queen's University, Kingston, Ont. 331p

Hickey,R.L., Gerlach,D.C. and Frey,F.A. (1984) Geochemical Variations in Volcanic Rocks from Central-South Chile (32-42° S). In: Andean Magmatism Chemical and Isotopic Constraints. (Eds. R.S.Harmon and B.A.Barreiro) Shiva Publishing, Nantwich 72-95

Hoffstetter,R., Fuenzilada,H. and Cecioni,G. (1957) Lexique Stratigraphique International, Amerique Latine, Fascicule 7, Chile. Centre Nacional de la Recherche Scientifique, Paris 444p

Hole,M.J., Saunders,A.D., Marriner,G.F. and Tarney,J. (1984) Subduction of pelagic sediments: implications for the origin of Ce-anomalous basalts from the Mariana Islands. J. Geol. Soc. London 141, 453-472

Hollingworth,S.E. (1964) Dating the uplift of the Andes of northern Chile. Nature 201, 17-20

Hollingworth,S.E. and Rutland,R.W.R. (1968) Studies of Andean uplift. Part I - Post Cretaceous evolution of the San Bartolo area, north Chile. Geol. Journ. 6, 49-62

Huete,C., Maksaev,V., Moscoso,R., Ulriksen,C. and Vergara,H. (1977) Antecedentes geocronologicas de rocas intrusivas y volcanicas en la Cordillera de los Andes Comprendida entre la Sierra Moreno y el Rio Loa y los 21° y 2° lat. sur, II Region, Chile. Rev. Geol. de Chile 4, 35-41

Jakes,P. and White,A.J.R. (1969) Structure of the Melanesian Arcs and correlation with distribution of magma types. Tectonophysics 8, 223-236

Jakes,P. and Gill,J. (1970) Rare earth elements and the island arc tholeiite series. Earth Planet. Sci. Lett. 9, 17-28

Jakes,P. and White,A.J.R (1972) Major and trace element abundances in volcanic rocks of orogenic areas. Geol. Soc. Am. Bull. 83, 29-40

James,D.E. (1971a) Andean crustal and upper mantle structure. J. Geophys. Res. 76, 3246-3271

James,D.E. (1971b) Plate tectonic model for the evolution of the central Andes. Geol. Soc. Am. Bull. 82, 3325-3346

James,D.E. (1978) On the origin of the calc-alkaline volcanics of the central Andes: a revised interpretation. Yb. Carnegie Inst. Wash. 77, 562-590

James,D.E. (1981a) The combined use of oxygen and radiogenic isotopes as indicators of crustal contamination. Ann. Rev. Earth Planet. Sci. 9, 311-344

James,D.E. (1981b) Role of subducted continental material in the genesis of calc-alkaline volcanics in the central Andes. Mem. Geol. Soc. Am. 154, 769-790

James,D.E. (1982) A combined O, Sr, Nd and Pb isotopic and trace element study of crustal contamination in central Andean lavas: I. Local geochemical variations. Earth Planet. Sci. Lett. 57, 47-62

James,D.E. (1984) Quantitative models for crustal contamination in the Central and Northern Andes. In: Andean Magmatism Chemical and Isotopic Constraints. (Eds. R.S.Harmon and B.A.Barreiro) Shiva Publishing, Nantwich 124-138

James,D.E. and Brooks,C. (1976) Preliminary Rb/Sr data on the minimum age of the central Andean basement complex. Yb. Carnegie Inst. Wash. 75, 213-216

James,D.E. and Murcia,L.A. (1984) Crustal contamination in northern Andean volcanics. J. Geol. Soc. London 141, 823-830

James,D.E., Brooks,C. and Cuyubamba,A. (1974) Strontium isotopic composition and K, Rb, Sr geochemistry of Mesozoic volcanic rocks of the Central Andes. Yb. Carnegie Inst. Wash. 72, 252-259

James,D.E., Brooks,C. and Cuyubamba,A. (1975) Early evolution of the Central Andean volcanic arc. Yb. Carnegie Inst. Wash. 74, 247-250

James,D.E., Brooks,C. and Cuyubamba,A. (1976) Andean Cenozoic volcanism: magma genesis in the light of strontium isotopic composition and trace element geochemistry. Geol. Soc. Am. Bull. 87, 592-600

Jordan,T.E., Isacks,B.I., Allmendinger,R.W., Berger,J.A., Ramos,V.A. and Ando,C.J. (1983) Andean tectonics related to geometry of subducted Nazca Plate. Geol. Soc. Am. Bull. 94, 341-361

Kaneoka,I. (1980) $^{40}Ar/^{39}Ar$ dating on volcanic rocks of the Deccan Traps, India. Earth Planet. Sci. Lett. 46, 233-243

Klerkx,J., Deutsch,S., Pichler,H. and Zeil,W. (1977) Strontium isotopic composition and element data bearing on the origin of Cenozoic volcanic rocks of the Central and Southern Andes. J. Volcanol. Geotherm. Res. 2, 49-71

Kontak,D.J., Clark,A.H. and Farrar,E. (1984) The magmatic evolution of the Cordillera Oriental, southeastern Peru. In: Andean Magmatism Geochemical and Isotopic Constraints. (Eds. R.S.Harmon and B.A.Barreiro) Shiva Publishing, Nantwich 203-219

Kulm,L.D., Dymond,J., Dasch,E.J. and Hussong,D.M. (1981) Nazca Plate: Crustal Formation and Andean Convergence. Mem. Geol. Soc. Am. 154 824p

Kussmaul,S., Hormann,P.K., Ploskonka,E. and Subieta,T. (1977) Volcanism and structure of southwest Bolivia. J. Volcanol. Geotherm. Res. 2, 73-111

Lahsen,A. (1982) Upper Cenozoic volcanism and tectonism in the Andes of northern Chile. Earth Sci. Rev. 18, 285-302

Langmuir,C.H., Vocke,R.D., Hanson,G.N. and Hart,S.R. (1978) A general mixing equation with application to Icelandic basalts. Earth Planet. Sci. Lett. 37, 380-392

Lanphere,M.A., Cameron,K.C. and Cameron,M. (1980) Sr isotope geochemistry of voluminous rhyolitic ignimbrites and related rocks, western Mexico. Nature 286, 594-596

Lehmann,B. (1978) A Precambrian core sample from the Altiplano/Bolivia. Geol. Rundsh. 67, 270-278

Levi,B. (1970) Burial metamorphic episodes in the Andean geosyncline, central Chile. Geol. Rundschau. 59, 994-1013

Levi,B., Aguirre,L. and Nystrom,J.O. (1982) Metamorphic gradients in burial metamorphosed vesicular lavas: comparison of basalt and spilite in Cretaceous basic flows from central Chile. Contrib. Mineral. Petrol. 80, 49-58

Lomnitz,C. (1962) On Andean structure. J. Geophys. Res. 67, 351-363

Longstaffe,F.J., Clark,A.H., McNutt,R.H. and Zentilli,M. (1983) Oxygen isotope compositions of Central Andean plutonic and volcanic rocks, latitudes 26-29° south. Earth Planet. Sci. Lett. 64, 9-18

Lopez-Escobar,L., Frey,F.A. and Vergara,M. (1977) Andesites and high-alumina basalts from the central-south Chile High Andes: Geochemical evidence bearing on their petrogenesis. Contrib. Mineral. Petrol. 63, 199-228

Lopez-Escobar,L., Frey,F.A. and Oyarzun,J. (1979) Geochemical characteristics of central Chile (33° - 34° S) granitoids. Contrib. Mineral. Petrol. 70, 439-450

Mahoney,J., MacDougall,J.D., Lugmair,G.W., Murali,A.V., Sankar,D.M. and Gopalan,K. (1982) Origin of the Deccan Trap flows of Mahabaleshwar inferred from Nd and Sr isotopic chemical evidence. Earth Planet. Sci. Lett. 60, 47-60

Maksaev,V. (1978) Cuadrangula Chitigua y sector occidental del cuadrangulo Cerro Palpana, Region de Antofagasta. Escala 1:50,000. Carta Geologica de Chile. Inst. Invest. Geologicas No.31 55p

Mammerikx,J., Herron,E. and Dorman,L. (1980) Evidence for two fossil spreading ridges in the southeast Pacific. Geol. Soc. Am. Bull. 91, 263-271

Margaritz,M., Whitford,D.J. and James,D.E. (1978) Oxygen isotopes and the origin of high $^{87}Sr/^{86}Sr$ andesites. Earth Planet. Sci. Lett. 40, 220-230

McBride,S.L., Caelles,J.C., Clark,A.H. and Farrar,E. (1976) Palaeozoic radiometric age provinces in the Andean basement, latitudes 25° - 30° S. Earth Planet. Sci. Lett. 29, 373-383

McCarthy,T.S. and Groves,D.I. (1979) The Blue Tier Batholith, northeastern Tasmania. Contrib. Mineral. Petrol. 71, 193-209

McCourt,W.J. (1981) The geochemistry and petrography of the Coastal batholith of Peru, Lima segment. J. Geol. Soc. London 138, 407-420

McCourt,W.J., Aspden,J.A. and Brook,M. (1984) New geological and geochronological data from the Colombian Andes: continental growth by multiple accretion. J. Geol. Soc. London 141, 831-845

McCulloch,M.T. and Perfit,M.R. (1981) $^{143}Nd/^{144}Nd$, $^{87}Sr/^{86}Sr$ and trace element constraints on the petrogenesis of Aleutian island arc magmas. Earth Planet. Sci. Lett. 56, 167-179

McCulloch,M.T. and Chappell,B.W. (1982) Nd isotopic characteristics of S- and I-type granites. Earth Planet. Sci. Lett. 58, 51-64

McLennan,S.M. and Taylor,S.R. (1981) Role of subducted sediments in island-arc magmatism: constraints from REE patterns. Earth Planet. Sci. Lett. 54, 423-430

McNutt,R.H., Crocket,J.H., Clark,A.H., Caelles,J.C., Farrar,E., Haynes,S.J. and Zentilli,M. (1975) Initial 87Sr/86Sr ratios of plutonic and volcanic rocks of the Central Andes between latitudes 26° and 29° south. Earth Planet. Sci. Lett. 27, 305-313

McNutt,R.H., Clark,A.H. and Zentilli,M. (1979) Lead isotopic compositions of Andean igneous rocks, latitudes 26° to 29° S: petrogenetic and metallogenetic implications. Econ. Geol. 74, 827-837

Meissnar,R.O., Fleueh,E.R., Stibane,F.R. and Berg,F. (1972) Dynamics of the active plate boundary in southwest Colombia. Tectonophysics 35, 115-136

Menzies,M.A. and Wass,S.Y. (1983) CO_2- and LREE-rich mantle below eastern Australia: a REE and isotopic study of alkaline magmas and apatite-rich mantle xenoliths from the Southern Highlands Province, Australia. Earth Planet. Sci. Lett. 65, 287-302

Menzies,M.A. Leeman,W.P. and Hawkesworth,C.J. (1984). Geochemical and isotopic evidence for the origin of continental flood basalts with particular reference to the Snake River Plain Idaho, U.S.A. Phil. Trans. R. Soc. Lond. A310, 643-660

Miyashiro,A. (1973) The Troodos ophiolite complex was probably formed as an island arc. Earth Planet. Sci. Lett. 19, 218-224.

Montano,J. (1976) Estudio geologico de la zona de Caracoles y areas vecinas, con enfasis en el sistema Jurasico. Provincia de Antofagasta, II Region, Chile. Tesis de doctorado. Depto. de Geologia, Univ. de Chile. 154p

Morris,J.D. and Hart,S.R. (1983) Isotopic and incompatible element constraints on the genesis of island arc volcanics from Cold Bay and Amak Island, Aleutians and implicatons for mantle structure. Geochim. Cosmochim. Acta 47, 2015-2030

Mortimer,C., Farrar,E. and Saric,N. (1974) K-Ar ages from Tertiary lavas of the northwest Chilean Andes. Geol. Rundsch. 63, 484-490

Nakamura,N. (1974) Determination of REE, Ba, Fe, Mg, Na, and K in carbonaceous and ordinary chondrites. Geochim. Cosmochim. Acta 38, 757-775

Noble,D.C., McKee,E.H., Farrar,E. and Petersen,U. (1974) Episodic Cenozoic volcanism and tectonism in the Andes of Peru. Earth Planet. Sci. Lett. 21, 213-220

Nohda,S. and Wasserburg,G.J. (1981) Nd and Sr isotopic study of volcanic rocks from Japan. Earth Planet. Sci. Lett. 52, 264-276

O'Callaghan,L.J. (in prep.) The relation between volcanic and plutonic rocks in northern Chile. PhD thesis, Open University

Offler,R., Aguirre,L., Levi,B. and Child,S. (1980) Burial metamorphism in rocks of the Western Andes of Peru. Lithos 13, 31-42

O'Nions,R.K., Carter,S.R., Evensen,N.M. and Hamilton,P.J. (1979) Geochemical and cosmochemical applications of Nd isotope analysis. Ann. Rev. Earth Planet. Sci. 7, 11-38

Oxburgh,E.R. and Turcotte,D.L. (1970) Thermal struture of island arcs. Geol. Soc. Am. Bull. 81, 1665-1688

Oxburgh,E.R. and Parmentier,E.M. (1978) Thermal processes in the formation of continental lithosphere. Phil. Trans. R. Soc. Lond. A288, 415-429

Pacci,D., Munizaga,F., Herve,F., Kawashita,K. and Cordani,U.G. (1980) Acerca de la edad Rb-Sr Precambrica de rocas de la Formacion Esquistos de Belen, Dept. de Parinacota, Chile. Rev. Geol. Chile 10

Palacios,C. (1978) The Jurassic palaeovolcanism in northern Chile. Diss. F.B. Geowiss. Univ. Tubingen 97p

Pearce,J.A. (1982) Trace element characteristics of lavas from destructive plate boundaries. In: Andesites: Orogenic Andesites and Related Rocks (Ed. R.S.Thorpe) John Wiley & Sons, London 525-548

Pearce,J.A. (1983) Role of the sub-continental lithosphere in magma genesis at active continental margins. In: Continental Basalts and Mantle Xenoliths (Eds. C.J.Hawkesworth and M.J.Norry) Shiva Publishing, Nantwich 230-249

Pearce,J.A. and Cann,J.R. (1973) Tectonic setting of basic volcanic rocks determined using trace element analyses. Earth Planet. Sci. Lett. 19, 290-300

Pearce,J.A. and Norry,M.J. (1979) Petrogenetic implications of Ti, Zr, Y and Nb variations in volcanic rocks. Contrib. Mineral. Petrol. 69, 33-47

Peccerillo,A. and Taylor,S.R. (1976) Geochemistry of Eocene calc-alkaline volcanic rocks from the Kastamonu area, northern Turkey. Bull. Volcanol. 39, 557-569

Perez,E. and Levi,B. (1961) Relacion estratigraphica entre la Formacion Moctezuma y el granito subyacente. Calama, Prov. de Antofagasta, Chile. Rev. Minerales 74, 39-48

Pichler,H. and Zeil,W. (1969) Die quatare "Andesit" Formation in der Hochkordillere Nord - Chiles. Geol. Rundsch. 58, 866-903

Pichler,H. and Zeil,W. (1972) The Cenozoic rhyolite-andesite association of the Chilean Andes. Bull. Volcanol. 35, 424-452

Pichler,H., Hormann,P.K. and Braun,A.F. (1976) First petrologic data on lavas of the volcano El Reventador (Eastern Ecuador). Munster. Forsch. Geol. Palaeont. 38/39, 129-141

Piepgras,D.J. and Wasserburg,G.J. (1980) Neodymium isotopic variations in seawater. Earth Planet. Sci. Lett. 50, 128-138

Pitcher,W.S. (1978) The anatomy of a batholith. J. Geol. Soc. London 135, 157-182

Pitcher,W.S. (1984) Phanerozoic plutonism in the Peuvian Andes. In: Andean Magmatism Geochemical and Isotopic Constraints. (Eds. R.S.Harmon and B.A.Barreiro) Shiva Publishing, Nantwich 152-167

Potts,P.J., Thorpe,O.W. and Watson,J.S. (1981) Determination of the rare-earth element abundances in 29 international rock standards by instrumental neutron activation analysis: a critical appraisal of calibration errors. Chem. Geol. 34, 331-352

Potts,P.J., Webb,P.C. and Watson,J.S. (1984) Energy-Dispersive X-Ray Fluorescence analysis of silicate rocks for major and trace elements. X-Ray Spectrometry 13, 2-15

Potts,P.J., Thorpe,O.W., Isaacs,M.C. and Wright,D.W. (1985) High-precision instrumental neutron-activation analysis of geological samples employing simultaneous counting with both planar and coaxial detectors. Chem. Geol. 48, 145-155

Puig,A., Herve,M., Suarez,M. and Saunders,A.D. (1984) Calc-alkaline and alkaline Miocene and calc-alkaline Recent volcanism in the southernmost Patagonian Cordillera, Chile. J. Volcanol. Geotherm. Res. 20, 149-163

Quirt,G.S. (1972) A potassium-argon geochronological investigation of the Andean mobile belt of north-central Chile. PhD thesis, Queen's University, Kingston, Ont. 240p

Ramirez,C.F. and Huete,C. (1981) Hoja Ollague. Escala 1:250,000. Carta Geologica de Chile. Inst. Invest. Geologicas No.40 48p

Ringwood,A.E. (1974) The petrological evolution of island arc systems. J. Geol. Soc. London 130, 183-204

Rogers,G., Saunders,A.D., Terrell,D.J., Verma,S.P. and Marriner,G.F. (in press) Geochemistry of Holocene volcanic rocks associated with ridge subduction in Baja California, Mexico.

Rogers,N.W. and Hawkesworth,C.J. (1982) Proterozoic age and cumulate origin for granulite xenoliths, Lesotho. Nature 299, 409-413

Roobol,M.J., Francis,P.W., Ridley,W.I., Rhodes,M. and Walker,G.P.L.(1976) Physico-chemical characters of the Andean volcanic chain between latitudes 21° and 22° south. In: Proceedings of the Symposium on Andean and Antarctic Volcanology Problems (Santiago, Chile, 1974) IAVCEI (Ed. O.Gonzalez-Ferran) 450-464

Ruiz,C., Aguirre,L., Corvalan,J., Klohn,C., Klohn,E. and Levi,B. (1965) Geologia y yacimientos metaliferos de Chile. Inst. Invest. Geologicas, Santiago 305p

Rutland,R.W.R. (1971) Andean orogeny and ocean floor spreading. Nature 233, 252-255

Rutland,R.W.R., Guest,J.E. and Grasty,R.L. (1965) Isotopic ages and Andean uplift. Nature 208, 677-678

Sacks,I.S. and Okada,H. (1974) A comparison of the anelasticity structure beneath South America and Japan. Phys. Earth Planet. Inter. 9, 211-219

Sacks,I.S., Snoke,J.A. and Linde,A.T. (1976) Volcanoes, Q, and seismicity in western South America. Yb. Carnegie Inst. Wash. 75, 216-223

Saunders,A.D. and Tarney,J. (1984) The geochemical characteristics of basaltic volcanism within back-arc basins. In: Volcanic Processes in Marginal Basins (Eds. B.P.Kokelaar and M.F.Howells) Spec. Publ. Geol. Soc. London No.16 59-76

Saunders,A.D., Tarney,J., Stern,C.R. and Dalziel,I.W.D. (1979) Geochemistry of Mesozoic marginal basin floor igneous rocks from southern Chile. Geol. Soc. Am. Bull. 90, 237-258

Saunders,A.D., Tarney,J. and Weaver,S.D. (1980) Transverse geochemical variations across the Antarctic Peninsula: implications for the genesis of calc-alkaline magmas. Earth Planet. Sci. Lett. 46, 344-360

Saunders,A.D., Fornari,D.J. and Morrison,M.A. (1982) The composition and emplacement of basaltic magmas produced during the development of continental margin basins: the Gulf of California, Mexico. J. Geol. Soc. London 139, 335-346

Sepulveda,P.J. and Naranjo,J.A. (1982) Hoja Carrera Pinto. Escala 1:100,000. Carta Geologica de Chile. Servicio Nacional de Geologia y Mineria. No.53

Servicio Nacional de Geologia y Mineria (1980) Mapa Geologica de Chile. Escala 1:1,000,000.

Shackleton,R.M., Ries,A.C., Coward,M.P. and Cobbold,P.R. (1979) Structure, metamorphism and geochronology of the Arequipa Massif of coastal Peru. J. Geol. Soc. London 136, 195-214

Siegers,A., Pichler,H. and Zeil,W. (1969) Trace element abundances in the "Andesite" Formation of northern Chile. Geochim. Cosmochim. Acta 33, 882-887

Staudigel,H., Hart,S.R. and Richardson,S.H. (1981) Alteration of the oceanic crust: processes and timing. Earth Planet. Sci. Lett. 52, 311-327

Stern,C.R. and Futa,K. (1982) Nd and Sr isotope ratios of calc-alkaline volcanic rocks from the southern Andes. Trans. Am. Geophys. Union 63, 456-457

Stern,C.R., Futa,K. and Muehlenbachs,K. (1984) Isotope and trace element data for orogenic andesites from the Austral Andes. In: Andean Magmatism Chemical and Isotopic Constraints (Eds. R.S.Harmon and B.A.Barreiro) Shiva Publishing, Nantwich 21-46

Stern,R.J. (1981) A common mantle source for western Pacific island arc and "hot spot" magmas - implications for layering in the upper mantle. Yb. Carnegie Inst. Wash. 80, 455-462

Stern,R.J. and Bibee,L.D. (1980) Esmeralda Bank: geochemistry of an active submarine volcano in the Mariana island arc and its implications for magmagenesis in island arcs. Yb. Carnegie Inst. Wash. 79, 465-472

Strekheisen,A. (1976) To each rock its proper name. Earth Sci. Rev. 12, 1-33

Taylor,H.P. (1980) The effects of assimilation of country rocks by magmas on $^{18}O/^{16}O$ and $^{87}Sr/^{86}Sr$ systematics in igneous rocks. Earth Planet. Sci. Lett. 47, 243-254

Thirlwall,M.F. and Jones,N.W. (1983) Isotope geochemistry and contamination mechanics of Tertiary lavas from Skye, northwest Scotland. In: Continental Basalts and Mantle Xenoliths (Eds. C.J.Hawkesworth and M.J.Norry) Shiva Publishing, Nantwich 186-208

Thomas,A. (1969) Resumen de la geologia de las hojas Chuiquicamata y Soledad, Provincia de Antofagasta. Inst. Invest. Geologicas. (inedito)

Thorpe,R.S. (1982) Andesites: Orogenic Andesites and Related Rocks (Ed.) John Wiley & Sons, London

Thorpe,R.S. (1984) The tectonic setting of active Andean volcanism. In: Andean Magmatism Chemical and Isotopic Constraints (Eds. R.S.Harmon and B.A.Barreiro) Shiva Publishing, Nantwich 4-8

Thorpe,R.S. and Francis,P.W. (1979a) Variations in Andean andesite compositions and their petrogenetic significance. Tectonophysics 57, 53-70

Thorpe,R.S. and Francis,P.W. (1979b) Petrogenetic relationships of volcanic and intrusive rocks of the Andes. In: Origin of Granite Batholiths Geochemical Evidence (Eds. M.P.Atherton and J.Tarney) Shiva Publishing, Nantwich 65-75

Thorpe,R.S., Potts,P.J. and Francis,P.W. (1976) Rare earth data and petrogenesis of andesite from the north Chilean Andes. Contrib. Mineral. Petrol. 54, 65-78

Thorpe,R.S., Francis,P.W. and Moorbath,S. (1979) Rare earth and strontium isotope evidence concerning the petrogenesis of north Chilean ignimbrites. Earth Planet. Sci. Lett. 42, 359-367

Thorpe,R.S., Francis,P.W. and Harmon,R.S. (1981) Andean andesites and crustal growth. Phil. Trans. R. Soc. Lond. A301, 305-320

Thorpe,R.S., Francis,P.W., Hammill,M. and Baker,M.C.W. (1982) The Andes. In: Andesites: Orogenic Andesites and Related Rocks (Ed. R.S.Thorpe) John Wiley & Sons, London 187-206

Thorpe,R.S., Francis,P.W. and O'Callaghan,L.J. (1984) Relative roles of source composition, fractional crystallisation and crustal contamination in the petrogenesis of Andean volcanic rocks. Phil. Trans. R. Soc. Lond. A310, 675-692

Tilton,G.R. and Barreiro,B.A. (1980) Origin of lead in Andean calc-alkaline lavas, southern Peru. Science 210, 1245-1247

Tindle,A.G. (1982) Petrogenesis of the Loch Doon granite intrusion, Southern Uplands of Scotland. PhD thesis, Open University (unpublished) 327p

Tindle,A.G. and Pearce,J.A. (1981) Petrogenetic modelling of in situ fractional crystallization in the zoned Loch Doon pluton, Scotland. Contrib. Mineral. Petrol. 78, 196-207

Tindle,A.G. and Pearce,J.A. (1983) Assimilation and partial melting of continental crust: evidence from the mineralogy and geochemistry of autoliths and xenoliths. Lithos 16, 185-202

Turner,P., Clemmey,H. and Flint,S. (1984) Palaeomagnetic studies of a Cretaceous molasse sequence in the central Andes (Coloso Formation, northern Chile). J. Geol. Soc. London 141, 869-876

Ulriksen,C. (1979) Regional geology, geochronology and metallogeny of the Coastal Coldillera between $23^{0}30'$ and 26^{0}S. MSc thesis, Dalhousie University, Canada 180p

Vergara,H. (1978) Cuadrangulo Quehuita y sector occidental del cuadrangulo Volcan Mino, Region de Tarapaca. Escala 1:50,000. Carta Geologica de Chile. Inst. Invest. Geologicas. No.32 44p

Verma,S.P. (1983) Magma genesis and chamber processes at Los Humeros caldera, Mexico - Nd and Sr isotope data. Nature 302, 52-55

Vidal,Ph., Cocherie,A. and LeFort,P. (1982) Geochemical investigations of the origin of the Manaslu leucogranite (Himalaya, Nepal). Geochim. Cosmochim. Acta 46, 2279-2292

Vollmer,R. (1976) Rb-Sr and U-Th-Pb systematics of alkaline rocks: the alkaline rocks from Italy. Geochim. Cosmochim. Acta 40, 283-295

Weaver,S.D., Saunders,A.D., Pankhurst,R.J. and Tarney,J. (1979) A geochemical study of magmatism associated with the initial stages of back-arc spreading. The Quaternary volcanics of Bransfield Strait, from South Shetland Islands. Contrib. Mineral. Petrol. 68, 151-169

Wernick,E. (1981) The Archaean of Brazil. Earth Sci. Rev. 17, 31-48

Wetzel,W. (1927) Beitrage zur Erdgeschichte der mittleren Atacama. Neus Jahrb. Mineral. Geol. Palaontol. 58, 505-578

White,W.M. and Patchett,J. (1984) Hf-Nd-Sr isotopes and incompatible element abundances in island arcs: implications for magma origins and crust-mantle evolution. Earth Planet. Sci. Lett. 67, 167-185

White,W.M., Tapia,M.D.M., Schilling,J.-G. (1979) The petrology and geochemistry of the Azores islands. Contrib. Mineral. Petrol. 69, 201-213

Whitford,D.J. Nicholls,I.A. and Taylor,S.R. (1979) Spatial variations in the geochemistry of Quaternary lavas across the Sunda arc in Java and Bali. Contrib. Mineral. Petrol. 70, 341-356

Wood,D.A. (1979) A variably veined suboceanic upper mantle - genetic significance for mid-ocean ridge basalts from geochemical evidence. Geology 7, 499-503

Wood,D.A., Tarney,J., Varet,J., Saunders,A.D., Bougault,H., Joron,J.-L.,Treuil,M. and Cann,J.R. (1979) Geochemistry of basalts drilled in the North Atlantic by IPOD Leg 49: implications for mantle heterogeneity. Earth Planet. Sci. Lett. 42, 77-97

York,D. (1969) Least squares fitting of a straight line with correlated errors. Earth Planet. Sci. Lett. 5, 320-324

Zeil,W. (1964) Geologie von Chile. Gebruder Borntraeger, Berlin 233p

Zeil,W. (1979) The Andes - a geological review. Gebruder Borntraeger, Berlin 260p

Zeil,W. and Pichler,H. (1967) Die Kanozoische Rhyolith-Formation im mittleren Abschnitt der Anden. Geol. Rundsch. 57, 48-81

Zeil,W., Damm,K.-W. and Pichowiak,S. (1980) Los plutones de la Cordillera de la Costa al Norte de Chile. In: Nuevos resultados de la investigacion geocientifica alemana en Latinoamerica. Deutsche Forschungsgemeinschaft, Bonn y el Instituto de Colaboracion Cientifica, Tubingen 112-122

Zentilli,M. (1974) Geological evolution and metallogenetic relationships in the Andes of northern Chile between 26^0 and 29^0 south. PhD thesis, Queen's University, Kingston, Ont. 446p

Appendix A
Sample Locations

Unit	Sample No.	Rock Type	Location
Limón Verde Schists	81009	Amphibolite	22°38'45" S 68°58'46" W
	81010	Gt. amphibolite	22°38'45" S 68°58'46" W
	81011	Gt.-bi.-qtz. schist	22°38'49" S 68°58'43" W
	81150	Gt. amphibolite	22°38'51" S 68°58'42" W
	81151	Gt.-bi.-qtz. schist	22°38'51" S 68°58'42" W
	81152	Gt.-bi. amphibolite	22°38'52" S 68°58'43" W
	80213	Amphibolite	22°38'46" S 68°58'45" W
	80214	Gt.-qtz.-musc. schist	22°38'46" S 68°58'45" W
Toco Formation	81087	Arenite	2°02'58" S 69°47'01" W
	81107	Hornfelsed arenite	22°11'13" S 69°44'34" W
	81122	Hornfelsed arenite	22°45'16" S 68°59'08" W
	81123	Hornfelsed arenite	22°45'32" S 68°59'16" W
	81124	Hornfelsed arenite	22°45'41" S 68°59'25" W
Limón Verde Pluton	81012	Aplite dyke	22°39'21" S 68°57'45" W
	81013	Granodiorite	22°39'21" S 68°57'45" W
	81014	Dolerite dyke	22°39'24" S 68°57'43" W
	81015	Granodiorite	22°39'24" S 68°57'38" W
	81016	Aplite dyke	22°39'28" S 68°57'29" W
	81017	Granite	22°39'15" S 68°57'48" W
	81018	Granodiorite	22°39'15" S 68°57'48" W
	81113	Granodiorite	22°35'00" S 68°55'29" W
	81114	Granite	22°35'24" S 68°55'55" W
	81115	Granite	22°39'19" S 68°56'13" W
	81116	Granodiorite	22°39'19" S 68°56'04" W
	81117	Granite	22°39'19" S 68°55'55" W
	81118	Granodiorite	22°39'11" S 68°55'38" W
	81119	Granite	22°39'03" S 68°55'29" W
	81120	Granodiorite	22°42'02" S 68°55'47" W
	81121	Quartz monzodiorite	22°45'49" S 68°58'41" W

Unit	Sample No.	Rock Type	Location	
Cerro Crespo Formation	81041	Crystal Tuff	22°43'47" S	69°03'15" W
	81042	Rhyolite	22°43'47" S	69°03'15" W
	81043	Rhyolite	22°43'44" S	69°03'11" W
	81044	Volcaniclastic	22°43'44" S	69°03'11" W
	81045	Rhyolite	22°43'39" S	69°03'15" W
	80195	Rhyolite	22°43'47" S	69°03'15" W
Agua Dulce Formation	81001	Sandstone	22°36'24" S	69°00'07" W
	81002	Conglomerate	22°36'21" S	69°00'09" W
	81003	Calc-arenite	22°36'19" S	69°00'09" W
	81004	Agglomerate	22°36'15" S	69°00'12" W
	81005	Ignimbrite	22°36'15" S	69°00'12" W
	81006	Crystal Tuff	22°36'15" S	69°00'12" W
	81092	Hornfelsed lava	22°10'08" S	69°38'22" W
	81093	Hornfelsed lava	22°09'52" S	69°40'32" W
La Negra Formation	8077	Basaltic andesite	22°21'08" S	70°15'15" W
	8078	Basaltic andesite		
	8079	Basaltic andesite		
	8080	Basaltic andesite		
	8081	Basaltic andesite		
	8088	Basaltic andesite		
	8087	Basaltic andesite		
	8086	Basaltic andesite		
	8085	Basaltic andesite		
	8084	Basaltic andesite		
	8083	Basaltic andesite		
	8082	Basaltic andesite		
	8089	Tuff		
	8090	Volcanic Breccia		
	8091	Basaltic andesite		
	8092	Basaltic andesite		

Unit	Sample No.	Rock Type	Location	
La Negra Formation (continued)	8092A	Basaltic andesite	22°21'08" S	70°15'15" W
	8093	Basaltic andesite		
	8094	Tuff		
	8095	Altered basaltic andesite		
	8096	Altered basaltic andesite		
	8097	Basaltic andesite		
	8098	Andesite	22°20'41" S	70°13'26" W
	81069	Basaltic andesite	22°09'57" S	79°12'07" W
	81069A	Basaltic andesite	22°09'57" S	70°12'07" W
	81070	Basaltic andesite	22°09'57" S	70°12'07" W
	81071	Basaltic andesite	22°10'06" S	70'11'10" W
	81072	Basaltic andesite	22°09'52" S	70°10'19" W
	81073	Basaltic andesite	22°09'37" S	70°10'27" W
	81074	Basaltic andesite	22°09'23" S	70°10'24" W
	81081	Andesite	22°08'31" S	69°59'34" W
	81082	Andesite	22°08'39" S	69°59'25" W
	81083	Andesite	22°10'08" S	69°55'32" W
	81084	Basaltic andesite	22°10'16" S	69°54'48" W
	81085	Andesite	22°09'36" S	69°54'05" W
	81086	Andesite	22°09'44" S	69°53'48" W
Gatico Pluton	8052	Hornfelsed lava	22°24'00" S	70°14'51" W
	8053	Hornfelsed lava	22°24'10" S	70°14'43" W
	8054	Quartz monzodiorite	22°24'36" S	70°14'36" W
	8055	Felsic dyke	22°24'36" S	70°14'36" W
	8057	Lava	22°24'36" S	70°14'36" W
	8058	Quartz diorite	22°24'00" S	70°14'15" W
	8059	Quartz gabbro	22°24'06" S	70°13'55" W
	8060	Aplite dyke	22°23'50" S	70°13'48" W
	8061	Felsic dyke	22°23'29" S	70°13'17" W
	8062	Quartz diorite	22°25'47" S	70°15'12" W

Unit	Sample No.	Rock Type	Location	
Gatico Pluton (continued)	8063	Dolerite dyke	22°25'47" S	70°15'12" W
	8064	Dolerite dyke	22°25'47" S	70°15'12" W
	8065	Feldspathic sweatout	22°26'50" S	70°15'27" W
	8066	Granodiorite	22°28'23" S	70°12'51" W
	8067	Granodiorite	22°28'13" S	70°12'34" W
	8068	Pegmatite dyke	22°27'58" S	70°15'14" W
	8069	Silicic vein	22°27'58" S	70°15'14" W
	8070	Altered granodiorite	22°27'58" S	70°15'14" W
	8071	Acid dyke	22°28'08" S	70°14'27" W
	8072	Granite	22°28'08" S	70°14'27" W
	8073	Quartz diorite	22°29'28" S	70°13'58" W
	8074	Quartz monzodiorite	22°29'28" S	70°13'58" W
	8075	Aplite dyke	22°29'28" S	70°13'58" W
	8076	Aplite dyke	22°29'28" S	70°13'58" W
Tocopilla Pluton	81075	Monzonite	22°06'37" S	70°10'02" W
	81076	Monzonite	22°08'21" S	70°08'21" W
	81077	Monzonite	22°06'42" S	70°09'45" W
	81078	Monzonite	22°07'21" S	70°08'31" W
	81079	Monzonite	22°06'49" S	70°08'15" W
	81080	Monzonite	22°06'19" S	70°05'24" W
	TOC 1	Monzontie	22°06'00" S	70°06'17" W
	TOC 2	Quartz monzodiorite	22°04'54" S	70°09'22" W
	TOC 3	Monzonite	22°04'54" S	70°09'22" W
	TOC 4	Monzonite	22°04'49" S	70°10'34" W
	TOC 5	Granite	22°02'28" S	70°11'09" W
	TOC 6	Granite	22°00'11" S	70°10'34" W
	TOC 7	Quartz monzodiorite	22°00'11" S	70°10'34" W

Unit	Sample No.	Rock Type	Location	
Cerro Colupito Pluton	81094	Quartz monzodiorite	22°13'31" S	69°58'42" W
	81095	Granodiorite	22°13'39" S	69°58'33" W
	81096	Granite	22°13'47" S	69°58'33" W
	81097	Autolith	22°13'47" S	69°58'33" W
	81098	Autolith	22°13'47" S	69°58'33" W
Sierra de la Cruz Pluton	8040	Granodiorite	22°16'37" S	69°42'33" W
	81099	Granite	22°16'13" S	69°45'52" W
	81100	Autolith	22°16'37" S	69°42'33" W
	81101	Andesitic dyke	22°14'52" S	69°43'25" W
	81102	Andesitic dyke	22°15'16" S	69°43'08" W
	81103	Andesitic dyke	22°15'41" S	69°43'08" W
	81104	Andesitic dyke	22°11'29" S	69°47'01" W
	81105	Tonalite	22°11'29" S	69°47'01" W
	81106	Tonalite	22°11'21" S	69°47'10" W
	81108	Andesitic dyke	22°13'39" S	69°45'17" W
	81109	Andesitic dyke	22°13'39" S	69°45'17" W
	81110	Quartz monzodiorite	22°12'18" S	69°45'52" W
	81111	Aplite dyke	22°12'42" S	69°45'52" W
Jurassic marine sediments	81007	Calcisiltstone	22°36'13" S	69°00'19" W
	81008	Glauconitic sand	22°36'15" S	69°00'21" W
	81026	Limestone	22°36'11" S	69°05'28" W
	81027	Bituminous calcilutite	22°36'13" S	69°05'30" W
	81028	Bituminous calcilutite	22°36'13" S	60°05'30" W
	81029	Bituminous calcilutite	22°36'13" S	69°05'30" W
	81030	Calcarenite	22°36'13" S	69°05'32" W
	81031	Calcilutite	22°36'15" S	69°05'49" W
	81032	Oolitic limestone	22°36'13" S	69°05'53" W
	81033	Oolitic limestone	22°36'11" S	69°05'56" W

Unit	Sample No.	Rock Type	Location	
Jurassic marine sediments (continued)	81034	Lutite	22°36'11" S	69°05'56" W
	81058	Lutite	22°41'13" S	69°12'05" W
Cretaceous continental sediments	81059	Arenite	22°41'15" S	69°12'10" W
	81060	Siltstone	22°41'15" S	69°12'17" W
Indio Muerto Formation	81053A	Dacite	22°36'03" S	69°16'59" W
	81054	Dacite	22°35'49" S	69°18'53" W
	81055	Andesite	22°35'39" S	69°18'43" W
	81056	Basaltic andesite	22°35'39" S	69°18'43" W
	81061	Andesitic dyke	22°41'05" S	69°12'34" W
	81062	Andesite	22°42'15" S	69°15'56" W
	81063	Andesite	22°42'06" S	69°16'28" W
	80201	Dacite	22°41'06" S	69°18'41" W
	80202	Basaltic andesite	22°38'58" S	69°16'59" W
	80204	Andesite	22°36'57" S	69°14'56" W
	80205	Basalt	22°36'58" S	69°14'48" W
	80206	Andesite	22°36'52" S	69°14'37" W
Augusta Victoria Formation	81130	Basaltic andesite	22°19'03" S	69°04'02" W
	81131	Basaltic andesite	22°19'19" S	69°04'02" W
	81132	Basaltic andesite	22°19'19" S	69°04'02" W
	81134	Basalt	22°18'39" S	69°04'37" W
	81135	Andesite	22°18'15" S	69°04'46" W
	81136	Basaltic andesite	22°17'42" S	69°06'29" W
	81137	Basaltic andesite	22°17'58" S	69°06'21" W
?	81142	Altered lava	22°17'02" S	69°23'48" W
Cerros de Montecristo Pluton	81125	Granodiorite	22°19'19" S	69°00'00" W
	81126	Quartz monzodiorite	22°19'28" S	69°00'02" W
	81127	Quartz monzodiorite	22°18'39" S	69°00'26" W
	81128	Quartz monzodiorite	22°18'31" S	69°00'35" W

Unit	Sample No.	Rock Type	Location	
Cerro de Montecristo Pluton (continued)	81129	Granodiorite	22°19'19" S	69°00'09" W
	81133	Quartz monzodiorite	22°19'52" S	69°04'02" W
	81138	Granite	22°16'13" S	69°04'54" W
	81139	Granodiorite	22°16'05" S	69°04'37" W
	81140	Granodiorite	22°15'08" S	69°11'50" W
	81141	Granodiorite	22°16'21" S	69°05'12" W
Cerritos Bayos Pluton	81038	Monzonite	22°41'50" S	69°09'42" W
	81039	Altered monzonite	22°43'03" S	69°07'05" W
	81040	Monzonite	22°43'36" S	69°07'06" W
	81046	Monzonite	22°40'24" S	69°09'13" W
	81047	Gabbro	22°40'18" S	69°09'14" W
	81048	Diorite	22°40'15" S	69°09'13" W
	81049	Felsic dyke	22°40'13" S	69°09'14" W
	81050	Aplite dyke	22°40'10" S	69°09'14" W
	81051	Monzodiorite	22°40'08" S	69°09'09" W
	81052	Diorite	22°40'05" S	69°09'09" W
	81053	Pegmatite dyke	22°41'03" S	69°09'18" W
	81057	Diorite	22°37'08" S	69°11'49" W
	80196	Granodiorite	22°43'55" S	69°05'49" W
	80197	Altered monzonite	22°43'37" S	69°05'40" W
	80198	Monzonite	22°40'47" S	69°07'55" W
	80199	Monzonite	22°40'44" S	69°08'06" W
	80200	Monzonite	22°42'31" S	69°11'47" W
	80203	Monzonite	22°36'45" S	69°16'08" W
	80207	Monzonite	22°37'36" S	69°10'32" W
Pampa Negra Pluton	81088	Quartz monzodiorite	22°10'08" S	69°37'13" W
	81089	Quartz monzodiorite	22°10'08" S	69°37'13" W
	81090	Quartz monzodiorite	22°10'08" S	69°37'13" W
	81091	Quartz gabbro	22°10'16" S	69°37'39" W

Unit	Sample No.	Rock type	Location	
Cerro Colorado Pluton	81066	Diorite	21°52'26" S	68°37'34" W
	80173	Gabbro	21°48'23" S	68°38'36" W
	80176	Diorite	21°48'47" S	68°38'36" W
	80180	Gabbro	21°52'10" S	68°39'10" W
	80187	Granodiorite	21°52'10" S	68°37'34" W
	80190	Gabbro	21°50'41" S	68°40'38" W
Cerro Negro Formation	81019	Crystal tuff	22°37'50" S	68°58'34" W
	81020	Dacite	22°37'44" S	68°58'41" W
	81021	Crystal tuff	22°37'41" S	68°58'36" W
	81022	Crystal tuff	22°37'34" S	68°58'36" W
	81023	Altered lava	22°37'26" S	68°58'43" W
	81024	Altered tuff	22°37'23" S	68°58'45" W
	81025	Crystal tuff	22°37'18" S	68°58'45" W
	80208	Altered lava	22°37'34" S	68°58'36" W
	81035	Sandstone	22°39'13" S	69°00'07" W
	81036	Altered lava	22°39'19" S	69°00'09" W
	81037	Altered lava	22°39'26" S	69°00'09" W
El Abra Pluton	80101	Granodiorite	21°55'41" S	68°50'41" W
	80102	Aplite dyke	21°55'41" S	68°50'41" W
	80103	Granite	21°55'41" S	68°50'41" W
	80104	Granodiorite	21°55'08" S	68°50'32" W
	80105	Granodiorite	21°55'24" S	68°50'15" W
	80106	Granodiorite	21°55'16" S	68°48'48" W
	80107	Quartz monzodiorite	21°55'41" S	68°48'12" W
	80108	Granodiorite	21°55'49" S	68°46'36" W

Unit	Sample No.	Rock type	Location	
Upper Tertiary Volcanics	A6-2	Dacite	21°56'30" S	68°32'30" W
	A31-1	Andesite	21°25'15" S	68°24'15" W
	A33-1	Andesite	21°25'00" S	68°21'30" W
	A168-1	Andestie	21°44'00" S	68°31'30" W
	B5	Dacite	19°52'00" S	67°34'00" W
	B43	Basaltic andesite	21°20'00" S	68°01'15" W
Monogenetic Centres	A791	Basaltic andesite	23°28'00" S	67°42'45" W
	7927	Basalt	21°58'00" S	68°21'48" W
	7888	Basaltic andesite	21°18'15" S	68°17'50" W
	80193	Dacite	22°32'45" S	69°00'05" W
	B1	Alkali basalt	19°48'51" S	67°38'17" W

Appendix B

Analytical Techniques

Appendix B(i) Modal Analyses

The modal proportions of minerals in plutonic rocks are presented in Appendix C. The data were obtained using a Swift Model E pointcounter fitted with an automated stage by counting 1500 points on each sample. Proportions are expressed as percentages: "tr" means that a particular mineral was observed but not point counted.

Appendix B(ii) Powder Preparation

Whenever possible, 2 - 4 kg of fresh rock samples were collected. These were split into 3 cm cubes using a hydraulic splitter (any excess weathered surfaces being discarded), and crushed to 0.5 cm pieces in a hardened steel jaw crusher. After cone and quartering about 100 g of the crushed rock were powdered to 200 mesh using an agate "Tema" mill.

Appendix B (iii) X-Ray Fluorescence Techniques - Open University

Energy dispersive X-ray fluorescence (EDXRF) techniques were used to analyse major elements for all samples and the trace elements Rb, Sr, Y, Zr, Nb and Ni for certain samples. Major elements were analysed using glass beads made by mixing a 4:1 lithium metaborate: tetraborate mixture (Spectroflux 100B) with pre-dried rock powder in the ratio of 6:1 and fusing in a platinum-gold alloy crucible in a muffle furnace at 1100°C for 20 minutes. Corrections were regularly made for flux weight losses during fusion. Loss on ignition data were acquired by heating pre-dried powder in a silica crucible at 1000°C for 40 minutes. Trace elements were

anlaysed using pressed powder pellets. These were made by thoroughly mixing 8 g of powder with a binder (Moviol), and compressing into a 3 cm diameter disc using a hydraulic press.

Samples were analysed using a Link Systems Meca 10 - 44 EDXRF spectrometer. This consisted of a low power (maximum 49W) silver anode side window X-ray tube operated in pulsed mode with maximum settings of 49kV or 1mA, and a Si(Li) detector with a resolution of 165eV at 5.9keV. The EDXRF was calibrated using international standards covering a wide range of compositions. For major elements glass beads were counted in duplicate for 500 seconds at 10 kV, 0.2 mA with no primary beam filter. Pressed powder pellets for trace elements were counted twice for 800 seconds at 45 kV, 0.3 mA with a 127 μm silver primary beam filter. Instrumental drift was monitored by analysing USGS AGV-1 (major elements) and USGS GSP-1 (trace elements) several times during each run.

Detection limits for the major elements are generally 0.05 wt.% except for the light elements Na, Mg, Al and Si where these values vary from 0.21 wt.% (Si) to 0.96 wt.% (Na). Precision is better than 1% (2σ) relative at > 2 wt.% oxide except for Al(2%), Mg(3%) and Na(10%). Detection limits are 6 ppm for Rb, Sr, Y, Nb and Ni, and 15 ppm for Zr. Precision for all elements is 2% at the 100 ppm level. Full details of the EDXRF system are given in Potts *et al.* (1984). The results of certain international standards analysed as unknowns are presented in Table B:1 and compared with the values in Abbey (1980).

Table B:1 Major element data for international standards analysed during the course of this study compared to their values in Abbey (1980). All data as wt.%

	JB-1		AGV-1		GSP-1		G2	
	Abbey (1980)	This work	Abbey (1980)	This work	Abbey (1980)	This work	Abbey (1980)	This work
SiO_2	52.60	52.09	59.61	59.35	67.32	67.19	69.22	69.46
TiO_2	1.34	1.32	1.06	1.07	0.66	0.68	0.48	0.50
Al_2O_3	14.62	14.51	17.19	17.10	15.28	15.00	15.40	15.41
Fe_2O_3	9.01	9.08	6.78	6.97	4.30	4.45	2.69	2.76
MnO	0.15	0.15	0.10	0.10	0.04	0.04	0.03	0.03
MgO	7.76	7.73	1.52	1.62	0.97	0.96	0.75	0.86
CaO	9.35	9.36	4.94	5.02	2.03	2.03	1.96	1.94
Na_2O	2.79	2.78	4.32	4.34	2.81	2.82	4.06	4.21
K_2O	1.42	1.37	2.92	2.93	5.51	5.56	4.46	4.55
P_2O_5	0.26	0.29	0.51	0.52	0.28	0.28	0.13	0.14

Appendix B(iv) X-Ray Fluorescence Techniques - Nottingham University

The trace elements Ba, Co, Cr, Ni, Nb, Rb, Sr, V, Y and Zr were analysed at Nottingham University using a Philips PW1400 wavelength dispersive X-ray fluorescene spectrometer. A rhodium X-ray tube was utilised throughout. Analyses were performed upon pressed powder pellets whose manufacture has been described above. Detection limits are 3 ppm. Operating conditions are as listed in Table B:2.

Rb and Sr were determined separately from the other trace elements using the measuring cycle given in Table B:3. Both elements were analysed at 75kV, 40mA using a LiF220 crystal; full procedural details are given in Harvey and Atkin (1981).

Several international standards were analysed as unknowns, and are compared with values given in Abbey (1980) in Table B:4.

Table B:2 XRF operating conditions at Nottingham University

Element	kV	mA	Crystal	Ct. (peak)	Ct. (bkd).
Ba	50	60	LiF220	20	10
Co	60	50	LiF220	20	20
Cr	50	60	LiF200	20	8
Ni	70	40	LiF200	10	4
Nb	75	40	LiF220	10	8
Y	75	40	LiF220	20	16
Zr	75	40	LiF220	20	20

Ct. (peak) normal counting time on the peak position

Ct. (bkd). normal counting time on the background

Table B:3 Measuring cycle for Rb and Sr determinations

	Position	Count time (secs)
(i)	Background: (Sr^{-})	4
(ii)	Peak: Sr-K	20
(iii)	Background: (Sr^{+}, Rb^{-})	4
(iv)	Peak: Rb-K	10
(v)	Background: (Rb^{+})	4

This cycle was repeated six times for each sample

Table B:4 Trace element data fro international standards analysed at Nottingham University during this study compared to values in Abbey (1980). All data in ppm.

	AGV-1		GSP-1		BR		NIM-G	
	Abbey (1980)	This work	Abbey (1980)	This work	Abbey (1980)	This work	Abbey (1980)	This work
Ba	1200	1223	1300	1274	1050	1036	120	110
Co	16	16	8	8	50	58	3	3
Cr	10	11	12	14	380	384	12	13
Ni	15	17	9	9	260	271	8	9
Nb	16	15	23	28	100	112	53	52
Rb	67	66	250	253	47	52	320	321
Sr	660	656	240	231	1300	1429	10	9
V	125	125	54	54	240	261	2	1
Y	19	24	29	30	30	31	145	147
Zr	230	233	500	499	250	253	300	298

Appendix B(v) INAA Analyses

Instrumental neutron activation analysis (INAA) was used to determine the concentrations of the following elements in selected samples:- La, Ce, Nd, Sm, Eu, Tb, Tm, Yb, Th, Ta, Hf, U, Co and Sc. The experimental technique is fully described in Potts et al. (1981, 1985).

Rock powders were dried overnight at 105°C, and 0.3 g of each powder were then weighed into polythene capsules which were heat sealed. Ten capsules were loaded into a further polythene "can", with an international standard and an internal standard (Ailsa Craig microgranite) positioned one third and two thirds of the way through the can. Laquered iron foils were inserted between the capsules and used to monitor the neutron flux.

Samples were irradiated in the centre two positions of a 270° core tube at the University of London Reactor Centre, Ascot in a thermal flux of 5×10^{12} n cm^{-2} s^{-1} for 24 - 30 hours of reactor time. After one week's "cooling" samples were counted at the Open University using two detectors: a low energy photon spectrometer (LEPS) and a coaxial Ge(Li) detector. The following counting procedure was employed:

(a) The iron foils were counted on the coaxial detector for 300 seconds each to provide data for the neutron flux correction.

(b) Each sample was counted for 800 seconds on the LEPS detector for Sm, and then on the coaxial detector for La, Co and Sc.

(c) Each sample was counted for 2.5×10^4 - 5×10^4 seconds using the LEPS detector for the remaining elements.

The areas of the photopeaks were calculated using the peak fitting software supplied with the EG and G ORTEC 7032A multichannel analyser system. All photopeak data were then corrected for neutron flux discrepancies and exponential decay of specific isotopes between standard and unknown, weight of sample and count time.

The mean and standard deviation data for the standards RGM-1 and Whin Sill from this work are compared with values given in Potts et al. (1981, 1985) in Table B:5. All data portrayed in chondrite-normalised diagrams are normalised to the values of Nakamura (1974).

Table B:5 INAA data for standards analysed during this study compared to their values in Potts et al. (1981, 1985).

	RGM-1			Whin Sill		
	Potts et al. (1981)	This work (n = 3)	2σ	Potts et al. (1985)	This work (n = 3)	2σ
La	23.7	26.1	1.4	25.5	25.6	0.55
Ce	47.3	48.0	2.1	57.5	58.4	1.67
Nd	20.3	20.6	2.9	32.9	33.2	1.71
Sm	4.55	4.27	0.30	7.27	7.40	0.23
Eu	0.62	0.65	0.03	2.25	2.30	0.05
Tb	0.64	0.66	0.03	1.09	1.11	0.09
Tm	0.41	0.38	0.03	0.41	0.45	0.05
Yb	2.54	2.54	0.10	2.54	2.60	0.11
Th	15.0	15.6	0.74	3.05	3.12	0.18
Ta	0.94	0.99	0.04	1.26	1.30	0.06
Hf	5.8	6.06	0.24	4.93	5.05	0.40
Co	1.9	1.97	0.12	47.4	47.2	3.1
Sc	-	5	-	-	29	-
U	-	-	-	0.90	0.73	0.20

Appendix B(vi) Mass Spectrometric Analyses

(a) General Chemistry

All techniques described below are performed in a laboratory with a small positive pressure generated by an air makeup unit with particle filters. Dissolutions are performed within laminar flow cupboards in teflon beakers and bombs. The teflon is cleaned by thorough rinsing in pyrex distilled H_2O, soaking for 24 hours in concentrated HNO_3 at 80°C, and finally further soaking for at least 24 hours in quartz distilled H_2O at 80°C. Tap water is purified by passage through a pyrex still which feeds a two-stage quartz still. Analar HCl and HNO_3 are double distilled in quartz stills, and then purified in subboiling teflon stills. HF is purified in similar subboiling stills.

Total procedural blanks for Sm and Nd are <1 ng and for Sr about 8 ng.

(b) Sr Chemistry

About 150 mg of rock powder is weighed into a PTFE beaker to which is added about 5 ml of 40% HF and 2 ml of concentrated HNO_3. This is evaporated to dryness in a teflon oven with clean air circulation at 80°C. A further 2 ml of concentrated HNO_3 is added and evaporated. When this solution is "damp" about 6 ml of 6M HCl are added at which stage complete dissolution should occur. The solution is evaporated and the residue redissolved in 1 ml of 2.5M HCl. Any residue is centrifuged off and the clear solution loaded onto a preconditioned cation exchange column containing 10 ml Bio-Rad AG50W x 8, 200 - 400 mesh resin. The sample is

washed in with 2 x 1 ml of 2.5M HCl and eluted with 40 ml 2.5M HCl. The Sr fraction is collected with a further 10 ml 2.5M HCl, and evaporated to dryness.

(c) Sm/Nd Chemistry

Volcanic samples for Sm and Nd analysis are dissolved as described for Sr analysis: solutions of plutonic samples, however, are made using the following procedure due to the difficulty experienced in dissolving minor phases which contain the bulk of the REE. About 150 mg of rock powder is weighed into a PTFE bomb to which is added about 5 ml of 40% HF and 2 ml of concentrated HNO_3. This is left to stand "cold" for several hours before being placed in a monel jacket in an oven at 180°C for at least 24 hours. The bomb is then placed in the clean air circulation oven at 80°C, and when dry a further 2 ml of concentrated HNO_3 are added. When this is "damp" about 6 ml 6M HCl are added, and the bomb is replaced in the monel jacket in an oven at 180°C overnight. Subsequent procedure is the same for both volcanic and plutonic samples.

The dissolved sample is loaded onto the Sr cation exchange column, and the elutions are the same as for Sr. However, once the Sr fraction has been collected the column is washed with a 1 ml H_2O, a further 21 ml 3M HNO_3 are eluted and 20 ml 3M HNO_3 are collected. This fraction, containing both Sm and Nd, is evaporated to dryness. To remove Ba from the REE this residue is then dissolved in 1 ml 90% CH_3COOH - 10% 5M HNO_3 and loaded onto a preconditioned anion exchange column containing 1 ml Bio-Rad AG1 x 8 200 - 400 mesh resin. This is washed in twice with 1 ml and eluted with 10 mls of the solution. Sm and Nd are

stripped off by eluting with 4 ml 0.05M HNO_3. The solution is evaporated to dryness. This residue is dissolved in 1 ml of a solution of 75% CH_3OH - 10% 8M CH_3COOH - 10% 5M HNO_3 - 5% H_2O (solution 1) and loaded onto a preconditioned anion exchange column containing 3 ml Bio-Rad AG1 x 8 200 - 400 mesh resin encased in a thermostatically controlled water jacket set at 25°C. After washing in twice with 1 ml of solution 1, 13 ml of solution 1 is eluted and Sm collected in the next 19 ml. (If Sm is not required then 32 ml of solution 1 is eluted). The water temperature is increased to 35°C, and the column eluted with 15 ml of a solution of 75% CH_3OH - 10% 8M CH_3COOH - 5% 5MHNO_3 - 10% H_2O (solution 2). The following 29 ml containing the Nd fraction are then collected and evaporated to dryness.

(d) REE Chemistry

Dissolutions for REE are the same as described above for Sm and Nd, but the final residue is dissolved in 1 ml 90% CH_3COOH - 10% 5M HNO_3. This is loaded onto a preconditioned anion exchange column containing 4 ml Bio-Rad AG1 x 8 200 - 400 mesh resin, and washed in twice with 1 ml of the solution. After eluting 35 ml the REE are stripped off with 10 ml 0.05M HNO_3 and evaporated to dryness. The residue is dissolved in 1 ml 90% CH_3OH - 10% 5M HNO_3 (solution 3) and loaded onto a preconditioned anion exchange column containing 3 ml Bio-Rad AG1 x 8 200 - 400 mesh resin. The sample is washed in twice with 1 ml of solution 3, and a further 3 ml are eluted. Dy, Er and Yb (HREE) are collected with the next 8 ml of solution 3. Nd, Sm, Eu and Gd (LREE) are collected by eluting 15 ml of 90% CH_3OH - 10% 0.01M HNO_3

(solution 4); a further elution of 3 ml 1.5M HNO_3 yields La and Ce.

(e) Spiking

The following spikes were used in this study for Sm, Nd and REE concentrations:

		96.66%	^{149}Sm		
		84.10%	^{145}Nd		
92.77%	^{139}La	89.67%	^{145}Nd	90.41%	^{161}Dy
92.11%	^{142}Ce	98.98%	^{149}Sm	91.54%	^{167}Er
		96.83%	^{151}Eu	95.97%	^{171}Yb
		91.61%	^{155}Gd		

Samples are weighed out on a 0.01 mg balance, and 1 - 2 drops of spike are added and weighed. Chemical separations are then performed as previously described.

(f) Mass spectrometry

The Sr fraction from the chemical separation is dissolved in about 0.5 ml H_2O and loaded onto a single outgassed Ta filament on which about 1 µl of 1M H_3PO_4 has been placed. A current is passed through the filament to dry the solution and when the sample is loaded the current is increased until the H_3PO_4 fumes off and the filament glows dull red. Sm concentrations, the LREE and La/Ce fractions are loaded in a similar manner. Nd fractions for isotopic abundance are dissolved in a small drop of H_2O on the Ta side filaments of an

outgassed triple filament assemblage with a Re centre filament. The sample is dried out very carefully, and the side filaments positioned orthogonally to the centre filament. Nd concentrations and the HREE fractions are loaded likewise.

The loaded filaments are placed in a six position turret in a Vacuum Generators Isomass 54E mass spectrometer. Sr and Nd isotopic abundances and Sm and Nd concentrations are run automatically by software developed by D.W. Wright and P.W.C. van Calsteren using a HP9845T computer. The REE are run semiautomatically. All analyses are performed at 10^{-7} torr and an accelerating potential of 8kV.

(g) Sr isotope abundance

Sr beams are managed to give an intensity 15pA at a filament current of 2.5A. The measuring cycle is: 88, 87, 86, 86.5, 85, 84. The 85 peak is eliminated when the Rb contribution to the 87 peak is 0.01%, and the 84 peak after the first set. All peaks are counted for four periods of 1.28 seconds after which the magnet is stepped to the next position. The intensities are calculated using a double interpolation algorithm (Dodson, 1978) corrected for zero, dynamic memory, and Rb interference if necessary. The $^{87}Sr/^{86}Sr$ ratio is corrected for mass fractionation assuming that the fractionation is linearly dependent on mass difference, and that $^{86}Sr/^{88}Sr = 0.1194$. Ratios are stored in sets of 10, the mean and the error are calculated and ratios are rejected that do not satisfy Chauvenet's criterion. If the total error for the set is still 100 ppm the whole set is rejected; if the error is 500 ppm the whole set is ignored. Chauvenet's criterion is tested again

for all stored ratios including the rejected ones, but not the ignored sets, to form a running mean. The run is terminated when at least 100 ratios are accumulated and the error is 20 ppm (1 σ). The NBS 987 standard gives $^{87}Sr/^{86}Sr = 0.71015 \pm 4$.

(h) Nd isotopic abundance

Instrumentation and software are the same as for Sr isotopic abundances given above. Nd beams are managed to give an intensity of about 7pA with a centre filament current of 3.9A and side filament currents of 2.0A. The measuring cycle is: 146, 144, 143, 142.5, 142, 147. The 147 peak is eliminated when the Sm contribution to the 144 peak is 0.01%. The $^{143}Nd/^{144}Nd$ ratio is corrected for mass fractionation assuming $^{146}Nd/^{144}Nd = 0.7219$. A run is terminated when at least 200 ratios are accumulated and the error is 10 ppm (1σ). BCR-1 gives $^{143}Nd/^{144}Nd = 0.512620 \pm 20$.

(i) Nd concentration

Nd concentrations are determined as above but the 145 peak is included to give a measuring cycle of: 146, 144, 143, 142.5, 142, 145, 147. Run termination conditions are the same as for Sr.

(j) Sm concentration

Sm beams are managed to give an intensity of about 3 pA at a filament current of 2.6A. The measuring cycle is: 149, 148, 147, 146.5, 146, 145. Run termination conditions are the same as for Sr.

(k) REE concentrations

Dy, Er and Yb beams are obtained with a centre filament current of 3.9A and side filament currents of about 1.8, 2.2 and 2.4A respectively. Eu, Sm, Nd and Gd beams are optimised with filament currents of about 1.3, 2.5, 2.7 and 2.9A respectively. Ce and La beams are obtained with filament currents of 2.4 and 2.6A. The computer program automatically corrects for input Sm, Nd and Ce interferences where necessary.

(1) Data Representation

All the isotopic data in this study (both original and quoted) has been normalised to the following values:

$^{86}Sr/^{88}Sr = 0.1194$

NBS 987: $^{87}Sr/^{86}Sr = 0.71022$ (= E. & A. $^{87}Sr/^{86}Sr = 0.70800$)

$^{146}Nd/^{144}Nd = 0.7219$

BCR-1 : $^{143}Nd/^{144}Nd = 0.51265$

The ε notation of DePaolo and Wasserburg (1976a) has been utilised for representation of isotopic data at any time (t) relative to a uniform reservoir (UR) at the same time. For Nd analyses the UR is assumed to be chondritic (CHUR).

$$\varepsilon_{Nd} = \left[\frac{(^{143}Nd/^{144}Nd)_{sample}^{(T)}}{(^{143}Nd/^{144}Nd)_{CHUR}^{(T)}} - 1 \right] \times 10^4$$

$$\varepsilon_{Sr} = \left[\frac{(^{87}Sr/^{86}Sr)_{sample}^{(T)}}{(^{87}Sr/^{86}Sr)_{UR}^{(T)}} - 1 \right] \times 10^4$$

Two types of Nd model ages - T^{CHUR}_{Nd} and T^{DM}_{Nd} - are used: T^{CHUR}_{Nd} represents the time elapsed since a rock last had

a Nd isotope ratio the same as CHUR given its present Sm/Nd ratio. T^{DM}_{Nd} is the analogous time since derivation from a depleted mantle reservoir. These parameters are calculated using:

$$T^{CHUR}_{Nd} = \frac{1}{\lambda} \ln \left[\left[\frac{(^{143}Nd/^{144}Nd)_{sample} - (^{143}Nd/^{144}Nd)_{CHUR}}{(^{147}Sm/^{144}Nd)_{sample} - (^{147}Sm/^{144}Nd)_{CHUR}} \right] + 1 \right]$$

$$T^{DM}_{Nd} = \frac{1}{\lambda} \ln \left[\left[\frac{(^{143}Nd/^{144}Nd)_{sample} - (^{143}Nd/^{144}Nd)_{DM}}{(^{147}Sm/^{144}Nd)_{sample} - (^{147}Sm/^{144}Nd)_{DM}} \right] + 1 \right]$$

Where: $\lambda^{147}Sm = 6.54 \times 10^{-12} a^{-1}$

$(^{143}Nd/^{144}Nd)_{CHUR} = 0.51264$

$(^{147}Sm/^{144}Nd)_{CHUR} = 0.1967$

$(^{143}Nd/^{144}Nd)_{DM} = 0.51310$

$(^{147}Sm/^{144}Nd)_{DM} = 0.2238$

$\lambda^{87}Rb = 1.42 \times 10^{-11} a^{-1}$

$(^{87}Sr/^{86}Sr)_{UR} = 0.7047$

$(^{87}Rb/^{86}Sr)_{UR} = 0.0847$

(m) Isochron calculations

The data for the isochron calculations were processed by a computer program written by D.W. Wright using the least squares approximation method of York (1969). 2σ blanket errors for Rb/Sr were taken as 2%, and for $^{87}Sr/^{86}Sr$ as 0.04%. A regression was termed an 'errorchron' when the M.S.W.D. was greater than 5.

Appendix C

Modal Mineralogy

(a) Limon Verde Pluton

Sample	Plag.	Kspar.	Qtz.	Amph.	Biot.	Oxide	Apat.	Sph.	Microcl.	Epidote
81118	28.5	7.5	19.9	31.4	11.3	0.4	0.2	0.8	-	Tr
81121	44.2	6.5	12.7	25.3	10.3	0.9	0.1	Tr	-	-
81115	22.9	20.0	28.0	13.3	10.7	1.1	0.1	0.7	-	0.7
81015	34.4	11.3	23.1	15.8	13.2	0.3	0.2	0.4	1.3	Tr
81120	42.5	12.6	33.1	3.7	5.4	1.8	0.4	0.5	-	Tr
81013	34.0	12.2	28.8	5.8	11.9	0.6	Tr	0.8	5.7	0.2
81114	44.3	24.8	25.4	3.1	0.9	1.5	Tr	Tr	-	-
81117	36.0	18.0	33.0	1.4	7.0	1.9	0.4	0.4	1.9	-
81018	37.3	11.5	36.8	1.1	9.5	0.5	0.1	0.9	1.5	0.8
81119	16.2	23.6	51.3	0.2	3.3	0.2	Tr	0.2	5.0	Tr

The following minerals were also observed in the samples indicated

Zircon: 81121, 81120, 81013
Allanite: 81117
Perthitic textures were developed in: 81015, 81013, 81117, 81018 and 81119

(b) Jurassic Plutons

Sample	Plag.	Kspar.	Qtz.	Cpx.	Opx.	Amph.	Biot.	Oxide	Apat.	Sphene	Tourm.
(i) Gatico											
8059	65.0	2.0	6.4	15.3	8.9	-	0.7	1.7	-	-	-
8062	62.2	3.4	4.7	19.2	7.1	-	1.1	2.3	Tr	-	-
8058	64.1	2.9	5.9	17.9	5.1	-	0.7	1.9	1.5	-	-
8074	41.2	8.3	9.9	26.9	-	2.7	8.5	2.3	0.2	-	-
8054	51.6	7.7	7.5	19.1	3.8	1.3	4.5	3.1	1.4	-	-
8073	55.4	6.0	10.2	15.2	4.5	-	5.1	3.3	0.3	-	Tr
8072	20.0	42.2	21.7	3.0	-	6.5	2.9	3.5	0.3	-	-
Zircon was observed in 8072											
(ii) Tocopilla											
TOC2	51.5	12.6	8.2	20.2	-	0.7	2.3	3.6	0.4	0.5	-
TOC7	52.5	10.8	12.4	12.8	-	3.0	5.5	1.9	0.4	-	0.7
TOC4	50.4	13.4	11.3	21.8	-	-	-	2.4	0.1	0.6	-
TOC5	38.3	21.4	24.7	3.1	Tr	3.2	8.3	0.9	Tr	0.1	-
TOC6	34.9	27.6	25.0	-	-	3.6	7.1	0.2	-	-	1.6
Zircon was observed in TOC7, TOC5, TOC6											
(iii) Colupito											
81094	55.0	12.0	8.8	-	-	16.1	4.0	2.7	-	Tr	-
81095	50.3	14.2	17.7	-	-	15.5	-	2.3	Tr	-	-
81096	41.1	22.1	18.5	-	-	15.1	0.1	2.7	Tr	0.1	-
Epidote was observed in 81096											
(iv) Sierra de la Cruz											
81105	53.3	5.8	17.9	0.2	-	10.8	11.1	0.9	Tr	-	-
81110	58.1	13.4	11.2	-	-	10.3	6.9	0.1	Tr	Tr	-
81106	61.4	1.6	17.7	19.3	-	-	-	Tr	-	Tr	-
81099	30.7	23.3	27.7	-	-	11.1	6.8	0.4	Tr	-	-
Zircon was observed in 81105											

(c) Cretaceous plutons

Sample	Plag.	Kspar.	Qtz.	Cpx.	Opx.	Amph.	Biot.	Oxide	Apat.	Sphene	Tourm.
(i) Cerros de Montecristo											
81127	48.6	21.2	11.8	9.5	-	5.5	Tr	3.0	0.4	-	-
81128	54.6	16.0	14.7	7.4	-	2.2	1.5	3.6	Tr	-	-
81133	41.3	20.3	12.0	7.1	-	16.3	Tr	3.0	Tr	-	-
81129	51.5	6.4	19.4	10.5	-	3.7	6.5	2.0	Tr	-	Tr
81125	53.8	9.7	18.4	10.2	-	0.4	4.2	2.8	0.5	-	-
81126	47.3	20.2	14.8	11.0	-	-	3.7	2.7	0.2	0.1	-
81139	38.5	18.3	26.4	-	-	10.6	4.1	1.8	Tr	0.3	-
81138	38.1	21.9	22.0	-	-	10.8	3.7	3.5	Tr	-	-
81141	40.2	21.1	19.0	-	-	10.2	7.7	1.8	Tr	-	-
81140	41.4	21.5	21.8	3.7	-	4.5	6.3	0.8	Tr	-	-

The following minerals were observed in the samples indicated
Epidote: 81127, 81126
Zircon: 81129, 81139, 81138, 81141, 81140
Tourmaline: 81129

(ii) Cerritos Bayos											
81052	70.5	2.2	2.0	21.3	-	-	-	3.8	Tr	0.2	-
81047	82.6	4.7	2.3	4.1	-	-	4.6	1.6	0.1	-	-
81051	61.1	10.5	3.7	17.4	2.3	-	3.7	1.0	0.3	-	-
81048	69.5	2.3	3.3	23.1	-	-	-	1.2	0.6	Tr	-

Zircon was observed in 81051

(iii) Pampa Negra											
81091	60.8	1.0	6.3	6.9	23.6	-	-	1.4	Tr	-	-
81088	51.6	10.7	10.4	22.1	-	-	-	3.0	0.3	-	1.9
81090	43.9	11.5	10.3	27.4	-	0.4	-	2.9	0.1	-	3.5
81089	45.2	15.3	12.1	24.4	-	-	0.1	2.3	0.4	0.1	0.1

Zircon was observed in 81089

(d) El Abra pluton

Sample	Plag.	Kspar.	Qtz.	Amph.	Biot.	Oxide	Apat.	Sph.	Zirc.
800107	52.7	22.8	16.6	3.1	3.2	1.2	0.3	0.1	Tr
80106	44.3	20.1	19.8	2.6	11.2	1.4	0.3	0.3	Tr
80101	42.2	20.4	21.3	6.2	7.7	2.2	Tr	-	Tr
80104	47.6	18.1	21.9	6.3	4.1	1.0	0.7	0.3	Tr
80108	46.2	20.6	22.6	4.1	4.0	2.1	0.2	0.2	Tr
80105	46.1	20.3	23.3	3.2	4.8	1.2	0.7	0.4	Tr
80103	17.2	48.5	33.9	-	0.3	0.1	Tr	-	-

Appendix D
Whole rock XRF data

	Limon Verde Schists				Cerro Crespo Formation				
Sample	81011	81150	81151	81152	81041	81042	81043	81045	81095
SiO_2	73.93	40.08	66.82	53.32	74.38	70.82	79.95	75.17	79.67
TiO_2	1.12	3.15	1.44	1.54	0.24	0.50	0.15	0.26	0.13
Al_2O_3	7.96	15.41	10.07	12.57	12.77	13.20	10.07	13.44	12.08
Fe_2O_3	8.92	16.78	11.15	10.28	2.33	3.13	1.89	2.25	1.25
MnO	0.86	0.64	0.35	0.17	0.13	0.18	0.07	0.03	0.04
MgO	2.90	6.32	4.77	9.91	0.20	0.19	0.17	n.d.	0.15
CaO	2.14	11.34	2.53	6.37	2.23	2.28	0.59	0.37	0.10
Na_2O	0.01	2.01	0.18	2.19	4.45	5.20	5.52	4.13	2.48
K_2O	1.32	0.42	2.47	1.74	1.78	2.18	0.13	4.00	3.01
P_2O_5	0.21	0.73	0.51	0.16	0.08	0.10	n.d.	n.d.	0.02
LOI	0.44	1.37	0.66	1.80	2.67	2.28	1.27	1.14	1.63
Total	99.82	98.60	100.96	99.97	101.26	100.03	99.80	100.78	100.55
Rb	57.1	7.5	118.5	75.4	50.7	53.3	3.9	96.0	96.4
Sr	14.6	166.7	21.8	74.9	69.5	134.2	165.3	47.1	104.4
Ba	694	98	-	398	178	4122	3537	552	514
Y	32	74	54	29	51	30	44	49	55
Zr	146	235	268	148	191	210	230	211	171
Nb	15	266	22	21	14	11	17	17	15
V	154	401	-	20	18	24	7	15	2
Cr	226	46	-	563	4	8	8	25	105
Ni	105	58	124	329	1	n.d.	5	1	6
Co	36	59	-	44	3	4	n.d.	2	n.d.

Limon Verde Pluton

Sample	81113	81114	81115	81117	81118	81119	81120	81121	81012	81015	81018
SiO_2	67.23	68.48	59.64	68.84	52.57	75.05	65.98	55.49	68.36	63.20	69.80
TiO_2	0.52	0.40	0.78	0.47	0.94	0.29	0.65	0.71	0.51	0.59	0.35
Al_2O_3	16.70	15.28	15.66	15.22	15.62	13.76	16.53	16.79	15.78	15.65	15.71
Fe_2O_3	3.79	3.21	7.77	3.98	9.92	0.85	4.33	8.46	3.96	5.49	2.69
MnO	0.11	0.07	0.17	0.08	0.25	0.04	0.08	0.17	0.09	0.13	0.06
MgO	0.95	0.57	3.36	0.64	5.85	0.43	1.49	5.23	1.58	3.85	1.26
CaO	2.68	2.18	6.19	2.42	7.95	2.85	3.63	7.44	4.08	5.49	3.09
Na_2O	5.91	5.83	3.74	5.19	2.85	5.02	4.45	3.09	4.05	3.57	3.42
K_2O	2.11	2.15	1.31	1.29	1.43	1.01	2.61	1.39	2.04	2.02	3.44
P_2O_5	0.11	0.09	0.15	0.08	0.18	0.04	0.17	0.15	0.12	0.12	0.12
LOI	1.06	1.21	1.10	0.73	1.30	0.50	1.41	1.74	0.81	1.24	1.12
Total	101.17	99.47	99.88	98.93	98.87	99.83	101.34	100.65	101.38	101.35	101.04
Rb	56.9	51.8	47.7	34.3	43.3	20.3	70.8	67.2	81.3	96.0	82.6
Sr	270.3	194.4	367.1	256.1	337.0	238.0	371.8	367.9	319.9	294.9	451.3
Ba	853	851	393	490	360	228	1267	297	582	298	915
Y	37	36	37	27	48	21	20	26	19	30	17
Zr	412	335	124	382	88	176	205	96	149	76	108
Nb	14	14	10	12	11	11	11	9	9	10	11
V	25	14	172	15	220	13	68	187	66	111	41
Cr	9	23	48	21	154	22	11	112	34	28	18
Ni	n.d.	1	10	n.d.	21	n.d.	n.d.	20	11	22	1
Co	5	4	20	6	31	n.d.	9	28	15	19	2

	Aqua Dulce Formation		La Negra Formation							
Sample	81004	81006	8077	8078	8079	8080	8081	8088	8087	8086
SiO_2	73.55	74.11	54.01	52.00	51.62	51.50	52.70	53.81	53.03	53.10
TiO_2	0.38	0.34	1.69	1.69	1.92	1.75	1.41	1.10	1.47	1.36
Al_2O_3	13.78	13.74	14.72	13.73	13.49	14.17	16.87	17.49	14.80	16.31
Fe_2O_3	2.48	2.26	11.59	12.90	12.56	11.46	8.56	9.12	11.50	10.46
MnO	0.02	0.02	0.39	0.41	0.33	0.40	9.38	0.15	0.33	0.15
MgO	1.11	0.48	3.16	4.40	4.13	3.91	3.69	3.38	3.91	3.16
CaO	0.43	0.88	5.42	6.00	6.59	6.71	6.40	8.30	6.88	7.01
Na_2O	3.99	5.44	3.95	3.79	3.15	4.17	3.73	3.67	3.71	3.88
K_2O	1.29	2.18	2.53	2.38	3.03	2.62	2.83	1.73	2.12	2.02
P_2O_5	n.d.	0.04	0.51	0.44	0.55	0.43	0.24	0.33	0.21	0.35
LOI	3.13	1.83	1.70	2.14	1.73	1.60	1.91	1.21	1.20	1.55
Total	100.15	101.31	99.67	99.88	99.10	98.72	98.71	100.02	99.15	99.35
Rb	47.2	44.7	91.2	84.5	113.6	108.6	130.1	48.1	77.5	59.3
Sr	89.9	94.9	235.2	178.8	212.8	217.0	310.3	402.0	247.5	317.7
Ba	-	-	521	475	525	517	464	385	297	381
Y	24	38	48	49	49	49	37	34	40	39
Zr	180	285	249	216	246	225	202	165	195	180
Nb	9	10	8	8	8	8	9	6	8	7
V	-	-	308	401	390	350	254	277	358	308
Cr	-	-	26	47	40	41	55	41	50	38
Ni	11	4	9	11	12	12	30	10	17	11
Co	-	-	23	32	32	28	24	24	32	25

La Negra Formation (continued)

Sample	8085	8084	8083	8082	8091	8092	8092A	8093	8097	8098
SiO_2	54.03	53.52	53.16	55.57	53.96	53.43	54.93	55.28	52.36	59.12
TiO_2	1.34	1.62	1.23	1.19	1.40	1.33	1.54	1.39	1.42	1.48
Al_2O_3	15.31	14.36	15.34	15.13	15.59	16.72	14.73	15.31	14.58	13.51
Fe_2O_3	10.54	11.58	10.03	9.31	10.89	9.72	10.75	10.31	11.70	10.59
MnO	0.26	0.25	0.31	0.21	0.43	0.49	0.41	0.39	0.30	0.28
MgO	4.01	3.78	4.57	4.62	4.56	3.38	3.73	3.31	2.98	2.17
CaO	6.96	6.73	6.64	7.15	5.14	5.70	4.22	4.31	4.75	3.70
Na_2O	3.23	3.73	3.49	3.39	3.78	4.06	3.49	4.03	4.06	4.45
K_2O	2.39	2.33	2.61	2.21	2.86	3.39	2.53	3.35	2.01	1.31
P_2O_5	0.29	0.36	0.25	0.30	0.36	0.31	0.41	0.41	0.37	0.46
LOI	1.42	1.15	1.72	1.40	2.13	2.03	2.34	1.92	4.79	3.94
Total	99.79	99.05	99.35	100.47	101.20	100.56	99.08	100.01	99.32	101.00
Rb	75.4	83.7	86.8	72.4	125.4	147.0	90.8	125.7	94.7	65.1
Sr	266.0	241.3	257.6	248.3	224.8	301.0	229.5	206.9	241.5	195.4
Ba	319	338	339	250	523	908	454	502	1649	490
Y	41	43	38	40	35	36	49	42	44	55
Zr	214	225	192	204	200	194	275	267	230	310
Nb	7	8	8	7	7	7	8	8	8	10
V	300	357	267	208	351	296	277	250	303	242
Cr	88	48	97	80	52	35	28	29	55	19
Ni	30	17	28	16	22	13	7	8	21	13
Co	32	29	32	26	27	24	21	23	32	22

Gatico Pluton

Sample	8054	8058	8059	8062	8066	8067	8072	8073	8074
SiO_2	55.63	54.19	53.10	53.61	60.72	58.46	64.98	55.98	54.75
TiO_2	1.06	0.67	0.66	0.71	1.24	0.94	1.07	1.11	1.06
Al_2O_3	15.08	16.76	17.51	17.38	13.86	15.81	14.39	15.92	15.41
Fe_2O_3	10.44	8.76	9.56	8.31	8.14	7.83	6.96	9.87	9.94
MnO	0.20	0.16	0.15	0.15	0.07	0.07	0.11	0.16	0.13
MgO	4.15	5.68	5.57	4.85	2.81	3.73	1.65	4.22	3.91
CaO	7.69	9.26	10.07	9.53	5.01	6.39	3.84	7.87	7.71
Na_2O	4.23	3.72	3.32	2.91	5.06	4.13	3.61	3.65	3.43
K_2O	1.25	0.96	0.69	0.88	0.72	2.18	3.71	1.47	1.43
P_2O_5	0.19	0.10	0.10	0.07	0.31	0.28	0.38	0.23	0.17
LOI	0.14	0.40	0.27	0.22	1.21	1.15	0.40	0.07	1.06
Total	100.06	100.66	100.00	98.62	99.15	100.97	101.10	100.55	99.00
Rb	33.4	25.3	16.4	21.0	20.6	62.4	120.4	47.7	48.7
Sr	294.8	315.8	342.8	327.1	239.3	292.3	159.8	279.1	283.7
Ba	299	226	175	225	79	357	448	273	255
Y	37.	25	20	21	49	38	49	36	31
Zr	96	47	67	80	237	143	152	135	65
Nb	5	6	5	4	9	6	10	7	5
V	216	154	200	186	189	158	107	231	232
Cr	65	127	126	84	49	68	12	72	68
Ni	14	22	20	16	10	17	8	14	16
Co	29	28	30	29	20	19	13	23	29

Tocopilla Pluton

Sample	81075	81076	81077	81078	81079	81080	TOC1	TOC2	TOC3	TOC4	TOC5	TOC6	TOC7
SiO_2	65.3	63.00	58.58	60.00	59.83	55.71	57.54	56.68	67.74	58.51	65.30	67.80	57.50
TiO_2	0.61	1.03	0.83	0.88	0.96	0.98	1.01	1.02	0.75	0.98	0.70	0.38	1.02
Al_2O_3	16.05	14.75	16.11	15.99	14.94	15.84	15.14	16.15	15.14	15.84	15.51	15.58	15.47
Fe_2O_3	3.45	6.96	7.26	7.20	7.32	9.78	8.69	8.16	3.20	6.34	5.43	3.84	9.57
MnO	0.04	0.10	0.12	0.16	0.15	0.16	0.10	0.10	0.03	0.08	0.08	0.08	0.16
MgO	2.00	1.87	3.30	3.16	3.31	4.23	3.25	3.31	1.76	3.74	2.14	1.27	3.88
CaO	4.56	3.68	5.25	3.81	4.35	6.89	5.60	7.04	3.97	8.11	3.94	3.68	7.09
Na_2O	5.13	3.72	4.17	4.89	3.65	2.95	3.65	4.27	7.63	5.31	4.06	4.17	3.40
K_2O	2.26	3.99	2.40	2.84	3.51	1.89	2.43	1.51	0.22	0.42	3.11	2.68	1.98
P_2O_5	0.10	0.30	0.20	0.16	0.16	0.23	0.23	0.25	0.20	0.27	0.17	0.09	0.18
LOI	1.00	1.08	1.62	1.65	1.65	1.59	1.15	0.93	0.64	1.09	0.73	0.95	0.23
Total	100.59	100.49	99.85	100.74	99.82	100.25	99.77	99.41	101.26	100.69	101.17	100.52	100.48
Rb	44.0	154.4	74.3	99.1	138.2	71.7	107.6	45.6	10.8	19.3	140.4	174.7	93.9
Sr	323.0	198.8	274.0	219.0	210.0	318.3	290.2	418.7	160.8	375.3	215.9	292.0	309.3
Ba	446	541	339	393	457	310	353	362	25	111	495	390	311
Y	20	47	28	27	36	32	33	34	30	36	27	18	29
Zr	160	314	172	196	249	112	189	106	258	131	185	107	138
Nb	6	1	6	7	8	7	4	3	6	6	6	5	6
V	99	99	153	161	148	248	214	216	197	221	84	73	269
Cr	24	15	36	30	43	32	34	59	37	44	36	16	47
Ni	4	8	12	9	11	12	13	16	12	18	13	10	15
Co	9	17	21	20	23	28	25	18	4	14	15	8	26

	Sierra de la Cruz Pluton					Cerro Colupito Pluton		
Sample	81099	81105	81106	81110	81111	81094	81095	81096
SiO_2	67.62	62.67	64.70	63.35	76.93	58.63	59.69	61.15
TiO_2	0.77	0.72	0.68	0.60	0.17	0.76	0.77	0.77
Al_2O_3	14.51	16.81	17.79	17.79	13.09	16.45	16.54	16.37
Fe_2O_3	5.01	5.54	1.02	4.41	1.12	7.70	6.83	6.67
MnO	0.07	0.08	0.02	0.08	0.01	0.17	0.11	0.14
MgO	1.96	2.73	2.16	2.05	0.27	3.08	3.27	2.66
CaO	3.63	5.44	7.65	5.10	0.85	6.18	5.83	5.52
Na_2O	3.70	4.08	5.54	4.80	3.23	3.56	4.27	3.62
K_2O	3.16	1.72	0.42	1.98	4.97	2.69	2.48	2.69
P_2O_5	n.d.	0.14	0.14	0.14	0.06	0.17	0.14	0.14
LOI	0.68	0.61	0.45	0.69	0.41	0.99	0.82	0.91
Total	101.10	100.64	100.57	100.98	101.10	100.38	100.75	100.63
Rb	135.0	42.8	4.9	71.0	164.0	79.6	53.0	72.2
Sr	196.9	378.4	468.7	346.1	82.9	336.1	340.5	315.4
Ba	275	264	127	233	241	440	354	394
Y	34	27	24	28	27	30	31	33
Zr	300	134	136	184	100	155	174	177
Nb	10	9	6	7	8	6	5	6
V	105	100	81	88	18	173	178	145
Cr	30	37	27	40	19	21	18	36
Ni	13	18	8	17	3	4	7	5
Co	16	20	3	15	4	21	14	17

Indio Muerto Formation

Sample	81053A	81054	81055	81056	80201	80202	80204	80205
SiO_2	65.88	67.88	57.99	53.84	66.12	55.88	60.32	51.66
TiO_2	0.51	0.65	1.11	1.72	0.62	1.43	1.18	1.45
Al_2O_3	16.36	14.75	17.18	17.30	14.50	15.96	15.96	16.46
Fe_2O_3	3.39	4.41	7.20	9.43	4.43	9.25	6.54	10.21
MnO	0.04	0.07	0.12	0.16	0.09	0.17	0.13	0.18
MgO	1.57	1.05	1.94	3.37	1.15	3.39	2.47	4.34
CaO	3.55	1.02	4.88	7.26	2.67	6.15	4.23	7.40
Na_2O	4.42	4.79	4.46	4.08	4.00	3.51	4.33	3.14
K_2O	2.99	4.61	2.57	1.70	4.53	2.82	3.03	1.32
P_2O_5	0.12	0.08	0.36	0.30	0.12	0.40	0.31	0.35
LOI	1.02	2.06	1.94	1.41	1.57	1.55	1.90	2.49
Total	99.85	101.37	99.75	100.57	99.79	100.52	100.40	99.00
Rb	269.7	50.7	70.8	44.7	244.7	103.1	104.0	39.5
Sr	224.9	623.6	452.6	494.5	352.2	350.4	354.7	433.2
Ba	931	699	755	674	871	880	792	752
Y	49	12	42	33	45	50	50	41
Zr	424	119	210	161	430	346	330	215
Nb	18	7	14	12	17	17	18	12
V	55	51	87	267	48	116	156	232
Cr	14	12	9	32	21	22	35	46
Ni	8	n.d.	n.d.	n.d.	10	5	14	22
Co	10	9	8	16	7	14	22	29

Augusta Victoria Formation

Sample	81130	81131	81132	81134	81135	81136	81137
SiO_2	53.29	55.34	53.50	50.50	58.05	53.23	52.14
TiO_2	0.93	0.77	1.08	1.40	1.11	1.50	1.44
Al_2O_3	17.25	16.80	17.09	17.68	16.45	17.09	17.97
Fe_2O_3	7.96	6.55	7.64	9.37	7.35	9.89	9.44
MnO	0.27	0.09	0.18	0.24	0.19	0.16	0.09
MgO	4.08	1.55	3.02	5.64	2.70	3.95	4.63
CaO	5.87	4.35	4.50	9.34	5.68	8.06	9.13
Na_2O	5.73	6.28	5.14	2.50	2.96	3.43	3.02
K_2O	2.48	3.84	3.63	0.49	2.91	1.08	0.93
P_2O_5	0.54	0.40	0.46	0.38	0.33	0.35	0.35
LOI	2.40	4.03	3.35	3.19	2.40	1.09	1.32
Total	100.80	100.02	99.59	100.73	100.12	99.83	100.46
Rb	59.3	104.8	110.7	10.5	87.5	36.5	32.2
Sr	829.3	145.2	492.3	445.2	349.5	363.2	481.1
Ba	1690	1643	1348	233	541	380	172
Y	26	14	20	33	39	45	29
Zr	227	224	212	162	283	242	187
Nb	24	30	32	13	15	12	14
V	177	104	176	262	152	228	212
Cr	45	16	33	62	60	25	62
Ni	19	6	16	28	11	7	13
Co	16	7	24	24	16	20	25

Cerritos Bayos Pluton

Sample	81038	81039	81040	81046	81047	81048	81049	81051	81052	81053
SiO_2	66.28	73.19	69.04	65.02	53.22	55.56	64.25	54.61	52.34	54.76
TiO_2	0.91	0.16	0.20	0.98	1.31	1.34	1.01	1.21	1.42	1.46
Al_2O_3	15.28	15.21	15.70	14.93	19.01	17.41	15.65	17.08	17.47	14.80
Fe_2O_3	5.07	0.03	1.85	4.77	8.47	3.97	1.52	8.40	7.79	2.39
MnO	0.05	n.d.	0.01	0.06	0.13	0.14	0.07	0.12	0.11	0.07
MgO	0.89	n.d.	0.26	1.19	3.58	5.14	2.76	4.44	5.38	6.34
CaO	2.85	1.55	1.22	2.78	8.65	11.38	8.43	8.02	9.93	13.02
Na_2O	4.22	7.95	5.36	3.27	3.44	4.10	5.09	3.58	4.44	4.17
K_2O	4.57	0.04	4.65	5.21	1.09	0.68	0.44	1.72	0.53	0.82
P_2O_5	0.24	n.d.	0.11	0.26	0.20	0.26	0.26	0.18	0.37	n.d.
LOI	0.64	2.33	1.42	1.36	0.30	0.80	0.72	0.11	1.09	1.28
Total	101.00	101.46	99.80	99.81	99.39	100.78	100.19	99.47	100.86	99.13
Rb	158.7	n.d.	81.6	151.9	29.6	14.0	9.5	62.8	16.4	26.4
Sr	362.3	308.1	390.1	316.6	546.4	553.3	516.9	454.6	667.7	492.6
Ba	750	41	1100	977	451	254	152	453	181	210
Y	43	12	14	52	22	30	47	27	32	25
Zr	289	120	126	357	91	141	313	168	70	134
Nb	17	11	10	20	7	10	14	9	9	9
V	48	9	17	54	261	210	109	220	224	216
Cr	13	9	27	17	78	83	43	71	108	107
Ni	4	n.d.	n.d.	4	13	10	4	17	13	5
Co	9	n.d.	3	8	27	9	6	27	13	7

Cerros de Montecristo Pluton

Sample	81125	81126	81127	81128	81129	81133	81138	81139	81141	81140
SiO_2	60.81	62.47	58.81	59.46	60.32	60.29	64.20	64.18	65.57	65.84
TiO_2	0.72	0.76	0.89	0.82	0.86	1.40	0.80	0.75	0.71	0.68
Al_2O_3	16.83	16.44	16.69	16.86	16.77	17.68	15.73	15.22	15.50	15.19
Fe_2O_3	6.10	5.62	6.67	6.38	6.27	6.59	5.57	5.17	4.86	4.68
MnO	0.10	0.08	0.10	0.10	0.10	0.11	0.09	0.11	0.08	0.08
MgO	2.84	2.37	3.44	2.88	3.02	2.97	2.10	1.72	2.08	2.06
CaO	5.61	4.71	5.97	5.56	5.56	5.43	3.98	3.72	3.86	3.69
Na_2O	3.75	3.80	3.62	3.56	3.49	4.17	3.99	3.61	3.55	3.59
K_2O	2.81	3.57	2.75	2.82	2.95	2.87	3.78	4.00	3.93	3.94
P_2O_5	0.14	0.18	0.19	0.21	0.20	0.20	0.18	0.13	0.19	0.18
LOI	0.37	1.06	0.90	1.09	0.52	0.98	0.89	1.06	0.78	0.63
Total	100.08	101.06	100.01	99.73	100.06	100.76	101.40	99.67	101.12	100.56
Rb	102.8	140.0	109.9	106.2	119.2	119.2	164.8	162.9	179.8	194.7
Sr	549.3	579.5	520.2	535.3	528.7	491.9	298.5	291.8	298.5	263.9
Ba	654	735	641	614	645	637	601	696	556	587
Y	23	25	23	22	22	119	36	33	25	26
Zr	147	231	185	191	207	217	300	322	255	250
Nb	11	12	12	11	12	8	14	17	12	13
V	117	97	140	138	144	128	101	87	86	80
Cr	23	31	31	41	57	30	22	30	55	34
Ni	9	8	13	16	21	19	8	8	8	8
Co	22	14	19	21	17	16	12	13	14	9

	Pampa Negra Pluton				Cerro Colorado Pluton[a]		
Sample	81088	81089	81090	81091	80173	80176	80180
SiO_2	55.41	58.24	5547	53.09	57.91	63.46	54.14
TiO_2	1.24	1.12	1.28	0.87	0.82	0.39	0.69
Al_2O_3	15.76	15.48	15.71	17.30	18.40	16.41	20.42
Fe_2O_3	9.35	8.17	8.69	9.12	5.84	4.06	5.86
MnO	0.15	0.17	0.15	0.15	0.16	0.11	0.13
MgO	4.12	3.32	4.09	5.29	1.32	0.70	2.06
CaO	7.15	6.21	6.65	8.88	3.55	2.36	6.51
Na_2O	2.77	3.14	3.13	2.64	3.95	4.54	3.97
K_2O	1.75	2.12	2.20	0.83	7.35	5.99	4.62
P_2O_5	0.25	0.23	0.15	0.09	0.41	0.15	0.54
LOI	1.19	1.16	1.58	0.76	0.59	1.70	0.11
Total	99.12	99.36	99.10	99.02	100.30	99.87	100.05
Rb	76.1	93.4	99.3	30.8	172.6	155.7	68.8
Sr	256.3	239.3	263.0	302.5	696.7	544.6	1223.8
Ba	364	425	373	230	752	573	870
Y	39	44	37	22	33	36	15
Zr	150	209	138	65	677	290	64
Nb	8	10	10	4	13	19	3
V	184	154	200	256	59	38	98
Cr	59	42	55	63	3	3	n.d.
Ni	16	12	16	16	n.d.	n.d.	n.d.
Co	25	22	22	33	-	-	-

a. Analyses from L.J. O'Callaghan (unpublished data)

	Cerro Negro Formation						El Abra Pluton				
Sample	81019	81020	81021	81022	81023	81025	80102	80103	80104	80106	80107
SiO_2	63.79	66.25	73.99	65.67	50.67	56.06	78.17	77.37	65.71	65.82	65.38
TiO_2	0.63	0.63	0.41	0.60	1.10	1.23	0.14	0.16	0.53	0.61	0.49
Al_2O_3	16.90	15.58	13.01	16.32	13.42	14.46	12.32	12.33	15.86	16.45	17.08
Fe_2O_3	4.21	3.62	1.88	2.52	6.41	6.62	0.65	0.78	4.23	4.15	3.68
MnO	0.04	0.09	0.02	0.03	0.08	0.09	0.02	0.01	0.08	0.05	0.06
MgO	1.63	0.50	0.18	0.69	2.66	4.09	n.d.	n.d.	1.77	1.98	1.31
CaO	4.52	5.15	2.21	3.79	11.02	7.45	0.51	0.69	3.69	3.66	4.22
Na_2O	4.00	3.29	0.33	3.25	2.94	4.22	3.28	3.10	3.69	4.22	4.86
K_2O	3.12	3.15	3.05	2.98	1.08	2.06	5.33	5.47	3.59	3.06	2.52
P_2O_5	0.13	0.22	0.12	0.17	0.42	0.47	n.d.	n.d.	0.15	0.14	0.19
LOI	0.52	1.60	5.04	3.79	9.37	2.81	0.28	0.41	0.65	0.82	0.53
Total	99.49	100.07	100.24	99.80	99.16	99.58	100.70	100.32	99.95	100.97	100.32
Rb	67.7	71.5	68.6	68.2	43.9	40.6	294.0	200.2	141.4	133.0	62.5
Sr	658.4	928.7	128.6	596.6	642.6	1541.0	41.4	93.9	486.0	505.6	748.1
Ba	736	630	593	720	415	-	67	350	765	721	808
Y	13	10	11	10	18	21	8	12	16	14	11
Zr	138	125	100	128	239	291	93	95	181	177	121
Nb	9	6	8	8	12	13	12	11	13	11	7
V	79	62	46	71	145	-	1	4	79	104	60
Cr	20	49	15	57	143	-	32	13	14	31	21
Ni	7	7	n.d.	8	58	65	5	5	10	14	13
Co	9	10	4	6	27	-	5	n.d.	13	14	12

	Upper Tertiary Volcanics						Monogenetic Centres				
Sample	A168-1	A6-2	A31-1	B43	A33-1	B5	A791[a]	7927[a]	7988[a]	80193	B1[b]
SiO_2	57.13	67.45	57.43	54.05	62.15	62.63	54.22	50.65	56.18	62.22	43.49
TiO_2	0.62	0.47	0.90	1.08	0.62	1.07	0.95	1.09	1.17	0.68	2.34
Al_2O_3	18.28	16.71	17.20	15.70	17.04	16.12	16.02	15.97	16.78	16.76	13.43
Fe_2O_3	7.39	3.07	7.32	8.52	5.40	5.40	8.46	9.33	7.94	4.93	13.19
MnO	0.17	0.04	0.10	0.12	0.10	0.07	0.13	0.14	0.10	0.08	0.18
MgO	3.85	1.43	3.84	6.22	2.09	2.33	7.66	6.26	4.61	2.62	8.95
CaO	7.27	3.75	6.65	7.37	4.85	4.25	7.88	8.20	6.95	4.89	12.30
Na_2O	4.52	5.06	3.90	3.25	3.86	4.72	3.14	3.62	3.75	3.78	3.12
K_2O	1.20	2.51	1.83	1.79	2.26	3.55	1.19	1.43	2.05	3.00	1.42
P_2O_5	0.23	0.15	0.25	0.26	0.26	0.40	0.20	0.22	0.27	0.18	0.74
LOI	0.39	0.09	0.45	0.62	1.70	0.25	0.10	2.22	0.41	1.75	-
Total	101.05	100.73	99.87	98.98	100.33	100.79	99.95	99.13	100.21	100.89	99.16
Rb	28.9	56.4	44.4	47.8	79.2	77.6	32.0	30.0	46.0	107.0	24.0
Sr	598.7	753.5	565.0	570.3	546.8	889.7	501.0	630.0	584.0	575.0	871.0
Ba	-	-	-	-	-	-	367	525	846	913	-
Y	20	8	18	24	17	16	21	31	21	21	27
Zr	125	141	161	161	201	279	115	124	156	208	190
Nb	6	5	8	11	9	21	11	11	11	10	47
V	-	-	-	-	-	-	190	213	190	81	-
Cr	-	-	-	-	-	-	120	56	35	19	-
Ni	41	13	42	79	8	17	81	28	11	9	127
Co	-	-	-	-	-	-	-	-	-	n.d.	-

a. Analyses from L.J. O'Callaghan (unpublished data)
b. Analysis from Thorpe *et al.* (1984)

Appendix E
INAA Data

	Limón Verde Schists			Cerro Crespo Formation	
Sample	81150[a]	81151[a]	81152[a]	81043	81045
La	41.8	50.8	17.8	27.3	39.4
Ce	100.0	113.0	41.9	56.5	83.0
Nd	50.8	49.3	21.0	32.2	36.6
Sm	11.8	7.82	4.61	6.3	8.2
Eu	4.06	1.98	1.26	1.10	1.39
Gd	9.05	9.61	5.20	–	–
Tb	–	–	–	1.03	1.20
Dy	12.4	9.56	4.80	–	–
Er	6.94	5.95	2.61	–	–
Tm	–	–	–	0.57	0.69
Yb	6.67	5.74	2.30	3.67	4.47
Hf	–	–	–	6.39	6.60
Ta	–	–	–	1.11	1.01
Th	–	–	–	15.40	12.75
U	–	–	–	–	–
Sc	–	–	–	6.50	9.30
Co	–	–	–	0.47	0.95

a Analysis by Isotope Dilution

Limón Verde Pluton

Sample	81013	81015	81018	81114	81115	81118	81120
La	24.9	11.1	5.9	30.8	20.7	19.3	26.0
Ce	46.0	26.7	14.5	64.6	48.0	57.7	52.0
Nd	17.5	16.9	10.7	33.1	26.4	36.0	22.0
Sm	3.4	3.9	2.8	7.1	6.1	7.9	4.3
Eu	0.90	0.90	0.84	2.33	1.42	2.13	1.47
Gd	-	-	-	-	-	-	-
Tb	0.51	0.68	0.40	1.05	0.95	1.25	0.57
Tm	0.31	0.39	0.19	0.54	0.52	0.75	0.28
Yb	2.03	2.83	1.25	3.59	3.30	4.86	1.71
Hf	4.65	2.99	3.12	9.59	3.72	3.16	6.51
Ta	0.31	0.26	0.83	0.70	0.84	0.62	0.42
Th	12.59	6.85	3.03	6.66	7.20	2.38	3.17
U	2.3	2.1	1.7	2.1	1.9	-	0.8
Sc	9.4	20.0	6.0	14.6	31.1	39.5	11.7
Co	10.0	20.1	5.9	2.2	19.7	30.3	7.3

La Negra Formation

Sample	8077	8080	8088	8086	8084	8092	8092A	8097	8098
La	23.0	24.6	16.4	18.5	18.1	19.0	24.0	18.5	27.9
Ce	59.4	62.2	40.0	44.0	46.0	44.0	59.0	46.0	65.5
Nd	35.6	38.6	25.4	26.8	-	28.6	37.9	30.0	39.2
Sm	9.0	9.3	5.8	6.7	7.2	6.7	8.7	7.7	9.8
Eu	1.91	2.32	1.60	1.79	1.80	1.81	2.15	1.82	2.29
Gd	-	-	-	-	-	-	-	-	-
Tb	1.47	1.46	0.87	1.03	1.17	1.01	1.35	1.20	1.53
Tm	0.79	0.74	0.45	0.54	0.61	0.52	0.74	0.62	0.77
Yb	4.64	4.54	2.86	3.40	3.98	3.15	4.40	3.94	4.93
Hf	6.90	6.28	4.23	4.80	5.70	4.75	6.69	6.19	8.12
Ta	0.41	0.39	0.23	0.25	0.39	0.32	0.46	0.38	0.52
Th	7.76	6.38	4.79	5.41	6.66	5.36	7.40	7.30	10.50
U	-	-	-	-	-	-	-	1.8	2.5
Sc	32.6	38.9	27.6	28.4	35.3	28.7	27.8	9.8	31.0
Co	24.4	27.1	21.0	23.1	24.0	21.5	19.4	29.7	19.1

	Gatico Pluton					Sierra de la Cruz	
Sample	8054	8058	8059	8062	8073	81105	81106
La	13.6	8.5	5.7	7.4	14.8	15.5	9.7
Ce	30.9	20.8	13.7	16.0	35.0	34.0	26.1
Nd	-	-	-	-	-	16.9	15.4
Sm	5.6	3.8	2.5	3.0	5.2	3.8	3.3
Eu	1.84	1.21	0.97	1.16	1.45	1.02	1.02
Gd	-	-	-	-	-	-	-
Tb	0.97	0.69	0.47	0.53	0.89	0.61	0.49
Tm	0.51	0.43	0.27	0.33	0.49	0.32	0.29
Yb	3.55	2.67	1.87	2.10	3.23	2.00	1.88
Hf	3.73	1.53	1.75	2.09	4.40	4.04	4.19
Ta	0.16	0.13	0.08	0.11	0.24	0.39	0.40
Th	3.31	2.39	1.73	1.81	4.55	5.40	6.24
U	-	-	-	-	-	0.9	2.1
Sc	35.7	34.3	35.6	31.7	32.6	13.5	13.4
Co	25.0	27.6	28.4	25.0	26.0	15.8	2.3

	Tocopilla Pluton					Cerro Colupito
Sample	81075	81076	81078	TOC4	TOC6	81094
La	10.4	34.2	20.4	14.5	17.6	14.8
Ce	20.4	74.1	44.6	37.4	38.0	34.3
Nd	11.9	42.0	24.1	23.0	17.5	19.4
Sm	3.0	9.2	5.6	5.5	3.7	4.7
Eu	0.84	1.76	1.24	1.12	0.69	1.07
Gd	-	-	-	-	-	-
Tb	0.45	1.24	0.83	0.83	0.53	0.72
Tm	0.25	0.69	0.43	0.48	0.32	0.42
Yb	1.66	4.10	2.62	2.88	2.06	2.68
Hf	4.69	8.86	5.40	4.57	2.77	4.78
Ta	0.37	0.68	0.43	0.36	0.39	0.35
Th	10.42	15.50	10.51	11.92	16.12	8.42
U	2.3	4.4	2.9	2.5	3.6	2.4
Sc	13.2	16.8	20.4	27.8	9.8	25.9
Co	6.7	13.1	18.1	11.6	8.2	19.1

Indio Muerto Formation

Sample	81053A	81054	81055	81056	80204[a]	80205[a]
La	37.5	16.7	31.0	25.1	33.8	23.9
Ce	81.0	32.4	67.0	51.0	76.4	52.7
Nd	36.2	15.2	31.7	28.0	38.5	28.0
Sm	7.7	2.8	6.9	5.5	8.34	6.27
Eu	1.15	0.86	1.96	1.74	1.86	1.64
Gd	–	–	–	–	6.89	6.58
Tb	1.24	0.33	1.11	0.94	–	–
Dy	–	–	–	–	7.95	5.80
Er	–	–	–	–	4.63	3.12
Tm	0.70	0.13	0.56	0.47	–	–
Yb	4.50	0.80	3.70	2.88	4.30	2.67
Hf	11.42	3.24	5.56	4.35	–	–
Ta	1.27	0.33	0.93	0.72	–	–
Th	31.50	4.11	8.12	5.68	–	–
U	–	–	–	–	–	–
Sc	13.1	6.5	16.0	26.0	–	–
Co	6.3	8.2	6.2	13.3	–	–

a Analysis by Isotope Dilution

	Augusta Victoria Formation				Cerros de Montecristo			
Sample	81130	81131[a]	81134	81136	81126	81129	81139	81140
La	74.9	44.6	16.6	21.3	27.2	26.5	30.1	28.5
Ce	146.5	97.6	38.6	49.5	47.2	55.8	65.0	59.7
Nd	66.9	39.1	23.0	29.5	27.2	26.8	31.4	28.0
Sm	11.0	6.48	5.1	6.9	5.4	5.5	6.5	6.0
Eu	2.89	1.32	1.55	1.85	1.12	1.14	1.17	0.98
Gd	-	4.55	-	-	-	-	-	-
Tb	0.98	-	0.87	1.19	0.65	0.67	0.87	0.79
Dy	-	3.02	-	-	-	-	-	-
Er	-	1.54	-	-	-	-	-	-
Tm	0.40	-	0.47	0.65	0.38	0.30	0.54	0.42
Yb	2.20	1.53	2.84	3.93	2.29	2.09	3.51	2.78
Hf	5.30	-	3.89	5.59	7.23	6.20	8.34	8.15
Ta	1.39	-	0.66	0.70	0.91	0.79	1.13	1.18
Th	20.20	-	3.60	5.71	22.4	18.70	20.9	22.59
U	5.3	-	1.0	1.9	6.5	5.7	6.2	7.4
Sc	15.7	-	26.5	30.0	14.0	16.2	14.2	12.0
Co	20.8	-	21.3	19.3	13.4	16.6	9.2	9.8

a Analysis by Isotope Dilution

	Cerro Negro Formation		Pampa Negra		Cerro Colorado Pluton		
Sample	81019	81020	81089	81091	80173	80176	80180
La	18.9	24.0	20.7	9.1	30.6	18.6	20.8
Ce	38.3	45.3	48.5	20.6	63.8	41.1	38.0
Nd	22.0	19.6	28.0	13.0	32.6	24.1	21.3
Sm	3.5	4.0	6.7	3.1	7.40	5.88	4.42
Eu	1.02	1.06	1.36	1.04	1.95	1.38	1.92
Gd	-	-	-	-	-	-	-
Tb	0.35	0.40	1.10	0.56	0.98	0.86	0.52
Tm	-	-	0.63	0.31	0.58	0.54	0.19
Yb	0.78	0.73	3.84	2.06	4.41	3.96	1.33
Hf	3.52	3.38	6.45	1.85	19.4	10.2	1.65
Ta	0.42	0.36	0.57	0.25	0.65	1.34	0.22
Th	4.78	5.16	7.60	2.55	9.32	21.2	2.44
U	-	-	2.1	0.7	4.1	4.3	0.8
Sc	8.3	8.3	24.8	33.5	8.8	3.6	9.6
Co	9.2	6.6	20.1	30.5	8.1	4.6	10.4

	El Abra Pluton			Upper Tertiary Volcanics		
Sample	80103	80104	80107	A31-1	A168-1	B43
La	31.7	28.4	23.5	21.7	15.8	26.5
Ce	63.6	59.6	43.4	44.7	30.7	53.0
Nd	22.6	26.5	19.8	22.0	14.8	29.0
Sm	3.79	5.04	3.44	4.57	3.55	5.89
Eu	0.40	0.98	0.92	1.20	0.98	1.48
Gd	-	-	-	-	-	-
Tb	0.30	0.57	0.32	0.55	0.51	0.75
Tm	0.23	0.26	0.13	0.25	0.30	0.36
Yb	1.99	1.88	0.89	1.57	1.97	2.01
Hf	4.09	5.49	3.55	4.12	3.22	4.16
Ta	1.88	1.08	0.48	0.39	0.28	0.62
Th	44.4	18.2	6.79	4.24	1.77	4.26
U	13.8	6.24	2.55	1.1	0.5	1.4
Sc	1.8	8.6	5.8	17.7	17.5	23.0
Co	1.6	10.4	8.4	23.2	23.9	30.2

	Monogenetic Centres					Standards	
Sample	A791[a]	7927[a]	7988[a]	80193	B1[b]	Whin Sill	RGM-1
La	15.7	17.5	24.5	34.6	47.5	25.6	26.1
Ce	35.0	40.0	53.0	66.3	96.1	58.4	48.0
Nd	18.7	20.5	26.2	27.8	49.0	33.2	20.6
Sm	4.0	4.5	5.3	4.7	8.8	7.40	4.27
Eu	1.12	1.30	1.43	1.22	-	2.30	0.65
Gd	-	-	-	-	-	-	-
Tb	0.61	0.79	0.72	0.51	1.1	1.11	0.66
Tm	-	0.38	0.28	0.25	-	0.45	0.38
Yb	1.69	2.84	1.60	1.44	2.0	2.60	2.54
Hf	3.20	3.60	4.20	5.04	4.5	5.05	6.06
Ta	0.48	0.88	0.89	0.73	3.5	1.30	0.99
Th	2.48	2.85	3.50	10.33	5.4	3.12	15.60
U	-	-	-	2.4	-	0.73	-
Sc	34.0	38.6	22.0	10.8	-	29[c]	5[c]
Co	-	-	-	12.5	-	46[c]	2
						n=4	n=3

a L.J. O'Callaghan (pers. comm.)
b Thorpe et al. (1984)
c Sc and Co values are used as the primary standard

Appendix F
Isotope Data

(i) Limon Verde Schists. Rb-Sr age 250 Ma

Sample	Rb	Sr	$^{87}Sr/^{86}Sr$	$(^{87}Sr/^{86}Sr)_{250}$	ε_{Sr}^{250}	Sm	Nd	$^{143}Nd/^{144}Nd$	$(^{143}Nd/^{144}Nd)_{250}$	ε_{Nd}^{250}
81150	7.5	166.7	0.70624±4	0.70578	+19.6	12.350	50.47	0.512646±42	0.512404	+1.67
81151	118.5	21.8	0.76647±2	0.71022	+82.6	9.390	48.40	0.512186±16	0.511994	-6.63
81152	75.4	74.9	0.71877±4	0.70840	+56.8	4.859	21.40	0.512491±24	0.512266	-1.01
81011	57.1	14.6	0.74146±4	0.70120	-45.4	4.614	22.79	0.512294±24	0.512094	-4.38

(ii) Limon Verde Pluton. Age 265.6 Ma

Sample	Rb	Sr	$^{87}Sr/^{86}Sr$	$(^{87}Sr/^{86}Sr)_i$	ε_{Sr}^{i}	Sm	Nd	$^{143}Nd/^{144}Nd$	$(^{143}Nd/^{144}Nd)_i$	ε_{Nd}^{i}
81013	81.3	319.9	0.70905±3	0.70627	+26.9					
81015	96.0	294.9	0.70999±3	0.70643	+29.2					
81018	82.6	451.3	0.70805±2	0.70605	+23.7					
81113	56.9	270.3	0.70844±3	0.70614	+24.9					
81114	51.8	194.4	0.70915±4	0.70623	+26.3	6.617	29.49	0.512449±10	0.512229	-1.35
81117	34.3	256.1	0.70791±4	0.70645	+29.3					
81118	43.3	337.0	0.70744±3	0.70603	+23.4	7.312	33.48	0.512456±12	0.512226	-1.40
81119	20.3	238.0	0.70742±4	0.70649	+30.0	6.169	40.49	0.512355±8	0.512195	-2.01
81120	70.8	371.8	0.70824±2	0.70615	+25.1					
81121	67.2	367.9	0.70772±4	0.70572	+19.0	3.794	17.05	0.512405±16	0.512171	-2.48

(iii) Cerro Crespo Formation. Age 232.7 Ma

81041	50.7	69.5	0.71354±3	0.70655	+30.3	6.77	35.70	0.512387±28	0.512212	-2.50
81042	53.3	134.2	0.71138±2	0.70757	+44.8	4.79	25.00	0.512472±20	0.512295	-0.88
81043	3.9	165.3	0.70815±4	0.70793	+49.8	5.59	28.90	0.512428±10	0.212250	-1.77
81045	96.0	47.1	0.72789±4	0.70831	+55.2	7.43	40.30	0.512408±16	0.512238	-2.00
80195	96.4	104.4	0.71502±3	0.70618	+24.9					

(iv) La Negra Formation. Age 186.5 Ma

Sample	Rb	Sr	$^{87}Sr/^{86}Sr$	$(^{87}Sr/^{86}Sr)_i$	ε^i_{Sr}	Sm	Nd	$^{143}Nd/^{144}Nd$	$(^{143}Nd/^{144}Nd)_i$	ε^i_{Nd}
8077	91.2	235.2	0.70644±3	0.70347	-14.3	8.170	34.70	0.512868±22	0.512694	+5.74
8078	84.5	178.8	0.70654±3	0.70292	-22.1	8.279	35.64	0.512821±30	0.512650	+4.88
8079	113.6	212.8	0.70713±3	0.70303	-20.4					
8080	108.6	217.0	0.70704±2	0.70321	-18.0					
8081	130.1	310.3	0.70657±3	0.70336	-15.9					
8088	48.1	402.0	0.70407±3	0.70315	-18.8					
8087	77.5	247.5	0.70545±3	0.70305	-20.3					
8086	59.3	317.7	0.70474±3	0.70330	-16.6	6.508	27.49	0.512775±26	0.512600	+3.90
8085	75.4	266.0	0.70535±3	0.70318	-18.4					
8084	83.7	241.3	0.70562±2	0.70296	-21.6	7.032	28.96	0.512918±20	0.512739	+6.62
8083	86.8	257.6	0.70573±3	0.70314	-18.9					
8082	72.4	248.3	0.70539±4	0.70315	-18.8					
8091	125.4	224.8	0.70757±3	0.70329	-16.9					
8092	147.0	301.0	0.70692±2	0.70318	-18.4	6.010	26.50	0.512892±34	0.512725	+6.34
8092A	90.8	229.5	0.70616±4	0.70312	-19.3					
8093	125.7	206.9	0.70785±4	0.70320	-18.2	8.167	34.63	0.512836±32	0.512662	+5.11
8097	94.7	241.5	0.70601±3	0.70301	-20.9	7.286	30.34	0.512868±16	0.512691	+5.68
8098	65.1	195.4	0.70559±3	0.70304	-20.5	9.446	39.46	0.512876±38	0.512699	+5.84

(v) Gatico Pluton. Age 158.3 Ma

8054	33.4	294.8	0.70395±3	0.70322	-18.4					
8058	25.3	315.8	0.70384±3	0.70332	-16.9					
8059	16.4	342.8	0.70362±3	0.70331	-17.0	2.420	9.45	0.512902±36	0.512740	+5.93
8062	21.0	327.1	0.70368±4	0.70326	-17.7	2.862	10.72	0.512939±16	0.512772	+6.55
8072	120.4	159.8	0.70819±3	0.70329	-17.4					
8073	47.7	279.1	0.70436±3	0.70325	-17.9	4.860	20.40	0.512920±24	0.512771	+6.53
8074	48.7	283.7	0.70451±4	0.70339	-15.9					

(vi) Sierra de la Cruz Pluton. Age 156.2 Ma

Sample	Rb	Sr	$^{87}Sr/^{86}Sr$	$(^{87}Sr/^{86}Sr)_i$	ε^i_{Sr}	Sm	Nd	$^{143}Nd/^{144}Nd$	$(^{143}Nd/^{144}Nd)_i$	ε^i_{Nd}
81099	135.0	196.9	0.70861±2	0.70421	- 4.3					
81105	42.8	378.4	0.70506±3	0.70433	- 2.6	3.668	16.74	0.512817±24	0.512682	+4.74
81106	4.9	468.7	0.70430±4	0.70423	- 4.0	3.166	14.65	0.512798±16	0.512664	+4.39
81110	71.0	346.1	0.70504±3	0.70373	-11.1					

(vii) Cerro Colupito Pluton. Assumed age 155 Ma

81094	79.6	336.1	0.70473±3	0.70322	-18.3	4.201	18.43	0.512769±44	0.512659	+4.26
81095	53.0	340.5	0.70447±3	0.70347	-14.8					
81096	72.2	315.4	0.70479±4	0.70333	-16.7					

(viii) Tocopilla Pluton. Age 154.6 Ma

81075	44.0	323.0	0.70491±3	0.70405	- 6.7	2.653	11.27	0.512785±28	0.512641	+3.90
81076	154.4	198.8	0.70845±4	0.70351	-14.3	8.357	39.26	0.512761±28	0.512601	+3.71
81077	74.3	274.0	0.70553±4	0.70381	-10.0					
81078	99.1	219.0	0.70699±4	0.70412	- 5.7	5.036	23.15	0.512832±20	0.512699	+5.03
81079	138.2	210.0	0.70821±3	0.70403	- 6.9					
81080	71.7	318.3	0.70509±4	0.70366	-12.2					
TOC1	107.6	290.2	0.70603±2	0.70367	-11.9					
TOC2	45.6	418.7	0.70463±4	0.70394	- 8.2					
TOC4	19.3	375.3	0.70424±4	0.70392	- 8.4	5.127	22.27	0.512852±16	0.512711	+5.27
TOC5	140.4	215.9	0.70828±4	0.70415	- 5.2	4.419	19.95	0.512770±24	0.512634	+3.77
TOC6	174.7	292.0	0.70777±4	0.70397	- 7.7	3.372	16.46	0.512799±18	0.512674	+4.55
TOC7	93.9	309.3	0.70556±4	0.70363	-12.6	4.45	19.12	0.512885±20	0.512743	+5.89

(ix) Indio Muerto Formation. Assumed Age 130 Ma

Sample	Rb	Sr	$^{87}Sr/^{86}Sr$	$(^{87}Sr/^{86}Sr)_i$	ε^i_{Sr}	Sm	Nd	$^{143}Nd/^{144}Nd$	$(^{143}Nd/^{144}Nd)_i$	ε^i_{Nd}
81053A	269.7	224.9	0.70861±3	0.70220	-33.3					
81054	50.7	623.6	0.70462±3	0.70418	- 5.1					
81055	70.8	452.6	0.70617±3	0.70534	+11.3	6.753	31.88	0.512505±22	0.512396	-1.50
81056	44.7	494.5	0.70535±4	0.70487	+ 4.6	5.697	26.32	0.512610±26	0.512499	+0.51

(x) Augusta Victoria Formation. Age 104.7 Ma

81130	59.3	829.3	0.70489±3	0.70458	+ 0.1	11.300	67.80	0.512755±18	0.512687	+3.55
81131	104.8	145.2	0.70741±3	0.70430	- 3.9	6.48	39.10	0.512828±26	0.512759	+4.95
81132	110.7	492.3	0.70514±4	0.70417	- 5.7	8.050	46.20	0.512846±30	0.512774	+5.24
81134	10.5	445.2	0.70433±4	0.70423	- 4.9	4.896	21.15	0.512782±20	0.512688	+3.57
81136	36.5	363.2	0.70451±3	0.70408	- 7.0	6.720	28.46	0.512803±32	0.512705	+3.90

(xi) Cerro Negro Formation. Assumed age 70 Ma

81019	67.7	658.4	0.70586±3	0.70457	- 0.7	3.50	22.00	0.512719±16	0.512675	+2.44
81020	71.5	928.7	0.70514±3	0.70492	+ 4.3	4.00	19.60	0.512733±20	0.512676	+2.46

(xii) Cerros de Montecristo Pluton. Age 101.7 Ma

81125	102.8	549.3	0.70479±3	0.70400	- 8.2					
81126	140.0	579.5	0.70548±4	0.70447	- 1.5	5.100	26.25	0.512675±16	0.512597	+1.71
81127	109.9	520.2	0.70498±3	0.70409	- 6.9					
81128	106.2	535.3	0.70492±2	0.70409	- 7.0					
81129	119.2	528.7	0.70501±3	0.70407	- 7.2	5.083	26.04	0.512697±26	0.512611	+1.99
81133	119.2	491.9	0.70593±3	0.70402	- 7.9					
81138	164.8	298.5	0.70633±4	0.70402	- 7.9					
81139	162.9	291.8	0.70684±4	0.70451	- 1.0	6.185	30.24	0.512687±16	0.512605	+1.87
81141	194.7	263.9	0.70636±3	0.70384	-10.4					

(xiii) Cerritos Bayos Pluton. Assumed age 100 Ma

Sample	Rb	Sr	$^{87}Sr/^{86}Sr$	$(^{87}Sr/^{86}Sr)_i$	ε^i_{Sr}	Sm	Nd	$^{143}Nd/^{144}Nd$	$(^{143}Nd/^{144}Nd)_i$	ε^i_{Nd}
81038	158.7	362.3	0.70680±2	0.70500	+ 5.9	7.041	33.15	0.512711±30	0.512627	+2.26
81040	81.6	390.1	0.70691±3	0.70605	+20.8					
81046	151.9	316.6	0.70715±3	0.70518	+ 8.5					
81047	29.6	564.4	0.70453±2	0.70431	- 3.8					
81048	14.0	553.3	0.70580±3	0.70570	+15.9	4.094	17.61	0.512731±20	0.512639	+2.49
81051	62.8	454.6	0.70476±3	0.70420	- 5.4	4.619	21.27	0.512748±20	0.512662	+2.94
81052	16.4	667.7	0.70564±4	0.70553	+13.6					
81053	26.4	492.6	0.70682±3	0.70660	+28.7					

(xiv) Pampa Negra Pluton. Age 79.2 Ma

81088	76.1	256.3	0.70514±3	0.70417	- 6.2					
81089	93.4	239.3	0.70547±3	0.70420	- 5.7	6.082	26.19	0.512670±20	0.512597	+1.15
81090	99.3	263.0	0.70548±2	0.70425	- 5.1					
81091	30.8	302.5	0.70455±4	0.70422	- 5.4	2.765	11.20	0.512623±26	0.512546	+0.15

(xv) Cerro Colorado Pluton. Age 65.5 Ma

	a	a								
80166	110.1	1145.5	0.70413±3	0.70387	-10.7					
80173	172.6	696.7	0.70439±3	0.70372	-12.8	6.738	30.81	0.512799±16	0.512742	+3.63
80176	155.7	544.6	0.70474±3	0.70397	- 9.3	5.358	22.35	0.512810±16	0.512748	+3.75
81080	68.8	1223.8	0.70400±3	0.70385	-10.9	4.064	19.45	0.512831±14	0.512779	+4.36
81087	152.8	798.9	0.70431±2	0.70380	-11.7					
80190	152.1	999.1	0.70432±2	0.70391	-10.1					

a L.J. O'Callaghan (pers. comm.)

(xvi) El Abra Pluton. Age 38.7 Ma

80103	200.2	93.9	0.70790±3	0.70451	- 2.0	3.431	20.89	0.512708±14	0.512683	+1.81
80104	141.4	486.0	0.70503±4	0.70457	- 1.2	4.485	24.12	0.512687±12	0.512659	+1.34
80107	62.5	748.1	0.70460±2	0.70447	- 2.7	3.183	18.46	0.512689±18	0.512663	+1.42

(xvii) Upper Tertiary Volcanics.

Sample	Age (Ma)	Rb	Sr	$^{86}Sr/^{87}Sr$	$(^{86}Sr/^{87}Sr)_i$	ε^i_{Sr}	Sm	Nd	$^{143}Nd/^{144}Nd$	$(^{143}Nd/^{144}Nd)_i$	ε^i_{Nd}
A168-1	15.2	28.9	598.7	0.70500±3	0.70497	+ 4.1	3.131	15.47	0.512548±38	0.512536	-1.65
A6-2	10.5	56.4	753.5	0.70554±2	0.70551	+11.6	2.757	15.92	0.512477±12	0.512470	-3.05
A31-1	5.7	44.4	565.0	0.70568±3	0.70566	+13.7	4.156	21.68	0.512453±20	0.512449	-3.58
B43	4.6	47.8	570.3	0.70678±3	0.70676	+29.3	5.385	27.40	0.512307±16	0.512303	-6.46
A33-1	3.6	79.2	546.8	0.70558±2	0.70556	+12.3	4.167	23.70	0.512431±20	0.512428	-4.05
B5	2.5	77.6	889.7	0.70566±3	0.70565	+13.6	8.184	52.71	0.512268±20	0.512266	-7.22

(xviii) Monogenetic Centres. Recent

Sample	Rb	Sr	$^{86}Sr/^{87}Sr$	ε_{Sr}	Sm	Nd	$^{143}Nd/^{144}Nd$	ε_{Nd}
A791[a]	32.0	501.0	0.70612±4	+20.1	4.000	18.70	0.512536±18	-2.03
7927[a]	30.0	630.0	0.70628±3	+22.4	4.500	20.50	0.512461±22	-3.49
7988[a]	46.0	584.0	0.70637±3	+23.7	5.300	26.20	0.512319±20	-6.26
80193	107.0	575.0	0.70498±4	+ 4.0	4.700	27.80	0.512674±28	+0.66
B1[b]	24.0	871.0	0.70386±2	-11.9	8.800	49.00	0.512679±24	+0.76

a Trace element data from L.J. O'Callaghan (pers. comm.); b Trace element data from Thorpe et al. (1984)

(xix) San Pedro

					c	c		
170	56[a]	638[a]	0.70649	+25.5	2.74	14.6	0.512354	-5.58
172	103[a]	504[a]	0.70640	+24.1	4.25	23.0	0.512353	-5.60
176	52[a]	518[a]	0.70616	+20.7	3.15	15.9	0.512431	-4.08
7901	38[b]	631[b]	0.70665	+27.6			0.512347	-5.72
7920	58[b]	584[b]	0.70681	+29.9			0.512359	-5.48
80010	71[b]	581[b]	0.70647	+25.1			0.512391	-4.86
80012	42[b]	624[b]	0.70642	+24.4			0.512279	-7.04
80025	63[b]	656[b]	0.70629	+22.6			0.512402	-4.64

a Data from Francis et al. (1977); b L.J. O'Callaghan (pers. comm.); c Hawkesworth et al. (1979a)

(xx) Other Recent volcanoes in North Chile

Sample	Rb[c]	Sr[c]	$^{87}Sr/^{86}Sr$	ε_{Sr}	Sm	Nd	$^{143}Nd/^{144}Nd$	ε_{Nd}
283[a]	47	584	0.70711	+34.1	4.49[d]	23.3[d]	0.512331	-6.03
200[b]	76	512	0.70677	+29.3	5.50[e]	22.1[e]	0.512355	-5.56
482[b]	68	441	0.70583	+16.0	5.59[d]	27.8[d]	0.512499	-2.75

a San Pablo Volcano; b Details of location in Thorpe et al. (1976); c Data from Francis et al. (1977); d Data from Hawkesworth et al. (1979a); e Data from Thorpe et al. (1976)

(xxi) Ecuador

	a	a			b	b		
EF7	21	638	0.70425±3	- 6.4	3.72	17.2	0.512895±10	+4.97
EF13	47	589	0.70429±3	- 5.8	3.96	18.8	0.512797± 8	+3.06
EF18	30	570	0.70405±3	- 9.2	3.35	15.7	0.512870± 8	+4.49
EF20	31	565	0.70416±3	- 7.7	3.37	15.8	0.512889±20	+4.86
EF21	19	852	0.70370±3	-14.2	4.02	20.5	0.512934± 8	+5.74
EF22	19	1144	0.70365±4	-14.9	5.68	32.4	0.512970±20	+6.44

a Data from Francis et al. (1977); b Hawkesworth et al. (1979a)